

Aspects of the Pathogenesis, Immunity and Treatment of Buruli ulcer

INAUGURALDISSERTATION

zur Erlangung der Würde eines Doktors der Philosophie
vorgelegt der Philosophisch-Naturwissenschaftlichen Fakultät der
Universität Basel

von

Raphael Bieri

aus Willisau LU

Basel, 2017

Originaldokument gespeichert auf dem Dokumentenserver
der Universität Basel edoc.unibas.ch

Genehmigt von der Philosophisch-Naturwissenschaftlichen Fakultät
auf Antrag von

Prof. Dr. Christian Münz

Prof. Dr. Gerd Pluschke

Basel, den 8. Dezember 2015

Prof. Dr. Jörg Schibler

Dekan

Summary

Buruli ulcer (BU) is a neglected tropical disease of the skin and subcutaneous tissue caused by infection with *Mycobacterium ulcerans*. The disease has been reported from over 30 countries worldwide with the highest prevalence in rural areas of West African countries. Clinically, *M. ulcerans* disease presents in different forms, ranging from small non-ulcerative nodules to large ulcers. The pathology of BU is largely attributable to the production of mycolactone, a lipid-like macrolide exotoxin with cytotoxic and immunosuppressive characteristics. Although mycolactone-induced cytotoxicity and tissue necrosis are the key elements of BU pathogenesis, the molecular mechanisms underlying these processes remained to be elucidated.

Within the framework of this PhD thesis, we could show that mycolactone binds to the 12-kDa FK506-binding protein and acts as a potent inhibitor of both mTORC1 and mTORC2. Inhibition of mTORC2 results in inactivation of Akt and dephosphorylation and activation of the Akt-targeted transcription factor FoxO3. Subsequent up-regulation of the FoxO3 target gene *Bim*, a pro-apoptotic member of the Bcl-2 protein family, was observed both *in vitro* and in human BU lesions. Moreover, *Bim* knockout mice were able to contain *M. ulcerans* infection and did not develop necrotic lesions with large clusters of extracellular bacilli typical for BU, highlighting the pivotal role of *Bim*-promoted apoptosis for BU pathogenesis.

In addition, we aimed at characterizing the nature of immune defense mechanisms conferring protection against BU. Specifically, we focused on the role of interferon- γ and of cellular immune effector mechanisms during the early intracellular stage of *M. ulcerans* infection. We could show that interferon- γ is critical for early host immunity against *M. ulcerans*, since mice lacking this cytokine showed a faster increase in bacterial burden and an accelerated pathogenesis, indicative of a reduced capacity to kill the bacilli during the early intracellular stage of the infection.

Finally, we evaluated the activity of the new tuberculosis drug candidate Q203 against *M. ulcerans* using the BU mouse foot pad infection model. In this project, we were able to demonstrate that Q203 has a higher activity against *M. ulcerans* than rifampicin, and might therefore be suited to replace rifampicin as the first line therapeutic option in the future.

Zusammenfassung

Buruli Ulkus (BU) ist eine vernachlässigte Erkrankung der Haut und des Unterhautgewebes, welche durch Infektion mit *Mycobacterium ulcerans* verursacht wird. Die Tropenkrankheit wurde weltweit in über 30 Ländern nachgewiesen, mit der höchsten Prävalenz in ländlichen Gebieten einiger westafrikanischer Länder. Klinisch präsentiert sich BU mit einem breiten Spektrum an Krankheitsbildern, welche von geschlossenen Läsionen bis hin zu offenen Ulzera reichen. Die Pathologie der Krankheit ist eng assoziiert mit der Produktion von Mykolacton, einem fettähnlichen Makrolidtoxin, welches zytotoxische und immunsuppressive Eigenschaften besitzt. Obwohl die Mykolacton-induzierte Zytotoxizität und die daraus resultierende Gewebenekrose für die Pathogenese der Krankheit von zentraler Bedeutung sind, mussten die zugrundeliegenden molekularen Mechanismen erst noch entschlüsselt werden.

Im Rahmen der vorliegenden Doktorarbeit konnten wir zeigen, dass Mykolacton an das 12-kDa FK506 Bindungsprotein bindet und dabei als potenter Inhibitor der beiden mTOR Komplexe wirkt. Die Inhibition vom mTOR Komplex 2 resultiert in der Inaktivierung der Kinase Akt und in der anschliessenden Dephosphorylierung und Aktivierung des von Akt regulierten Transkriptionsfaktors FoxO3. Die darauffolgende Hochregulation der Expression des FoxO3-regulierten Genes *Bim*, einem proapoptischen Mitglied der Bcl-2 Proteinfamilie, wurde sowohl *in vitro* als auch in humanen BU Läsionen beobachtet. Des Weiteren konnten wir zeigen, dass *Bim* Knockout Mäuse fähig sind, Infektionen mit *M. ulcerans* zu kontrollieren und dass sie keine der für BU typischen nekrotischen Läsionen mit grossen Akkumulationen von extrazellulären Bakterien entwickeln, was die entscheidende Rolle der *Bim*-abhängigen Apoptose für die Pathogenese von BU unterstreicht.

Ein zusätzliches Ziel dieser Doktorarbeit war es, die Immunabwehr-Mechanismen, welche zum Schutz vor BU beitragen, genauer zu charakterisieren. Ein spezifischer Fokus lag dabei auf der Rolle von Interferon- γ und auf den zellulären Immuneffektormechanismen während der frühen intrazellulären Phase der Infektion mit *M. ulcerans*. Dabei konnten wir zeigen, dass Interferon- γ für die frühe Immunabwehr gegen *M. ulcerans* wichtig ist, da wir bei Interferon- γ -defizienten Mäusen eine schnellere

Zunahme der Bakterienlast und einen beschleunigten Krankheitsverlauf beobachtet haben, was darauf hinweist, dass die Fähigkeit dieser Tiere, intrazelluläre Bakterien während des frühen Stadiums der Infektion zu bekämpfen, reduziert ist.

Des Weiteren testeten wir die Aktivität von Q203, einem möglichen neuen Medikament zur Behandlung der Tuberkulose, in einem BU Mausmodell. Hierbei konnten wir zeigen, dass Q203 eine höhere Aktivität gegen *M. ulcerans* besitzt als Rifampicin und daher geeignet sein könnte, Rifampicin in der Zukunft als Primärtherapie zu ersetzen.

Acknowledgements

My PhD studies were carried out at the Swiss Tropical and Public Health Institute in Basel from June 2012 until December 2015. None of this would have been possible without the support and help of many great friends and colleagues, whom I would like to acknowledge here.

First and foremost, I would like to thank my boss Professor Gerd Pluschke, for giving me the opportunity to do my PhD in his group, for his constant support, the freedom to work on my own and to develop my own ideas, as well as for giving me the possibility to present my work on scientific meetings.

I would also like to express my gratitude to Professor Christian Münz, University of Zurich, for joining my PhD committee as a co-referee, to Professor Karl-Heinz Altmann, ETH Zurich, for participating at my thesis defense as an external expert and to Professor Till Voss for chairing my thesis defense.

Very special thanks to all the current and past members of the Molecular Immunology group at the Swiss TPH, it was the utmost pleasure to work with you! Thank you for all the help, for sharing the coffee breaks and for the wonderful time we spent together!

Especially, I would like to acknowledge Nicole Scherr, Miriam Bolz, Theresa Ruf, Jean-Pierre Dangy and Sarah Kerber for sharing some of their projects with me, for their technical support and for all the fruitful discussions we had together. A special thank goes to Nicole for her constant support and for reading and correcting my manuscripts and my thesis. Miriam, thank you for introducing me into the work under BSL-3 conditions, you really helped me a lot expanding my technical skills. In addition, I would like to thank our secretary Susi who was always very helpful and did a fantastic job.

At the EPFL in Lausanne, I want to thank Professor Stewart Cole and the group members for allowing me to use their BSL-3 animal facility and for integrating me as if I were a normal member of their lab. Special thanks go to Claudia Sala for supporting me with

many issues concerning BSL-3 lab activities and to Cécile Hayward-Scherrer for booking hotel rooms and solving IT problems. Philippe, Anthony, Jérémie, Andrej, Chloé and Charlotte, I really enjoyed the coffee and lunch breaks as well as the after-work beers with you! Furthermore, I am grateful to the animal care takers, especially Morgane Nicod and Nicolas Fabbroni, who always took care of my mice.

This work would not have been possible without the collaboration of many other people that have shared their technologies and compounds with us. I especially would like to thank Professor Karl-Heinz Altmann and team members Philipp Gersbach and Matthias Gehringer for providing us with synthetic mycolactone and mycolactone derivatives which allowed us to decipher the molecular mechanisms of mycolactone cytotoxicity.

I sincerely acknowledge having received financial support for the project through the Stop Buruli Initiative supported by the UBS-Optimus Foundation.

Further, I would like to thank my flat mate Elias for the great past few years and numerous people at the Swiss TPH for creating such a wonderful working atmosphere, for sharing coffee and lunch breaks and for all the memorable evenings and events we spent together. It was a great time and I will always look back with a smile to this wonderful time. Thank you very much, Fabrice, Alex, Remo, Philipp, Laura, Nadja, Sämi, Urs, Beni, Philipp, Tobi, Paola, Arianna, Angelika, Nathalie and Lucienne.

Finally, I'm deeply grateful to my parents, to my sister Alexandra, to my brother Lukas, to my grandparents and to all of my friends for their constant support and encouragement throughout my whole PhD studies.

Table of contents

Summary	I
Zusammenfassung	II
Acknowledgements	IV
Table of contents	VI
List of abbreviations	VIII
Introduction	1
History and epidemiology of Buruli ulcer	1
Evolution, reservoir and transmission of <i>M. ulcerans</i>	3
Pathogenesis of Buruli ulcer	4
Cellular effects of mycolactone.....	6
Immune responses against <i>M. ulcerans</i>	9
Diagnosis and Treatment.....	9
Apoptosis.....	13
The mTOR signaling pathway and its role in apoptosis.....	15
Rapamycin and its derivatives.....	17
ATP-competitive mTOR kinase inhibitors	18
Objectives	29
Results	30
Chapter 1: Mycolactone binds to FKBP12 and promotes Bim-dependent apoptosis in Buruli ulcer through inhibition of mTOR	30
Chapter 2: Interferon- γ is a Crucial Activator of Early Host Immune Defense against <i>Mycobacterium ulcerans</i> Infection in Mice	69
Chapter 3: The anti-TB drug candidate Q203 is highly active against <i>Mycobacterium ulcerans</i> , the causative agent of Buruli ulcer	93
General Discussion	114
What has been learned about the molecular mechanisms underlying the cytotoxic activity of mycolactone and their impact on the pathogenesis of Buruli ulcer?.....	114

Could the new mechanistic insights into mycolactone cytotoxicity be used for the development of a novel therapeutic approach?.....	118
What is the significance of the mTORC2-Akt-FoxO3-Bim pathway for the immunosuppression mediated by mycolactone?.....	119
What is the impact of this work for the understanding of immunity and for the treatment of Buruli ulcer?.....	121
Conclusions	123
References	124
Appendix.....	127
Chapter 1: Mycolactone binds to FKBP12 and promotes Bim-dependent apoptosis in Buruli ulcer through inhibition of mTOR	127
Chapter 3: The anti-TB drug candidate Q203 is highly active against Mycobacterium ulcerans, the causative agent of Buruli ulcer.....	148
Curriculum Vitae.....	161

List of abbreviations

AFB	acid-fast bacilli
AT ₂ R	angiotensin type II receptor
BCG	Bacille Calmette-Guérin
Bim	Bcl-2 interacting mediator of cell death
BU	Buruli ulcer
CMI	cell-mediated immunity
CYP450	cytochrome P450
DED	death effector domain
DISC	death-inducing signaling complex
DTH	delayed-type hypersensitivity
EPFL	école polytechnique fédérale de Lausanne
ER	endoplasmatic reticulum
FADD	Fas-Associated protein with Death Domain
FDA	US Food and Drug Administration
FKBP12	12-kDa FK506-binding protein
FoxO	forkhead box O
FRB	FKBP12-rapamycin binding domain
GBUI	Global Buruli Ulcer Initiative
HE	Haematoxylin/Eosin
hPXR	human pregnane X receptor
IFN γ	interferon- γ
Ig	Immunoglobulin
IL	interleukin
IPA	imidazo(1,2- α)pyridine carboxamide
IS	insertional sequence
M. liflandii	Mycobacterium liflandii
M. leprae	Mycobacterium leprae
M. marinum	Mycobacterium marinum
M. pseudoshottsii	Mycobacterium pseudoshottsii
M. tuberculosis	Mycobacterium tuberculosis

Abbreviations

M. ulcerans	Mycobacterium ulcerans
MAC	mitochondrial apoptosis-inducing channel
MDR	multiple drug resistant
MIC	minimal inhibitory concentration
MOI	multiplicity of infection
MPM	mycolactone-producing mycobacteria
MPT	mitochondria permeability transition
mSIN1	mammalian stress-activated protein kinase interacting protein
mTOR	mammalian target of rapamycin
Nec-1	necrostatin-1
NFAT	nuclear factor of activated T-cells
NO	nitric oxide
NTD	neglected tropical disease
PARP-1	nuclear Poly(ADP-ribose) polymerase-1
PCD	programmed cell death
PCR	polymerase chain reaction
PDK1	phosphoinositide-dependent kinase 1
PI3K	phosphoinositide 3-kinase
PIKK	phosphoinositide 3-kinase-related protein kinase
PKC α	protein kinase C α
QcrB	b subunit of the electron transport complex ubiquinol - cytochrome c reductase
qPCR	quantitative real-time polymerase chain reaction
R/S	rifampicin streptomycin combination therapy
Raptor	regulatory-associated protein of mTOR
Rictor	rapamycin-insensitive companion of mTOR
S6K1	ribosomal protein S6 kinase 1
siRNA	short interfering RNA
TB	tuberculosis
TKIs	ATP-competitive mTOR kinase inhibitors
TLR	toll-like receptor
TNF α	tumor necrosis factor alpha

Abbreviations

WASP	Wiskott-Aldrich syndrome protein family
WHO	World Health Organization
Wisko	wiskostatin
WT	wild-type
XDR	extensive drug resistant
ZN	Ziehl-Neelsen / Methylene blue
zVAD	zVAD.fmk
3-MA	3-methyladenine
4E-BP1	eukaryotic initiation factor 4E-binding protein 1

Introduction

Buruli ulcer (BU) is a chronic necrotizing disease of the skin and subcutaneous tissue caused by infection with *Mycobacterium ulcerans* (*M. ulcerans*), a relative of *Mycobacterium tuberculosis* (*M. tuberculosis*) and *Mycobacterium leprae* (*M. leprae*), the two causative pathogens of tuberculosis and leprosy, respectively. *M. ulcerans* is unique in the sense that it produces mycolactone, a cytotoxic and immunosuppressive lipid-like macrolide exotoxin responsible for the pathophysiology of the disease [1,2]. After a long time of disregard, the World Health Organization (WHO) recognized BU in 1998 as an emerging health problem and consequently launched the Global Buruli Ulcer Initiative (GBUI) aiming to intensify and coordinate the control and research activities of this devastating skin disease [3].

Despite intensified research efforts during the last 15 years, many of the central molecular mechanisms underlying the pathogenesis of BU still remain obscure and a practical and well-tolerated anti-BU treatment is not available.

History and epidemiology of Buruli ulcer

The first report on BU was published in 1948 by *MacCallum et al.* describing the clinical symptoms of six patients with ulcerative lesions of the skin in the Bairnsdale district in Australia. In the same study, the disease causing pathogen, later referred to as *Mycobacterium ulcerans* (*M. ulcerans*), was isolated from one of the lesions and described as a bacterium with a lower optimal growth temperature than *M. tuberculosis* [4]. A few years later, the Buruli County in Uganda was identified as a hot-spot of the disease and from this time onwards the disease became more generally known as Buruli ulcer (BU) [5]. In the 1970's, cases were also reported from various other places in Africa including regions that nowadays belong to Cameroon, Nigeria and the Democratic Republic of the Congo [6–8]. Since then, BU has been widely distributed and is today reported from over thirty countries worldwide. It affects South East Asian countries such as Indonesia, Papua New Guinea and Malaysia as well as countries in Central and South America including Mexico, Peru or Suriname [9,10]. After tuberculosis and leprosy, BU is considered to be the third most common mycobacterial disease

worldwide, however, in some high burden West African countries, the disease is more prevalent than leprosy [11,12]. In 2014, there were 2200 new cases of BU worldwide which is most likely an underestimation of the exact numbers since only 12 of the affected 33 countries reported data to the WHO (Figure 1) [13]. In addition, the remote locations of most endemic areas and as a consequence the limited access of many of the patients to the health care systems may potentiate this underestimation [11].

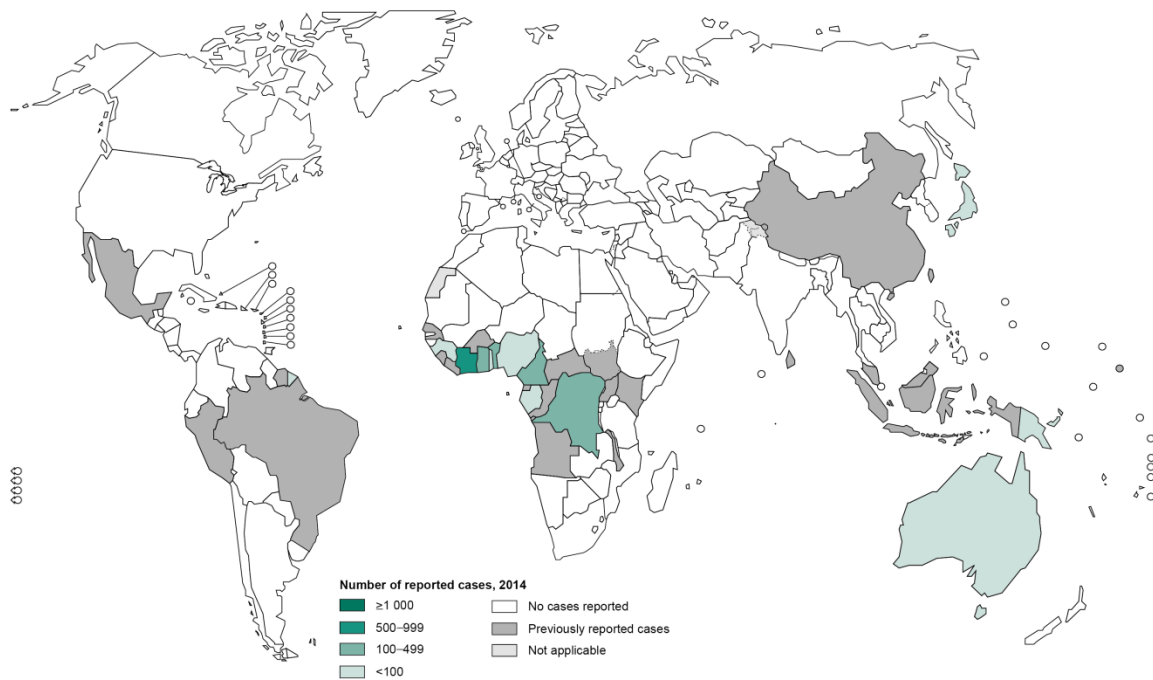


Figure 1: Geographical distribution of BU in 2014 [13].

Although BU affects people at all ages, most of the patients are children between the age of 4 and 15 years [9]. No gender differences in BU incidence have been observed among children and adults [14]. About 80 % of the ulcers are found on the limbs, most of them are located on the lower extremities [9].

In BU endemic countries, the disease mostly occurs close to wetlands with slow-flowing water courses or stagnant water. In several countries including Nigeria, Liberia or Australia, the emergence of the disease has been attributed to environmental disturbances in water management, for example for energy production, agriculture or mining [14].

Evolution, reservoir and transmission of *M. ulcerans*

It is assumed that *M. ulcerans* has evolved from a common progenitor of *Mycobacterium marinum* (*M. marinum*), an intracellular environmental bacterium living in aquatic niches, occasionally causing relatively minor granulomatous skin lesions in humans [15,16]. Like *M. ulcerans*, *M. marinum* optimally grows at 28 °C – 32 °C but only poorly at 37 °C [16]. The close relationship of *M. ulcerans* and *M. marinum* was identified using comparative genomics showing that the two species share over 98 % of genomic DNA sequence identity. Moreover, it was proposed that all *M. ulcerans* strains diverged from a common *M. marinum* progenitor [15,17]. During the evolutionary divergence from *M. marinum*, *M. ulcerans* has undergone some major genetic changes. Firstly and probably most importantly, *M. ulcerans* has acquired a 174 kb virulence plasmid called pMUM through horizontal gene transfer. This plasmid encodes the polyketide synthases required for the production of the macrolide exotoxin mycolactone, the only virulence factor of *M. ulcerans* identified to date [18,19]. Secondly, *M. ulcerans* has integrated the two insertion sequence elements IS2404 and IS2606 into its genome. While these two elements are absent in *M. marinum*, they have been expanded to high copy numbers in the genome of *M. ulcerans*, constituting the molecular target for the most sensitive method of BU diagnosis, the polymerase chain reaction (PCR) [20]. The genomic expansion of IS2404 to 213 copies and of IS2606 to 91 copies resulted in the disruption of over 110 genes, extensive pseudogene formation, genomic rearrangement and genome reduction [2,21]. The evolution of the *M. ulcerans* genome indicates that this pathogen underwent a series of adaptations allowing its transition from an environmental to a host-adapted niche [21]. For example, the acquisition of the immunosuppressive toxin mycolactone, the loss or modification of cell wall antigens, the slow replication time of around 72 hours as well as the thermosensitivity of *M. ulcerans* altogether favor a long-term survival in a mammalian host [21–23].

During the evolution, two different but closely related lineages of *M. ulcerans* causing human disease have emerged. The so-called ancestral lineage of is more closely related to *M. marinum* and causes only sporadic disease in China, Japan, Mexico and South America. In contrast, BU in Africa, Australia and South East Asia is primarily caused by the classical lineage of *M. ulcerans* containing the most pathogenic genotypes, resulting in a higher prevalence in these countries [24]. Strains of these two lineages are, together

with the few other mycolactone-producing mycobacteria (MPM) including the fish and frog pathogens, commonly known as *M. ulcerans* [25].

Despite intensive research in the last few years, the reservoir and the exact mode of transmission of *M. ulcerans* still remain unclear [9]. Like its progenitor *M. marinum*, *M. ulcerans* is considered as an environmental bacterium and its DNA has been detected in the environment [26,27]. In addition, research has focused on invertebrates or vertebrates as potential animal reservoirs and indeed *M. ulcerans* DNA has been detected in animals such as water bugs and aquatic snails [9,23]. Since then, mainly water bugs were suspected to play a major role in the transmission of BU, however, their role still remains questionable as these insects rarely bite humans [9,28,29]. In Australia, possums with skin lesions caused by *M. ulcerans* have recently been identified as a potential mammalian reservoir and mosquitos as possible vectors [30,31]. While possums represent a potential animal reservoir for *M. ulcerans* in Australia, a comparable animal reservoir could not be identified in Africa [32,33]. Furthermore, the mode of transmission from a potential animal reservoir or from the environment to humans is still unclear and several possibilities such as an involvement of insect bites or a direct transmission from an environmental reservoir to humans, for example after skin trauma, have been discussed [9].

Pathogenesis of Buruli ulcer

The pathogenesis of BU entirely relies on the presence of the cytotoxic and immunosuppressive macrolide toxin mycolactone [1]. Due to the low optimal growth temperature of the bacteria and hence a strong tropism for the skin, BU is predominantly a disease of the skin and the subcutaneous fat tissue with very restricted systemic dissemination. Furthermore, the disease progresses only slowly, probably as a result of the long generation time of *M. ulcerans* [34].

The first clinical sign of the disease is typically a movable, subcutaneous nodule which can be observed after an estimated incubation time of 2 to 3 months (Figure 2, A). From this initial nodular stage, the disease may develop into a non-ulcerative plaque or oedema (Figure 2, B and C, respectively). As the infection progresses, a massive destruction of the subcutaneous adipose tissue can be observed, resulting in the collapse

of the epidermis and the formation of characteristic ulcers with undermined edges (Figure 2, D) [2,34]. Complementary to these descriptions, the WHO introduced a classification system which is primarily based on the size of the lesions. Lesions grouped into category I are smaller than 5 cm in diameter whereas lesions with a diameter of 5 – 15 cm are classified into category II. Category III finally contains lesions with a diameter of over 15 cm, lesions in the region of head and neck, mixed forms such as osteomyelitis, lesions with involvement of joints and disseminated forms of the disease [35]. Interestingly, BU lesions are often described as painless and it was speculated for a long time whether this analgesic effect might be the result of the local destruction of nerve fibers [36]. However, a recent study indicates the painless nature of BU lesions most likely comes from mycolactone-induced signaling through angiotensin type II receptors (AT₂R), resulting in neuronal hyperpolarization and analgesia [37].

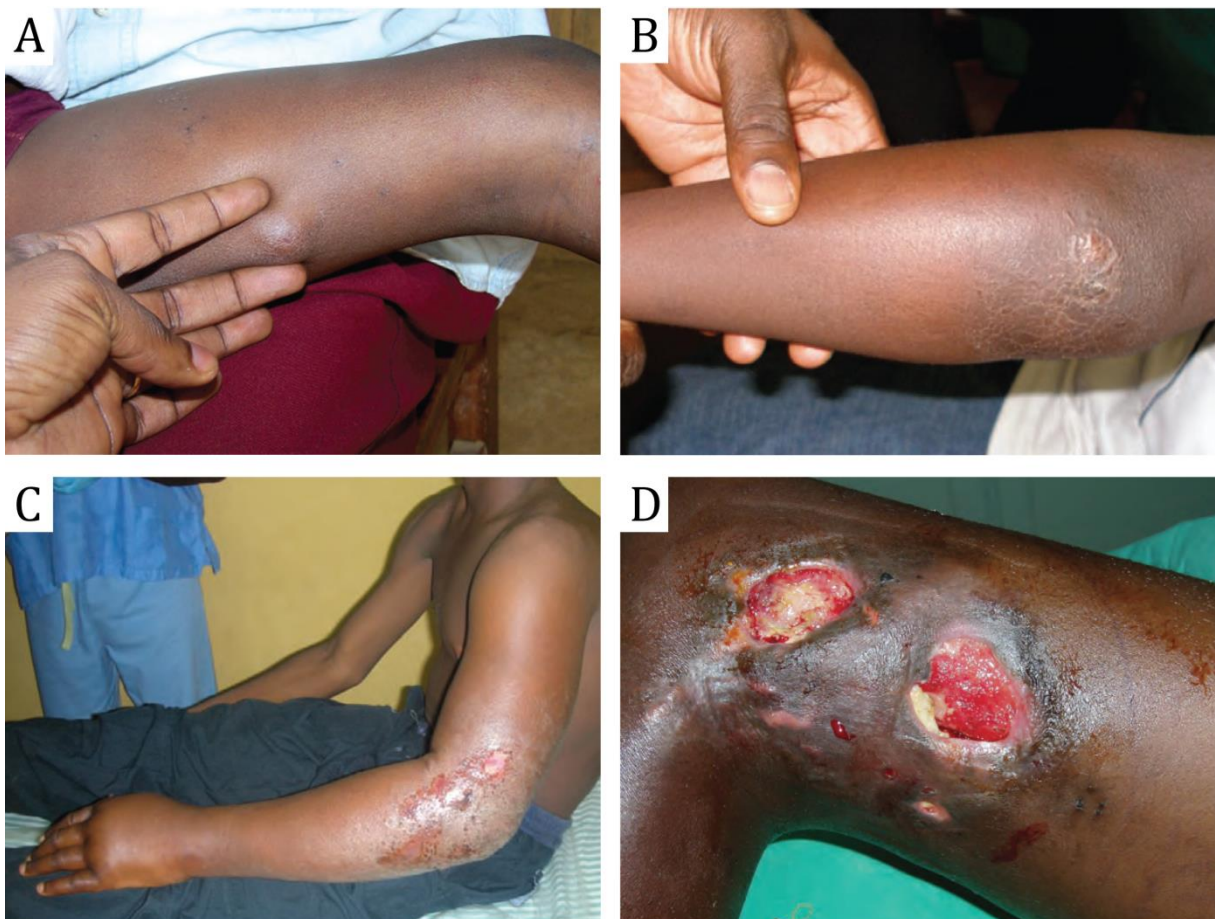


Figure 2: Illustration of the typical clinical presentations of the three non-ulcerative BU forms, the nodule (A), the plaque (B) and the oedema (C). In (D), a medium sized ulcer is shown as an example for the open forms of BU [35].

After the infection and an early intramacrophage growth phase, it is assumed that small clusters of acid-fast bacilli (AFB) are formed which produce a protective cloud of mycolactone, preventing their elimination by infiltrating immune cells. With the proliferation of the AFB and increasing mycolactone concentrations, a central necrotic area develops and infiltrating immune cells are killed by the toxin [34,38–41]. Additional histopathological hallmarks of BU are the presence of fat cell ghosts, epidermal hyperplasia and the absence of significant cellular infiltration [34,42]. However, this immunosuppressive phenotype of active BU lesions is reverted during antibiotic treatment into an inflammatory phenotype characterized by extensive infiltration of lymphocytes, macrophages and Langhans' giant cells as well as by the presence of intracellular bacteria and of bacterial debris in phagocytic cells. In addition, the formation of granulomatous and organized lymphoid structures can be observed during antibiotic treatment [11,14,40].

Cellular effects of mycolactone

The existence of a virulence factor produced by *M. ulcerans* was already postulated in the 1960's, however, it was not until 1999 that mycolactone could be isolated by the group of Pamela Small [1,43]. Mycolactone is a polyketide macrolide-lipid like molecule and the only virulence factor identified of this pathogen to date [2]. In the last few years, the availability of synthetic mycolactone, which seems to have identical biological properties as the natural A/B forms purified from bacterial cultures, has facilitated the research on this molecule [44–47].

The production of mycolactone is essential to the pathophysiology of BU as it causes the two determining characteristics of the ulcers: extensive cytotoxicity and pronounced immunosuppression [2]. The prominent role of mycolactone for BU pathogenesis is further supported by studies showing that intradermal injection of the toxin is sufficient to induce the formation of BU-like lesions in animal models and that mycolactone-deficient *M. ulcerans* mutants are not virulent [1,41].

Mycolactone consists of a 12-membered lactone core and an upper and a lower polyketide side chain (Figure 3) [1], rendering the molecule highly hydrophobic and thus it is thought that mycolactone enters mammalian cells by passive diffusion [48].

Using a fluorescent mycolactone derivative it was demonstrated that the toxin localizes to the cytosol, pointing to the presence of a cytosolic receptor for mycolactone [48]. In active BU lesions, it is assumed that mycolactone is largely retained in the extracellular matrix formed around the bacterial colonies [49].

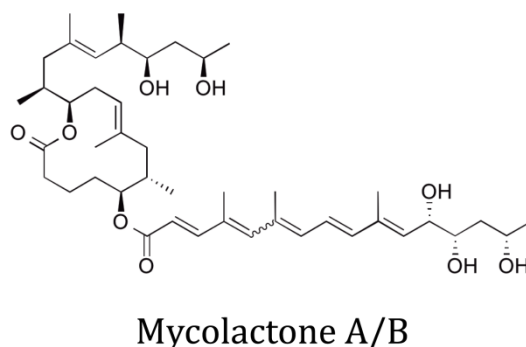


Figure 3: Chemical structure of the *M. ulcerans* virulence factor mycolactone A/B.

The production of mycolactone is dependent on the 174 kb virulence plasmid pMUM that is present in all MPM. This plasmid encodes the polyketide synthases required for the synthesis of the toxin [18]. Six different variants of mycolactones named A to F have been described so far which differ in their potency and their geographical distribution. The most virulent *M. ulcerans* strains from Africa mainly produce mycolactone A/B, the most potent form of the toxin. Mycolactone A/B is composed of a 3:2 ratio of the Z-/E-isomers of the C-4-C-5 bond in the lower side chain. Mycolactone C and D on the other hand are less potent and the predominant mycolactone species produced by the Australian and Asian strains, respectively [47,50]. In addition to these variants produced by the human pathogenic strains of *M. ulcerans*, mycolactone E and F are produced by the fish pathogen and frog pathogens which have been previously also referred to as *M. pseudoshottsii* and *M. liflandii* [51–53]. Importantly, all of these mycolactones contain the same lactone core but possess a lower side chain that varies in length, position of the double bonds and in the number and position of hydroxyl groups, resulting in different cytotoxicities [53,54]. This suggests that the lower side chain of mycolactone is largely responsible for the biological activity of the molecule, which was recently confirmed in structure-activity relationship studies using different synthetic mycolactones [47].

Although mycolactone was not yet identified in the late 1970's, it was already known at this time that sterile filtrates of *M. ulcerans* cultures contained a highly cytotoxic substance that induced the rounding up, detachment and cell death of L929 fibroblasts [55]. Today, L929 fibroblasts are still the most sensitive cell type identified and are frequently used as a reporter cells. Furthermore, it was shown for the same cell line that mycolactone induces cell cycle arrest at the G₁/G₀ phase [1]. Interestingly, different cell types show different susceptibilities to mycolactone-induced cytotoxicity and die after different times of exposure. For instance, while immature dendritic cells are rather sensitive and die within the first 48 hours of mycolactone treatment, J774 macrophages and Jurkat T-cells are more resistant and only die after prolonged incubation times [56–58]. Although mycolactone cytotoxicity is absolutely central for the pathogenesis of BU, the molecular mechanisms underlying this process still remain obscure.

In contrast to mycolactone-induced cytotoxicity, much more is known about the mycolactone-mediated immunosuppression, the second functional feature of the toxin. It is known that mycolactone modulates local and systemic immune responses [59,60], for example by blocking the activation of different immune cells including T-cells, dendritic cells, monocytes and macrophages [56,58,61,62], by interfering with T-cell homing [63], or by reducing the expression of T-cell receptors as well as co-stimulatory molecules including CD40 and CD86 [56,58]. Furthermore, mycolactone interferes with the phagocytic activity of macrophages [59,60] and the ability of monocytes, macrophages and dendritic cells to produce the cytokine tumor necrosis factor alpha (TNF α) [61,62,64,65]. Additionally, the production of various other cytokines including interleukin (IL)-6, IL-8 and IL-10 is strongly reduced in both primary human monocytes and macrophages as result of mycolactone exposure [61]. Interestingly, this almost complete loss of proteins responsible for a proper functioning of immune system might be explained by a recent study showing that mycolactone interferes with protein translocation into the endoplasmic reticulum (ER), leading to the degradation of nearly all glycosylated and secreted proteins [66].

Finally, the well-characterized cytoskeletal rearrangements observed in mycolactone-treated cells have recently been associated with uncontrolled ARP2/3-mediated actin polymerization as a result of mycolactone-induced activation of members from the Wiskott-Aldrich syndrome protein family (WASP) of actin regulators [67].

Immune responses against *M. ulcerans*

There is only limited data on the development of immune responses against *M. ulcerans* and it is not entirely clear to which extent mycolactone might interfere. In Tuberculosis (TB) endemic areas where Bacille Calmette-Guérin (BCG) vaccination is frequent, the analysis of *M. ulcerans*-specific immune responses is further complicated by the broad cross-reactivity of *M. ulcerans* antigens with antigens from *M. tuberculosis* and *M. bovis* [40]. In studies using filtrates from *M. ulcerans* cultures Immunoglobulin (Ig) G and IgM antibody responses were found in sera of BU patients. However, they could also be identified in TB patients as well as in BCG-vaccinated individuals [68,69]. In BU non-endemic areas, the highly immunogenic 18 kDa small heat shock protein of *M. ulcerans* which has also a homologue in *M. leprae* but not in *M. tuberculosis* and *M. bovis* was successfully used in seroepidemiological studies to distinguish between BU patients and healthy household contacts [70]. However, the sera from some people living in BU endemic areas who did not develop active disease also contained *M. ulcerans*-specific IgG, indicating the generation of protective humoral responses in exposed, but otherwise healthy individuals [70–72]. This is in line with findings from reports on spontaneous healing of BU patients [73,74].

On the other hand, it was reported that the control of *M. ulcerans* infection may be predominantly dependent on a T_H1 cellular immune response [2,40]. Indeed, the T_H1-specific cytokine interferon- γ (IFN γ) was found to be strongly expressed in both nodules and ulcers of human BU patients, suggesting that a T_H1 response might be induced at an early stage of infection [75]. Furthermore, spontaneous healing is often correlated with a positive delayed hypersensitivity against *M. ulcerans* antigens, indicative of cell-mediated immunity [68,76].

Diagnosis and Treatment

For the laboratory diagnosis of BU, there are currently four methods available. At rural treatment centers, microscopy can be used for direct smear examination from wound exudates stained with Ziehl-Neelsen/Methylene blue (ZN) to detect AFB. This method is easily applicable and delivers rapid results. However, it has a low sensitivity, does not show whether the bacilli are viable or not and cannot discriminate between BU and

cutaneous tuberculosis [77,78]. The other three methods require more sophisticated equipment which is often only available in bigger hospitals or in reference laboratories. Today, the gold standard for BU diagnosis is a polymerase chain reaction (PCR) targeting the genomic multi-copy insertional sequence 2404 (IS2404), since it has the highest sensitivity and specificity of all four methods [77]. However, stringent quality control measures should be implemented on a regular basis to ensure the accuracy of the obtained PCR results as issues with false-positivity or false-negativity have been raised [20,79].

In vitro cultivation of *M. ulcerans* is the only possibility allowing the discrimination between viable and non-viable organisms and can additionally be used for monitoring the treatment efficiency and the development of drug resistance. However, the slow growth of the bacteria and the low sensitivity restrict the use of this method for immediate patient care [77].

Histopathology requires highly trained personnel performing invasive sampling procedures in the form of patient biopsies. In addition to supporting the diagnosis, this technique can be used for studying treatment response and wound healing and can provide new mechanistic insights into disease pathogenesis by answering basic biological questions [20,40,41,80–82].

According to the latest recommendations by the WHO, suspected BU cases should be laboratory confirmed by at least one of the four methods introduced above. Preferably, positive results from two different tests should be obtained to minimize misdiagnosis based on false-positivity or false-negativity and it is recommended that at least 70 % of all reported cases should be laboratory confirmed by PCR [20].

Typical indications used for the differential diagnosis of BU are the presence of ulcerative lesions with undermined edges, lymphadenopathy as well as the absence of fever and pain [11].

For the laboratory confirmation of BU, different sampling methods exist depending on the nature of the lesion (open or closed) and the diagnosis method of choice. For early and closed lesions, fine-needle aspiration is commonly used whereas open, ulcerative lesions can be swabbed with a cotton swab [20,83]. Both of these sample types can be used for diagnosis by microscopy, PCR and cultivation. In order to perform histopathological analysis, punch biopsies or surgical excisions are however required [20].

Because of the difficult diagnosis of BU in rural settings, there is a strong need for new point-of-care diagnostic tests [20]. In particular, the detection of mycolactone in human lesions or *M. ulcerans*-specific antibodies would be promising approaches for the development of a new highly specific and easily applicable diagnostic test [84].

Until the implementation of antibiotic therapy in 2004 by the WHO, surgical removal of the infected tissue including a wide margin of healthy tissue was considered to be the most effective treatment of BU [35,85]. However, surgery followed by skin grafting can involve multiple operations and resulted in an average hospitalization of more than 3 months [86]. Furthermore, the relapse rates after surgery without the combination of antibiotic therapy were still in the range of 20 % [87].

It was already known from studies performed in the 1970's that rifampicin can be used to effectively treat small BU lesions [11]. However, it was not before 2004 when the WHO started to recommend antibiotic therapy to effectively treat BU. The antibiotic regimen recommended by the WHO is based on a combination of oral rifampicin (10 mg/kg) and intramuscular streptomycin (15 mg/kg) (R/S) daily during a period of 8 weeks [88]. As a direct consequence of the introduction of the antibiotic therapy, relapse rates could be reduced to around 2 % and the requirement for surgical interventions has diminished [89,90]. However, despite the effectivity of the R/S treatment there is still a strong need for intensive wound care, surgical removal of necrotic tissue, for covering of large parts of damaged skin by skin grafting as well as for correcting deformities in order to prevent disabilities [11]. Although the use of R/S combination therapy seems to be well tolerated by the majority of patients, the therapy has the disadvantage of a daily need for intramuscular injections of streptomycin [85]. Hence, research efforts are driven towards a replacement of streptomycin with clarithromycin, a less toxic drug that can be orally delivered [91–94].

Histopathological studies indicate that the production of mycolactone declines early after start of R/S treatment [95]. This leads to a rapid onset of local cellular immune responses defined by chronic leukocyte infiltration, formation of defined granulomas, efficient phagocytosis of extracellular bacilli and finally to clearance of the infection. After eight weeks of R/S treatment, most of the bacteria display a beaded appearance, reflecting their killing [40,95–97]. As a consequence of the massive activation of the immune system during the course of antibiotic therapy, a temporary worsening of the status of the lesions or the development of new lesions may occur, a phenomenon called

“paradoxical reaction”. This can be resolved by simple wound care and does not need additional treatment [40,80].

It was already noticed in the 1970`s that the application of heat might be an attractive approach to treat BU as *M. ulcerans* grows optimally at temperatures between 28 °C – 32 °C and does not grow at temperatures above 37 °C [98,99]. This so-called thermotherapy has been proven an attractive and cheap alternative to the antibiotic treatment since application of heat is nowadays easily possible by using bags filled with phase change material [100]. By performing a follow-up clinical trial these promising results of the thermotherapy were confirmed in a larger patient cohort carried out in Cameroon [101]. Finally, major efforts have been undertaken for the development of a vaccine against BU [102,103].

Apoptosis

The process of cell death is a fundamental part of life and is of great importance for the development of organisms as well as for the regulation of the immune system and for host defense against bacterial or viral infections [104]. However, excessive cell death is also responsible for several pathological conditions, including Parkinson's, Alzheimer's or Huntington's disease [105].

On account of this, it is not surprising that several forms of genetically programmed cell death mechanisms, so-called programmed cell death (PCD), exist. The most intensively studied form of PCD is apoptosis and knowledge of the mechanisms involved in this process was first gained during studies of the cell death occurring during the development of the nematode *Caenorhabditis elegans* [106,107].

During apoptosis, cells undergo several biochemical and morphological changes. A key event happening during the onset of apoptosis is the activation of a family of cysteine aspartyl proteases, so-called caspases, whose proteolytic activities are essential for this process. Caspases are further subdivided into initiator caspases that cleave the inactive pro-forms of effector caspases, thereby activating them. Effector caspases cleave other protein substrates in the cell and are responsible for the cellular degradation [108].

Additionally, when undergoing apoptosis, cells start to shrink, lose their attachment to the surrounding, their chromatin condenses and the plasma membrane starts blebbing. These blebs are the progenitors of apoptotic bodies, small cytoplasmic fragments encapsulated in cell membranes which may contain functional organelles surrounded by intact plasma membranes [109–111]. Another biochemical feature of apoptotic cells is the presentation of phosphatidylserine, a normally inward-facing phospholipid of the plasma membrane, as a cell surface marker that results in efficient phagocytosis of the dying cell by recruited macrophages, thereby minimizing the damage to the surrounding tissue [112].

Apoptosis can be triggered by two different cellular pathways, the extrinsic (death receptor) or the intrinsic (mitochondrial) apoptosis pathway [113,114].

Extrinsic apoptosis is activated by clustering and binding of transmembrane receptors such as CD95/APO-1/Fas with its corresponding trimeric ligands, in this case APO-1/FasL. This results in the recruitment of the adaptor molecule Fas-Associated protein with Death Domain (FADD) to the Fas receptor. FADD then associates with procaspase-8

via dimerization of the death effector domain (DED), resulting in the formation of a death-inducing signaling complex (DISC) and auto-catalytic cleavage of procaspase-8. Activated caspase-8 in turn activates other downstream caspases including caspase-3 and caspase-7, finally leading to the destruction of the cell [110,115].

In contrast, the intrinsic apoptosis pathway is directly activated at the mitochondria by non-receptor-mediated stimuli such as radiation, hypoxia or toxins that cause changes in the inner mitochondrial membrane resulting in an opening of the mitochondrial permeability transition (MPT) pore, loss of the mitochondrial membrane potential and release of the pro-apoptotic cytochrome c into the cytosol [116]. Cytosolic cytochrome c binds and activates Apaf-1, leading to the recruitment of procaspase-9 and the formation of an apoptosis inducing complex named apoptosome. As a consequence, procaspase-9 is activated, resulting in the recruitment and activation of the downstream caspase-3 and subsequent cleavage of a number of key substrates responsible for the execution of apoptosis [117–119].

The mitochondrial apoptosis pathway is regulated by members of the Bcl-2 family of proteins which are either pro- or anti-apoptotic. For instance, Bmf, Bak and Bax are pro-apoptotic Bcl-2 family members and Bcl-2, Bcl-x_L and Bcl-w are anti-apoptotic. These proteins are of special relevance for the intrinsic apoptosis, as they can directly control the mitochondrial membrane permeability for cytochrome c, thereby determining whether a cell is committed to apoptosis or not [120].

The Bcl-2 interacting mediator of cell death (Bim), an important member of the pro-apoptotic Bcl-2 family proteins, is alternatively spliced and as a consequence exists in a variety of different isoforms [121,122]. The most prominent splice variants of Bim are Bim-short, Bim-long and Bim-extra-long (Bim_S, Bim_L and Bim_{EL}) that are all cytotoxic [123]. Bim acts by binding in a heterodimeric complex to anti-apoptotic Bcl-2 family proteins, thereby allowing the pro-apoptotic proteins Bax and Bak to form an oligomeric pore in the outer mitochondrial membrane, the so-called mitochondrial apoptosis-inducing channel (MAC) [114,124]. Furthermore, a direct interaction of Bim with Bax and Bak has been demonstrated, suggesting that Bim can directly activate these two proteins to form a MAC [125–127]. MAC formation leads to mitochondrial cytochrome c release, the formation of the apoptosome, activation of the initiator caspase-9, subsequent activation of the effector caspases-3, -6, and -7 and finally to cellular degradation [114].

The mTOR signaling pathway and its role in apoptosis

The mammalian target of rapamycin (mTOR) is a highly conserved serine/threonine kinase belonging to the family of the phosphoinositide 3-kinase (PI3K)-related protein kinases (PIKK) [128]. mTOR is a master regulator of a number of important cellular processes including cell growth, metabolism, cytoskeletal organization and survival [129]. As such, mTOR is implicated in various disease states where cellular growth and homeostasis are deregulated, for example in cancer, metabolic disorders or ageing [128].

mTOR interacts with several proteins to form two distinct multi-protein complexes named mTOR complex 1 (mTORC1) and 2 (mTORC2) (Figure 4). mTORC1 is composed of the catalytic subunit mTOR, the regulatory-associated protein of mTOR (Raptor), mLST8/G β L, Deptor and proline-rich Akt substrate 40 [130]. This complex is regulated by various environmental signals such as growth factors, nutrients and cellular stress [128]. The PI3K/Akt pathway is an important up-stream mediator of mTORC1, since it is the central pathway integrating external growth factors through PI3K-dependent activation of Akt [131]. mTORC1 controls cellular proliferation and growth by promoting the biosynthesis of proteins, lipids and organelles and it inhibits catabolic processes such as autophagy [129]. The biosynthesis of proteins is controlled by mTORC1 through phosphorylation of the ribosomal protein S6 kinase 1 (S6K1) and of the eukaryotic translation initiation factor 4E-binding protein 1 (4E-BP1) [132]. When 4E-BP1 is phosphorylated by mTORC1, it dissociates from the eukaryotic translation initiation factor 4E, thereby allowing for the recruitment of the translation initiation factor to the 5' end of the mRNAs, resulting in the start of protein translation [133]. In addition, phosphorylation of S6K1 by mTORC1 results in the activation of multiple proteins that promote translation initiation and elongation [128]. Furthermore, active mTORC1 signaling inhibits macroautophagy, a catabolic process induced by starvation, which eventually results in the destruction of the whole cell [134].

The second complex, mTORC2, is composed of mTOR, the rapamycin-insensitive companion of mTOR (Rictor), mLST8/G β L, Protor, Deptor, and mammalian stress-activated protein kinase interacting protein (mSIN1) [129]. In contrast to mTORC1, little is known about the up-stream regulation of mTORC2. Generally, it is thought that growth factors stimulate mTORC2, either directly or indirectly [128]. Originally,

mTORC2 was identified in *Saccharomyces cerevisiae* as a regulator of actin cytoskeleton organization, which was later also confirmed in mammalian cells [135–137]. In these studies it has been observed that knocking down mTORC2 components results in perturbed actin polymerization and cell morphology. The underlying molecular mechanisms are not yet fully understood, however, it is thought that mTORC2 regulates these mechanisms by phosphorylation of the protein kinase C α (PKC α), phosphorylation and relocalization of the focal adhesion-associated adaptor protein paxillin, and by the loading of the two Rho-GTPases RhoA and Rac1 with GTP [135,137].

Beside the regulation of the cytoskeletal organization, mTORC2 has been implicated in the control of cell survival, cell proliferation and metabolism [128,129]. These processes are all highly dependent on the activation state of Akt, which positively regulates them through phosphorylation of a set of diverse proteins [138]. The activity of Akt is determined by the phosphorylation status at two specific sites: Ser308, which is targeted by phosphoinositide-dependent kinase 1 (PDK1) and Ser473, a site that has been demonstrated to be specifically phosphorylated by mTORC2 and required for full activation of this kinase [139–141]. Subsequently, several reports reconfirmed that mTORC2 specifically phosphorylates Akt at Ser473 by showing that ablation of mTORC2 components blocks Akt phosphorylation at this site, resulting in impairment of the phosphorylation of some, but not all, Akt targets [142,143]. For instance, the transcription factors forkhead box O1 and 3 (FoxO1, FoxO3) are dephosphorylated upon depletion of mTORC2 [144]. These transcription factors are normally excluded from the nucleus upon phosphorylation by Akt, followed by ubiquitination and proteolytic degradation. In mTORC2 depleted cells, FoxO transcription factors are devoid of phosphorylation and as a result retained in the nucleus where they can promote apoptosis by inducing the expression of pro-apoptotic Bcl-2 family proteins such as Bim or by activating cell-extrinsic apoptosis pathways including Fas receptor signaling [145].

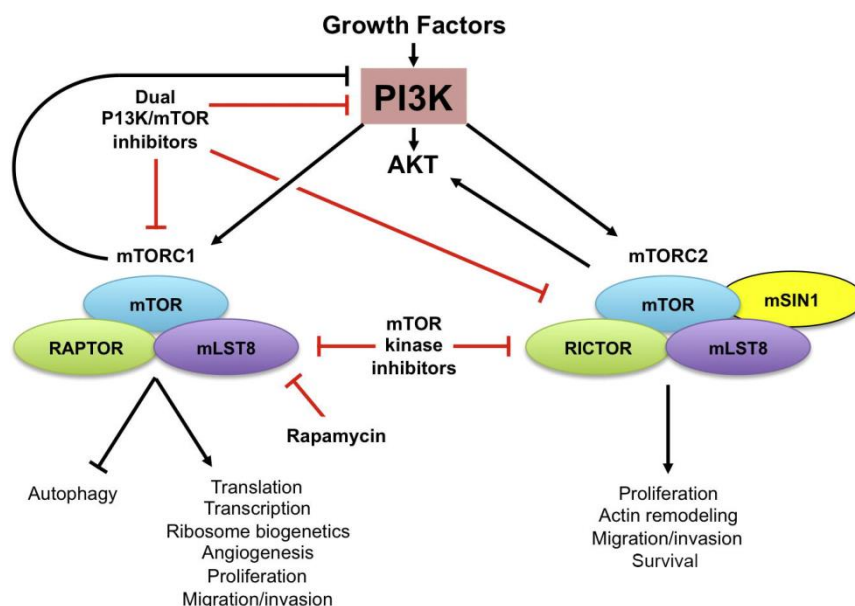


Figure 4: Overview of the mTOR signaling pathway. mTOR exists in two different multi-protein complexes named mTORC1 and mTORC2 that are both activated in response to growth factor stimulation. mTOR is essential for the regulation of multiple cellular functions, including proliferation, actin remodeling and survival. Adapted from [146].

Rapamycin and its derivatives

The natural mTOR inhibitor rapamycin (Sirolimus), a macrolide produced by the bacterium *Streptomyces hydropiscus*, was originally used as an antifungal and immunosuppressive agent. The discovery of mTOR as the target of rapamycin and the compound's inherent anti-proliferative characteristics have led to the discovery of rapamycin as a potential anti-cancer agent [147]. Upon entering the cells, rapamycin forms a complex with the intracellular 12-kDa FK506-binding protein (FKBP12) and this complex interacts with the FKBP12-rapamycin binding domain (FRB) of mTOR, thus inhibiting the kinase activity of mTORC1. In contrast, FKBP12/rapamycin cannot physically interact with mTORC2 and as a consequence does not inhibit its functions [129,135,137]. However, prolonged exposure to rapamycin has been shown to inhibit mTORC2 in some cell types by blocking the assembly of the complex, leading to inhibition of Akt signaling [148,149]. This indirect inhibition of mTORC2 can be

explained by a progressive sequestration of mTOR in a complex with FKBP12/rapamycin, reducing its availability for the formation of mTORC2 [128].

The poor water solubility and limitations in the bioavailability of rapamycin have driven efforts to improve these characteristics and have resulted in the generation of the first rapamycin analogs (rapalogs), including everolimus (RAD001, Novartis, Basel) and temsirolimus (CCI-779, Wyeth, NJ) (Figure 5) [150,151]. Despite the introduction of chemical modifications during the generation of rapalogs, these compounds preserve their binding to FKBP12 and subsequent interaction with mTOR, thus maintaining a conserved mode of action [149].

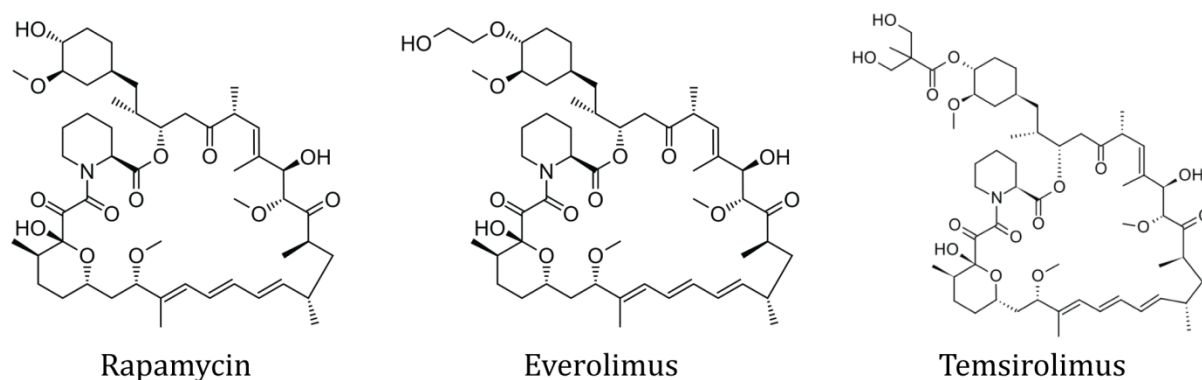


Figure 5: Chemical structure of Rapamycin (left) and of its derivatives Everolimus (middle) and Temsirolimus (right).

ATP-competitive mTOR kinase inhibitors

Limitations in the success of rapamycin-based therapies in the clinics have led to the development of a second generation of mTOR inhibitors that are known as ATP-competitive mTOR kinase inhibitors (TKIs). As the name already says, this class of mTOR inhibitors directly targets the kinase domain of mTOR, thereby inhibiting its catalytic activity. The mechanistic advantage of this class of inhibitors is the blockage of the kinase activity of both mTOR complexes, resulting in the inhibition of mTORC1 and mTORC2 [128,152]. In the last few years, numerous TKIs have been developed, including PP242, WAY-600 and AZD-8055 (Figure 6) [153]. The therapeutic benefit of TKIs over rapalogs for the treatment of cancer originates from their ability to block

mTORC2-dependent phosphorylation of Akt [154]. However, the major disadvantage of TKIs restricting their use in the clinics is their potential toxicity as it has been anticipated that global inhibition of mTOR results in higher levels of toxicity in non-diseased tissue [149]. For instance, the dual mTOR inhibitor PP242 has recently been shown to promote mTORC2-specific apoptosis in arteries in a rat model of pulmonary arterial hypertension due to increased levels of the pro-apoptotic protein Bim [155]. Nevertheless, TKIs have a great potential for the treatment of many different cancers and some of them are already successfully used in the clinics as illustrated by the example of Imatinib (Gleevec), a TKI administered for the treatment of chronic myeloid leukemia [156].

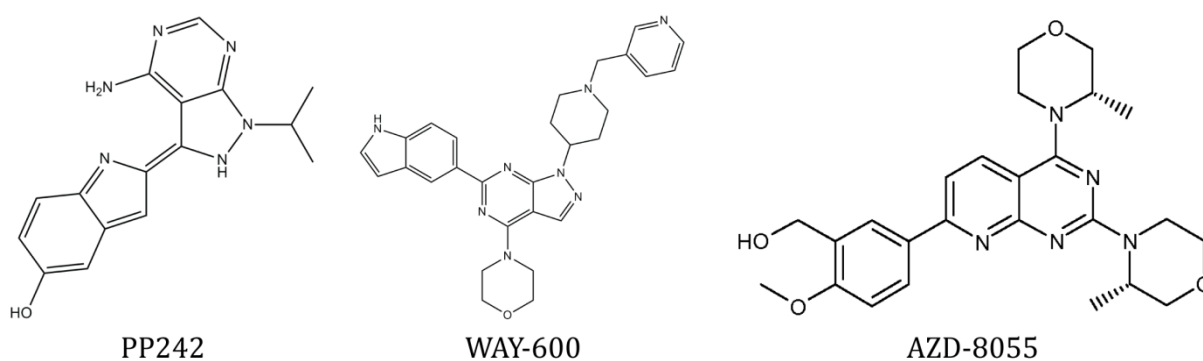


Figure 6: Chemical structures of the TKIs PP242 (left), WAY-600 (middle) and AZD-8055 (right).

References

1. George KM, Chatterjee D, Gunawardana G, Welty D, Hayman J, Lee R, et al. Mycolactone: a polyketide toxin from *Mycobacterium ulcerans* required for virulence. *Science*. 1999;283: 854–857.
2. Demangel C, Stinear TP, Cole ST. Buruli ulcer: reductive evolution enhances pathogenicity of *Mycobacterium ulcerans*. *Nat Rev Microbiol*. 2009;7: 50–60. doi:10.1038/nrmicro2077
3. WHO | The history of GBUI. Available: <http://www.who.int/buruli/gbui/en/>. Accessed 9 November 2015.
4. Maccallum P, Tolhurst JC, Buckle G, Sissons HA. A new mycobacterial infection in man. *J Pathol Bacteriol*. 1948;60: 93–122. doi:10.1002/path.1700600111
5. Epidemiology of *Mycobacterium ulcerans* infection (Buruli ulcer) at Kinyara, Uganda. *Trans R Soc Trop Med Hyg*. 1971;65: 763–775.
6. Ravisse P. [Skin ulcer caused by *Mycobacterium ulcerans* in Cameroon. I. Clinical, epidemiological and histological study]. *Bull Société Pathol Exot Ses Fil*. 1977;70: 109–124.
7. Oluwasanmi JO, Solanke TF, Olurin EO, Itayemi SO, Alabi GO, Lucas AO. *Mycobacterium ulcerans* (Buruli) skin ulceration in Nigeria. *Am J Trop Med Hyg*. 1976;25: 122–128.
8. Smith JH. Epidemiologic observations on cases of Buruli ulcer seen in a hospital in the Lower Congo. *Am J Trop Med Hyg*. 1970;19: 657–663.
9. Merritt RW, Walker ED, Small PLC, Wallace JR, Johnson PDR, Benbow ME, et al. Ecology and Transmission of Buruli Ulcer Disease: A Systematic Review. *PLoS Negl Trop Dis*. 2010;4: e911. doi:10.1371/journal.pntd.0000911
10. Johnson PDR, Stinear T, Small PLC, Pluschke G, Merritt RW, Portaels F, et al. Buruli Ulcer (*M. ulcerans* Infection): New Insights, New Hope for Disease Control. *PLoS Med*. 2005;2: e108. doi:10.1371/journal.pmed.0020108
11. Walsh DS, Portaels F, Meyers WM. Buruli ulcer: Advances in understanding *Mycobacterium ulcerans* infection. *Dermatol Clin*. 2011;29: 1–8. doi:10.1016/j.det.2010.09.006
12. Debacker M, Aguiar J, Steunou C, Zinsou C, Meyers WM, Guédénon A, et al. *Mycobacterium ulcerans* Disease (Buruli Ulcer) in Rural Hospital, Southern Benin, 1997–2001. *Emerg Infect Dis*. 2004;10: 1391–1398. doi:10.3201/eid1008.030886
13. WHO | World Health Organization. Available: http://apps.who.int/neglected_diseases/ntddata/buruli/buruli.html. Accessed 9 November 2015.
14. Portaels F, Silva MT, Meyers WM. Buruli ulcer. *Clin Dermatol*. 2009;27: 291–305. doi:10.1016/j.clindermatol.2008.09.021
15. Stinear TP, Jenkin GA, Johnson PD, Davies JK. Comparative genetic analysis of *Mycobacterium ulcerans* and *Mycobacterium marinum* reveals evidence of recent divergence. *J Bacteriol*. 2000;182: 6322–6330.
16. Tobin DM, Ramakrishnan L. Comparative pathogenesis of *Mycobacterium marinum* and *Mycobacterium tuberculosis*. *Cell Microbiol*. 2008;10: 1027–1039. doi:10.1111/j.1462-5822.2008.01133.x
17. Yip MJ, Porter JL, Fyfe JAM, Lavender CJ, Portaels F, Rhodes M, et al. Evolution of *Mycobacterium ulcerans* and other mycolactone-producing mycobacteria from a common *Mycobacterium marinum* progenitor. *J Bacteriol*. 2007;189: 2021–2029. doi:10.1128/JB.01442-06
18. Stinear TP, Mve-Obiang A, Small PLC, Frigui W, Pryor MJ, Brosch R, et al. Giant plasmid-encoded polyketide synthases produce the macrolide toxin of *Mycobacterium ulcerans*. *Proc Natl Acad Sci U S A*. 2004;101: 1345–1349. doi:10.1073/pnas.0305877101
19. Stinear TP, Pryor MJ, Porter JL, Cole ST. Functional analysis and annotation of the virulence plasmid pMUM001 from *Mycobacterium ulcerans*. *Microbiol Read Engl*. 2005;151: 683–692. doi:10.1099/mic.0.27674-0
20. WHO | Laboratory diagnosis of buruli ulcer. Available: http://www.who.int/buruli/laboratory_diagnosis/en/. Accessed 9 November 2015.

21. Stinear TP, Seemann T, Pidot S, Frigui W, Reysset G, Garnier T, et al. Reductive evolution and niche adaptation inferred from the genome of *Mycobacterium ulcerans*, the causative agent of Buruli ulcer. *Genome Res.* 2007;17: 192–200. doi:10.1101/gr.5942807
22. Rondini S, Käser M, Stinear T, Tessier M, Mangold C, Dernick G, et al. Ongoing genome reduction in *Mycobacterium ulcerans*. *Emerg Infect Dis.* 2007;13: 1008–1015. doi:10.3201/eid1307.060205
23. Doig KD, Holt KE, Fyfe JAM, Lavender CJ, Eddyani M, Portaels F, et al. On the origin of *Mycobacterium ulcerans*, the causative agent of Buruli ulcer. *BMC Genomics.* 2012;13: 258. doi:10.1186/1471-2164-13-258
24. Käser M, Rondini S, Naegeli M, Stinear T, Portaels F, Certa U, et al. Evolution of two distinct phylogenetic lineages of the emerging human pathogen *Mycobacterium ulcerans*. *BMC Evol Biol.* 2007;7: 177. doi:10.1186/1471-2148-7-177
25. Pidot SJ, Asiedu K, Käser M, Fyfe JAM, Stinear TP. *Mycobacterium ulcerans* and Other Mycolactone-Producing Mycobacteria Should Be Considered a Single Species. *PLoS Negl Trop Dis.* 2010;4: e663. doi:10.1371/journal.pntd.0000663
26. Williamson HR, Benbow ME, Campbell LP, Johnson CR, Sopoh G, Barogui Y, et al. Detection of *Mycobacterium ulcerans* in the environment predicts prevalence of Buruli ulcer in Benin. *PLoS Negl Trop Dis.* 2012;6: e1506. doi:10.1371/journal.pntd.0001506
27. Bratschi MW, Ruf M-T, Andreoli A, Minyem JC, Kerber S, Wantong FG, et al. *Mycobacterium ulcerans* persistence at a village water source of Buruli ulcer patients. *PLoS Negl Trop Dis.* 2014;8: e2756. doi:10.1371/journal.pntd.0002756
28. Marion E, Eyangoh S, Yeramian E, Doannio J, Landier J, Aubry J, et al. Seasonal and Regional Dynamics of *M. ulcerans* Transmission in Environmental Context: Deciphering the Role of Water Bugs as Hosts and Vectors. *PLoS Negl Trop Dis.* 2010;4. doi:10.1371/journal.pntd.0000731
29. Doannio JMC, Konan KL, Dosso FN, Koné AB, Konan YL, Sankaré Y, et al. [*Micronecta* sp (Corixidae) and *Diplonychus* sp (Belostomatidae), two aquatic Hemiptera hosts and/or potential vectors of *Mycobacterium ulcerans* (pathogenic agent of Buruli ulcer) in Cote d'Ivoire]. *Médecine Trop Rev Corps Santé Colon.* 2011;71: 53–57.
30. Fyfe JAM, Lavender CJ, Handasyde KA, Legione AR, O'Brien CR, Stinear TP, et al. A major role for mammals in the ecology of *Mycobacterium ulcerans*. *PLoS Negl Trop Dis.* 2010;4: e791. doi:10.1371/journal.pntd.0000791
31. Johnson PDR, Azuolas J, Lavender CJ, Wishart E, Stinear TP, Hayman JA, et al. *Mycobacterium ulcerans* in mosquitoes captured during outbreak of Buruli ulcer, southeastern Australia. *Emerg Infect Dis.* 2007;13: 1653–1660. doi:10.3201/eid1311.061369
32. O'Brien CR, Handasyde KA, Hibble J, Lavender CJ, Legione AR, McCowan C, et al. Clinical, microbiological and pathological findings of *Mycobacterium ulcerans* infection in three Australian Possum species. *PLoS Negl Trop Dis.* 2014;8: e2666. doi:10.1371/journal.pntd.0002666
33. Durnez L, Suykerbuyk P, Nicolas V, Barrière P, Verheyen E, Johnson CR, et al. Terrestrial small mammals as reservoirs of *Mycobacterium ulcerans* in benin. *Appl Environ Microbiol.* 2010;76: 4574–4577. doi:10.1128/AEM.00199-10
34. Junghanss T, Johnson RC, Pluschke G. 42 - *Mycobacterium ulcerans* Disease. In: White JFJHJKLJ, editor. *Manson's Tropical Infectious Diseases (Twenty-Third Edition)*. London: W.B. Saunders; 2014. pp. 519–531.e2. Available: <http://www.sciencedirect.com/science/article/pii/B9780702051012000431>
35. WHO | Treatment of *Mycobacterium ulcerans* disease (Buruli Ulcer). Available: <http://www.who.int/buruli/treatment/en/>. Accessed 9 November 2015.
36. Goto M, Nakanaga K, Aung T, Hamada T, Yamada N, Nomoto M, et al. Nerve Damage in *Mycobacterium ulcerans*-Infected Mice: Probable Cause of Painlessness in Buruli Ulcer. *Am J Pathol.* 2006;168: 805–811. doi:10.2353/ajpath.2006.050375
37. Marion E, Song O-R, Christophe T, Babonneau J, Fenistein D, Eyer J, et al. Mycobacterial Toxin Induces Analgesia in Buruli Ulcer by Targeting the Angiotensin Pathways. *Cell.* 2014;157: 1565–1576. doi:10.1016/j.cell.2014.04.040

38. Torrado E, Fraga AG, Castro AG, Stragier P, Meyers WM, Portaels F, et al. Evidence for an intramacrophage growth phase of *Mycobacterium ulcerans*. *Infect Immun*. 2007;75: 977–987. doi:10.1128/IAI.00889-06
39. Silva MT, Portaels F, Pedrosa J. Pathogenetic mechanisms of the intracellular parasite *Mycobacterium ulcerans* leading to Buruli ulcer. *Lancet Infect Dis*. 2009;9: 699–710. doi:10.1016/S1473-3099(09)70234-8
40. Schütte D, Pluschke G. Immunosuppression and treatment-associated inflammatory response in patients with *Mycobacterium ulcerans* infection (Buruli ulcer). *Expert Opin Biol Ther*. 2009;9: 187–200. doi:10.1517/14712590802631854
41. Bolz M, Ruggli N, Ruf M-T, Ricklin ME, Zimmer G, Pluschke G. Experimental infection of the pig with *Mycobacterium ulcerans*: a novel model for studying the pathogenesis of Buruli ulcer disease. *PLoS Negl Trop Dis*. 2014;8: e2968. doi:10.1371/journal.pntd.0002968
42. Guarner J, Bartlett J, Whitney EAS, Raghunathan PL, Stienstra Y, Asamoia K, et al. Histopathologic features of *Mycobacterium ulcerans* infection. *Emerg Infect Dis*. 2003;9: 651–656.
43. Connor DH, Lunn HF. *Mycobacterium ulcerans* infection (with comments on pathogenesis). *Int J Lepr*. 1965;33: Suppl:698–709.
44. Song F, Fidanze S, Benowitz AB, Kishi Y. Total synthesis of the mycolactones. *Org Lett*. 2002;4: 647–650.
45. Song F, Fidanze S, Benowitz AB, Kishi Y. Total Synthesis of Mycolactones A and B. *Tetrahedron*. 2007;63: 5739–5753. doi:10.1016/j.tet.2007.02.057
46. Gersbach P, Jantsch A, Feyen F, Scherr N, Dangy J-P, Pluschke G, et al. A ring-closing metathesis (RCM)-based approach to mycolactones A/B. *Chem Weinh Bergstr Ger*. 2011;17: 13017–13031. doi:10.1002/chem.201101799
47. Scherr N, Gersbach P, Dangy J-P, Bomio C, Li J, Altmann K-H, et al. Structure-Activity Relationship Studies on the Macrolide Exotoxin Mycolactone of *Mycobacterium ulcerans*. *PLoS Negl Trop Dis*. 2013;7: e2143. doi:10.1371/journal.pntd.0002143
48. Snyder DS, Small PLC. Uptake and cellular actions of mycolactone, a virulence determinant for *Mycobacterium ulcerans*. *Microb Pathog*. 2003;34: 91–101.
49. Marsollier L, Brodin P, Jackson M, Korduláková J, Tafelmeyer P, Carbonnelle E, et al. Impact of *Mycobacterium ulcerans* biofilm on transmissibility to ecological niches and Buruli ulcer pathogenesis. *PLoS Pathog*. 2007;3: e62. doi:10.1371/journal.ppat.0030062
50. Mve-Obiang A, Lee RE, Portaels F, Small PLC. Heterogeneity of mycolactones produced by clinical isolates of *Mycobacterium ulcerans*: implications for virulence. *Infect Immun*. 2003;71: 774–783.
51. Ranger BS, Mahrous EA, Mosi L, Adusumilli S, Lee RE, Colorni A, et al. Globally distributed mycobacterial fish pathogens produce a novel plasmid-encoded toxic macrolide, mycolactone F. *Infect Immun*. 2006;74: 6037–6045. doi:10.1128/IAI.00970-06
52. Hong H, Stinear T, Skelton P, Spencer JB, Leadlay PF. Structure elucidation of a novel family of mycolactone toxins from the frog pathogen *Mycobacterium* sp. MU128FXT by mass spectrometry. *Chem Commun Camb Engl*. 2005; 4306–4308. doi:10.1039/b506835e
53. Hong H, Demangel C, Pidot SJ, Leadlay PF, Stinear T. Mycolactones: immunosuppressive and cytotoxic polyketides produced by aquatic mycobacteria. *Nat Prod Rep*. 2008;25: 447–454. doi:10.1039/b803101k
54. Kishi Y. Chemistry of mycolactones, the causative toxins of Buruli ulcer. *Proc Natl Acad Sci U S A*. 2011;108: 6703–6708. doi:10.1073/pnas.1015252108
55. Hockmeyer WT, Krieg RE, Reich M, Johnson RD. Further characterization of *Mycobacterium ulcerans* toxin. *Infect Immun*. 1978;21: 124–128.
56. Coutanceau E, Decalf J, Martino A, Babon A, Winter N, Cole ST, et al. Selective suppression of dendritic cell functions by *Mycobacterium ulcerans* toxin mycolactone. *J Exp Med*. 2007;204: 1395–1403. doi:10.1084/jem.20070234
57. George KM, Pascopella L, Welty DM, Small PL. A *Mycobacterium ulcerans* toxin, mycolactone, causes apoptosis in guinea pig ulcers and tissue culture cells. *Infect Immun*. 2000;68: 877–883.

58. Boulkroun S, Guenin-Macé L, Thoulouze M-I, Monot M, Merckx A, Langsley G, et al. Mycolactone suppresses T cell responsiveness by altering both early signaling and posttranslational events. *J Immunol Baltim Md* 1950. 2010;184: 1436–1444. doi:10.4049/jimmunol.0902854
59. Adusumilli S, Mve-Obiang A, Sparer T, Meyers W, Hayman J, Small PLC. Mycobacterium ulcerans toxic macrolide, mycolactone modulates the host immune response and cellular location of *M. ulcerans* in vitro and in vivo. *Cell Microbiol*. 2005;7: 1295–1304. doi:10.1111/j.1462-5822.2005.00557.x
60. Coutanceau E, Marsollier L, Brosch R, Perret E, Goossens P, Tanguy M, et al. Modulation of the host immune response by a transient intracellular stage of Mycobacterium ulcerans: the contribution of endogenous mycolactone toxin. *Cell Microbiol*. 2005;7: 1187–1196. doi:10.1111/j.1462-5822.2005.00546.x
61. Simmonds RE, Lali FV, Smallie T, Small PLC, Foxwell BM. Mycolactone inhibits monocyte cytokine production by a posttranscriptional mechanism. *J Immunol Baltim Md* 1950. 2009;182: 2194–2202. doi:10.4049/jimmunol.0802294
62. Pahlevan AA, Wright DJ, Andrews C, George KM, Small PL, Foxwell BM. The inhibitory action of Mycobacterium ulcerans soluble factor on monocyte/T cell cytokine production and NF-kappa B function. *J Immunol Baltim Md* 1950. 1999;163: 3928–3935.
63. Guenin-Macé L, Carrette F, Asperti-Boursin F, Bon AL, Caleechurn L, Bartolo VD, et al. Mycolactone impairs T cell homing by suppressing microRNA control of L-selectin expression. *Proc Natl Acad Sci*. 2011;108: 12833–12838. doi:10.1073/pnas.1016496108
64. Torrado E, Adusumilli S, Fraga AG, Small PLC, Castro AG, Pedrosa J. Mycolactone-mediated inhibition of tumor necrosis factor production by macrophages infected with Mycobacterium ulcerans has implications for the control of infection. *Infect Immun*. 2007;75: 3979–3988. doi:10.1128/IAI.00290-07
65. Phillips R, Sarfo FS, Guenin-Macé L, Decalf J, Wansbrough-Jones M, Albert ML, et al. Immunosuppressive Signature of Cutaneous Mycobacterium ulcerans Infection in the Peripheral Blood of Patients with Buruli Ulcer Disease. *J Infect Dis*. 2009;200: 1675–1684. doi:10.1086/646615
66. Hall BS, Hill K, McKenna M, Ogbechi J, High S, Willis AE, et al. The Pathogenic Mechanism of the Mycobacterium ulcerans Virulence Factor, Mycolactone, Depends on Blockade of Protein Translocation into the ER. *PLoS Pathog*. 2014;10: e1004061. doi:10.1371/journal.ppat.1004061
67. Guenin-Macé L, Veyron-Churlet R, Thoulouze M-I, Romet-Lemonne G, Hong H, Leadlay PF, et al. Mycolactone activation of Wiskott-Aldrich syndrome proteins underpins Buruli ulcer formation. *J Clin Invest*. 2013;123: 1501–1512. doi:10.1172/JCI66576
68. Dobos KM, Spotts EA, Marston BJ, Horsburgh CR, King CH. Serologic response to culture filtrate antigens of Mycobacterium ulcerans during Buruli ulcer disease. *Emerg Infect Dis*. 2000;6: 158–164. doi:10.3201/eid0602.000208
69. Okenu DMN, Ofielu LO, Easley KA, Guarner J, Spotts Whitney EA, Raghunathan PL, et al. Immunoglobulin M antibody responses to Mycobacterium ulcerans allow discrimination between cases of active Buruli ulcer disease and matched family controls in areas where the disease is endemic. *Clin Diagn Lab Immunol*. 2004;11: 387–391.
70. Diaz D, Döbeli H, Yeboah-Manu D, Mensah-Quainoo E, Friedlein A, Soder N, et al. Use of the immunodominant 18-kiloDalton small heat shock protein as a serological marker for exposure to Mycobacterium ulcerans. *Clin Vaccine Immunol* CVI. 2006;13: 1314–1321. doi:10.1128/CVI.00254-06
71. Yeboah-Manu D, Röltgen K, Opare W, Asan-Ampah K, Quenin-Fosu K, Asante-Poku A, et al. Sero-epidemiology as a tool to screen populations for exposure to Mycobacterium ulcerans. *PLoS Negl Trop Dis*. 2012;6: e1460. doi:10.1371/journal.pntd.0001460
72. Röltgen K, Bratschi MW, Ross A, Aboagye SY, Ampah KA, Bolz M, et al. Late onset of the serological response against the 18 kDa small heat shock protein of Mycobacterium ulcerans in children. *PLoS Negl Trop Dis*. 2014;8: e2904. doi:10.1371/journal.pntd.0002904
73. Revill WD, Morrow RH, Pike MC, Ateng J. A controlled trial of the treatment of Mycobacterium ulcerans infection with clofazimine. *Lancet*. 1973;2: 873–877.

74. Gordon CL, Buntine JA, Hayman JA, Lavender CJ, Fyfe JA, Hosking P, et al. Spontaneous clearance of *Mycobacterium ulcerans* in a case of Buruli ulcer. *PLoS Negl Trop Dis*. 2011;5: e1290. doi:10.1371/journal.pntd.0001290
75. Phillips R, Horsfield C, Mangan J, Laing K, Etuaful S, Awuah P, et al. Cytokine mRNA expression in *Mycobacterium ulcerans*-infected human skin and correlation with local inflammatory response. *Infect Immun*. 2006;74: 2917–2924. doi:10.1128/IAI.74.5.2917-2924.2006
76. Stanford JL, Revill WD, Gunthorpe WJ, Grange JM. The production and preliminary investigation of Burulin, a new skin test reagent for *Mycobacterium ulcerans* infection. *J Hyg (Lond)*. 1975;74: 7–16.
77. Portaels F, WHO. Laboratory diagnosis of buruli ulcer: a manual for health care providers. Available: <http://apps.who.int/iris/handle/10665/111738>. Accessed 9 November 2015
78. Beissner M, Herbinger K-H, Bretzel G. Laboratory diagnosis of Buruli ulcer disease. *Future Microbiol*. 2010;5: 363–370. doi:10.2217/fmb.10.3
79. Eddyani M, Lavender C, de Rijk WB, Bomans P, Fyfe J, de Jong B, et al. Multicenter External Quality Assessment Program for PCR Detection of *Mycobacterium ulcerans* in Clinical and Environmental Specimens. *PLoS ONE*. 2014;9: e89407. doi:10.1371/journal.pone.0089407
80. Ruf M-T, Chauty A, Adeye A, Ardant M-F, Kousse mou H, Johnson RC, et al. Secondary Buruli Ulcer Skin Lesions Emerging Several Months after Completion of Chemotherapy: Paradoxical Reaction or Evidence for Immune Protection? *PLoS Negl Trop Dis*. 2011;5: e1252. doi:10.1371/journal.pntd.0001252
81. Andreoli A, Ruf M-T, Sopoh GE, Schmid P, Pluschke G. Immunohistochemical monitoring of wound healing in antibiotic treated Buruli ulcer patients. *PLoS Negl Trop Dis*. 2014;8: e2809. doi:10.1371/journal.pntd.0002809
82. Ogbechi J, Ruf M-T, Hall BS, Bodman-Smith K, Vogel M, Wu H-L, et al. Mycolactone-Dependent Depletion of Endothelial Cell Thrombomodulin Is Strongly Associated with Fibrin Deposition in Buruli Ulcer Lesions. *PLoS Pathog*. 2015;11: e1005011. doi:10.1371/journal.ppat.1005011
83. Yeboah-Manu D, Danso E, Ampah K, Asante-Poku A, Nakobu Z, Pluschke G. Isolation of *Mycobacterium ulcerans* from swab and fine-needle-aspiration specimens. *J Clin Microbiol*. 2011;49: 1997–1999. doi:10.1128/JCM.02279-10
84. Sarfo FS, Phillips RO, Rangers B, Mahrous EA, Lee RE, Tarelli E, et al. Detection of Mycolactone A/B in *Mycobacterium ulcerans*-Infected Human Tissue. *PLoS Negl Trop Dis*. 2010;4: e577. doi:10.1371/journal.pntd.0000577
85. Converse PJ, Nuermberger EL, Almeida DV, Grosset JH. Treating *Mycobacterium ulcerans* disease (Buruli ulcer): from surgery to antibiotics, is the pill mightier than the knife? *Future Microbiol*. 2011;6: 1185–1198. doi:10.2217/fmb.11.101
86. Asiedu K, Etuaful S. Socioeconomic implications of Buruli ulcer in Ghana: a three-year review. *Am J Trop Med Hyg*. 1998;59: 1015–1022.
87. K Kibadi JBM-Y. [Relapse after surgical treatment of mycobacterium ulcerans infection (buruli ulcer): study of risk factors in 84 patients in the Democratic Republic of the Congo]. *Médecine Trop Rev Corps Santé Colon*. 2009;69: 471–4.
88. WHO | Provisional guidance on the role of specific antibiotics in the management of *Mycobacterium ulcerans* disease (Buruli ulcer). Available: <http://www.who.int/buruli/information/antibiotics/en/index1.html>. Accessed 9 November 2015.
89. Chauty A, Ardant M-F, Adeye A, Euverte H, Guédénon A, Johnson C, et al. Promising Clinical Efficacy of Streptomycin-Rifampin Combination for Treatment of Buruli Ulcer (*Mycobacterium ulcerans* Disease). *Antimicrob Agents Chemother*. 2007;51: 4029–4035. doi:10.1128/AAC.00175-07
90. Sarfo FS, Phillips R, Asiedu K, Ampadu E, Bobi N, Adentwe E, et al. Clinical efficacy of combination of rifampin and streptomycin for treatment of *Mycobacterium ulcerans* disease. *Antimicrob Agents Chemother*. 2010;54: 3678–3685. doi:10.1128/AAC.00299-10
91. Gordon CL, Buntine JA, Hayman JA, Lavender CJ, Fyfe JAM, Hosking P, et al. All-Oral Antibiotic Treatment for Buruli Ulcer: A Report of Four Patients. *PLoS Negl Trop Dis*. 2010;4: e770. doi:10.1371/journal.pntd.0000770

92. Chauty A, Ardant M-F, Marsollier L, Pluschke G, Landier J, Adeye A, et al. Oral treatment for *Mycobacterium ulcerans* infection: results from a pilot study in Benin. *Clin Infect Dis Off Publ Infect Dis Soc Am*. 2011;52: 94–96. doi:10.1093/cid/ciq072
93. Almeida D, Converse PJ, Ahmad Z, Dooley KE, Nuermberger EL, Grosset JH. Activities of Rifampin, Rifapentine and Clarithromycin Alone and in Combination against *Mycobacterium ulcerans* Disease in Mice. *PLoS Negl Trop Dis*. 2011;5. doi:10.1371/journal.pntd.0000933
94. Friedman ND, Athan E, Hughes AJ, Khajehnoori M, McDonald A, Callan P, et al. *Mycobacterium ulcerans* Disease: Experience with Primary Oral Medical Therapy in an Australian Cohort. *PLoS Negl Trop Dis*. 2013;7: e2315. doi:10.1371/journal.pntd.0002315
95. Schütte D, UmBoock A, Pluschke G. Phagocytosis of *Mycobacterium ulcerans* in the course of rifampicin and streptomycin chemotherapy in Buruli ulcer lesions. *Br J Dermatol*. 2009;160: 273–283. doi:10.1111/j.1365-2133.2008.08879.x
96. Schütte D, Um-Boock A, Mensah-Quainoo E, Itin P, Schmid P, Pluschke G. Development of Highly Organized Lymphoid Structures in Buruli Ulcer Lesions after Treatment with Rifampicin and Streptomycin. *PLoS Negl Trop Dis*. 2007;1: e2. doi:10.1371/journal.pntd.0000002
97. Ruf M-T, Sopoh GE, Brun LV, Dossou AD, Barogui YT, Johnson RC, et al. Histopathological Changes and Clinical Responses of Buruli Ulcer Plaque Lesions during Chemotherapy: A Role for Surgical Removal of Necrotic Tissue? *PLoS Negl Trop Dis*. 2011;5: e1334. doi:10.1371/journal.pntd.0001334
98. Meyers WM, Shelly WM, Connor DH. Heat treatment of *Mycobacterium ulcerans* infections without surgical excision. *Am J Trop Med Hyg*. 1974;23: 924–929.
99. Eddyani M, Portaels F. Survival of *Mycobacterium ulcerans* at 37 degrees C. *Clin Microbiol Infect Off Publ Eur Soc Clin Microbiol Infect Dis*. 2007;13: 1033–1035. doi:10.1111/j.1469-0691.2007.01791.x
100. Junghanss T, Um Boock A, Vogel M, Schuette D, Weinlaeder H, Pluschke G. Phase Change Material for Thermo-therapy of Buruli Ulcer: A Prospective Observational Single Centre Proof-of-Principle Trial. *PLoS Negl Trop Dis*. 2009;3: e380. doi:10.1371/journal.pntd.0000380
101. Vogel M, Bayi PF, Ruf M-T, Bratschi MW, Bolz M, Um Boock A, et al. Local heat application for the treatment of Buruli ulcer: results of a phase II open label single center non comparative clinical trial. *Clin Infect Dis Off Publ Infect Dis Soc Am*. 2015; doi:10.1093/cid/civ883
102. Einarsdottir T, Huygen K. Buruli ulcer. *Hum Vaccin*. 2011;7: 1198–1203. doi:10.4161/hv.7.11.17751
103. Bolz M, Kerber S, Zimmer G, Pluschke G. Use of Recombinant Virus Replicon Particles for Vaccination against *Mycobacterium ulcerans* Disease. *PLoS Negl Trop Dis*. 2015;9: e0004011. doi:10.1371/journal.pntd.0004011
104. Chaabane W, User SD, El-Gazzah M, Jaksik R, Sajjadi E, Rzeszowska-Wolny J, et al. Autophagy, apoptosis, mitoptosis and necrosis: interdependence between those pathways and effects on cancer. *Arch Immunol Ther Exp (Warsz)*. 2013;61: 43–58. doi:10.1007/s00005-012-0205-y
105. Radi E, Formichi P, Battisti C, Federico A. Apoptosis and oxidative stress in neurodegenerative diseases. *J Alzheimers Dis JAD*. 2014;42 Suppl 3: S125–152. doi:10.3233/JAD-132738
106. Nikolettou V, Markaki M, Palikaras K, Tavernarakis N. Crosstalk between apoptosis, necrosis and autophagy. *Biochim Biophys Acta*. 2013;1833: 3448–3459. doi:10.1016/j.bbamcr.2013.06.001
107. Horvitz HR. Genetic control of programmed cell death in the nematode *Caenorhabditis elegans*. *Cancer Res*. 1999;59: 1701s–1706s.
108. McIlwain DR, Berger T, Mak TW. Caspase Functions in Cell Death and Disease. *Cold Spring Harb Perspect Biol*. 2013;5: a008656. doi:10.1101/cshperspect.a008656
109. Green DR. Apoptotic pathways: ten minutes to dead. *Cell*. 2005;121: 671–674. doi:10.1016/j.cell.2005.05.019
110. Elmore S. Apoptosis: A Review of Programmed Cell Death. *Toxicol Pathol*. 2007;35: 495–516. doi:10.1080/01926230701320337
111. Ghavami S, Hashemi M, Ande SR, Yeganeh B, Xiao W, Eshraghi M, et al. Apoptosis and cancer: mutations within caspase genes. *J Med Genet*. 2009;46: 497–510. doi:10.1136/jmg.2009.066944

112. Bratton DL, Fadok VA, Richter DA, Kailey JM, Guthrie LA, Henson PM. Appearance of phosphatidylserine on apoptotic cells requires calcium-mediated nonspecific flip-flop and is enhanced by loss of the aminophospholipid translocase. *J Biol Chem.* 1997;272: 26159–26165.
113. Kroemer G, Galluzzi L, Brenner C. Mitochondrial membrane permeabilization in cell death. *Physiol Rev.* 2007;87: 99–163. doi:10.1152/physrev.00013.2006
114. Adams JM. Ways of dying: multiple pathways to apoptosis. *Genes Dev.* 2003;17: 2481–2495. doi:10.1101/gad.1126903
115. Los M, Wesselborg S, Schulze-Osthoff K. The Role of Caspases in Development, Immunity, and Apoptotic Signal Transduction: Lessons from Knockout Mice. *Immunity.* 1999;10: 629–639. doi:10.1016/S1074-7613(00)80062-X
116. Saelens X, Festjens N, Walle LV, Gurp M van, Loo G van, Vandenabeele P. Toxic proteins released from mitochondria in cell death. *Oncogene.* 2004;23: 2861–2874. doi:10.1038/sj.onc.1207523
117. Fulda S, Debatin K-M. Extrinsic versus intrinsic apoptosis pathways in anticancer chemotherapy. *Oncogene.* 2006;25: 4798–4811. doi:10.1038/sj.onc.1209608
118. Adrain C, Slee EA, Harte MT, Martin SJ. Regulation of apoptotic protease activating factor-1 oligomerization and apoptosis by the WD-40 repeat region. *J Biol Chem.* 1999;274: 20855–20860.
119. Bratton SB, Walker G, Srinivasula SM, Sun XM, Butterworth M, Alnemri ES, et al. Recruitment, activation and retention of caspases-9 and -3 by Apaf-1 apoptosome and associated XIAP complexes. *EMBO J.* 2001;20: 998–1009. doi:10.1093/emboj/20.5.998
120. Cory S, Adams JM. The Bcl2 family: regulators of the cellular life-or-death switch. *Nat Rev Cancer.* 2002;2: 647–656. doi:10.1038/nrc883
121. O'Connor L, Strasser A, O'Reilly LA, Hausmann G, Adams JM, Cory S, et al. Bim: a novel member of the Bcl-2 family that promotes apoptosis. *EMBO J.* 1998;17: 384–395. doi:10.1093/emboj/17.2.384
122. U M, Miyashita T, Shikama Y, Tadokoro K, Yamada M. Molecular cloning and characterization of six novel isoforms of human Bim, a member of the proapoptotic Bcl-2 family. *FEBS Lett.* 2001;509: 135–141.
123. Ley R, Ewings KE, Hadfield K, Cook SJ. Regulatory phosphorylation of Bim: sorting out the ERK from the JNK. *Cell Death Differ.* 2005;12: 1008–1014. doi:10.1038/sj.cdd.4401688
124. Willis SN, Fletcher JL, Kaufmann T, van Delft MF, Chen L, Czabotar PE, et al. Apoptosis initiated when BH3 ligands engage multiple Bcl-2 homologs, not Bax or Bak. *Science.* 2007;315: 856–859. doi:10.1126/science.1133289
125. Czabotar PE, Colman PM, Huang DCS. Bax activation by Bim? *Cell Death Differ.* 2009;16: 1187–1191. doi:10.1038/cdd.2009.83
126. Gavathiotis E, Reyna DE, Davis ML, Bird GH, Walensky LD. BH3-triggered structural reorganization drives the activation of proapoptotic BAX. *Mol Cell.* 2010;40: 481–492. doi:10.1016/j.molcel.2010.10.019
127. Mérimo D, Giam M, Hughes PD, Siggs OM, Heger K, O'Reilly LA, et al. The role of BH3-only protein Bim extends beyond inhibiting Bcl-2-like prosurvival proteins. *J Cell Biol.* 2009;186: 355–362. doi:10.1083/jcb.200905153
128. Zoncu R, Efeyan A, Sabatini DM. mTOR: from growth signal integration to cancer, diabetes and ageing. *Nat Rev Mol Cell Biol.* 2011;12: 21–35. doi:10.1038/nrm3025
129. Laplante M, Sabatini DM. mTOR signaling at a glance. *J Cell Sci.* 2009;122: 3589–3594. doi:10.1242/jcs.051011
130. Kim DH, Sabatini DM. Raptor and mTOR: subunits of a nutrient-sensitive complex. *Curr Top Microbiol Immunol.* 2004;279: 259–270.
131. Manning BD, Cantley LC. United at last: the tuberous sclerosis complex gene products connect the phosphoinositide 3-kinase/Akt pathway to mammalian target of rapamycin (mTOR) signalling. *Biochem Soc Trans.* 2003;31: 573–578. doi:10.1042/
132. Gibbons JJ, Abraham RT, Yu K. Mammalian target of rapamycin: discovery of rapamycin reveals a signaling pathway important for normal and cancer cell growth. *Semin Oncol.* 2009;36 Suppl 3: S3–S17. doi:10.1053/j.seminoncol.2009.10.011

133. Hara K, Yonezawa K, Kozlowski MT, Sugimoto T, Andrabi K, Weng QP, et al. Regulation of eIF-4E BP1 phosphorylation by mTOR. *J Biol Chem.* 1997;272: 26457–26463.
134. Foster KG, Fingar DC. Mammalian target of rapamycin (mTOR): conducting the cellular signaling symphony. *J Biol Chem.* 2010;285: 14071–14077. doi:10.1074/jbc.R109.094003
135. Sarbassov DD, Ali SM, Kim D-H, Guertin DA, Latek RR, Erdjument-Bromage H, et al. Rictor, a novel binding partner of mTOR, defines a rapamycin-insensitive and raptor-independent pathway that regulates the cytoskeleton. *Curr Biol CB.* 2004;14: 1296–1302. doi:10.1016/j.cub.2004.06.054
136. Loewith R, Jacinto E, Wullschlegel S, Lorberg A, Crespo JL, Bonenfant D, et al. Two TOR Complexes, Only One of which Is Rapamycin Sensitive, Have Distinct Roles in Cell Growth Control. *Mol Cell.* 2002;10: 457–468. doi:10.1016/S1097-2765(02)00636-6
137. Jacinto E, Loewith R, Schmidt A, Lin S, Ruegg MA, Hall A, et al. Mammalian TOR complex 2 controls the actin cytoskeleton and is rapamycin insensitive. *Nat Cell Biol.* 2004;6: 1122–1128. doi:10.1038/ncb1183
138. Manning BD, Cantley LC. AKT/PKB Signaling: Navigating Downstream. *Cell.* 2007;129: 1261–1274. doi:10.1016/j.cell.2007.06.009
139. Alessi DR, James SR, Downes CP, Holmes AB, Gaffney PR, Reese CB, et al. Characterization of a 3-phosphoinositide-dependent protein kinase which phosphorylates and activates protein kinase Balpha. *Curr Biol CB.* 1997;7: 261–269.
140. Hemmings BA, Restuccia DF. PI3K-PKB/Akt Pathway. *Cold Spring Harb Perspect Biol.* 2012;4: a011189. doi:10.1101/cshperspect.a011189
141. Sarbassov DD, Guertin DA, Ali SM, Sabatini DM. Phosphorylation and regulation of Akt/PKB by the rictor-mTOR complex. *Science.* 2005;307: 1098–1101. doi:10.1126/science.1106148
142. Guertin DA, Stevens DM, Thoreen CC, Burds AA, Kalaany NY, Moffat J, et al. Ablation in mice of the mTORC components raptor, rictor, or mLST8 reveals that mTORC2 is required for signaling to Akt-FOXO and PKCalpha, but not S6K1. *Dev Cell.* 2006;11: 859–871. doi:10.1016/j.devcel.2006.10.007
143. Jacinto E, Facchinetti V, Liu D, Soto N, Wei S, Jung SY, et al. SIN1/MIP1 Maintains rictor-mTOR Complex Integrity and Regulates Akt Phosphorylation and Substrate Specificity. *Cell.* 2006;127: 125–137. doi:10.1016/j.cell.2006.08.033
144. Calnan DR, Brunet A. The FoxO code. *Oncogene.* 2008;27: 2276–2288. doi:10.1038/onc.2008.21
145. Fu Z, Tindall DJ. FOXOs, cancer and regulation of apoptosis. *Oncogene.* 2008;27: 2312–2319. doi:10.1038/onc.2008.24
146. Zaytseva YY, Valentino JD, Gulhati P, Mark Evers B. mTOR inhibitors in cancer therapy. *Cancer Lett.* 2012;319: 1–7. doi:10.1016/j.canlet.2012.01.005
147. Alvarado Y, Mita MM, Vemulapalli S, Mahalingam D, Mita AC. Clinical activity of mammalian target of rapamycin inhibitors in solid tumors. *Target Oncol.* 2011;6: 69–94. doi:10.1007/s11523-011-0178-5
148. Sarbassov DD, Ali SM, Sengupta S, Sheen J-H, Hsu PP, Bagley AF, et al. Prolonged rapamycin treatment inhibits mTORC2 assembly and Akt/PKB. *Mol Cell.* 2006;22: 159–168. doi:10.1016/j.molcel.2006.03.029
149. Liu Q, Thoreen C, Wang J, Sabatini D, Gray NS. mTOR Mediated Anti-Cancer Drug Discovery. *Drug Discov Today Ther Strateg.* 2009;6: 47–55. doi:10.1016/j.ddstr.2009.12.001
150. Napoli KL, Taylor PJ. From beach to bedside: history of the development of sirolimus. *Ther Drug Monit.* 2001;23: 559–586.
151. Hartford CM, Ratain MJ. Rapamycin: Something Old, Something New, Sometimes Borrowed and Now Renewed. *Clin Pharmacol Ther.* 2007;82: 381–388. doi:10.1038/sj.clpt.6100317
152. Yu K, Toral-Barza L, Shi C, Zhang W-G, Lucas J, Shor B, et al. Biochemical, cellular, and in vivo activity of novel ATP-competitive and selective inhibitors of the mammalian target of rapamycin. *Cancer Res.* 2009;69: 6232–6240. doi:10.1158/0008-5472.CAN-09-0299
153. Lv X, Ma X, Hu Y. Furthering the design and the discovery of small molecule ATP-competitive mTOR inhibitors as an effective cancer treatment. *Expert Opin Drug Discov.* 2013;8: 991–1012. doi:10.1517/17460441.2013.800479

154. Roper J, Richardson MP, Wang WV, Richard LG, Chen W, Coffee EM, et al. The Dual PI3K/mTOR Inhibitor NVP-BEZ235 Induces Tumor Regression in a Genetically Engineered Mouse Model of PIK3CA Wild-Type Colorectal Cancer. PLoS ONE. 2011;6: e25132. doi:10.1371/journal.pone.0025132
155. Dmitry Goncharov, Tatiana V. Kudryashova, Steven M. Kawut, Elena A. Goncharova. Dual mTORC1/mTORC2 Inhibitor PP242 Induces mTORC2-Specific Bim-Dependent Apoptosis In Small PAs And Reverses Hypoxia-Induced Pulmonary Vascular Remodeling In Rats. Available: http://www.atsjournals.org/doi/abs/10.1164/ajrccm-conference.2014.189.1_MeetingAbstracts.A5562. Accessed 9 November 2015.
156. Moen MD, McKeage K, Plosker GL, Siddiqui MAA. Imatinib: a review of its use in chronic myeloid leukaemia. *Drugs*. 2007;67: 299–320

Objectives

Within the framework of this thesis, specific objectives were:

1. to unravel the molecular mechanisms underlying the cytotoxic activity of mycolactone by making use of cellular systems, the BU mouse foot pad model as well as biopsies from human BU patients.
2. to contribute to the understanding of the nature of immune effector mechanisms conferring protection against BU with a focus on the role of interferon- γ and of cellular immune defense mechanisms during the early intracellular stage of *M. ulcerans* infection.
3. to evaluate the activity of a new tuberculosis drug candidate against *M. ulcerans*.

Results Chapter 1

Mycolactone binds to FKBP12 and promotes Bim-dependent apoptosis in Buruli ulcer through inhibition of mTOR

Raphael Bieri^{1,2}, Nicole Scherr^{1,2}, Marie-Thérèse Ruf^{1,2}, Jean-Pierre Dangy^{1,2}, Flurina Pletscher³, Philipp Gersbach⁴, Matthias Gehringer⁴, Thomas Junghanss⁵, Karl-Heinz Altmann⁴ and Gerd Pluschke^{1,2*}

¹Swiss Tropical and Public Health Institute, Socinstrasse 57, 4002 Basel, Switzerland

²University of Basel, Petersplatz 1, 4003 Basel, Switzerland

³Department of Biomedicine at University of Basel and University Hospital Basel, Hebelstrasse 20, 4031 Basel, Switzerland,

⁴Department of Chemistry and Applied Biosciences, Institute of Pharmaceutical Sciences, Swiss Federal Institute of Technology (ETH) Zurich, Vladimir-Prelog-Weg 1-5 / 10, 8093 Zurich, Switzerland

⁵Section of Clinical Tropical Medicine, Heidelberg University Hospital, Im Neuenheimer Feld 324, 69120 Heidelberg, Germany

* Corresponding author

Working Manuscript

Abstract

Mycolactone, the macrolide exotoxin produced by *Mycobacterium ulcerans*, is central to the pathogenesis of the necrotic skin disease Buruli ulcer (BU). Using two complex synthetic probe molecules, we demonstrate that mycolactone binds to the 12-kDa FK506-binding protein and acts as a potent mTOR inhibitor. In contrast to the immunosuppressive drug rapamycin, a non-cytotoxic inhibitor of mTORC1, mycolactone also shows powerful inhibition of mTORC2 activity, resulting in inactivation of Akt and dephosphorylation and activation of the Akt-targeted transcription factor FoxO3. Subsequent up-regulation of the FoxO3 target gene *Bim* was observed both *in vitro* and in human BU lesions. Further highlighting the key role of Bim-dependent apoptosis in BU pathogenesis, Bim knockout mice were able to contain *M. ulcerans* infections and did not develop any of the typical necrotic BU lesions with large clusters of extracellular bacteria.

Introduction

The cytotoxic and immunosuppressive macrolide exotoxin mycolactone A/B (in the following simply referred to as “mycolactone”) (Fig. 1) is the key virulence factor of *Mycobacterium ulcerans* (*M. ulcerans*), the causative pathogen of the chronic necrotizing skin disease Buruli ulcer (BU). After tuberculosis and leprosy, BU is the third most common mycobacterial disease in humans and leads to massive subcutaneous tissue destruction and the formation of ulcers with characteristic undermined edges [1–3]. Mycolactone is regarded as essential for BU pathogenesis, as mycolactone-deficient *M. ulcerans* mutants are avirulent and intradermal injection of the toxin in animal models is sufficient to induce the formation of BU-like lesions [4]. Despite the severity of the disease, the formation of extensive skin lesions is not accompanied by pain, since mycolactone induces analgesia by targeting the angiotensin pathways [5].

Mycolactone has been shown to have pleiotropic cellular effects. It is highly cytotoxic and immunosuppressive, induces cytoskeletal rearrangements and blocks protein translocation to the ER [1,6–8].

Mycolactone-induced cytoskeletal rearrangements have been recently associated with mycolactone binding to the Wiskott-Aldrich syndrome protein family (WASP) regulators of actin polymerization, resulting in blockade of WASP autoinhibition and uncontrolled ARP2/3-mediated actin polymerization, a process that was partly suppressed by co-administration of the N-WASP inhibitor Wiskostatin [7].

Like rapamycin, an immunosuppressant produced by *Streptomyces hygroscopicus*, mycolactone belongs to the group of natural macrolides. Rapamycin acts as inhibitor of the mammalian target of rapamycin (mTOR), a serine/threonine protein kinase involved in the regulation of cell fate decisions including cell proliferation, cell survival, transcription and translation. mTOR interacts with several proteins to form two different complexes named mTOR complex 1 (mTORC1) and 2 (mTORC2). These two mTOR complexes have distinct sensitivities to rapamycin and different downstream outputs. Rapamycin forms a complex with the intracellular 12-kDa FK506-binding protein (FKBP12), which directly interacts and inhibits mTORC1, but not mTORC2. Short-term rapamycin treatment does not inhibit mTORC2 because the FKBP12-rapamycin complex cannot bind to intact mTORC2. However, it was shown that long-term treatment reduces mTORC2 signaling in some cell types by suppressing mTORC2 assembly [9–12]. One of the main targets of mTORC2 is Akt, a serine/threonine protein

kinase controlling cellular survival processes and inhibiting apoptosis pathways through phosphorylation of different target proteins. Most importantly, mTORC2 phosphorylates Akt at Ser473, which is required for maximal Akt activation [13]. Defective phosphorylation of Akt associated with depletion or inhibition of mTORC2 has been demonstrated to impair phosphorylation of several Akt targets including the two transcription factors forkhead box O1 and 3 (FoxO1, FoxO3) [14,15]. These transcription factors are normally excluded from the nucleus through phosphorylation by Akt, resulting in their ubiquitination and proteolytic degradation. In contrast, nuclear FoxOs are devoid of phosphorylation and can promote apoptosis by inducing the expression of the pro-apoptotic Bcl-2 family member Bim. Additionally, they can activate cell-extrinsic apoptosis pathways such as Fas receptor signaling [16].

Despite the fact that mycolactone-induced cell death is the central element of BU pathogenesis, the molecular mechanisms underlying this process are still completely unknown.

In the present study we have used well-defined synthetic mycolactone and mycolactone derivatives in order to decipher the molecular mechanisms of mycolactone cytotoxicity. Two distinct biotin-tagged mycolactone analogs were designed and used as molecular probes for target identification. By applying several complementary approaches, we show that the toxin acts as a potent mTOR inhibitor, thus causing up-regulation of the FoxO3 target gene *Bim* via the mTORC2-Akt-FoxO3 axis and finally Bim-dependent apoptosis.

Results

Synthesis of Mycolactone and Mycolactone Derivatives

The synthesis of mycolactone and a truncated derivative **1** has been described previously by our group [17,18]. For target identification, biotin tags were introduced as an extension of the upper side chain (**2**) or as a replacement of the lower polyene side chain (**3**). In both cases, a diethylenglycol carbamoyl spacer was used for connecting biotin to the mycolactone scaffold. As for the natural product, the synthesis of mycolactone derivatives **1-3** proceeded through macrocyclic alkyl iodide **4** as a common advanced intermediate (Fig 1). The syntheses of these derivatives are summarized in Supplementary Schemes S1 – S3 (Appendix Chapter 1).

Mycolactone treatment results in up-regulation of Bim and Bim-dependent apoptosis

To investigate whether mycolactone-exposed mammalian cells die by apoptosis, programmed necrosis or autophagy, L929 fibroblasts were treated with 80 nM (60 ng/ml) synthetic mycolactone [18]. Treatment was in the presence of either the pan-caspase inhibitor zVAD.fmk (zVAD) [19], the autophagy inhibitor 3-methyladenine (3-MA) [20] or necrostatin-1 (Nec-1), a selective inhibitor of programmed necrosis targeting the central RIP-1 kinase [21]. Since mycolactone has recently been demonstrated to bind to and activate the Wiskott-Aldrich syndrome protein family (WASP) of actin regulators [7], the effect of the WASP inhibitor wiskostatin (Wisko) on mycolactone-induced cytotoxicity was also assessed [22]. While mycolactone-treated L929 fibroblasts showed no signs of cell death after 24 hours of mycolactone exposure, about 75 % of the cells had died after 48 hours (Fig. 2a). Only the pan-caspase inhibitor zVAD significantly reduced mycolactone-induced cytotoxicity (Fig. 2a), demonstrating that mycolactone-treated cells die by apoptosis. Surprisingly, co-administration of the N-WASP inhibitor Wiskostatin did not decrease, but even enhance mycolactone cytotoxicity (Fig. 2a).

To dissect the molecular mechanism of mycolactone-mediated cytotoxicity, we performed a quantitative RT-PCR screen of 84 genes involved in the regulation of apoptosis, necrosis and autophagy. Expression of these genes was profiled in L929

fibroblasts at different times after the start of mycolactone treatment. While the expression of genes involved in the regulation of necrosis or autophagy was not or only marginally affected by the toxin, mycolactone treatment resulted in a strong up-regulation of the transcription of the genes encoding the pro-apoptotic BH3-only protein Bim (Bim_{EL} isoform) and the Fas death receptor (Supplementary Table 1, Appendix Chapter 1). The pro-apoptotic BH-3 only protein Bim binds to anti-apoptotic Bcl-2 family proteins, thereby allowing the pro-apoptotic proteins Bax and Bak to form oligomeric pores, the so-called mitochondrial apoptosis-induced channels (MAC), in the outer mitochondrial membrane. As a result, cytochrome c is released into the cytoplasm and the initiator caspase-9 as well as the downstream effector caspases-3, -6, and -7 are activated, which ultimately leads to cellular demolition [23,24].

Experiments with a second set of primers reconfirmed up-regulation of Bim and Fas receptor mRNA levels in L929 fibroblasts treated for 24 hours with mycolactone (18- and 9-fold increase, respectively; Fig. 2b). No changes were observed for DMSO control cells (Supplementary Fig. 1a). When expression of these two highly regulated genes was analyzed at the protein level by Western blot analysis of whole cell lysates, a good correlation between the increase in mRNA and protein levels was observed (Fig. 2c).

In addition to the up-regulation of Bim and Fas, cleaved caspase-8 emerged in L929 fibroblasts after 24 hours of mycolactone treatment (Fig. 2c), suggesting activation of the extrinsic apoptotic pathway in association with the up-regulation of the Fas receptor. Detection of Bim, Fas and cleaved caspase-8 thus immediately preceded the onset of apoptosis (Fig. 2a). Additional markers, such as cleavage of caspase-3, cleavage of the caspase-3 target nuclear Poly(ADP-ribose) polymerase-1 (PARP-1) [21,25] (Fig. 2c), as well as the release of mitochondrial cytochrome c (Fig. 2d) provided further evidence for the induction of apoptosis.

Next, we assessed whether mycolactone-induced apoptosis is dependent on the observed induced expression of Fas and/or Bim. Therefore, we silenced these factors through RNA interference. Bim and Fas knockdown efficiencies in transfected cells were monitored by quantitative RT-PCR (Supplementary Fig. 1b) and Western blot analysis (Fig. 2e). While knockdown of Bim completely protected L929 fibroblasts from mycolactone-induced apoptosis, ablation of Fas did not diminish cell death significantly compared to untransfected cells or to cells transfected with a non-targeting control short interfering RNA (siRNA) (Fig. 2f).

Mycolactone is a natural mTORC1/2 inhibitor

It has been suggested that mycolactone shares structural features with the immunosuppressive macrolide rapamycin [1]. We therefore hypothesized that mycolactone might also act as an mTOR inhibitor and that the mode of action may be comparable to that of cytotoxic mTORC1/2 inhibitors, such as PP242 and WAY-600 [15,26], which induce Bim-dependent apoptosis. To verify this hypothesis, we tested, whether mycolactone treatment has an effect on the phosphorylation of the mTORC1 targeted ribosomal protein S6 at residue Ser235/236 (pS6 (Ser235/236)) and the mTORC2 targeted protein kinase Akt at residue Ser473 (pAkt (Ser473)) [9]. Western Blot analysis of whole cell lysates of mycolactone- or rapamycin-treated L929 fibroblasts showed that mycolactone treatment completely abolished phosphorylation of both S6 and Akt (Fig. 3a). As expected, rapamycin was found to have a strong effect on S6 phosphorylation due to inhibition of mTORC1, while it is a weaker inhibitor of mTORC2, as shown by its less pronounced effects on Akt phosphorylation (Fig. 3a). No changes in the phosphorylation of the S6 protein and Akt were found in the DMSO controls. Neither mycolactone nor rapamycin treatment affected total expression of the S6 and Akt proteins (Fig. 3a).

Qualitatively similar effects as for L929 fibroblasts were also observed with Jurkat cells, a non-adherent human T lymphocyte cell line. However, Jurkat cells died 24 hours later than L929 fibroblasts and mycolactone-induced effects were generally delayed and less pronounced for this cell line (Supplementary Fig. 2). These results are consistent with previous findings on the lower sensitivity of Jurkat cells towards mycolactone compared to L929 fibroblasts [27,28]. Collectively, however, the results obtained for both, L929 fibroblasts and Jurkat cells, identified mycolactone as a potent inhibitor of mTORC1 and mTORC2, which causes dephosphorylation and inactivation of the Akt kinase.

Mycolactone induces Bim-dependent apoptosis via the mTORC2-Akt-FoxO3 signaling axis

In a next step we investigated whether the mycolactone-induced mTORC2-dependent inactivation of Akt results in dephosphorylation and transcriptional activation of the directly Akt-targeted transcription factor FoxO3 [14–16], thus potentially leading to the

up-regulation of the FoxO3 target genes *Bim* and *Fas* [16] and ultimately to Bim-dependent apoptosis.

Western blot analysis of whole cell lysates revealed complete dephosphorylation of FoxO3 at the Akt target site Thr32 after 12 hours of mycolactone treatment of L929 fibroblasts (Fig. 3b) [15], which correlates well with the time course of Akt inactivation (Fig. 3a), but also with the up-regulation of Bim and Fas and the induction of Bim-dependent apoptosis (Fig. 2a-c). Dephosphorylation of FoxO3 was also observed to a weaker extent for rapamycin-treated L929 fibroblasts, but not for untreated control cells (Fig. 3b). Neither mycolactone nor rapamycin affected expression of the FoxO3 protein itself (Fig. 3b).

In RNA interference experiments knockdown of FoxO3 significantly reduced mycolactone-induced apoptosis (Fig. 3c). Since FoxO3 seemed to play a pivotal role in mycolactone-mediated cytotoxicity, we next investigated whether transcriptional activity of FoxO3 in fact constitutes the molecular basis for the observed mycolactone-mediated up-regulation of Bim and Fas (Fig. 2b,c). To this end, we analyzed the expression levels of FoxO3, Bim and Fas in FoxO3 knockdown cells by quantitative RT-PCR and by Western blot analysis. Intriguingly, the massive up-regulation of Bim and Fas upon mycolactone treatment was strongly reduced in FoxO3 knockdown cells, thus confirming that FoxO3 is the main transcriptional regulator of Bim-dependent apoptosis in mycolactone-treated cells (Fig. 3d and Supplementary Fig. 1c).

The lower (C5) side chain of mycolactone is required for mTOR inhibition and Bim-dependent apoptosis

Our previous structure-activity relationship studies with synthetic mycolactone derivatives have demonstrated that the lower (C5) side chain of mycolactone is crucial to its cytotoxic activity [18]. To test whether this side chain is required for the mTOR inhibitory activity and the subsequent induction of Bim-dependent apoptosis, L929 fibroblasts were treated with either mycolactone or compound **1** (Fig. 1), a mycolactone derivative with a truncated lower side chain [18]. Whole cell lysates were analyzed by Western blotting for phosphorylation of S6 and Akt proteins, as well as for the levels of Bim. As expected, mycolactone-treated L929 fibroblasts displayed a complete inhibition of mTORC1/2 followed by a massive up-regulation of Bim (Fig. 4a). In contrast, no

inhibition of mTORC1/2 and no up-regulation of Bim was observed for **1**-treated cells (Fig. 4a), confirming that the lower side chain of mycolactone is indeed required for mTOR inhibition and subsequent induction of Bim-dependent apoptosis.

Mycolactone acts through binding to the 12-kDa FK506-binding protein (FKBP12)

Since mycolactone showed potent mTOR inhibitory activity and is known to be highly immunosuppressive [1], we next investigated whether it binds, like rapamycin, to the intracellular 12-kDa FK506-binding protein (FKBP12). Streptavidin-coated ELISA plates were incubated with synthetic biotinylated mycolactone derivatives **2** or **3** (Fig. 1). Compound **2** has a biotin tag attached to the upper side chain *via* a diethylenglycol-carbamoyl linker while compound **3** incorporates a biotinylated diethylenglycol-based replacement of the lower side chain of the toxin. It should be noted that we had previously found a butyl-carbamoyl analog of **2** (containing a butyl residue instead of a biotinylated diethylenglycol extension) to be only marginally less cytotoxic than natural mycolactone [18]. After compound treatment, plates were incubated with recombinant FKBP12 protein and bound FKBP12 protein was detected using anti-FKBP12 antibodies. While compound **2**, the derivative with an unmodified O-linked polyunsaturated lower side chain, displayed binding to FKBP12 (Fig. 4b), **3**, which contains the biotin label attached to a substitute of the lower side chain, showed only background binding to FKBP12 (Fig. 4c).

To analyze whether mycolactone binding to FKBP12 is in fact relevant for the cytotoxic activity of mycolactone, we performed a competition assay using FK506 (Tacrolimus), an immunosuppressive drug binding to the conserved active site of FKBP12 [29–31]. Strikingly, we found that administration of a 1000-fold excess of FK506 completely protected L929 fibroblasts from mycolactone-induced apoptosis. A significant level of protection from mycolactone cytotoxicity was already achieved at a molar ratio of 10 (Fig. 4d).

Taken together, our data show that mycolactone binds to FKBP12 and that this complex induces Bim-dependent apoptosis via the mTORC2-Akt-FoxO3 signaling axis. The model of the mode of action of mycolactone inferred from these experiments is depicted in Figure 4e.

Up-regulation of Bim in human BU lesions

One of the main features of the pathogenesis of BU is the destruction of subcutaneous adipose tissue, leading to the collapse of the epidermis and the formation of characteristic ulcers with undermined edges [1]. To reconfirm that these events are triggered by mycolactone via the mTORC2-Akt-FoxO3-Bim axis, we performed further analyses with primary human adipocytes and clinical specimens from BU patients.

We found that the sensitivity of primary human adipocytes to mycolactone was comparable to that of L929 fibroblasts. However, adipocytes died later and only started to undergo apoptosis after five days of mycolactone treatment (Supplementary Fig. 3a). As for L929 fibroblasts, a complete inhibition of mTORC1/2 (Supplementary Fig. 3b) as well as a massive up-regulation of Bim was observed for adipocytes treated with 16 nM or 80 nM mycolactone both at mRNA (8-fold up-regulation, Supplementary Fig. 3c) and at protein levels (Supplementary Fig. 3b).

Immunohistochemical staining of tissue specimens from BU patients revealed up-regulation of Bim in BU lesions (Fig. 5). Punch biopsies taken at the border of ulcerative BU lesions comprising epidermis, dermis and subcutis showed characteristic histopathological hallmarks of BU, including the presence of epidermal hyperplasia, fat cell ghosts and extensive necrosis. Small clusters of solid stained acid-fast bacilli (Fig. 5b,c) were dispersed in the necrotic areas (Region 2 in Fig. 5a). In this region consisting of completely necrotic tissue devoid of living and infiltrating cells, no Bim-staining was observed (Fig. 5e). However, in the neighboring layers with better preserved tissue infiltrated by immune cells (Regions 1 and 3 in Fig. 5a), a substantial number of cells expressing high levels of Bim were found (Fig. 5d,f).

Containment of infection and lack of tissue necrosis in *M. ulcerans*-infected Bim knockout mice

To confirm that Bim-mediated apoptosis plays a key role in the pathogenesis of BU, we infected C57Bl/6 wild-type (WT) and homozygous Bim knockout mice (Bim^{-/-}) by injection of *M. ulcerans* bacteria into the left hind foot pad. Additionally, homozygous Fas (Fas^{-/-}) knockout mice were included in the experiment to reconfirm the results of the *in vitro* knockdown analyses (Fig. 2f) that suggested no involvement of the Fas pathway in mycolactone cytotoxicity. Disease progression was monitored by weekly measurements

of the foot pad thickness using a caliper. In contrast to the *Bim*^{-/-} mice, all WT and *Fas*^{-/-} mice started to show swelling of feet and reddening of the skin four weeks after infection (Fig. 6a,b). Histopathologically, these macroscopic signs in the susceptible mice correlated with edema formation and massive tissue necrosis (Fig. 6c,d). Quantitative IS2404 RT-PCR analysis [32] of footpad lysates revealed that bacterial multiplication was significantly impaired in the *Bim*^{-/-} mice (Fig. 6f). As expected for active BU lesions, large numbers of extracellular acid-fast bacilli were found throughout the infected footpads of WT and *Fas*^{-/-} mice (Fig. 6e). In contrast, only small numbers of acid-fast bacilli were found in the footpads of the *Bim*^{-/-} mice, primarily at the injection sites (Fig. 6e). Close vicinity of these small bacterial clusters to nuclei were indicative of uptake of the acid-fast bacteria by phagocytes (Fig. 6e).

Discussion

Cytotoxicity and immunosuppression mediated by mycolactone, the macrolide exotoxin produced by *M. ulcerans*, play key roles in the pathogenesis of BU. Using structurally well-defined synthetic mycolactone and mycolactone derivatives, we show that the toxin is an mTOR inhibitor that binds to the 12-kDa FK506-binding protein (FKBP12). In contrast to the non-cytotoxic rapamycin, which primarily acts as an inhibitor of mTORC1 and therefore only marginally interferes with the pro-survival Akt signaling, mycolactone also efficiently inhibits mTORC2, thereby activating a cytotoxic program via the mTORC2-Akt-FoxO3-Bim axis. For all mammalian cell types studied here, the sequence of events leading from the inhibition of mTORC2 to Bim-promoted apoptosis took at least 24 hours. This time lapse between the start of exposure to mycolactone and the onset of apoptosis has prevented recognition of the involvement of mTOR inhibition in mycolactone-mediated apoptosis in previous short time experiments [33]. For the same reason the potency of mycolactone has been often underestimated and the concentrations employed in some of the published studies on the activities of mycolactone at 'non-toxic' concentrations were in fact performed at toxic mycolactone concentrations.

In vitro, ablation of Bim expression by siRNA completely protected cells from mycolactone-induced cell death. Bim is also of fundamental importance for BU pathogenesis *in vivo*, as demonstrated by its high level of expression in cells surrounding the necrotic core of human BU lesions. Furthermore, Bim-deficient mice were completely resistant to tissue necrosis induced by infection with *M. ulcerans*. As a consequence of the resistance to mycolactone-mediated apoptosis, bacterial multiplication was significantly reduced in the Bim-deficient mice. This finding indicates that infiltrating phagocytes can contain the infection if they are not killed by the toxin produced by the internalized bacilli. While knockdown of Bim led to a complete protection from mycolactone cytotoxicity, ablation of FoxO3 had only a partial protective effect. This may be due to compensating functions by other FoxO family members.

The rather uncommon observation of a concomitant activation of cell-extrinsic (Fas, caspase-8) and cell-intrinsic (Bim) apoptosis pathways could possibly be a passive side-effect of FoxO3 activation by mycolactone. However, cooperation between these two pathways in terminating immune responses by efficiently deleting activated T-cells has

been demonstrated *in vivo* [34,35], possibly contributing to the immunosuppressive properties of mycolactone.

A recent study showed that mycolactone induces cytoskeletal rearrangement via blockage of WASP autoinhibition, leading to uncontrolled ARP2/3-mediated actin polymerization [7]. In our experiments the N-WASP inhibitor wiskostatin failed to block mycolactone-mediated cell death and even enhanced apoptosis. Cytoskeletal rearrangements might as well be triggered by the inhibition of mTORC2, since it has been demonstrated that the ablation of mTORC2 components affects actin polymerization, resulting in perturbed cell morphology [36].

Beyond the identification of the signaling cascade underlying mycolactone cytotoxicity, the results presented here also have major implications for mycolactone-induced immunosuppression, the second key feature of BU pathogenesis. The almost identical kinetics of mTOR inhibition in mycolactone- and rapamycin-treated cells as well as the demonstration of mycolactone binding to FKBP12 suggests that mycolactone and rapamycin might mediate systemic immunosuppression by similar pathways. This hypothesis is supported by studies showing that mycolactone can be traced in peripheral blood and peripheral lymph nodes of *M. ulcerans* infected mice, leading to a substantial down-regulation of T cell responses [37–39]. Since rapamycin-FKBP12 cannot directly bind and inhibit fully assembled mTORC2 [9], these similarities between rapamycin and mycolactone may suggest that mycolactone interferes with mTORC2 signaling by suppressing mTORC2 assembly, as previously demonstrated for rapamycin [9–12].

Our finding that the diffusible macrolide toxin mycolactone is a highly potent natural mTOR inhibitor does not only explain the molecular basis of mycolactone-mediated local pathogenesis and systemic immunosuppression, but may also open new perspectives for the development of a novel class of mTOR inhibitors with potential applications for the treatment of autoimmune diseases, organ graft rejection or cancer.

Acknowledgements

We thank Prof. Gerhard Christofori for critical reading of the manuscript. This work was supported by the Stop Buruli consortium funded by the UBS Optimus Foundation.

Author Contributions

R. B. and G. P. conceived the study and wrote the paper; N. S., M. G. and KH. A. corrected the manuscript; R. B. performed most of the experiments; N. S., MT. R., JP. D., F. P., P. G. and M. G. performed research and/or provided technical advice; G. P., KH. A. and T. J. provided vital reagents and materials.

Competing Financial Interests

The authors have no competing financial interests.

Figures

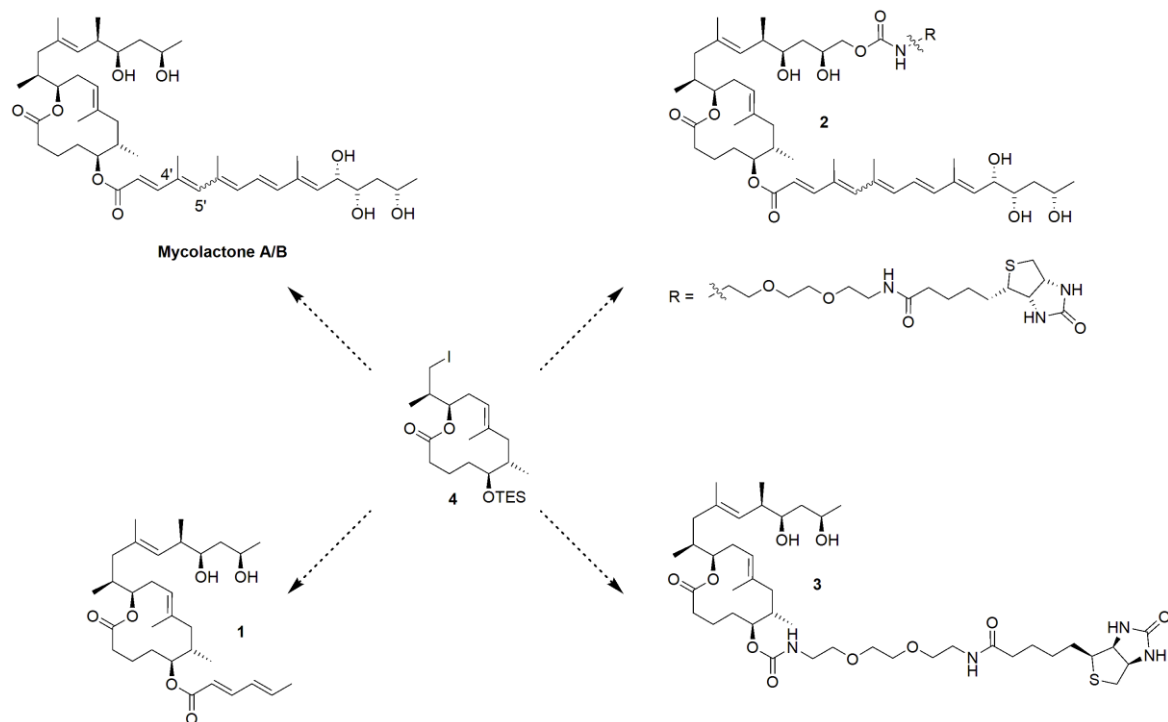


Figure 1: Structures of mycolactone A/B and of synthetic mycolactone derivatives 1-3.

Chemical structures of mycolactone A/B, truncated derivative **1** and biotin-tagged analogs **2** and **3**. All compounds were prepared from key intermediate **4**.

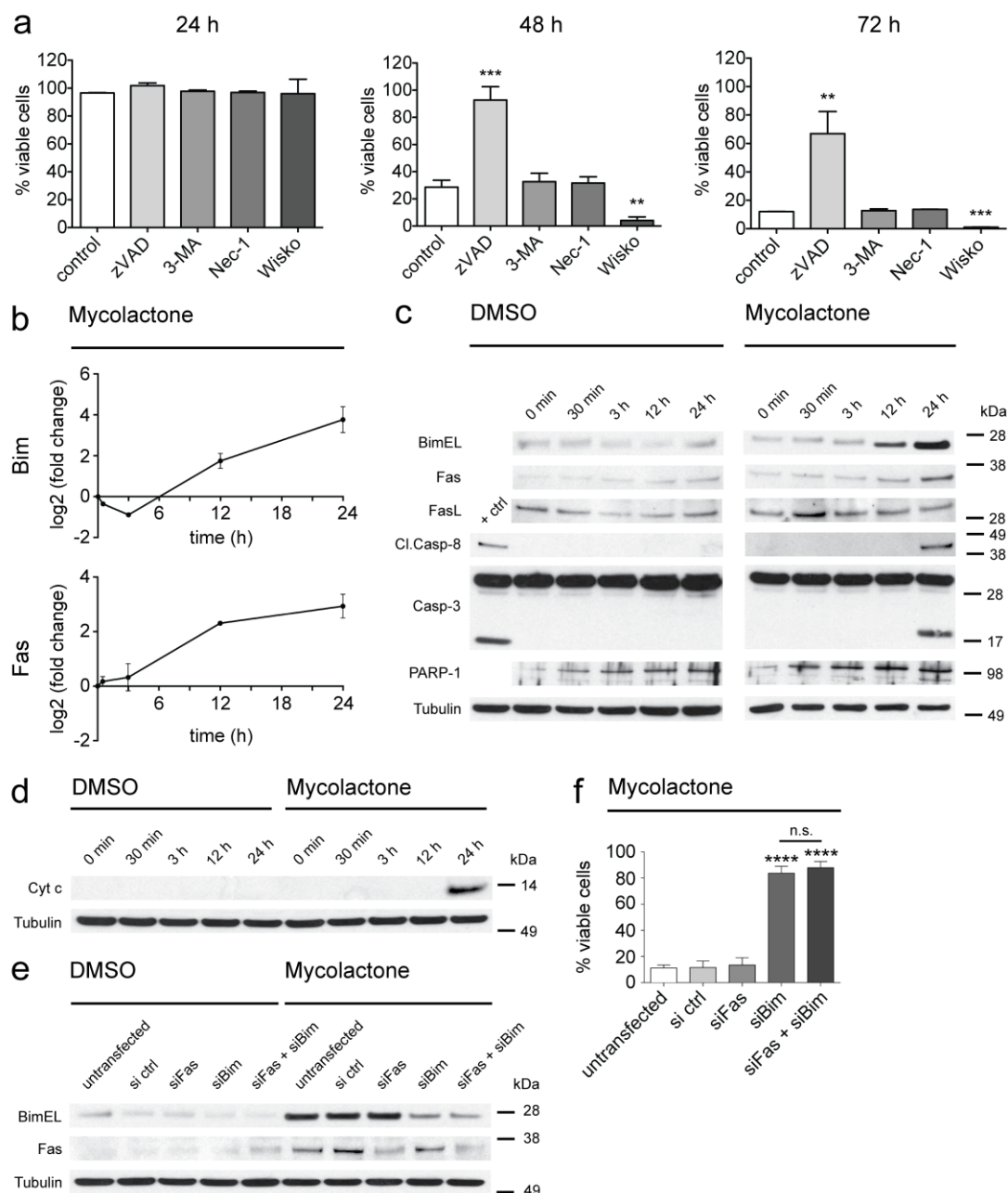


Figure 2: Mycolactone up-regulates Bim and induces Bim-dependent apoptosis in L929 fibroblasts.

(a) Mycolactone-treated L929 fibroblasts die by apoptosis. Cells were pre-treated for 1 h with 10 μ M zVAD, 200 μ M 3-MA, 10 μ M Nec-1 or 1 μ M Wisko prior to the addition of mycolactone. Cell viability was assessed by FACS analysis after 24 (left), 48 (middle), and 72 (right) hours. (b) Up-regulation of Bim and Fas mRNA expression as determined by qRT-PCR. Values are displayed as log₂ (fold change). Mean values across duplicate samples are shown, and error bars represent the s.d. (c) Up-regulation of Bim and Fas protein levels, and the presence of cleaved caspase-8, downstream caspase-3 and PARP-

1 as determined by Western blot. **(d)** Cytochrome c release from mitochondria as determined by Western blot using cytoplasmic fractions of mycolactone- or DMSO-treated L929 fibroblasts. **(e)** Protein levels of Bim and Fas in transfected L929 fibroblasts. **(f)** Knockdown of Bim - but not Fas - completely protects L929 fibroblasts from mycolactone-induced cytotoxicity. Cells were transfected with 10 nM siRNA control (si ctrl), siFas, siBim or siFas+ siBim 6 h prior to mycolactone addition and cell viability was assessed by FACS. Western blot data in **(c-e)** are representative of three independent experiments. α -Tubulin served as loading control. The bar graphs in **a** and **f** show mean values across duplicate samples, and the error bars represent the s.d. of three independent experiments. Two-tailed Student's t test. ****, $P \leq 0.0001$, ***, $P \leq 0.001$, **, $P \leq 0.01$, n. s., not significant.

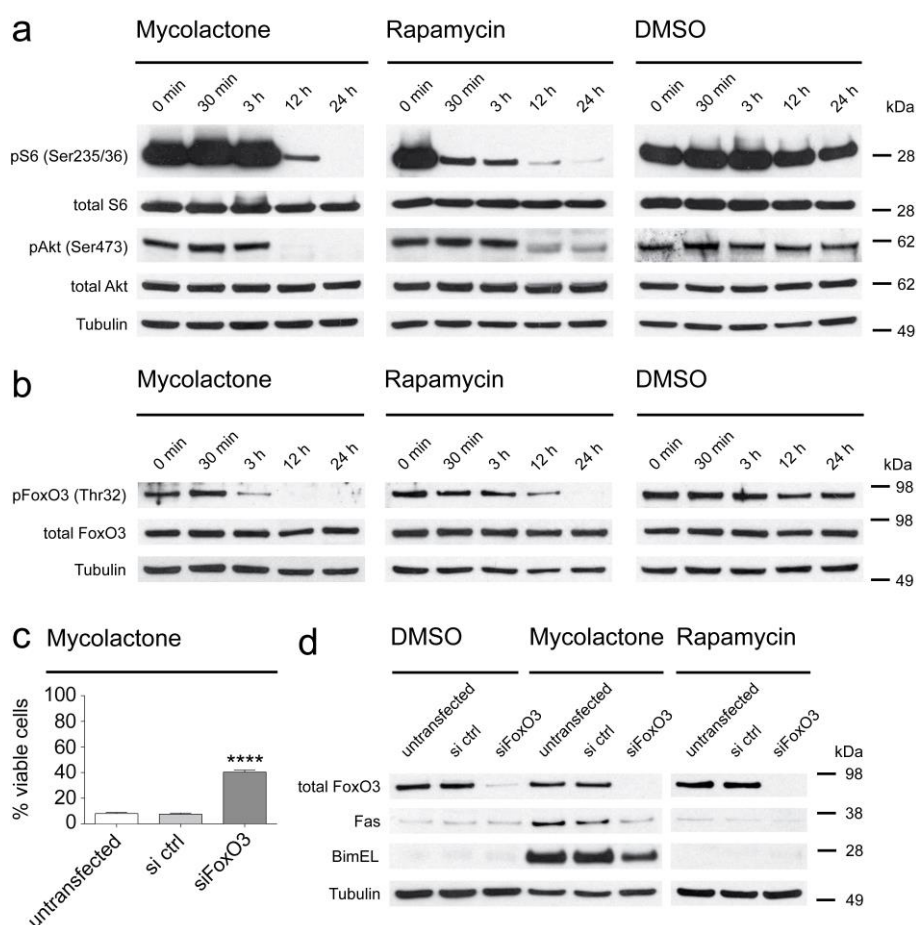


Figure 3: Mycolactone is an mTOR inhibitor and induces Bim-dependent apoptosis via the mTORC2-Akt-FoxO3 signaling axis.

(a) Mycolactone is a potent mTORC1/2 inhibitor. Western blot analysis for phospho-S6 ribosomal protein (Ser235/236) (pS6 (Ser235/36)), total S6 ribosomal protein (total S6), phospho-Akt (Ser473) (pAkt (Ser473)) and total Akt in L929 fibroblasts treated with 80 nM mycolactone (left), 80 nM rapamycin- (middle) or DMSO (right). (b-d) Mycolactone-induced mTORC2 inhibition results in dephosphorylation and activation of the transcription factor FoxO3, subsequent up-regulation of Bim and Fas and finally in Bim-dependent apoptosis. (b) Akt-dependent phosphorylation of the transcription factor FoxO3 is inhibited in mycolactone-treated cells, resulting in its transcriptional activation. Western blot analysis for phospho-FoxO3 (Thr32) (pFoxO3 (Thr32)) and total FoxO3 in L929 fibroblasts treated with 80 nM mycolactone (left), 80 nM rapamycin (middle) or DMSO (right). (c) Knockdown of FoxO3 protects L929 fibroblasts from mycolactone-induced apoptosis. Cells were transfected with 30 nM siRNA control (si

ctrl) or siFoxO3 6 h prior to mycolactone treatment and cell viability was assessed by FACS. Mean values across duplicate samples are shown, and the error bars represent the s.d. of three independent experiments. Two-tailed Student's t test. ****, $P \leq 0.0001$. **(d)** Knockdown of FoxO3 in L929 fibroblasts resulted in a strong decrease of the two FoxO3 targets Fas and Bim as demonstrated by Western blot for total FoxO3, Fas and Bim 24 h after addition of 80 nM mycolactone or DMSO. Western blot data in **(a,b,d)** are representative of three independent experiments. α -Tubulin served as loading control.

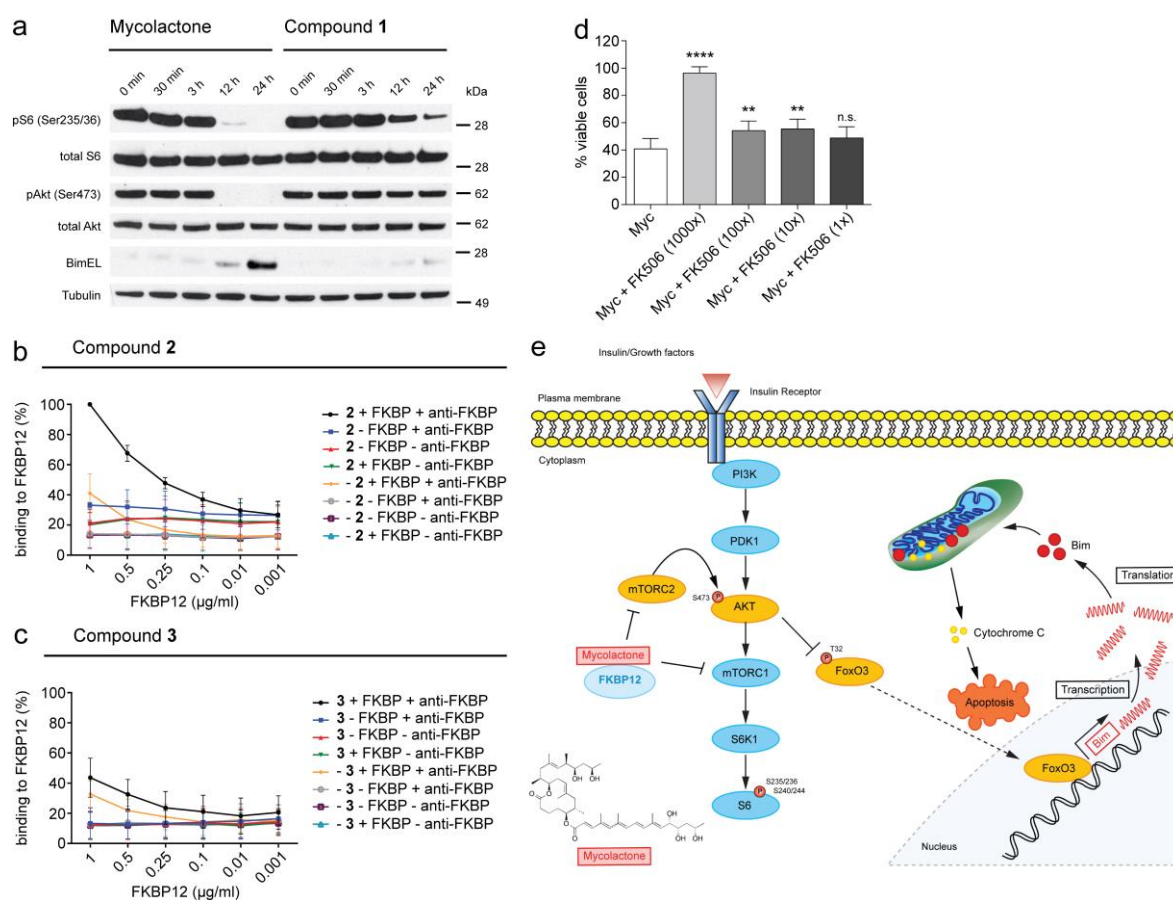


Figure 4: Mycolactone-induced apoptosis is dependent on the interaction with the 12-kDa FK506-binding protein (FKBP12).

(a) Cells treated with compound **1** showed no mTORC1/2 inhibition and no up-regulation of Bim. Western blot analysis for pS6 (Ser235/236), total S6, pAkt (Ser473), total Akt and Bim in L929 fibroblasts treated with 80 nM mycolactone or **1**. α -Tubulin served as loading control. Western blot data are representative of three independent experiments. (b,c) Recombinant human FKBP12 protein binds to compound **2** (b), but not to compound **3** (c) as shown by ELISA. The graphs show mean values across duplicate samples, and the error bars represent the s.d. of three independent experiments. (d) Treatment with the FKBP12 binding competitor FK506 (Tacrolimus) protects L929 fibroblasts from mycolactone-induced apoptosis. Cells were treated with mycolactone in combination with FK506 at a molar ratio of 1/1000 (1000x), 1/100 (100x), 1/10 (10x) and 1/1 (1x) and cell viability was assessed by FACS analysis. Mean values across duplicate samples are shown, and the error bars represent the s.d. of three independent experiments. Two-tailed Student's t test. ****, $P \leq 0.0001$, **, $P \leq 0.01$, n. s.,

not significant. (e) Model of the mycolactone-induced apoptosis pathway. FKBP12, 12-kDa FK506-binding protein; mTORC1, 2, mammalian target of rapamycin complex 1, 2; AKT, serine/threonine protein kinase AKT (protein kinase B); FoxO3, Forkhead box O3; Bim, Bcl-2-like protein 11; PI3K, Phosphatidylinositol-4,5-bisphosphate 3-kinase; PDK1, 3-Phosphoinositide-dependent protein kinase-1; S6K1, ribosomal protein S6 kinase beta-1; S6, ribosomal protein S6.

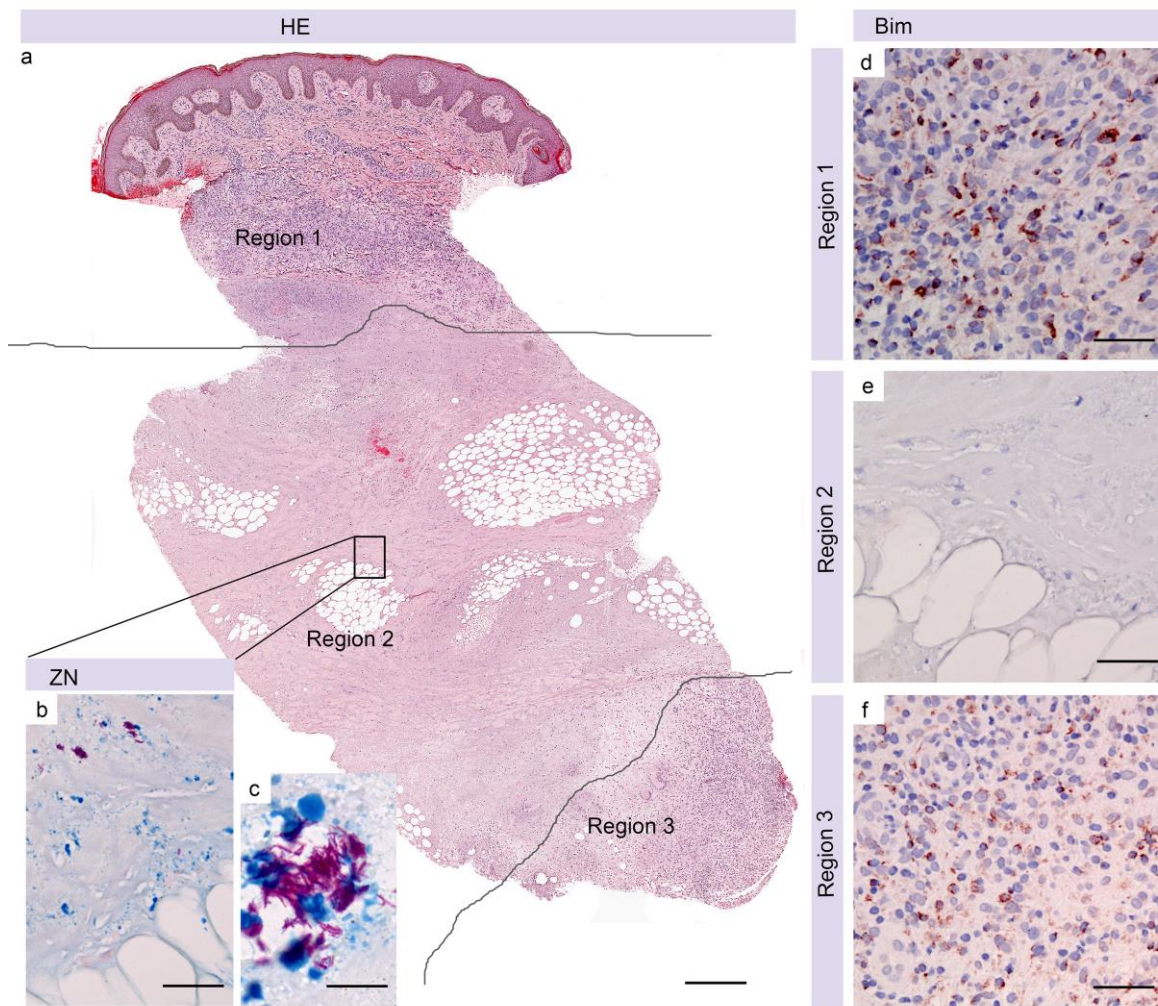


Figure 5: High expression levels of Bim in human BU lesions.

(a-f) Histological sections of a punch biopsy were either stained with Haematoxylin-Eosin (HE) (a), Ziehl-Neelsen (ZN) to stain for mycobacteria (b,c) or with an anti-Bim antibody (d-f), counterstain Haematoxylin. (a) Punch biopsy of a lesion with typical histopathological hallmarks of a BU infection: large necrotic areas, fat cell ghosts, absence of infiltration (Region 2) in the necrotic core and the presence of solid stained acid-fast bacilli (b,c). The necrotic core is surrounded by infiltrating immune cells (Region 1, Region 3). No intact (and no Bim-positive) cells are present in the necrotic core (Region 2, e). Bim-positive cells were found in large numbers in the infiltrated regions (d,e). Scale bars, 350 μm (a), 40 μm (b, d-f), 11 μm (c).

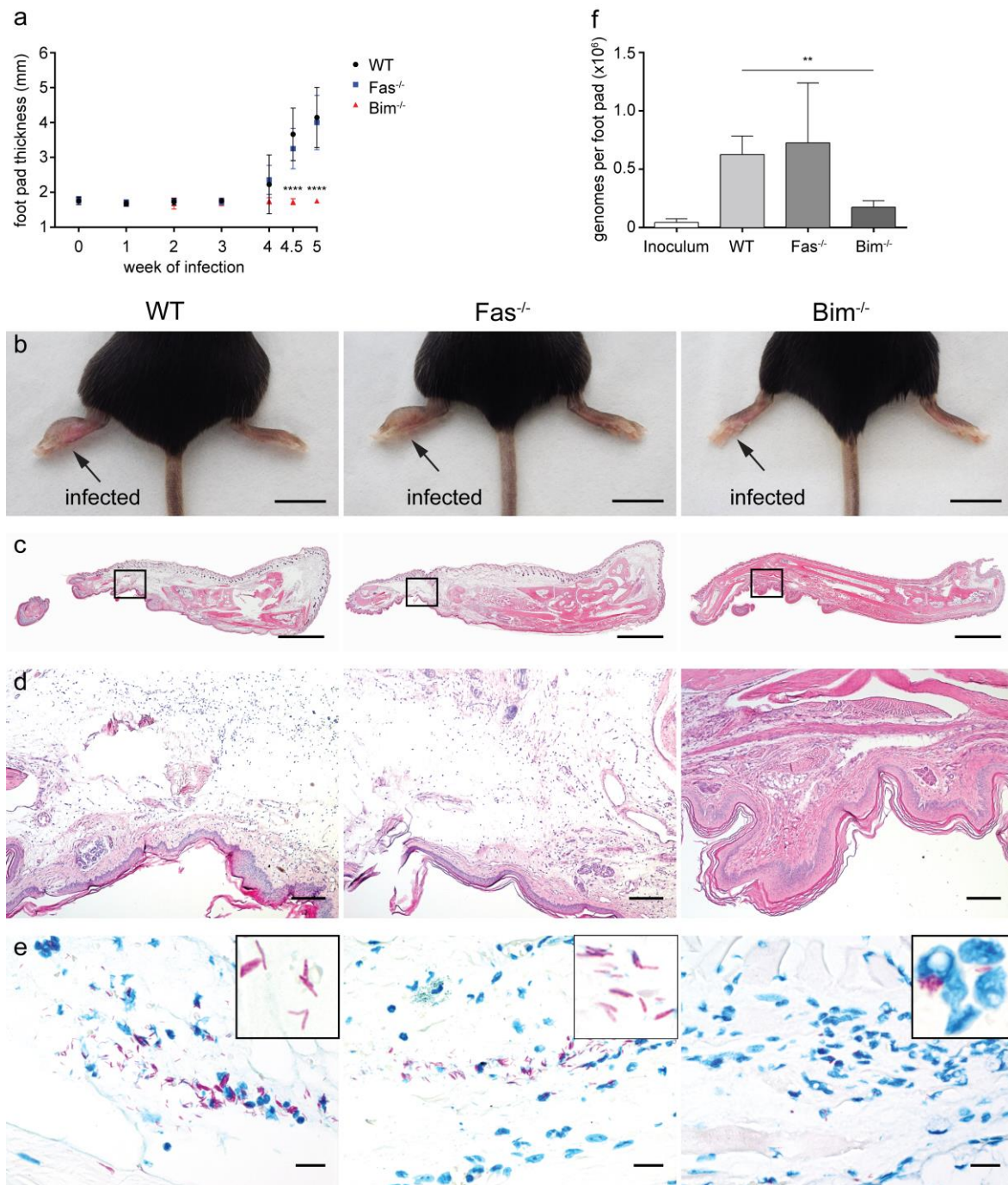
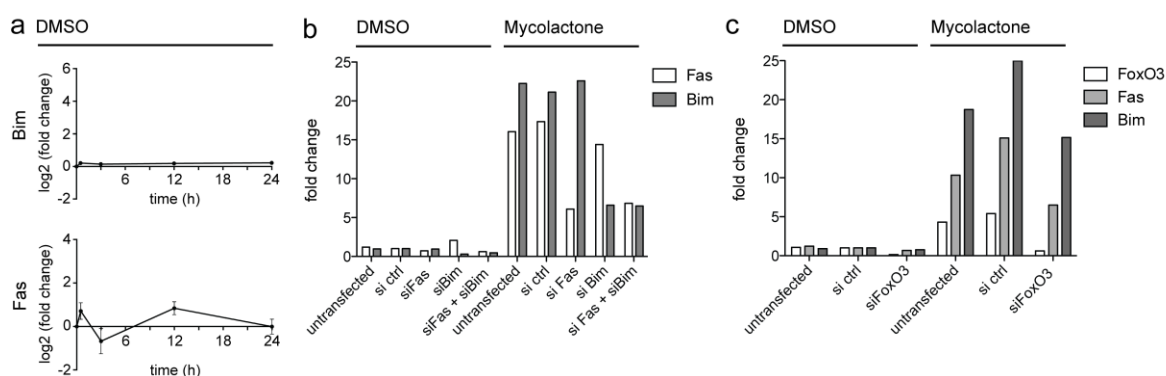


Figure 6: Bim knockout mice are resistant to the pathogenesis of BU.

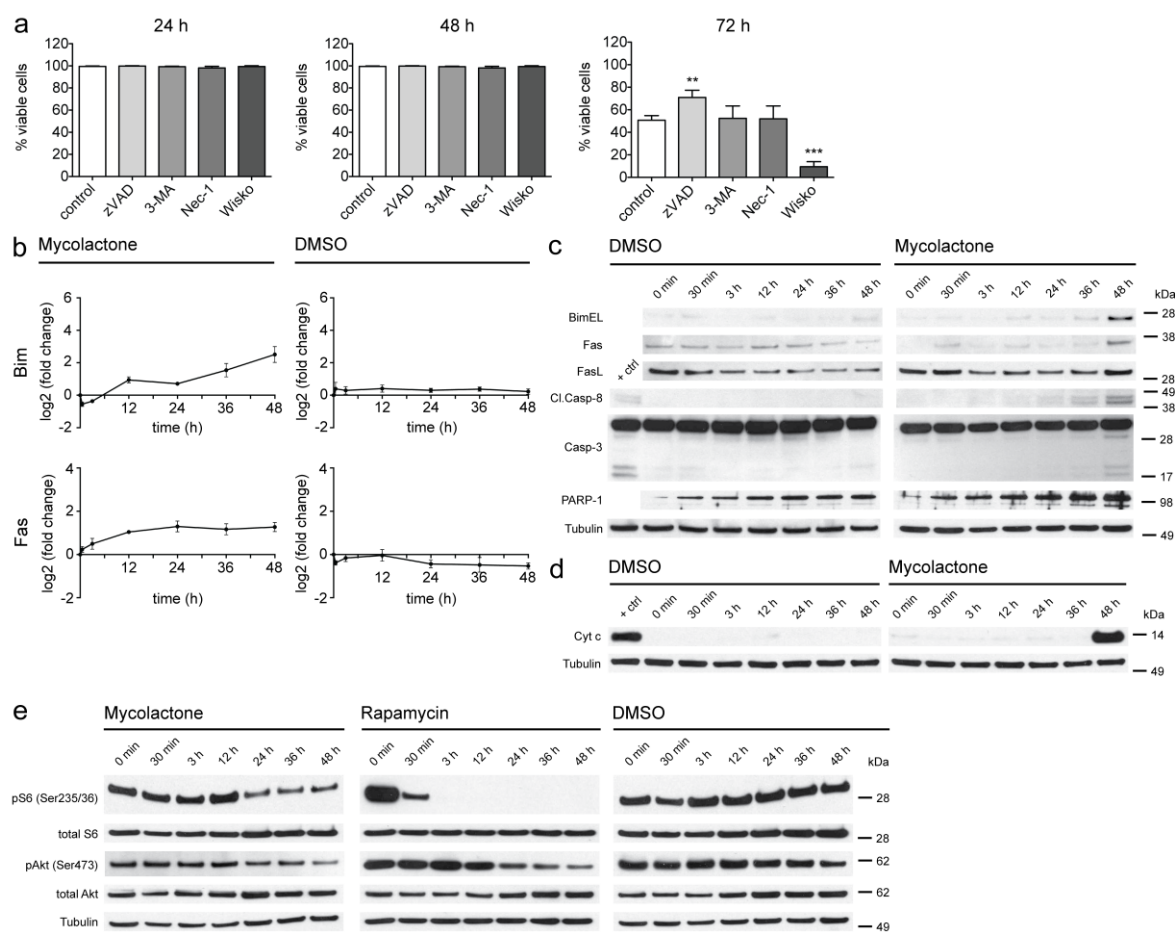
(a-f) Left hind foot pads of 8 week old female C57Bl/6 wild-type (WT), Fas homozygous knockout (Fas^{-/-}) and Bim homozygous knockout (Bim^{-/-}) mice were infected with *M. ulcerans*. (a) Progression of the infection as determined by weekly measurements of the foot pad thickness. Mean values are shown; the error bars represent the s.d. (n = 6 per genotype). (b) Representative images of a WT (left), Fas^{-/-} (middle) and Bim^{-/-} (right)

mouse 5 weeks after infection. Scale bars, 1 cm. **(c-e)** Histologic sections of foot pads from mice infected with *M. ulcerans* stained with Hematoxylin/Eosin (HE) **(c,d)** or Ziehl-Neelsen/Methylene blue (ZN) to stain for mycobacteria **(e)**. **(f)** Quantification of *M. ulcerans* in foot pad lysates by quantitative RT-PCR for the insertion sequence IS2404. Genomes per foot pad are shown. Values are displayed as mean, the error bars represent the s.d. (n = 3 per genotype). Scale bars, 1 cm **(b)**, 3 mm **(c)**, 160 μm **(d)**, 20 μm **(e)**. P values in **a** and **f** were calculated using two-tailed Student's t test. ****, $P \leq 0.0001$, **, $P \leq 0.01$.



Supplementary Figure 1: Mycolactone up-regulates Bim and Fas mRNA expression via activation of FoxO3.

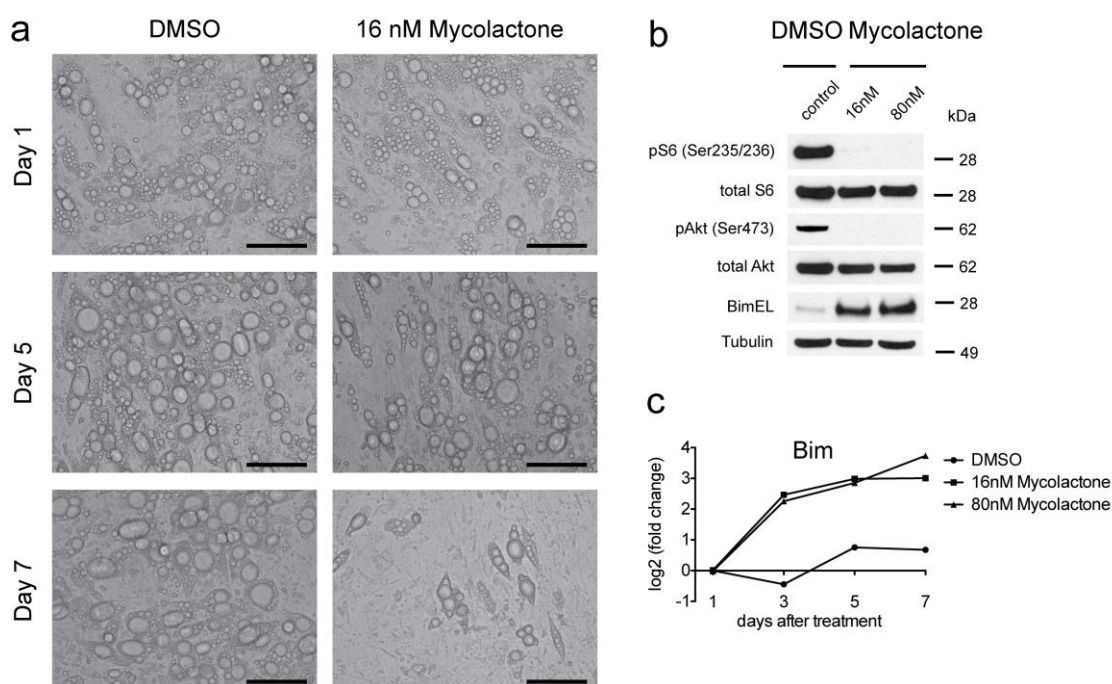
(a) Stable Bim and Fas mRNA expression levels in DMSO control L929 fibroblasts. mRNA expression was assessed over time by qRT-PCR. Values are displayed as log₂ (fold change). Mean values across duplicate samples are displayed, and error bars represent the s.d. **(b)** Determination of Fas and Bim knockdown efficiencies in transfected L929 fibroblasts by qRT-PCR. Fas and Bim mRNA expression levels were assessed 24 h after treatment with 80 nM mycolactone or DMSO. **(c)** Knockdown of FoxO3 in L929 fibroblasts results in a strong decrease of Fas and Bim. FoxO3, Fas and Bim mRNA expression 24 h after addition of 80 nM mycolactone or DMSO as determined by qRT-PCR. Values in **(b,c)** are shown as fold change, one of two independent similar experiment is shown.



Supplementary Figure 2: Mycolactone is an mTORC1/2 inhibitor and induces FoxO3- and Bim-dependent apoptosis in the more resistant Jurkat cells.

(a) Mycolactone-treated Jurkat cells die by apoptosis. Jurkat cells were pre-treated for 1 h with 10 μ M zVAD, 200 μ M 3-MA, 10 μ M Nec-1 or 1 μ M Wisko prior to the addition mycolactone. Cell viability was assessed by FACS analysis after 24 (left), 48 (middle) and 72 (right) hours. The bar graphs display mean values across duplicate samples, and the error bars represent the s.d. of three independent experiments. Two-tailed Student's t test. **, $P \leq 0.01$; ***, $P \leq 0.001$. **(b,c)** Mycolactone up-regulates Bim and Fas in Jurkat cells. **(b)** Up-regulation of Bim and Fas mRNA expression in mycolactone-treated (left) but not in DMSO-treated (right) cells as determined by qRT-PCR. Values are displayed as log₂ (fold change). Mean values across duplicate samples are shown, and error bars represent the s.d. **(c)** Up-regulation of Bim and Fas protein levels, and the detection of cleaved caspase-8, downstream caspase-3 and PARP-1 as determined by Western blot. **(d)** Cytochrome c release from mitochondria in Jurkat cells. Cytochrome c levels were

analyzed by Western blot using cytoplasmic fractions of Jurkat cells treated with mycolactone or DMSO. Whole cell lysates of mycolactone-treated Jurkat cells (48 h) served as positive control (+ ctrl). **(e)** Mycolactone acts as an mTORC1/2 inhibitor in Jurkat cells. Western blot analysis for phospho-S6 ribosomal protein (Ser235/236) (pS6 (Ser235/36)), total S6 ribosomal protein (total S6), phospho-Akt (Ser473) (pAkt (Ser473)) and total Akt in Jurkat cells treated with 80 nM mycolactone (left), 80 nM rapamycin (middle) or DMSO (right). Western blots in **(c-e)** are representative of three independent experiments. α -Tubulin served as loading control.



Supplementary Figure 3: Treatment of primary human adipocytes with mycolactone results in complete inhibition of mTORC1/2 and the up-regulation of Bim.

(a) Phase contrast microscopy images of primary human adipocytes treated for 1, 5 or 7 days with 16 nM mycolactone or DMSO. Bars, 100 μ m. (b) Mycolactone treatment of primary human adipocytes induces complete mTORC1/2 inhibition and a strong up-regulation of Bim. Western blot analysis of primary human adipocytes whole cell lysates for pS6 (Ser235/236), total S6, pAkt (Ser473), total Akt and Bim after 5 days treatment with 16 nM or 80 nM mycolactone or DMSO control. α -Tubulin served as loading control. (c) Up-regulation of Bim mRNA expression levels by mycolactone in primary human adipocytes as determined by qRT-PCR. Cells were either treated with 16 nM or 80 nM mycolactone or DMSO. Values are displayed as log₂ (fold change). One of two independent similar experiments is shown.

Methods

Compounds

The synthesis of mycolactone A/B, compound **1** and key intermediate **4** have been described previously [17,18]. The synthesis of biotin conjugates **2** and **3** starting from **4** is described in detail in Supplementary Schemes S1 – S3 (Appendix Chapter 1). All intermediates were fully characterized and all final compounds were purified by preparative HPLC.

Cell culture, flow cytometric analysis, siRNA transfection and competition with FK506

L929 fibroblasts were purchased from ATCC and Jurkat cells were a kind gift from J.-P. Bourquin's laboratory (University of Zurich). Cells were grown in RPMI 1640 medium supplemented with 10 % heat-inactivated FCS (Sigma) and 2 mM glutamine and incubated at 37 °C and 5 % CO₂.

For all experiments, highly defined synthetic mycolactone A/B (mycolactone) [17] dissolved in DMSO was used, an attractive alternative to the commonly used heterogeneous extracts purified by lipid chromatography. For all experiments, toxin-free DMSO at a concentration of 0.012 % served as solvent control.

For flow cytometric analysis, 24'000 L929 fibroblasts or 100'000 Jurkat cells were seeded into 24-well plates. L929 cells were allowed to adhere overnight, whereas Jurkat cells were plated directly prior to mycolactone treatment. Synthetic mycolactone (80 nM) or DMSO (control) were added in a volume of 600 µl medium. For experiments involving additional inhibitors, cells were pre-treated for 1 h with indicated concentrations of zVAD.fmk (Promega), 3-Methyladenine (Sigma), Necrostatin-1 (Sigma) or wiskostatin (Sigma) prior to mycolactone addition. Inhibitors were re-fed every 24 h. For flow cytometric analysis, cells were stained with Annexin V-FITC and PI (AnnexinV kit, Calbiochem) according to the manufacturer's recommendations. Stained cells were analyzed by flow cytometry using a BD FACS Calibur Flow Cytometer at indicated times and cell death was quantified using the CellQuest Pro Software (Becton Dickinson).

For the generation of transient knockdowns, L929 fibroblasts were transfected with si ctrl (ON-TARGETplus Non-targeting Pool, Thermo Scientific), siFas, siBim or siFoxO3 (ON-TARGETplus SMART Pool siRNAs, Thermo Scientific) with a final concentration of 10 nM using HiPerFect® Transfection Reagent (Qiagen) following the manufacturer's instructions. Six hours after transfection, cells were adherent and mycolactone was added. Cell death was quantified 48 h after transfection by Annexin V / PI staining and flow cytometric analysis as described above. Fas, Bim and FoxO3 expression levels of transfected cells were analyzed by quantitative RT-PCR and by Western Blot.

siRNA target sequences used: siFas: 5'-GUAAAUACAUCCCGAGAAU-3', 5'-CGAUGAAGAGCAUGGUUUA-3', 5'-GAAAUCGCCUAUGGUUGUU-3' and 5'-GUGAAACCAUACCAAUGAA-3', siBim: 5'-GGAGACGAGUUCAACGAAA-3', 5'-UUACAACUGUUACGCUUUA-3', 5'-GAAGACCACCCUCAAUUGG-3' and 5'-GCAACCUUCUGAUGUAAGU-3' and siFoxO3: 5'-UCGCAACGAUCCAAUGAUG-3', 5'-CCACAGCGACGUCAUGAUG-3', 5'-GGAGUUUGGUCAAUCAGAA-3' and 5'-GUGCAAACCUUCCCGUCAU-3'.

For the FK506 competition experiments, cells were pre-treated for 1 h with indicated concentrations of FK506 (Invivogen) or DMSO solvent control before addition of 20 nM mycolactone. FK506 was re-fed every 12 h and cell viability was assessed after 36 h by Annexin V / PI staining and flow cytometric analysis as described above.

Quantitative RT-PCR

For the quantitative RT-PCR screen, L929 fibroblasts were treated for indicated times with 80 nM mycolactone followed by total RNA extraction from cells using the RNeasy® Mini Kit (Qiagen), and reverse-transcribed in cDNA with the RT² First Strand Kit (Qiagen) according to the manufacturer's instructions. While extracting RNA, DNase treatment was performed using the RNase-Free DNase Set (Qiagen). The initial screening experiment (Supplementary Table 1, Appendix Chapter 1) was performed two times independently using the RT² Profiler™ PCR array system (Qiagen, Mouse Cell Death PathwayFinder™) on a StepOnePlus Real Time PCR System (Applied Biosystems) with RT² SYBR® green ROX™ qPCR Mastermix (Qiagen) according to the manufacturer's protocol. Transcript expression levels were normalized against the housekeeping genes actin beta (Actb), hypoxanthine-guanine phosphoribosyltransferase (Hprt) and heat

shock protein 90 kDa alpha, class B member 1 (Hsp90ab1) and displayed as fold changes or log2 (fold change). Up-regulation of Bcl2l11 (Bim) and Fas gene transcription in L929 fibroblasts was reconfirmed in a second step using newly designed primers and also assessed in Jurkat cells and primary human adipocytes. The following primers were used: mActb: fwd: 5'- CTCTGGCTCCTAGCACCATGAAGA-3', rev: 5'- GTAAAACGCAGCTCAGTAACAGTCCG-3', mHprt: fwd: 5'- TCCTCCTCAGACCGCTTTT-3', rev: 5'-CCTGGTTCATCATCGCTAATC-3', mHsp90ab1: fwd: 5'-TACTCGGCTTTCCCGTCA-3', rev: 5'-GCCTGAAAGGCAAAGGTCT-3', mFas: fwd: 5'- AAACCAGACTTCTACTGCGATTCT-3', rev: 5'- GGGTTCCATGTTCCACACGA-3', mBim: fwd: 5'-GGAGACGAGTTCAACGAAACTT-3', rev: 5'-AACAGTTGTAAGATAACCATTTGAGG-3', hActb: fwd: 5'-GCACAGAGCCTCGCCTT-3', rev: 5'-CCTTGCACATGCCGGAG-3', hHprt: fwd: 5'-TGACCTTGATTTATTTTGCATACC-3', rev: 5'-CGAGCAAGACGTTTCAGTCCT-3', hHsp90ab1: fwd: 5'-AACCGCATCTATCGCATGA-3', rev: 5'-CATCAGGAACTGCAGCATTG-3', hFas: 5'-GTGGACCCGCTCAGTACG-3', rev: 5'-TCTAGCAACAGACGTAAGAACCA-3', hBim: fwd: 5'-CATCGCGGTATTTCGGTTC-3', rev: 5'-GCTTTGCCATTTGGTCTTTTTT-3'. For determination of expression levels of transfected cells, the following primers were used: mFas, mBim (described above) and mFoxO3: fwd: 5'-GATAAGGGCGACAGCAACAG-3', rev: 5'-CATTCTGAACGCGCATGA-3'.

Western Blot

Cells were treated with indicated concentrations of mycolactone, rapamycin, compound **1** or DMSO and cell lysates were prepared at indicated time points in ice-cold RIPA-plus buffer (Sigma) complemented with 1 mM DTT, 1 mM NaF, 2 mM NaVO₄ and protease inhibitor cocktail (Sigma). Cell fractionation was performed using the Cell Fractionation Kit Standard (ab109719, abcam®).

For SDS-PAGE, equal amounts of cell lysates were loaded on precast 10 % Bis-Tris Gels (NuPAGE Novex®, Life Technologies) with MES running buffer and transferred to nitrocellulose membranes using the iBlot dry-blotting system (Novex®, Life Technologies) according to the manufacturer's recommendations. Membranes were blocked in 5 % milk in PBS/Tween-20 overnight at 4 °C and incubated with specific primary antibodies in 5 % BSA in TBS/Tween-20 overnight at 4 °C. Membranes were washed and incubated with peroxidase-conjugated secondary antibodies in 5 % milk PBS/Tween-20 for 1 h at room temperature. Blots were developed using the ECL

Western Blotting Substrate (Pierce). For phospho antibodies, the LumiGLO Reserve Substrate (KPL) was used. Antibodies used: Fas (AP00027PU-N, Acris), FasL (sc-6237, Santa Cruz Biotechnology), Bim (#2819, Cell Signaling), mouse Cleaved Caspase-8 (#8592, Cell Signaling), human Cleaved Caspase-8 (#9496, Cell Signaling), Cytochrome C (ab133504, abcam®), Caspase-3 (#9662, Cell Signaling), PARP-1 (sc-7150, Santa Cruz Biotechnology), pS6 (Ser235/236) (#2211, Cell Signaling), total S6 (#2217, Cell Signaling), pAkt (Ser473) (#9271, Cell Signaling), total Akt (#9272, Cell Signaling), pFoxO1 (Thr24) / pFoxO3 (Thr32) (#9464, Cell Signaling), total FoxO3 (#2497, Cell Signaling) and alpha-Tubulin (T9026, Sigma).

ELISA

NeutrAvidin Coated High Capacity Plates (Thermo Scientific) were blocked for 1 h with SuperBlock® T20 (TBS) Blocking Buffer (Thermo Scientific) and incubated for 2 h with 2 µg/ml compound **2** or **3** / TBS-T. Plates were subsequently washed with TBS-T, incubated for 1 h with recombinant human FKBP12 protein (Cayman Chemical) diluted in blocking buffer at indicated concentrations, washed again with TBS-T and incubated for 1 h with 0.33 µg/ml mouse anti-FKBP antibody (Sino Biological) diluted in blocking buffer. Plates were washed again with TBS-T and bound FKBP12 antibodies were detected using an Alkaline Phosphatase (AP) conjugated goat anti-mouse IgG antibody (Sigma) diluted 1:20'000 in blocking buffer and the Alkaline Phosphatase Yellow (pNPP) Liquid Substrate System (Sigma). The whole ELISA was performed at 37 °C and under light-protection.

Primary human adipocytes

Pools of subcutaneous human pre-adipocytes were purchased from Zen-Bio. Cells were expanded *in vitro* in DMEM / F12 (Sigma) containing 10 % heat-inactivated FBS, 1 % HEPES, 1 % sodium pyruvate, 1 % penicillin-streptomycin solution (Invitrogen) and 5 ng/ml bFGF (Sigma). When the pre-adipocytes reached confluence, cells were drifted to adipogenic differentiation by cultivating them for 14 days in DMEM / F12 medium supplemented with 10 % FBS, 1 % penicillin-streptomycin solution, 1 µM

Dexamethasone (Sigma), 0.5 mM 3-Isobutyl-1-Methylxanthine (Sigma), 100 μ M Indomethacin (Sigma) and 10 μ g/ml Actrapid HM (Novo Nordisk).

After 14 days, adipogenic differentiation was checked by performing an Oil Red O staining and cells were analyzed by quantitative RT-PCR, Western Blot and phase contrast microscopy.

For phase contrast microscopy, cells were treated for indicated times with 16 nM mycolactone or DMSO solvent control and analyzed at room temperature with an Olympus IX50 Osiris Microscope equipped with a LCPlanFL (40x/0.6) Objective (Olympus). Pictures were taken with a Colorview III camera (Olympus) and the CellSens 1.9 software (Olympus). For adjustment of brightness and contrast levels, Adobe Photoshop CS6 was used.

Immunohistochemistry

Punch biopsies of untreated laboratory reconfirmed Buruli ulcer patients were analyzed. The tissue was surgically removed and immediately transferred into 10 % neutral buffered formalin solution (4 % paraformaldehyde) for 24 h at room temperature (tissue fixation). Afterwards samples were stored and transported in 70 % ethanol, embedded into paraffin and cut into 5 μ m sections with a microtome.

After deparaffinization and rehydration sections were either directly stained with Haematoxylin/Eosin (HE) or Ziehl-Neelsen/Methylenblue (ZN) according to WHO standard protocols (see reference WHO diagnosis booklet) or further processed for immunohistochemistry (IHC). For IHC, antigen retrieval was performed with citrate buffer, pH 6.0, (Dako® Education guide: Immunohistochemical Staining methods). Endogenous peroxidase was inactivated by applying 0.3 % H₂O₂ for 20 min and prevention of unspecific binding was achieved by incubation with 1.5 % goat serum (Vectorlabs) for 30 min. Primary antibodies specific for Bim (#2933, Cell Signaling, 1:100) were diluted in phosphate buffered saline (PBS) containing 0.1 % Tween-20 and added to the slides for 1 h at room temperature. After incubation with a matching biotin-conjugated secondary antibody (goat anti-rabbit, #BA1000, Vectorlabs, 1:200) staining was performed using the Vector ABC elite and the NovaRED system (Vectorlabs). Haematoxylin (Sigma) was used as a counter stain.

Slides were analyzed at room temperature with a DM2500 Microscope (Leica) equipped with the Leica Okular HC Plan s (10x/25) and the Leica Objective HC PL Fluotar (20x/0.5) or the Leica Objective HCX PL Fluotar (100x/1.3, Leica Type N Immersion liquid). Pictures were taken either with an Aperio scanner or with a Leica DFC 420 camera and the Leica application Suite 4.3.0 software. For adjustment of brightness levels, Adobe Photoshop CS6 was used.

Mouse procedures

Mice were maintained in specific pathogen-free facilities at the école polytechnique fédérale de Lausanne (EPFL, Switzerland). All studies were performed under BSL-3 conditions either in 8 weeks old female C57Bl/6 wild type mice or mice homozygous for the lymphoproliferation spontaneous mutation (Fas^{lpr}) or homozygous Bim knockout mice ($Bcl2l1^{tm1.1Ast}$), respectively (Jackson Laboratory). For the infection of mice, the *M. ulcerans* strain S1013 isolated in 2010 from the ulcerative lesion of a Cameroonian BU patient was used [40]. Bacteria were grown for 6 weeks in Bac/T medium (Biomérieux, 251011), pelleted by centrifugation and resuspended in sterile PBS to a stock concentration of 125 mg/ml wet weight corresponding to 2.20×10^5 CFU/ml as determined by plating serial dilutions on 7H9 agar plates (Difco, 271310). Mice were subcutaneously infected with 30 μ l of a 1/100 dilution of the stock solution in sterile PBS into the hind left foot pad. Progression of the infection was followed by weekly measurements of the foot pad thickness using a caliper. At week 5, mice were euthanized and pictures of the feet were taken using a compact camera (WG-20, RICOH). Afterwards, foot pads were aseptically removed for determination of bacterial load by quantitative RT-PCR or for histopathological analysis.

Determination of bacterial load by quantitative RT-PCR

For preparation of foot pad lysates, mouse feet designated for quantification of *M. ulcerans* bacteria were removed above the ankle after euthanasia, cut into 4 pieces with a scalpel and transferred to hard tissue grinding tubes (MK28-R, Precellys, KT03961-1-008.2). Afterwards, 750 μ l sterile PBS was added and homogenization was performed using a Precellys 24-Dual tissue homogenizer (3 x 20 s at 5000 rpm with 30 s break).

The lysate was transferred into a new tube and the remaining, still intact tissue was homogenized for a second time after adding 750 µl of sterile PBS. After homogenization, the two lysates were pooled and used for DNA extraction.

DNA was isolated from 100 µl of a 1/20 dilution of the foot pad lysate as described by Lavender and Fyfe [32]. Isolated DNA was analyzed for IS2404 by quantitative RT-PCR as previously described [32]. Ct values were converted into number of genomes per foot pad by using the standard curve established by Fyfe *et al.* [41].

Histopathology

Mouse feet designated for histopathological analysis were removed above the ankle and transferred to 10 % neutral-buffered Formalin solution (4 % formaldehyde, Sigma, HT501128-4L) and fixed during 24 hours at room temperature. Afterwards, the feet were decalcified in 0.6 M EDTA and 0.25 M citric acid for 14 days at 37 °C and transferred to 70 % ETOH for storage. After dehydration and paraffin embedding, 5 µm thin sections were cut, de-paraffinised, rehydrated, and stained with Haematoxylin/Eosin (HE, Sigma, 51275-500ML, J.T. Baker, 3874) or Ziehl-Neelsen/Methylene blue (ZN, Sigma, 21820-1L and 03978-250ML) to stain for mycobacteria according to WHO standard protocols. Stained sections were mounted using Eukitt® mounting medium (Fluka, 03989) and pictures were taken with a Leica® DM2500B microscope or with an Aperio scanner.

Statistics

Two-sided Student's *t* test was used for statistical analysis (Prism GraphPad). We assumed normality and equal distribution of variance between the different groups compared.

Study approval

Analyzed human tissue samples were collected during another trial (ISRCTN72102977) and were reanalysed for the current purpose. Ethical approval for analyzing patient specimens was obtained from the National Ethics Committee of Cameroon and the

Ethics Committee of the Heidelberg University Hospital, Germany. Written informed consent from the patients or the guardians of the patients exists.

All animal experiments were approved by and performed according to the guidelines and regulations of the local animal welfare committee of the Canton of Vaud, Switzerland (authorization number 2657).

References

1. Demangel C, Stinear TP, Cole ST. Buruli ulcer: reductive evolution enhances pathogenicity of *Mycobacterium ulcerans*. *Nat Rev Microbiol*. 2009;7: 50–60. doi:10.1038/nrmicro2077
2. Guarner J, Bartlett J, Whitney EAS, Raghunathan PL, Stienstra Y, Asamo K, et al. Histopathologic features of *Mycobacterium ulcerans* infection. *Emerg Infect Dis*. 2003;9: 651–656.
3. Junghans T, Johnson RC, Pluschke G. 42 - *Mycobacterium ulcerans* Disease. *Manson's Tropical Infectious Diseases (Twenty-Third Edition)*. London: W.B. Saunders; 2014. pp. 519–531.e2. Available: <http://www.sciencedirect.com/science/article/pii/B9780702051012000431>. Accessed 9 November 2015.
4. George KM, Chatterjee D, Gunawardana G, Welty D, Hayman J, Lee R, et al. Mycolactone: a polyketide toxin from *Mycobacterium ulcerans* required for virulence. *Science*. 1999;283: 854–857.
5. Marion E, Song O-R, Christophe T, Babonneau J, Fenistein D, Eyer J, et al. Mycobacterial toxin induces analgesia in buruli ulcer by targeting the angiotensin pathways. *Cell*. 2014;157: 1565–1576. doi:10.1016/j.cell.2014.04.040
6. Gama JB, Ohlmeier S, Martins TG, Fraga AG, Sampaio-Marques B, Carvalho MA, et al. Proteomic analysis of the action of the *Mycobacterium ulcerans* toxin mycolactone: targeting host cells cytoskeleton and collagen. *PLoS Negl Trop Dis*. 2014;8: e3066. doi:10.1371/journal.pntd.0003066
7. Guenin-Macé L, Veyron-Churlet R, Thoulouze M-I, Romet-Lemonne G, Hong H, Leadlay PF, et al. Mycolactone activation of Wiskott-Aldrich syndrome proteins underpins Buruli ulcer formation. *J Clin Invest*. 2013;123: 1501–1512. doi:10.1172/JCI66576
8. Hall BS, Hill K, McKenna M, Ogbechi J, High S, Willis AE, et al. The Pathogenic Mechanism of the *Mycobacterium ulcerans* Virulence Factor, Mycolactone, Depends on Blockade of Protein Translocation into the ER. *PLoS Pathog*. 2014;10: e1004061. doi:10.1371/journal.ppat.1004061
9. Laplante M, Sabatini DM. mTOR signaling in growth control and disease. *Cell*. 2012;149: 274–293. doi:10.1016/j.cell.2012.03.017
10. Dazert E, Hall MN. mTOR signaling in disease. *Curr Opin Cell Biol*. 2011;23: 744–755. doi:10.1016/j.ceb.2011.09.003
11. Phung TL, Ziv K, Dabydeen D, Eyiah-Mensah G, Riveros M, Perruzzi C, et al. Pathological angiogenesis is induced by sustained Akt signaling and inhibited by rapamycin. *Cancer Cell*. 2006;10: 159–170. doi:10.1016/j.ccr.2006.07.003
12. Sarbassov DD, Ali SM, Sengupta S, Sheen J-H, Hsu PP, Bagley AF, et al. Prolonged rapamycin treatment inhibits mTORC2 assembly and Akt/PKB. *Mol Cell*. 2006;22: 159–168. doi:10.1016/j.molcel.2006.03.029
13. Sarbassov DD, Guertin DA, Ali SM, Sabatini DM. Phosphorylation and regulation of Akt/PKB by the rictor-mTOR complex. *Science*. 2005;307: 1098–1101. doi:10.1126/science.1106148
14. Guertin DA, Stevens DM, Thoreen CC, Burds AA, Kalaany NY, Moffat J, et al. Ablation in mice of the mTORC components raptor, rictor, or mLST8 reveals that mTORC2 is required for signaling to Akt-FOXO and PKC α , but not S6K1. *Dev Cell*. 2006;11: 859–871. doi:10.1016/j.devcel.2006.10.007
15. Janes MR, Limon JJ, So L, Chen J, Lim RJ, Chavez MA, et al. Effective and selective targeting of leukemia cells using a TORC1/2 kinase inhibitor. *Nat Med*. 2010;16: 205–213. doi:10.1038/nm.2091
16. Fu Z, Tindall DJ. FOXOs, cancer and regulation of apoptosis. *Oncogene*. 2008;27: 2312–2319. doi:10.1038/onc.2008.24
17. Gersbach P, Jantsch A, Feyen F, Scherr N, Dangy J-P, Pluschke G, et al. A ring-closing metathesis (RCM)-based approach to mycolactones A/B. *Chem Weinh Bergstr Ger*. 2011;17: 13017–13031. doi:10.1002/chem.201101799
18. Scherr N, Gersbach P, Dangy J-P, Bomio C, Li J, Altmann K-H, et al. Structure-Activity Relationship Studies on the Macrolide Exotoxin Mycolactone of *Mycobacterium ulcerans*. *PLoS Negl Trop Dis*. 2013;7: e2143. doi:10.1371/journal.pntd.0002143
19. Slee EA, Zhu H, Chow SC, MacFarlane M, Nicholson DW, Cohen GM. Benzylloxycarbonyl-Val-Ala-Asp (OMe) fluoromethylketone (Z-VAD.FMK) inhibits apoptosis by blocking the processing of CPP32. *Biochem J*. 1996;315: 21–24.

20. Wu Y-T, Tan H-L, Shui G, Bauvy C, Huang Q, Wenk MR, et al. Dual role of 3-methyladenine in modulation of autophagy via different temporal patterns of inhibition on class I and III phosphoinositide 3-kinase. *J Biol Chem*. 2010;285: 10850–10861. doi:10.1074/jbc.M109.080796
21. Lazebnik YA, Kaufmann SH, Desnoyers S, Poirier GG, Earnshaw WC. Cleavage of poly(ADP-ribose) polymerase by a proteinase with properties like ICE. *Nature*. 1994;371: 346–347. doi:10.1038/371346a0
22. Peterson JR, Lokey RS, Mitchison TJ, Kirschner MW. A chemical inhibitor of N-WASP reveals a new mechanism for targeting protein interactions. *Proc Natl Acad Sci*. 2001;98: 10624–10629. doi:10.1073/pnas.201393198
23. Willis SN, Fletcher JI, Kaufmann T, van Delft MF, Chen L, Czabotar PE, et al. Apoptosis initiated when BH3 ligands engage multiple Bcl-2 homologs, not Bax or Bak. *Science*. 2007;315: 856–859. doi:10.1126/science.1133289
24. Adams JM. Ways of dying: multiple pathways to apoptosis. *Genes Dev*. 2003;17: 2481–2495. doi:10.1101/gad.1126903
25. Tewari M, Quan LT, O'Rourke K, Desnoyers S, Zeng Z, Beidler DR, et al. Yama/ CPP32 beta, a mammalian homolog of CED-3, is a CrmA-inhibitable protease that cleaves the death substrate poly(ADP-ribose) polymerase. *Cell*. 1995;81: 801–809.
26. Yu K, Toral-Barza L, Shi C, Zhang W-G, Lucas J, Shor B, et al. Biochemical, cellular, and in vivo activity of novel ATP-competitive and selective inhibitors of the mammalian target of rapamycin. *Cancer Res*. 2009;69: 6232–6240. doi:10.1158/0008-5472.CAN-09-0299
27. Boulkroun S, Guenin-Macé L, Thoulouze M-I, Monot M, Merckx A, Langsley G, et al. Mycolactone suppresses T cell responsiveness by altering both early signaling and posttranslational events. *J Immunol Baltim Md 1950*. 2010;184: 1436–1444. doi:10.4049/jimmunol.0902854
28. Guenin-Macé L, Carrette F, Asperti-Boursin F, Bon AL, Caleechurn L, Bartolo VD, et al. Mycolactone impairs T cell homing by suppressing microRNA control of L-selectin expression. *Proc Natl Acad Sci*. 2011;108: 12833–12838. doi:10.1073/pnas.1016496108
29. Harding MW, Galat A, Uehling DE, Schreiber SL. A receptor for the immunosuppressant FK506 is a cis-trans peptidyl-prolyl isomerase. *Nature*. 1989;341: 758–760. doi:10.1038/341758a0
30. Siekierka JJ, Hung SH, Poe M, Lin CS, Sigal NH. A cytosolic binding protein for the immunosuppressant FK506 has peptidyl-prolyl isomerase activity but is distinct from cyclophilin. *Nature*. 1989;341: 755–757. doi:10.1038/341755a0
31. Galat A. Peptidylprolyl cis/trans isomerases (immunophilins): biological diversity--targets--functions. *Curr Top Med Chem*. 2003;3: 1315–1347.
32. Lavender CJ, Fyfe JAM. Direct detection of *Mycobacterium ulcerans* in clinical specimens and environmental samples. *Methods Mol Biol Clifton NJ*. 2013;943: 201–216. doi:10.1007/978-1-60327-353-4_13
33. Simmonds RE, Lali FV, Smallie T, Small PLC, Foxwell BM. Mycolactone inhibits monocyte cytokine production by a posttranscriptional mechanism. *J Immunol Baltim Md 1950*. 2009;182: 2194–2202. doi:10.4049/jimmunol.0802294
34. Hughes PD, Belz GT, Fortner KA, Budd RC, Strasser A, Bouillet P. Apoptosis regulators Fas and Bim cooperate in shutdown of chronic immune responses and prevention of autoimmunity. *Immunity*. 2008;28: 197–205. doi:10.1016/j.immuni.2007.12.017
35. Weant AE, Michalek RD, Khan IU, Holbrook BC, Willingham MC, Grayson JM. Apoptosis regulators Bim and Fas function concurrently to control autoimmunity and CD8+ T cell contraction. *Immunity*. 2008;28: 218–230. doi:10.1016/j.immuni.2007.12.014
36. Laplante M, Sabatini DM. mTOR signaling at a glance. *J Cell Sci*. 2009;122: 3589–3594. doi:10.1242/jcs.051011
37. Sarfo FS, Le Chevalier F, Aka N, Phillips RO, Amoako Y, Boneca IG, et al. Mycolactone diffuses into the peripheral blood of Buruli ulcer patients--implications for diagnosis and disease monitoring. *PLoS Negl Trop Dis*. 2011;5: e1237. doi:10.1371/journal.pntd.0001237

38. Coutanceau E, Decalf J, Martino A, Babon A, Winter N, Cole ST, et al. Selective suppression of dendritic cell functions by *Mycobacterium ulcerans* toxin mycolactone. *J Exp Med*. 2007;204: 1395–1403. doi:10.1084/jem.20070234
39. Yeboah-Manu D, Peduzzi E, Mensah-Quainoo E, Asante-Poku A, Ofori-Adjei D, Pluschke G, et al. Systemic suppression of interferon-gamma responses in Buruli ulcer patients resolves after surgical excision of the lesions caused by the extracellular pathogen *Mycobacterium ulcerans*. *J Leukoc Biol*. 2006;79: 1150–1156. doi:10.1189/jlb.1005581
40. Bratschi MW, Bolz M, Minyem JC, Grize L, Wantong FG, Kerber S, et al. Geographic distribution, age pattern and sites of lesions in a cohort of Buruli ulcer patients from the Mapé Basin of Cameroon. *PLoS Negl Trop Dis*. 2013;7: e2252. doi:10.1371/journal.pntd.0002252
41. Fyfe JAM, Lavender CJ, Johnson PDR, Globan M, Sievers A, Azuolas J, et al. Development and application of two multiplex real-time PCR assays for the detection of *Mycobacterium ulcerans* in clinical and environmental samples. *Appl Environ Microbiol*. 2007;73: 4733–4740. doi:10.1128/AEM.02971-06

Results Chapter 2

Interferon- γ is a Crucial Activator of Early Host Immune Defense against *Mycobacterium ulcerans* Infection in Mice

Raphael Bieri^{1,2}, Miriam Bolz^{1,2}, Marie-Thérèse Ruf^{1,2} and Gerd Pluschke^{1,2*}

¹Swiss Tropical and Public Health Institute, Socinstrasse 57, 4002 Basel, Switzerland

²University of Basel, Petersplatz 1, 4003 Basel, Switzerland

* Corresponding author

Article published in:
PLOS Neglected Tropical Diseases

Abstract

Buruli ulcer (BU), caused by infection with *Mycobacterium ulcerans*, is a chronic necrotizing human skin disease associated with the production of the cytotoxic macrolide exotoxin mycolactone. Little is known about the type of immune responses elicited against this pathogen and the effector functions conferring protection against BU. While histopathological analyses of advanced BU lesions have demonstrated a mainly extracellular localization of the toxin producing acid fast bacilli, there is growing evidence for an early intra-macrophage growth phase of *M. ulcerans*. This has led us to investigate whether interferon- γ might play an important role in containing *M. ulcerans* infections. In an experimental Buruli ulcer mouse model we found that interferon- γ is indeed a critical regulator of early host immune defense against *M. ulcerans* infections. Interferon- γ knockout mice displayed a faster progression of the infection compared to wild-type mice. This accelerated progression was reflected in faster and more extensive tissue necrosis and oedema formation, as well as in a significantly higher bacterial burden after five weeks of infection, indicating that mice lacking interferon- γ have a reduced capacity to kill intracellular bacilli during the early intra-macrophage growth phase of *M. ulcerans*.

This data demonstrates a prominent role of interferon- γ in early defense against *M. ulcerans* infection and supports the view that concepts for vaccine development against tuberculosis may also be valid for BU.

Author Summary

Mycobacterium ulcerans is the causative agent of Buruli ulcer (BU), a slow progressing ulcerative skin disease. The mode of transmission of *M. ulcerans* remains unknown and only little is known about the early stages of the disease and the nature of protective immune responses against this pathogen.

Given the increasing evidence for an early intracellular growth phase of *M. ulcerans*, we aimed at evaluating the impact of cell-mediated immunity for immunological defense against *M. ulcerans* infections. By comparing wild-type and interferon- γ -deficient mice in a BU mouse model, we could demonstrate that interferon- γ is a critical regulator of early host immune defense against *M. ulcerans* infections, indicative of an important role of early intracellular multiplication of the pathogen. In mice lacking interferon- γ the bacterial burden increased faster, resulting in accelerated pathogenesis. The observed differences between the two mouse strains were most likely due to differences in the capacity of macrophages to kill intracellular bacilli during the early stages of infection.

Introduction

Buruli ulcer (BU), caused by infection with *Mycobacterium ulcerans* (*M. ulcerans*), is a progressive disease of the skin and subcutaneous tissue. The disease is primarily affecting West African rural communities, but has also been reported from America, Australia and Asia. The pathogenesis of BU is mainly attributed to mycolactone, a macrolide exotoxin produced by *M. ulcerans* [1]. Mycolactone is essential for bacterial virulence and is highly cytotoxic for a wide range of mammalian cell types *in vitro* and *in vivo*, including fibroblasts, keratinocytes and adipocytes [1–4]. Injection of the toxin induces the formation of necrotic non-inflammatory lesions similar to BU lesions. Additionally to the induction of apoptosis, mycolactone possesses immunosuppressive characteristics and has been demonstrated to downregulate local and systemic immune responses [5,6], by interfering with the activation of immune cells such as T-cells, dendritic cells, monocytes and macrophages [7–10]. Furthermore, exposure to mycolactone results in complete inhibition of tumor necrosis factor alpha (TNF α) production by monocytes and macrophages, affects T-cell homing and interferes with the expression of T-cell receptors as well as co-stimulatory molecules including CD40 and CD86 [6–12].

Despite these immunosuppressive features of mycolactone, sera of individuals living in BU endemic regions frequently contain *M. ulcerans*-specific antibodies, demonstrating that many individuals develop immune responses associated with exposure to *M. ulcerans* without developing clinical disease [13,14]. Moreover, high mRNA levels for the cytokines interferon- γ (IFN γ), interleukin-1 β and TNF- α were found in human BU lesions, indicating that the innate immune system is activated at the site of infection [15]. Reports on spontaneous healing of BU [16,17], and a partial protective effect of Bacille Calmette-Guérin (BCG) vaccination in humans and experimentally infected mice [18–21] are all factors indicating that clearance of the *M. ulcerans* infection by the immune system is possible, in particular before large clusters of mycolactone producing extracellular bacteria have formed. These clusters are located in necrotic subcutaneous tissue of advanced BU lesions and are no longer reached by infiltrating leukocytes.

Antibodies against surface antigens of *M. ulcerans* do not seem to have a protective effect [22], indicating that cellular, and in particular type 1 helper (T_H1) cell responses [1,23] are more important in immune defense against BU than humoral responses.

IFN γ is critical for host defense against intracellular pathogens. In *Mycobacterium tuberculosis* (*M. tuberculosis*) infections, IFN γ produced by T_H1 cells, but also CD8 cytotoxic T (T_c) cells and NK cells, renders the macrophage competent to kill intracellular bacteria by overcoming the pathogen-induced block in phagosome-lysosome fusion and by producing microbicidal effectors such as nitric oxide (NO), resulting in host cell apoptosis and clearance of the bacteria [24–27]. In the early phase of an *M. ulcerans* infection an intra-macrophage growth phase seems to play an important role [6,28]. Protection mediated by IFN γ stimulated macrophages seems to be impaired by the suppression of IFN γ production after local build-up of mycolactone [29]. Here we have re-evaluated the role of IFN γ for host immune defense against *M. ulcerans* by comparing progression of the infection in IFN γ knockout and wild-type mice experimentally challenged with a fully virulent *M. ulcerans* isolate.

Methods

Ethical statement

This study was carried out in strict accordance with the Rules and Regulations for the Protection of Animal Rights (Tierschutzverordnung) of the Swiss Federal Food Safety and Veterinary Office. The protocol was granted ethical approval by the Veterinary Office of the county of Vaud, Switzerland (Authorization Number: 2657).

Mouse procedures

Mice were kept in specific pathogen-free facilities at the Ecole Polytechnique Fédérale de Lausanne (EPFL), Switzerland. All experiments were performed under BSL-3 conditions either in 8 weeks old female C57Bl/6 wild type mice or mice homozygous for the *Ifng^{tm1Ts}* targeted mutation (*IFN γ ^{-/-}*, B6.129S7-*Ifng^{tm1Ts}*/J, Jackson Laboratory). Animals were infected with the *M. ulcerans* strain S1013 isolated in 2010 from the ulcerative lesion of a BU patient from Cameroon [30]. The bacteria were cultivated from a low passage cell bank for six weeks in Bac/T medium (Biomerieux, 251011), pelleted by centrifugation and diluted in sterile PBS to a stock concentration of 125 mg/ml wet weight. Mice were infected subcutaneously into the hind left foot pad with 30 μ l (about 1×10^4 bacilli) of an appropriate dilution of the stock suspension in sterile PBS. Progression of the infection was followed by weekly measurements of the food pad thickness using a caliper. At weeks 1, 3, 5 and 8, groups of mice were euthanized and pictures of the feet were taken using a compact camera (WG-20, RICOH). The food pads were aseptically removed for determination of the bacterial load by quantitative real-time PCR (qPCR) or for histopathological analysis.

Determination of bacterial load by qPCR

Feet designated for the quantification of *M. ulcerans* were cut into 4 pieces using a scalpel and transferred to hard tissue grinding tubes (MK28-R, Precellys, KT03961-1-008.2). Next, 750 μ l sterile PBS was added and feet were homogenized using a Precellys 24-Dual tissue homogenizer (3 x 20 s at 5000 rpm with 30 s break). The lysates were transferred into new tubes and the remaining tissues were homogenized for a second

time after adding 750 µl of sterile PBS. The two lysates were pooled and used for DNA isolation. The DNA was extracted from 100 µl of a 1/20 dilution of the foot pad lysates as described by Lavender and Fyfe [31] and the isolated DNA was analyzed for insertion sequence (IS) 2404 by qPCR as previously described [31]. The number of genomes per foot pad was calculated according to the standard curve established by Fyfe *et al.* [32].

Histopathology

Mouse feet used for histopathological analysis were fixed in 10 % neutral-buffered formalin solution (4 % formaldehyde, Sigma, HT501128-4L) for 24 hours at room temperature, decalcified in 0.6 M EDTA and 0.25 M citric acid for 14 days at 37 °C and transferred to 70 % EtOH for storage. After dehydration and embedding in paraffin, 5 µm thin sections were cut. Sections were then deparaffinised, rehydrated, and stained with Haematoxylin/Eosin (HE, Sigma, 51275-500ML, J.T. Baker, 3874) or Ziehl-Neelsen/Methylene blue (ZN, Sigma, 21820-1L and 03978-250ML) to stain for mycobacteria according to WHO standard protocols [33]. Finally, the sections were mounted with Eukitt mounting medium (Fluka, 03989) and pictures were taken with an Aperio scanner or with a Leica DM2500B microscope.

Western Blot analysis

10 µg of *M. ulcerans* whole cell lysate was resolved on a 1-well 4-12 % gradient gel (NuPAGE Novex 4-12 % Bis-Tris Gel, Invitrogen, NP0330BOX) using MES running buffer and transferred to nitrocellulose membranes with the iBlot dry-blotting system (Novex, Life Technologies) according to the manufacturer's recommendations. The membrane was blocked in 5 % skim milk / PBS overnight at 4 °C, cut into thin strips and incubated with the indicated sera diluted 1:400 in 1 % skim milk / PBS-Tween-20 for 1.5 hours. After washing in 1 % skim milk / PBS-Tween-20, the membrane was incubated for 1 hour with HRP-conjugated goat anti-mouse IgG γ -chain secondary antibody (Southern Biotech, 1030-05) diluted 1:4000 in 1 % skim milk / PBS-Tween-20. Blots were developed using the ECL Western Blotting Substrate (Pierce, 32106).

Statistics

For statistical analysis, Student's *t* test was used (Prism GraphPad). We assumed normality and equal distribution of variance between the different groups analyzed.

Results

***M. ulcerans* infections progress faster in mice lacking IFN γ**

In order to evaluate the role of IFN γ in host immune defense against *M. ulcerans* infections, we infected 8 weeks old female C57Bl/6 wild-type (WT) mice and mice homozygous for the *Ifng*^{tm1Ts} targeted mutation (IFN γ ^{-/-}) into the left hind foot pad with 1×10^4 *M. ulcerans* bacilli. Progression of the disease was followed by weekly measurements of the foot pad thickness with a caliper. While all IFN γ ^{-/-} mice displayed strong swelling of the infected foot pads after 5 weeks of infection, no swelling was observed for the WT animals (Fig 1A). Six weeks after infection, some of the WT animals also started to show swelling of the infected feet. However, there was still a significant difference in foot pad thickness between the two different groups, which only resolved by week 8 (Fig 1A).

Complementary to the determination of the foot pad thickness, we documented the disease progression with pictures of the infected feet at 1, 3, 5 and 8 weeks after infection (Fig 1B). At week 5 infected foot pads of the WT mice did not show any macroscopic difference to the non-infected right control foot pads (Fig 1B). In contrast, the infected feet of the IFN γ ^{-/-} mice were swollen and showed signs of inflammation (Fig 1B). Although the difference in the food pad thickness resolved after 8 weeks of infection, the infected feet of the IFN γ ^{-/-} animals were more inflamed and clearly more ravaged at this time point (Fig 1B).

IFN γ -deficient mice display more extensive tissue necrosis and oedema formation than WT mice

Histopathological analysis of representative foot pads was performed to evaluate whether the increased foot pad thickness in IFN γ ^{-/-} mice at week 5 was caused by cellular infiltration or mainly by oedema formation. While no changes in tissue integrity were observed after 1 week of infection in both groups (Fig 2, A1-A3 and B1-B3), IFN γ ^{-/-} mice displayed massive oedema formation and tissue necrosis after 5 weeks of infection (Fig 2, B5, B4 and B6, respectively). Both are typical hallmarks of BU pathogenesis [34,35]. In contrast, the foot pads of the WT animals were devoid of oedema formation or tissue necrosis at this time point (Fig 2, A4-A6). Eight weeks after infection the foot

pads of the IFN γ ^{-/-} mice were still more oedematous and necrotic than those of the WT animals and the infection even affected the adjacent joints and legs (Fig 2, A7-A9 and B7-B9).

Enhanced bacterial multiplication in IFN γ -deficient mice

Next, we assessed whether the more severe course of *M. ulcerans* infection in the IFN γ ^{-/-} mice was associated with a higher bacterial burden in these animals. The bacterial load in footpads of WT and mutant mice was determined 1, 3, 5 and 8 weeks after infection by qPCR [22,31,32]. Strikingly, the bacterial load in the mice lacking IFN γ was significantly (3.5 fold) higher after 5 weeks of infection than in WT mice (Fig 3A), correlating with the strong foot pad swelling observed at this time point in only the mutant mice (Fig 1, A and B). As for the foot pad thickness, the differences in the bacterial load had resolved 8 weeks after infection (Fig 3A).

To reconfirm the qPCR results we stained tissue sections of whole foot pads with ZN to detect AFB. After 3 weeks of infection, only few AFB were found which were predominantly intracellular (Fig 3, B1 and B2). As for the qPCR analysis (Fig 3A), no difference in the total number of AFB was observed between the two groups at this time point. However, a trend to less extracellular bacterial debris and more viable extracellular bacilli was observed for IFN γ ^{-/-} foot pads at this time (S1 Fig).

In contrast, more AFB were detected in the IFN γ ^{-/-} mice 5 weeks after infection (Fig 3, C3 and C4), as compared to the WT controls (Fig 3, C1 and C2), which was again correlating with the results of the qPCR analysis (Fig 3A). At this time point, AFB were present as a mix of intra- and extracellular bacteria (Fig 3C). Interestingly, while the bacterial load was different for the two groups at this time point, no marked differences in the total cell infiltration was observed (Fig 3C). In line with the findings from the qPCR analysis (Fig 3A), the differences in the bacterial load had resolved 8 weeks after infection (S2 Fig).

Lack of antibody responses against *M. ulcerans* after 5 and 8 weeks of infection

To evaluate whether the stronger increase in the bacterial load between weeks 3 and 5 in the IFN γ ^{-/-} mice (Fig 3A) was caused by a diminished innate immune response as a

result of the lack activating IFN γ or rather by reduced antibody-mediated immune responses against *M. ulcerans*, we tested the reactivity of sera of infected mice with *M. ulcerans* whole cell lysates by Western Blot analysis. A complete absence of specific antibodies was observed both for WT and IFN γ ^{-/-} mice after 5 and 8 weeks of infection (Fig 4). Together with the observed presence of less extracellular debris in IFN γ ^{-/-} mice during the early phase of the infection (S1 Fig), this indicates that CMI is critical for host immunity against *M. ulcerans* infections.

Discussion

Evidence for an early intra-macrophage growth phase of *M. ulcerans* has led to the suggestion that the immune effector mechanisms protecting against *M. ulcerans* infection are similar to those active against *M. tuberculosis* [36–38]. However, in contrast to this closely related pathogen, *M. ulcerans* has the capacity to produce the cytotoxic macrolide mycolactone, which eventually kills the host cells and causes the characteristic necrotizing pathology of BU [1,35]. In the case of *M. tuberculosis* infection, the host immune response involves cell-mediated immunity (CMI) accompanied by a delayed type hypersensitivity (DTH) reaction [39]. Similarly, several reports showed that CMI and DTH responses are frequently induced in BU patients [38,40–45].

If CMI is required for immunological defense against *M. ulcerans* infections, IFN γ which is produced primarily by T_H1, but also by T_C and NK cells, is likely to play a critical role in this process by activating macrophages to kill intracellular bacteria at an early stage of infection. To test this hypothesis, we have used an experimental BU mouse model and compared the disease progression in WT and IFN γ ^{-/-} mice during active infection with a highly virulent *M. ulcerans* strain recently isolated from the lesion of a BU patient [30]. Our study conclusively demonstrates a key role of IFN γ for early immune defense against *M. ulcerans* infection *in vivo*, as mice lacking this cytokine suffered from an accelerated and more severe pathology associated with a significantly higher bacterial burden after 5 weeks of infection. These results indicate that CMI and IFN γ -dependent activation of the bactericidal activity of macrophages helps to contain the infection during its largely intracellular early stages. Further support for this hypothesis came from our histopathological analysis, where a trend to lower levels of extracellular acid-fast debris was found in the IFN γ ^{-/-} mice at the early intracellular stages of the infection. Moreover, these findings are in line with the observation of *Torrado et al.* who have reported that IFN γ -dependent phagosome maturation and NO production are required to control the intracellular proliferation of *M. ulcerans in vitro* [29]. In the same report, it is described, that IFN γ -deficient mice show increased susceptibility only for mycolactone-negative or intermediate virulent, but not for highly virulent *M. ulcerans* strains [29]. However, these at first view contradictory results can be explained by the fact that the mice infected by *Torrado et al.* with a highly virulent *M. ulcerans* strain were only monitored over a period of 20 days post infection, a time frame that is too narrow

to detect the differences between WT and IFN γ ^{-/-} mice, as we did not observe them before 5 weeks of infection.

In conclusion, our results indicate that the outcome of an infection with *M. ulcerans* may depend strongly on cellular immune defense mechanisms. IFN γ is likely to play an important role both as an element of innate immunity in the very early phase of host-pathogen interaction after inoculation and also in the subsequent development of protective adaptive cellular immune responses. Innate and adaptive immune defense mechanisms seem to be strong enough in the majority of exposed individuals living in BU endemic areas to protect them from developing clinical disease [13,14]. However, when the immune response of an individual is too weak to kill the intracellular bacteria, BU disease may develop. Intracellular multiplication of the bacteria may take place and small accumulations of bacteria found as globus-like structures [46,47] may represent the origin for the formation of large clusters of mycolactone producing *M. ulcerans* bacteria. As a result of mycolactone-induced host cell apoptosis, necrotic areas are forming around the bacteria. Furthermore, in the advanced BU lesions viable leukocyte infiltrates are no longer found close to the infection foci in the necrotic subcutaneous tissue, indicating that the accumulation of mycolactone is preventing macrophages and other defense cells from reaching the now extracellular pathogens before they are killed. As a result, a chronic *M. ulcerans* infection may develop, leading to the formation of large BU lesions, often resulting in severe morbidity and disability and requiring long and costly hospitalization [35].

Acknowledgements

We would like to thank Dr. Masato Murakami, Vincent Romanet, Caroline Stork, Patricia Barzaghi Rinaudo and Ernesta Dammassa from Novartis Basel for their technical support and providing access to the lab equipment for histopathology as well as Peter Schmid for the Aperio scans of the foot pads.

Figures

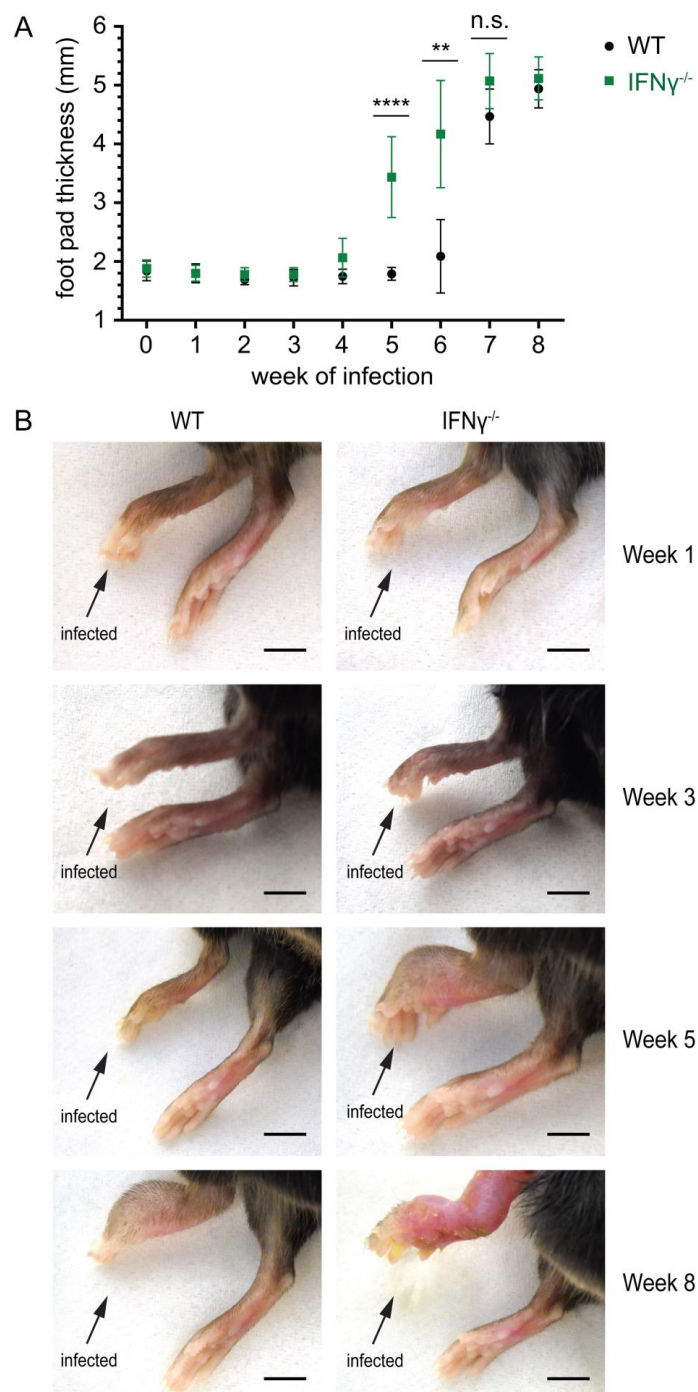


Fig 1. Faster progression of *M. ulcerans* infection in IFN γ -deficient mice.

WT and IFN $\gamma^{-/-}$ mice were infected into the left hind foot pad with *M. ulcerans* and the progression of the disease was followed by weekly measurements of the food pad thickness (A) and documented with pictures of the infected feet (B). (A) IFN $\gamma^{-/-}$ mice

exhibited an accelerated progression of *M. ulcerans* infection. At weeks 5 and 6, the foot pad thickness was significantly higher in IFN γ ^{-/-} mice than in WT animals. Mean values of the foot pad thickness (mm) are shown, the error bars represent the S.D.. P values were calculated using two-tailed Student's t test. ****, P \leq 0.0001, **, P \leq 0.01, n.s., not significant. (B) Pictures of representative feet taken 1, 3, 5 and 8 weeks after infection. At week 5, all mice deficient for IFN γ ^{-/-} had swollen feet. No swelling was observed in WT mice at this time point. Eight weeks after infection, foot pad swelling was observed for both WT and IFN γ ^{-/-} mice but the macroscopic disease symptoms were more severe in mice lacking IFN γ . Scale bars represent 5 mm.

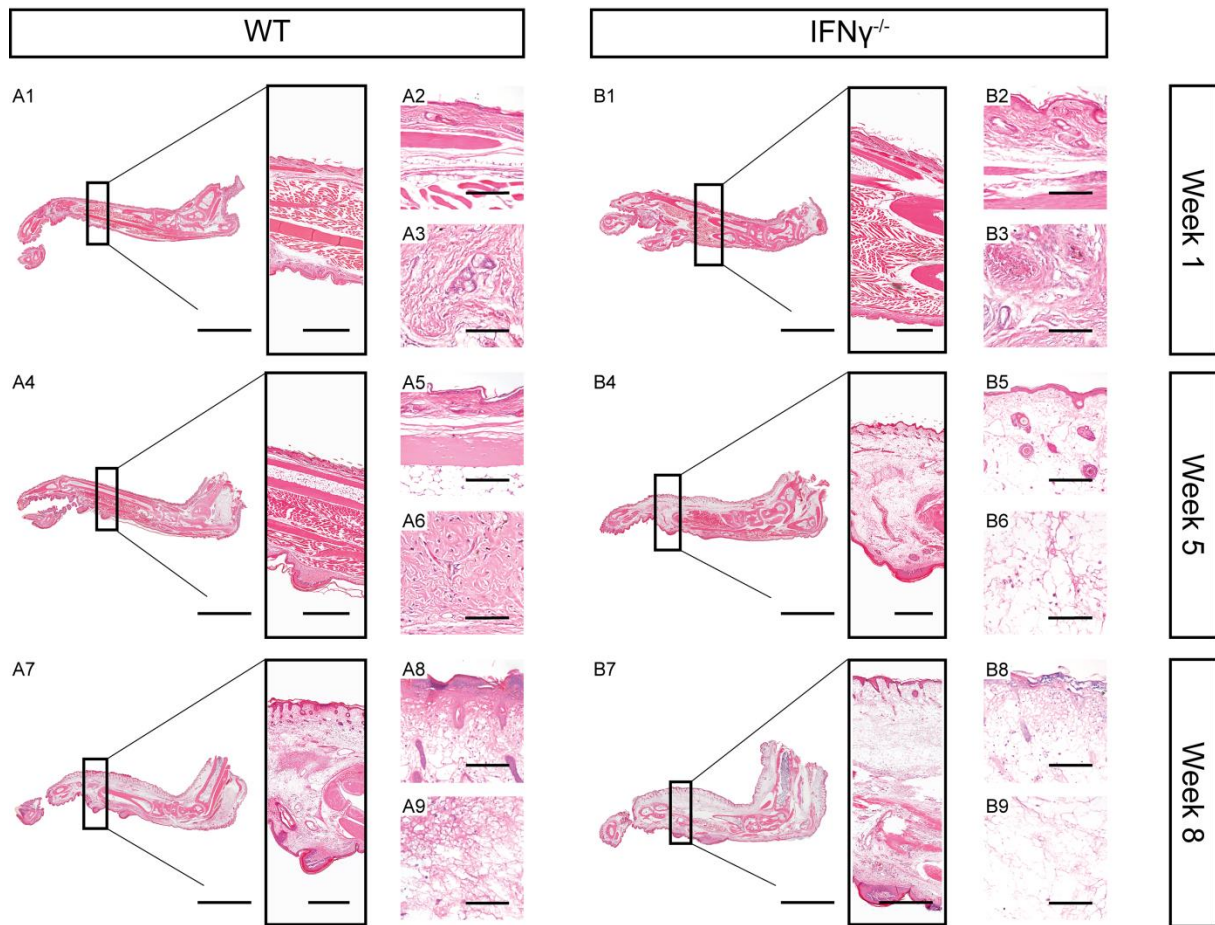


Fig 2. Extensive tissue necrosis and oedema formation in mice lacking IFN γ .

HE stained histologic sections of foot pads from representative WT (A) and IFN γ ^{-/-} (B) mice 1, 5 and 8 weeks after infection with *M. ulcerans*. Scale bars represent 5 mm (A1, A4, A7, B1, B4 and B7, left), 1 mm (A1, A4, A7, B1, B4 and B7, box), 150 μ m (A2, A5, A8, B2, B5 and B8) and 80 μ m (A3, A6, A9, B3, B6 and B9).

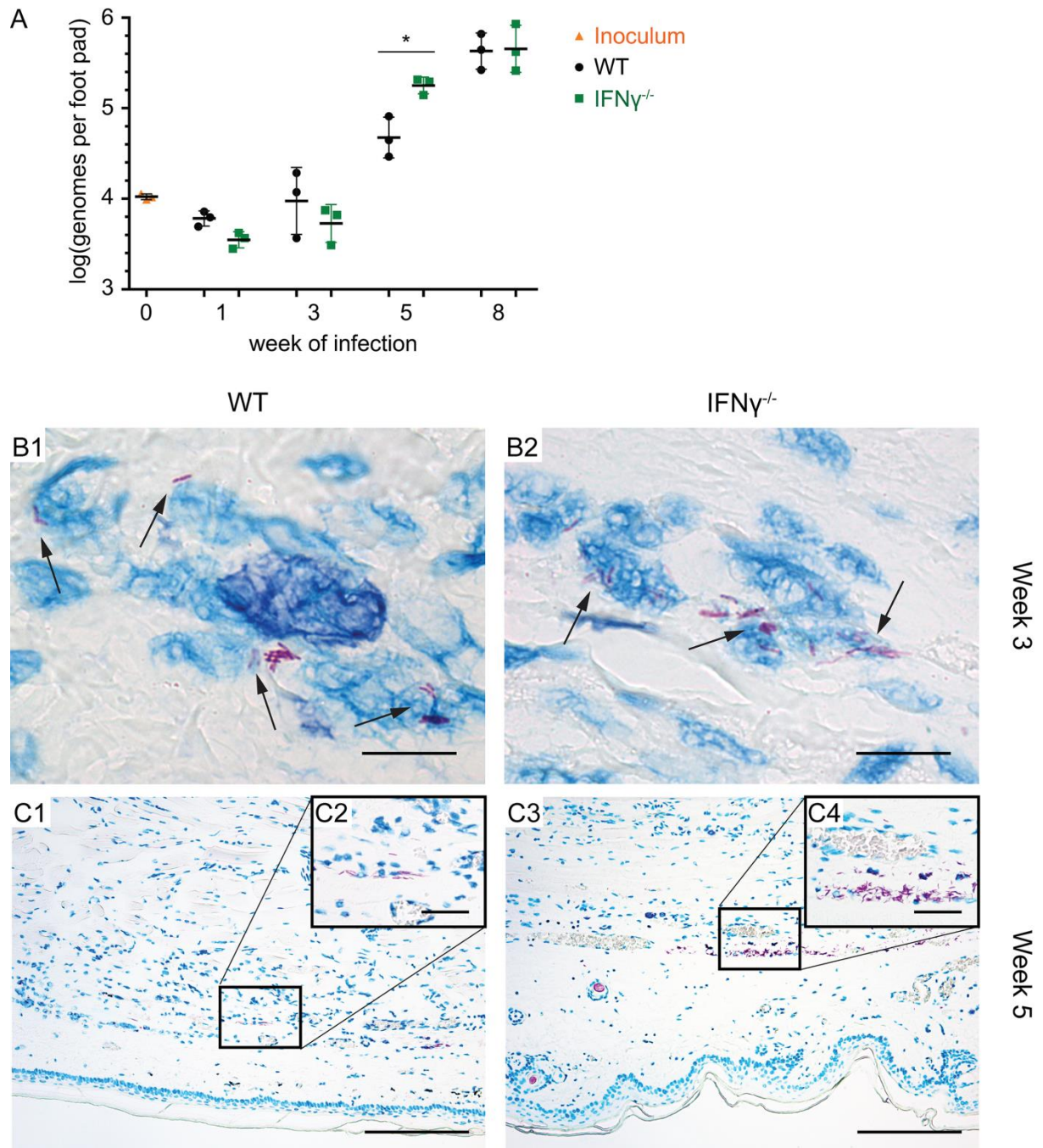


Fig 3. IFN γ -deficient mice have a significantly higher bacterial burden 5 weeks after infection.

WT and IFN γ ^{-/-} mice were infected with *M. ulcerans* and the bacterial load was determined by IS2404-specific qPCR (A). The distribution of AFB in the footpads was assessed by histopathological analysis at week 3 (B) and week 5 (C). (A) IFN γ ^{-/-} mice had a significantly higher bacterial burden as compared to WT animals 5 weeks after infection with *M. ulcerans*. Values are displayed as mean, the error bars represent the

S.D. (n = 3 per genotype). P values were calculated using two-tailed Student's t test. *, P ≤ 0.05. (B and C) 5 μm tissue sections of foot pads from representative WT (left) and IFN γ ^{-/-} (right) mice stained with ZN for visualization of AFB after 3 (B) or 5 (C) weeks of infection. AFB were predominantly intracellular at week 3 (B1 and B2, black arrows) whereas a mix of intra- and extracellular bacilli was found after 5 weeks of infection (C). At week 5, more AFB were present in IFN γ ^{-/-} foot pads (C2 and C4), no difference in the total immune cell infiltration between the two groups was observed (C1 and C3). Scale bars represent 8 μm (B1 and B2), 160 μm (C1 and C3) and 40 μm (C2 and C4).

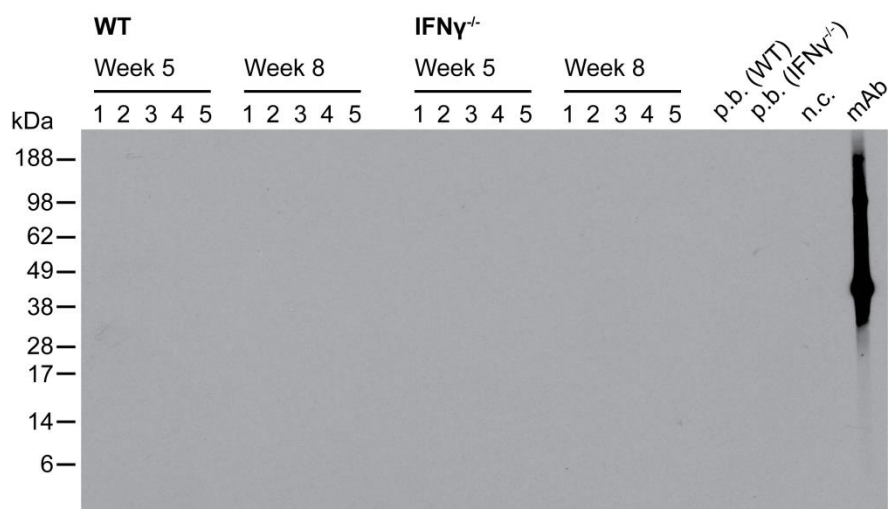
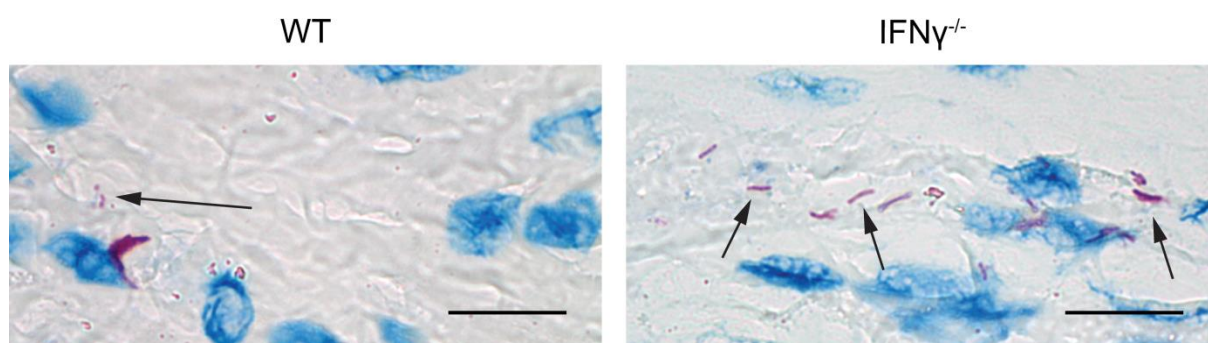


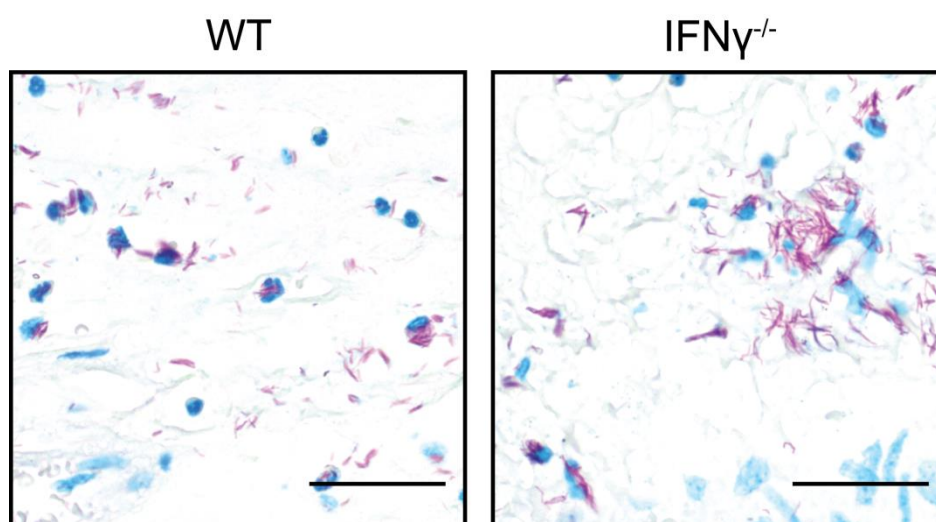
Fig 4. Absence of specific antibody responses against *M. ulcerans* in infected WT and IFN γ ^{-/-} mice.

Sera of WT and IFN γ ^{-/-} mice were analyzed 5 and 8 weeks after infection for the presence of specific IgG antibody responses against *M. ulcerans* by Western blotting on *M. ulcerans* whole cell lysate. A monoclonal antibody specific for the *M. ulcerans* antigen MUL3720 served as positive control.



S1 Fig. IFN γ -deficient mice show lower amounts of bacterial debris and higher numbers of intact extracellular bacteria 3 weeks after infection.

Histologic analysis of foot pad sections from representative WT (left) and IFN γ ^{-/-} (right) infected for 3 weeks of infection with *M. ulcerans*. Arrows indicate bacterial debris (left) or intact AFB (right). Scale bars, 8 μ m.



S2 Fig. No differences in the amount of AFB after 8 weeks of infection.

Histologic sections of foot pads from representative WT (left) and IFN γ ^{-/-} (right) mice infected for 8 weeks with *M. ulcerans* stained with ZN for AFB visualization. Scale bars, 30 μ m.

References

1. Demangel C, Stinear TP, Cole ST. Buruli ulcer: reductive evolution enhances pathogenicity of *Mycobacterium ulcerans*. *Nat Rev Microbiol*. 2009;7: 50–60. doi:10.1038/nrmicro2077
2. George KM, Chatterjee D, Gunawardana G, Welty D, Hayman J, Lee R, et al. Mycolactone: a polyketide toxin from *Mycobacterium ulcerans* required for virulence. *Science*. 1999;283: 854–857.
3. Bolz M, Ruggli N, Ruf M-T, Ricklin ME, Zimmer G, Pluschke G. Experimental infection of the pig with *Mycobacterium ulcerans*: a novel model for studying the pathogenesis of Buruli ulcer disease. *PLoS Negl Trop Dis*. 2014;8: e2968. doi:10.1371/journal.pntd.0002968
4. Hall B, Simmonds R. Pleiotropic molecular effects of the *Mycobacterium ulcerans* virulence factor mycolactone underlying the cell death and immunosuppression seen in Buruli ulcer. *Biochem Soc Trans*. 2014;42: 177–183. doi:10.1042/BST20130133
5. Adusumilli S, Mve-Obiang A, Sparer T, Meyers W, Hayman J, Small PLC. *Mycobacterium ulcerans* toxic macrolide, mycolactone modulates the host immune response and cellular location of *M. ulcerans* in vitro and in vivo. *Cell Microbiol*. 2005;7: 1295–1304. doi:10.1111/j.1462-5822.2005.00557.x
6. Coutanceau E, Marsollier L, Brosch R, Perret E, Goossens P, Tanguy M, et al. Modulation of the host immune response by a transient intracellular stage of *Mycobacterium ulcerans*: the contribution of endogenous mycolactone toxin. *Cell Microbiol*. 2005;7: 1187–1196. doi:10.1111/j.1462-5822.2005.00546.x
7. Simmonds RE, Lali FV, Smallie T, Small PLC, Foxwell BM. Mycolactone inhibits monocyte cytokine production by a posttranscriptional mechanism. *J Immunol Baltim Md 1950*. 2009;182: 2194–2202. doi:10.4049/jimmunol.0802294
8. Pahlevan AA, Wright DJ, Andrews C, George KM, Small PL, Foxwell BM. The inhibitory action of *Mycobacterium ulcerans* soluble factor on monocyte/T cell cytokine production and NF-kappa B function. *J Immunol Baltim Md 1950*. 1999;163: 3928–3935.
9. Coutanceau E, Decalf J, Martino A, Babon A, Winter N, Cole ST, et al. Selective suppression of dendritic cell functions by *Mycobacterium ulcerans* toxin mycolactone. *J Exp Med*. 2007;204: 1395–1403. doi:10.1084/jem.20070234
10. Boulkroun S, Guenin-Macé L, Thoulouze M-I, Monot M, Merckx A, Langsley G, et al. Mycolactone suppresses T cell responsiveness by altering both early signaling and posttranslational events. *J Immunol Baltim Md 1950*. 2010;184: 1436–1444. doi:10.4049/jimmunol.0902854
11. Torrado E, Adusumilli S, Fraga AG, Small PLC, Castro AG, Pedrosa J. Mycolactone-mediated inhibition of tumor necrosis factor production by macrophages infected with *Mycobacterium ulcerans* has implications for the control of infection. *Infect Immun*. 2007;75: 3979–3988. doi:10.1128/IAI.00290-07
12. Guenin-Macé L, Carrette F, Asperti-Boursin F, Bon AL, Caleechurn L, Bartolo VD, et al. Mycolactone impairs T cell homing by suppressing microRNA control of L-selectin expression. *Proc Natl Acad Sci*. 2011;108: 12833–12838. doi:10.1073/pnas.1016496108
13. Diaz D, Döbeli H, Yeboah-Manu D, Mensah-Quainoo E, Friedlein A, Soder N, et al. Use of the immunodominant 18-kiloDalton small heat shock protein as a serological marker for exposure to *Mycobacterium ulcerans*. *Clin Vaccine Immunol CVI*. 2006;13: 1314–1321. doi:10.1128/CVI.00254-06
14. Yeboah-Manu D, Röltgen K, Opore W, Asan-Ampah K, Quenin-Fosu K, Asante-Poku A, et al. Seroepidemiology as a tool to screen populations for exposure to *Mycobacterium ulcerans*. *PLoS Negl Trop Dis*. 2012;6: e1460. doi:10.1371/journal.pntd.0001460
15. Phillips R, Horsfield C, Mangan J, Laing K, Etuaful S, Awuah P, et al. Cytokine mRNA expression in *Mycobacterium ulcerans*-infected human skin and correlation with local inflammatory response. *Infect Immun*. 2006;74: 2917–2924. doi:10.1128/IAI.74.5.2917-2924.2006
16. Revill WD, Morrow RH, Pike MC, Ateng J. A controlled trial of the treatment of *Mycobacterium ulcerans* infection with clofazimine. *Lancet*. 1973;2: 873–877.

17. Gordon CL, Buntine JA, Hayman JA, Lavender CJ, Fyfe JA, Hosking P, et al. Spontaneous clearance of *Mycobacterium ulcerans* in a case of Buruli ulcer. *PLoS Negl Trop Dis*. 2011;5: e1290. doi:10.1371/journal.pntd.0001290
18. Dobos KM, Spotts EA, Marston BJ, Horsburgh CR, King CH. Serologic response to culture filtrate antigens of *Mycobacterium ulcerans* during Buruli ulcer disease. *Emerg Infect Dis*. 2000;6: 158–164. doi:10.3201/eid0602.000208
19. Okenu DMN, Ofielu LO, Easley KA, Guarner J, Spotts Whitney EA, Raghunathan PL, et al. Immunoglobulin M antibody responses to *Mycobacterium ulcerans* allow discrimination between cases of active Buruli ulcer disease and matched family controls in areas where the disease is endemic. *Clin Diagn Lab Immunol*. 2004;11: 387–391.
20. Smith PG, Revill WD, Lukwago E, Rykushin YP. The protective effect of BCG against *Mycobacterium ulcerans* disease: a controlled trial in an endemic area of Uganda. *Trans R Soc Trop Med Hyg*. 1976;70: 449–457.
21. Fraga AG, Martins TG, Torrado E, Huygen K, Portaels F, Silva MT, et al. Cellular immunity confers transient protection in experimental Buruli ulcer following BCG or mycolactone-negative *Mycobacterium ulcerans* vaccination. *PloS One*. 2012;7: e33406. doi:10.1371/journal.pone.0033406
22. Bolz M, Kerber S, Zimmer G, Pluschke G. Use of Recombinant Virus Replicon Particles for Vaccination against *Mycobacterium ulcerans* Disease. *PLoS Negl Trop Dis*. 2015;9: e0004011. doi:10.1371/journal.pntd.0004011
23. Einarsdottir T, Huygen K. Buruli ulcer. *Hum Vaccin*. 2011;7: 1198–1203. doi:10.4161/hv.7.11.17751
24. Ismail N, Olano JP, Feng H-M, Walker DH. Current status of immune mechanisms of killing of intracellular microorganisms. *FEMS Microbiol Lett*. 2002;207: 111–120.
25. Gutierrez MG, Master SS, Singh SB, Taylor GA, Colombo MI, Deretic V. Autophagy is a defense mechanism inhibiting BCG and *Mycobacterium tuberculosis* survival in infected macrophages. *Cell*. 2004;119: 753–766. doi:10.1016/j.cell.2004.11.038
26. Purdy GE, Russell DG. Lysosomal ubiquitin and the demise of *Mycobacterium tuberculosis*. *Cell Microbiol*. 2007;9: 2768–2774. doi:10.1111/j.1462-5822.2007.01039.x
27. Herbst S, Schaible UE, Schneider BE. Interferon Gamma Activated Macrophages Kill Mycobacteria by Nitric Oxide Induced Apoptosis. *PLoS ONE*. 2011;6: e19105. doi:10.1371/journal.pone.0019105
28. Torrado E, Fraga AG, Castro AG, Stragier P, Meyers WM, Portaels F, et al. Evidence for an intramacrophage growth phase of *Mycobacterium ulcerans*. *Infect Immun*. 2007;75: 977–987. doi:10.1128/IAI.00889-06
29. Torrado E, Fraga AG, Logarinho E, Martins TG, Carmona JA, Gama JB, et al. IFN-gamma-dependent activation of macrophages during experimental infections by *Mycobacterium ulcerans* is impaired by the toxin mycolactone. *J Immunol Baltim Md 1950*. 2010;184: 947–955. doi:10.4049/jimmunol.0902717
30. Bratschi MW, Bolz M, Minyem JC, Grize L, Wantong FG, Kerber S, et al. Geographic distribution, age pattern and sites of lesions in a cohort of Buruli ulcer patients from the Mapé Basin of Cameroon. *PLoS Negl Trop Dis*. 2013;7: e2252. doi:10.1371/journal.pntd.0002252
31. Lavender CJ, Fyfe JAM. Direct detection of *Mycobacterium ulcerans* in clinical specimens and environmental samples. *Methods Mol Biol Clifton NJ*. 2013;943: 201–216. doi:10.1007/978-1-60327-353-4_13
32. Fyfe JAM, Lavender CJ, Johnson PDR, Globan M, Sievers A, Azuolas J, et al. Development and application of two multiplex real-time PCR assays for the detection of *Mycobacterium ulcerans* in clinical and environmental samples. *Appl Environ Microbiol*. 2007;73: 4733–4740. doi:10.1128/AEM.02971-06
33. Portaels F, Organization WH. Laboratory diagnosis of buruli ulcer: a manual for health care providers. World Health Organization; 2014. Available: <http://apps.who.int/iris/handle/10665/111738>. Accessed 9 November 2015.
34. Guarner J, Bartlett J, Whitney EAS, Raghunathan PL, Stienstra Y, Asamo K, et al. Histopathologic features of *Mycobacterium ulcerans* infection. *Emerg Infect Dis*. 2003;9: 651–656.

35. Junghanss T, Johnson RC, Pluschke G. 42 - Mycobacterium ulcerans Disease. Manson's Tropical Infectious Diseases (Twenty-Third Edition). London: W.B. Saunders; 2014. pp. 519–531.e2. Available: <http://www.sciencedirect.com/science/article/pii/B9780702051012000431>. Accessed 9 November 2015.
36. Ernst JD. The immunological life cycle of tuberculosis. *Nat Rev Immunol*. 2012;12: 581–591. doi:10.1038/nri3259
37. O'Garra A, Redford PS, McNab FW, Bloom CI, Wilkinson RJ, Berry MPR. The immune response in tuberculosis. *Annu Rev Immunol*. 2013;31: 475–527. doi:10.1146/annurev-immunol-032712-095939
38. Phillips R, Horsfield C, Kuijper S, Sarfo SF, Obeng-Baah J, Etuaful S, et al. Cytokine Response to Antigen Stimulation of Whole Blood from Patients with Mycobacterium ulcerans Disease Compared to That from Patients with Tuberculosis. *Clin Vaccine Immunol*. 2006;13: 253–257. doi:10.1128/CVI.13.2.253-257.2006
39. Cooper AM. Cell-mediated immune responses in tuberculosis. *Annu Rev Immunol*. 2009;27: 393–422. doi:10.1146/annurev.immunol.021908.132703
40. Gooding TM, Johnson PDR, Smith M, Kemp AS, Robins-Browne RM. Cytokine Profiles of Patients Infected with Mycobacterium ulcerans and Unaffected Household Contacts. *Infect Immun*. 2002;70: 5562–5567. doi:10.1128/IAI.70.10.5562-5567.2002
41. Gooding TM, Kemp AS, Robins-Browne RM, Smith M, Johnson PDR. Acquired T-helper 1 Lymphocyte Energy Following Infection with Mycobacterium ulcerans. *Clin Infect Dis*. 2003;36: 1076–1077. doi:10.1086/368315
42. Prévot G, Bourreau E, Pascalis H, Pradinaud R, Tanghe A, Huygen K, et al. Differential production of systemic and intralésional gamma interferon and interleukin-10 in nodular and ulcerative forms of Buruli disease. *Infect Immun*. 2004;72: 958–965.
43. Kiszewski AE, Becerril E, Aguilar LD, Kader ITA, Myers W, Portaels F, et al. The local immune response in ulcerative lesions of Buruli disease. *Clin Exp Immunol*. 2006;143: 445–451. doi:10.1111/j.1365-2249.2006.03020.x
44. Westenbrink BD, Stienstra Y, Huitema MG, Thompson WA, Klutse EO, Ampadu EO, et al. Cytokine Responses to Stimulation of Whole Blood from Patients with Buruli Ulcer Disease in Ghana. *Clin Diagn Lab Immunol*. 2005;12: 125–129. doi:10.1128/CDLI.12.1.125-129.2005
45. Peduzzi E, Groeper C, Schütte D, Zajac P, Rondini S, Mensah-Quainoo E, et al. Local activation of the innate immune system in Buruli ulcer lesions. *J Invest Dermatol*. 2007;127: 638–645. doi:10.1038/sj.jid.5700593
46. Schütte D, UmBoock A, Pluschke G. Phagocytosis of Mycobacterium ulcerans in the course of rifampicin and streptomycin chemotherapy in Buruli ulcer lesions. *Br J Dermatol*. 2009;160: 273–283. doi:10.1111/j.1365-2133.2008.08879.x
47. Ruf M-T, Schütte D, Chauffour A, Jarlier V, Ji B, Pluschke G. Chemotherapy-associated changes of histopathological features of Mycobacterium ulcerans lesions in a Buruli ulcer mouse model. *Antimicrob Agents Chemother*. 2012;56: 687–696. doi:10.1128/AAC.05543-11

Results Chapter 3

The anti-TB drug candidate Q203 is highly active against Mycobacterium ulcerans, the causative agent of Buruli ulcer

Nicole Scherr^{1,2#}, Raphael Bieri^{1,2#}, Paul Schneide³, Kevin Pethe⁴, Matthias Witschel³, and
Gerd Pluschke^{1,2*}

¹Swiss Tropical and Public Health Institute, Socinstrasse 57, 4002 Basel, Switzerland

²University of Basel, Petersplatz 1, 4003 Basel, Switzerland

³BASF SE, Carl-Bosch-Strasse 38, 67056 Ludwigshafen, Germany

⁴Lee Kong Chian School of Medicine and School of Biological Sciences, Nanyang Technological University,
30 Biopolis Street, #B2-15a, Singapore 138671, Singapore

Contributed equally

* Corresponding author

Working Manuscript

Abstract

Imidazo(1,2- α)pyridine amines (IPA) represent one of the novel classes of compounds exhibiting high potency against *M. tuberculosis*. Among them, the TB drug candidate Q203 has outstanding activity and pharmacological properties. Here we tested Q203 and a pre-selected panel of IPA compounds for activity against *Mycobacterium ulcerans*, the causative agent of the neglected tropical skin disease Buruli ulcer (BU). We found several compounds with MIC values in the nanomolar range, outperformed however by Q203, which showed a MIC of <1 nM. Based on the promising *in vitro* activities, Q203 and IPA-7 were selected for *in vivo* testing in a mouse foot pad model of established BU infection. Q203, but not IPA-7, had a striking activity when administered orally three times per week at 0.5 mg/kg for a period of four weeks. While a strong increase in foot pad thickness was observed for the controls and the IPA-7 treated mice during the four week treatment course, Q203 caused a complete regression of foot pad swelling. Furthermore, histopathological analyses revealed absence of typical hallmarks of BU histopathology, such as tissue necrosis and edema formation after completion of Q203 treatment. These findings make Q203 a potent drug candidate for the treatment of BU.

Introduction

A high-throughput phenotypic screen on macrophages infected with *Mycobacterium tuberculosis* carried out by Pethe et al. has led to the identification of two compounds belonging to the imidazo(1,2- α)pyridine amide (IPA) family [1–4]. Both molecules showed activity in the micromolar range against extra- and intracellular bacteria and were also found effective when tested on multi-drug resistant (MDR) clinical isolates. An extensive lead optimization program led to the selection of the IPA Q203, showing extracellular/intracellular MIC₅₀ values of 2.7 nM and 0.28 nM, respectively [4,5]. Apart from its high *in vitro* potency, Q203 displayed desirable safety and pharmacokinetic profiles. Acute toxicity tests in mice indicated that concentrations up to 1000 mg/kg were tolerated without clinical signs of toxicity [4]. Pharmacokinetic studies in mice revealed a terminal half-life of nearly one day and a bioavailability of 90 %. In a mouse model of established tuberculosis, four weeks of treatment with Q203 at 0.4, 2 and 10 mg per kg body weight reduced the bacterial load by 90 %, 99 % and 99.9 % [4]. Recently, another representative of the powerful IPA compound family [6,7], designated ND-09759, was shown to have activities in the nanomolar range [8] and to efficiently decrease the bacterial burden in lungs and spleens of *M. tuberculosis* infected mice.

Similar to bedaquiline, a bactericidal diarylquinolone drug approved for clinical treatment of TB, members of the IPA family interfere with ATP synthesis. While bedaquiline binds to the F₀-subunit of the mycobacterial ATP synthase and disturbs the proton gradient serving as an uncoupler [9–11], Q203 targets the b subunit of the electron transport complex ubiquinol - cytochrome c reductase (*QcrB*). Interaction with the Q_p quinone binding site of the b subunit results in the exclusion of the substrate, and finally in an impaired ATP production [2,4,12]. As a major drawback, adverse effects such as nausea, headaches, arthralgia and arrhythmias have been described for bedaquiline, therefore its use is limited to patients suffering from MDR or XDR TB [13].

Since the IPA compound family has good overall druggable properties and holds with the optimized IPA Q203 one of the currently most promising candidate drugs for the treatment of TB, we initiated a study in which we tested the activity of a selected panel of IPA compounds, including Q203, on *M. ulcerans*. Potent drugs against Buruli ulcer (BU) are urgently needed, since the currently recommended 8-weeks combination therapy with rifampicin and streptomycin entails disadvantages. Streptomycin requires daily intramuscular injections and has been shown to cause ototoxicity and

nephrotoxicity [14,15] while rifampicin may be prone to cause resistances [16]. Thus, the evaluation of TB candidate drugs for application in BU is an attractive approach for identifying potential new treatment options.

Results

IPA compounds show potent *in vitro* inhibitory activity against *M. ulcerans*

By performing resazurin-based medium-throughput screens as previously described [17], we tested a pre-selected panel of 85 published and/or commercially available IPA compounds for activity against two *M. ulcerans* strains isolated from Cameroonian BU patients. Based on the determined minimal inhibitory concentrations we grouped the compounds into activity categories (Supplementary Table 1, Appendix Chapter 3). 20/85 (24 %) compounds were highly active with a MIC <0.1 µg/ml, with 8 of them having a MIC <0.01 µg/ml and a single compound - Q203 - even displaying a MIC <0.001 µg/ml (Figure 1A and 1B).

The SAR study of the IPA against *M. ulcerans* was found to yield largely similar results as the SAR study against *M. tuberculosis* [5]. Small residues like halogen, methyl or ethyl were tolerated on the imidazopyridine core, while the optimum activity of the substitution pattern depended on the amide residue. For the amide residue, p-phenylbenzylamides, preferentially substituted with p-Cl, showed very high activities in the cell based assay. They were followed by p-(dialkylamino)benzylamides and p-alkoxybenzylamides. Aliphatic, heterocyclic or branched amides had significantly reduced activities. Recently, pharmacokinetic data for the p-phenylbenzylamides were described, indicating some limitations due to their high lipophilicity and superior pharmacokinetic properties for the Q203 substitution pattern. The IPA compounds Q203 and IPA-7 were selected from the pool of the nine highly active compounds for more detailed profiling.

MIC values for Q203 and IPA-7 were determined by performing resazurin-based metabolic activity assays with four *M. ulcerans* clinical isolates belonging to the classical lineage [18]. The strains tested included two low passage clinical isolates from Cameroon (S1013 and S1298), and one isolate each from Togo (S1014) and from Australia (S1251). The measured MIC values were in the range of 0.6 ng/ml (1 nM) for Q203 and 10 ng/ml (25 nM) for IPA-7 (Figure 2). The dose-response data showed a sharp threshold for Q203, while the curve progression was less steep for IPA-7.

Next, we performed time-kill kinetic assays by cultivating strain S1013 in liquid broth medium in the presence of different concentrations of Q203 and IPA-7 (equivalent to 0.25x, 1x, 2x, 4x, 8x and 16x the respective MIC) for different time periods (0, 3, 7, 14, 21

and 28 days), before plating the bacteria for CFU determination. After incubation of plates for 16 weeks at 30 °C, CFUs were enumerated and *in vitro* kill-kinetic curves were generated (Figure 3). The results of the kill kinetic assays confirmed the MIC and dose-response data obtained with the metabolic activity assays (Figure 2). Q203 exerted strong bactericidal effects (4- \log_{10} CFU/ml reduction, 99.99 % killing) when bacteria were exposed for at least 14 days to minimally 1x the MIC. For IPA-7, a reduction in bacterial numbers could also be observed after two weeks of drug treatment, but killing was less complete when bacteria were exposed to 1x or 2x the MIC concentration (Figure 3).

Q203 shows potent *in vivo* activity against *M. ulcerans*

To monitor the response to antibiotic treatment *in vivo*, we infected BALB/c mice by foot pad injection with *M. ulcerans*. Progression of the infection was followed by weekly measurements of the foot pad thickness using a caliper (Figure 4A). Five weeks after infection, when the mice started to show swelling of the infected feet (Figure 4A), the treatment was initiated by orally administering either rifampicin (10 mg/kg), Q203 (0.5 mg/kg), IPA-7 (0.5 mg/kg) or a solvent control three times per week for a period of four weeks. A strong increase in foot pad thickness was observed for the controls and the IPA-7 treated mice during the four week treatment course (Figure 4A). Due to the severe progression of the infection, these animals had to be sacrificed after completion of the treatment. In contrast, a complete regression of the foot pad swelling was observed for the Q203 treated mice already 1.5 weeks after start of treatment (Figure 4A). The foot pad thickness of these mice returned to normal levels and did not increase again for the entire observation period of 10 weeks post treatment (Figure 4A). For rifampicin treated mice, the foot pad thickness reached a plateau after 2 weeks of treatment and started again to slightly increase after completion of treatment (Figure 4A). Responses to the suboptimal treatment with rifampicin (10 mg/kg three times a week instead of the recommended daily administration) varied strongly between animals (Supplementary Figure 1). The outcome of the different treatments is illustrated in Figure 4B where pictures of representative mice at the end of the treatment are shown. Histopathological analyses of foot pads taken at the end of the treatment revealed for the foot pads of the infected control animals (Figure 5A) and the IPA-7 treated mice

(Figure 5B) oedema formation and tissue necrosis, two typical hallmarks of BU histopathology [19,20]. Oedema formation and tissue necrosis were also present in foot pads of mice treated with rifampicin, however, to a much lower extent (Figure 5C). Strikingly, the foot pads of mice treated with Q203 looked almost identical to the non-infected control foot pads (Figure 5, D1 and E1, respectively) and were completely devoid of oedema (Figure 5, D2) and tissue necrosis (Figure 5, D3).

An IS2404-specific qPCR [21–23] was used to monitor the amounts of *M. ulcerans* DNA in the infected foot pads. In addition, tissue sections were stained with ZN to assess the integrity of AFBs. The qPCR analysis showed strongly increasing bacterial loads for the control mice and IPA-7 treated mice during the four week treatment period (Figure 6A). These findings are in line with the histopathological analyses, showing large extracellular clusters of solid-stained AFB for these mice (Figure 6, B1 and B2, C1 and C2, respectively). In the mice treated with rifampicin, bacterial multiplication was halted during the four weeks of treatment, but the amount of DNA started again to increase after completion of treatment (Figure 6A). As for the foot pad thickness values, a large in-group variance was observed at week 15 (Figure 6A). Compared to the controls and IPA-7 treated mice the bacteria were present in smaller extracellular clusters (Figure 6, D1) and presented as a mix of solid-stained and beaded AFB (Figure 6, D2). In Q203 treated mice the amount of *M. ulcerans* DNA increased slightly during treatment, but dropped after completion of treatment (Figure 6A). Only small numbers of AFB were found in the tissue sections (Figure 6, E1), with the vast majority of these bacilli having a beaded, not solid-stained appearance (Figure 6, E2).

Discussion

Screening of a panel of IPA compounds allowed for the identification of a series of derivatives with high *in vitro* activities (MIC < 0.01 µg/ml) against *M. ulcerans*, with Q203 ranking at the top (MIC < 0.001 µg/ml). Q203 represents the most active derivative of a lead optimization program for *M. tuberculosis* and it has been shown to have MIC₅₀ values of 2.7 nM (in culture broth medium) and 0.28 nM (inside macrophages) [4]. While the majority of potent anti-tubercular agents are less active against *M. ulcerans* (N. Scherr, personal communication), Q203 displayed an even higher activity (MIC₅₀ = 0.5 nM) against *M. ulcerans*. This was unexpected since Q203 is more than 5000 fold less effective against *M. marinum* (MIC₅₀ = 3.5 µM) (Petthe et al., 2013), a close relative of *M. ulcerans* [24]. *M. ulcerans* has diverged from a common ancestor with *M. marinum* by uptake of a virulence plasmid and by drastic genome reduction [25]. Higher susceptibility to Q203 may thus be related to gene loss or inactivation. In the IPA lead optimization program that resulted in the development of Q203, the activity against *M. tuberculosis* was mainly improved through the introduction of a long and hydrophobic group at the R3 position [4]. This seems to be also relevant for an increase in potency against *M. ulcerans*, making Q203 an exceptionally active compound when compared with the *in vitro* activities of currently used BU drugs such as rifampicin (0.13 µg/ml), streptomycin (0.25 µg/ml), ciprofloxacin (1 µg/ml), clarithromycin (0.25 µg/ml) and amikacin (1 µg/ml) [26–28]. To our knowledge, MIC values in the low nanomolar range against *M. ulcerans* have never been observed before.

By using the BU mouse foot pad model, we evaluated the *in vivo* activity of Q203, IPA-7 and rifampicin. As expected, three applications of rifampicin (10 mg/kg) per week for a period of four weeks were not sufficient to achieve complete cure. The high *in vitro* activity of IPA-7 did not translate into a good *in vivo* potency at the chosen regimen, which was however highly effective for Q203. Ten weeks after treatment completion, the group of Q203 treated animals was still devoid of relapses. Histopathological analysis showed after treatment with Q203 predominantly beaded and intracellular AFB, reconfirming the efficient killing of the bacteria.

To the best of our knowledge, a complete cure of all mice infected with *M. ulcerans* has never been accomplished before by a one month treatment with a single antibiotic administered only 3 times per week. If clinical development of Q203 against *M.*

tuberculosis will be successful, this also holds great promises for the development of an alternative drug treatment regimen for *M. ulcerans*.

Acknowledgements

We would like to thank Dr. Masato Murakami, Vincent Romanet, Caroline Stork, Ernesta Dammassa and Patricia Barzaghi Rinaudo from Novartis Basel for providing access to the lab equipment for histopathology as well as Peter Schmid for the Aperio scans of the foot pads.

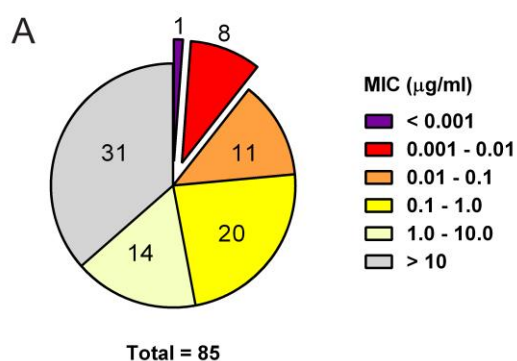
Author Contributions

N.S., R. B. and G. P. conceived the study and wrote the paper; N.S. and R. B. performed the experiments; P.S., M.W., K.P., and G.P. provided technical advice and vital reagents and materials.

Competing Financial Interests

The authors have no competing financial interests.

Figures



B

Number	Structure
Q203 (1)	
2	
3	
4	
5	
6	
7	
8	
9	

Figure 1: IPA compounds display very good *in vitro* activity against *M. ulcerans*.

All 85 IPA compounds were tested *in vitro* by performing resazurin-based metabolic activity assays using two Cameroonian strains. The resulting MIC values were classified into six activity categories and presented in total numbers in the pie diagram (A). The chemical structures of the 9 IPA compounds with MIC values <math>< 0.1 \mu\text{g/ml}</math> are shown in (B).

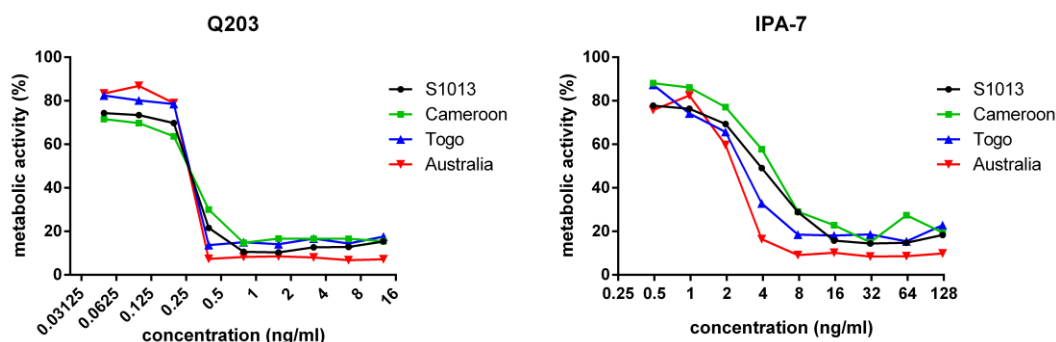


Figure 2: *In vitro* dose-response curve of Q203 and IPA-7 against different *M. ulcerans* strains of the classical lineage.

Metabolic activities of patient isolates originating from Cameroon (black circles and green squares), Togo (blue triangles) and Australia (red triangles) are displayed as mean values of duplicate samples. One representative of three independent experiments is shown.

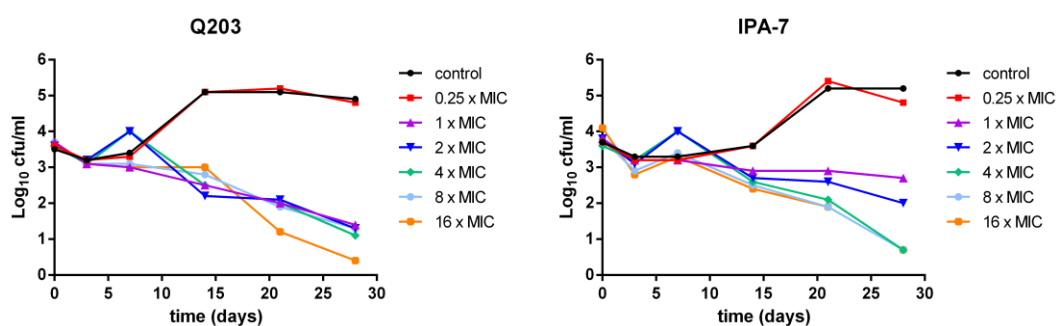


Figure 3: Time-to-kill kinetic assays of Q203 and IPA-7 against *M. ulcerans*.

Cameroonian strain S1013 was incubated with different compound concentrations (multiples of the respective minimal inhibitory concentration) for 0, 3, 7, 14, 21 and 28 days. Bacteria were then spread on 7H10 agar without compound and CFUs were counted after 16 weeks of growth at 30 °C.

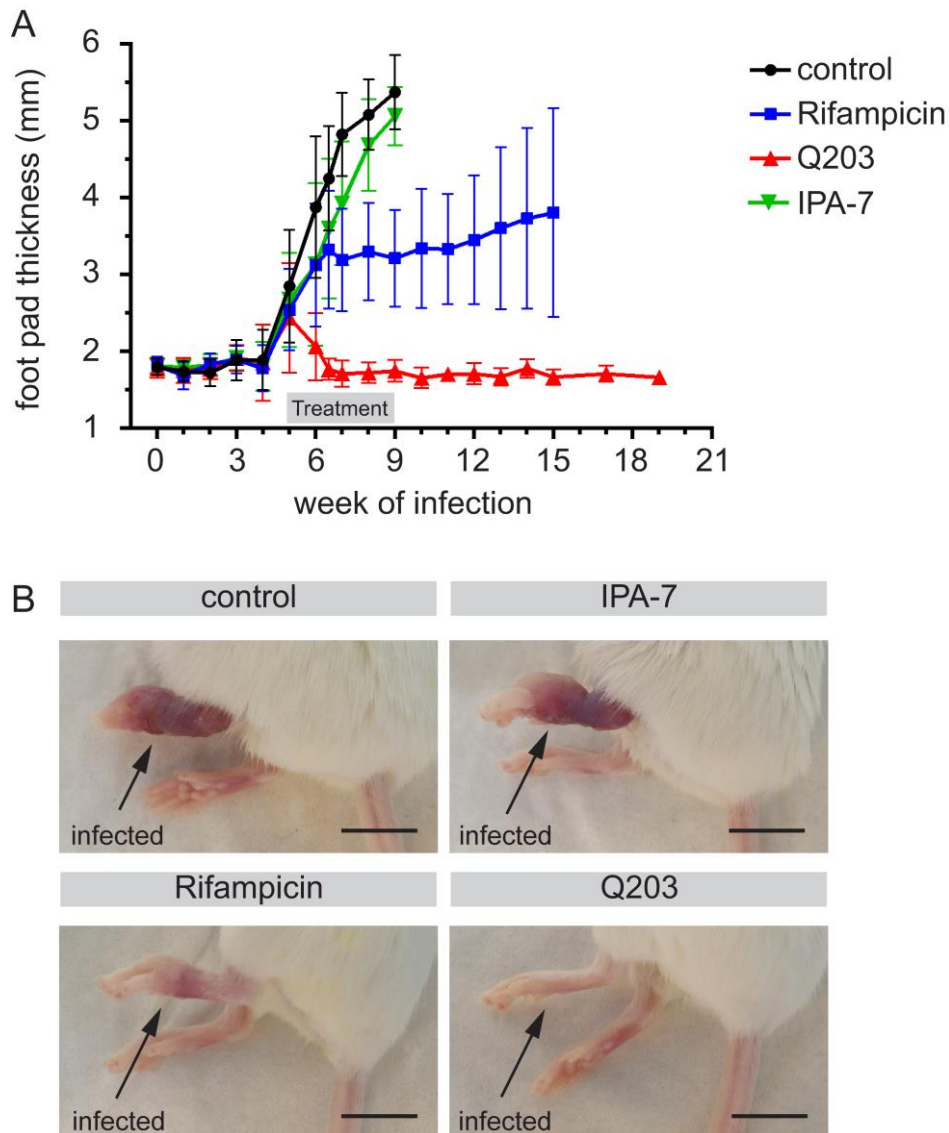


Figure 4: Response to antibiotic treatment in *M. ulcerans* infected mouse foot pads.

(A and B) Mice were infected with *M. ulcerans* into the left hind foot pad and the progression of the disease was followed by weekly measuring the foot pad thickness (A) and by taking pictures at the end of the treatment (B). After 5 weeks of infection, treatment was started by administering either rifampicin (blue squares), Q203 (red triangles), IPA-7 (green triangles) or solvent control (black circles) 3 times per week during a period of 4 weeks. (A) Mean values of the foot pad thickness (mm) are shown, and error bars represent the S.D. (B) Pictures of representative feet taken at the end of the treatment (week 9).

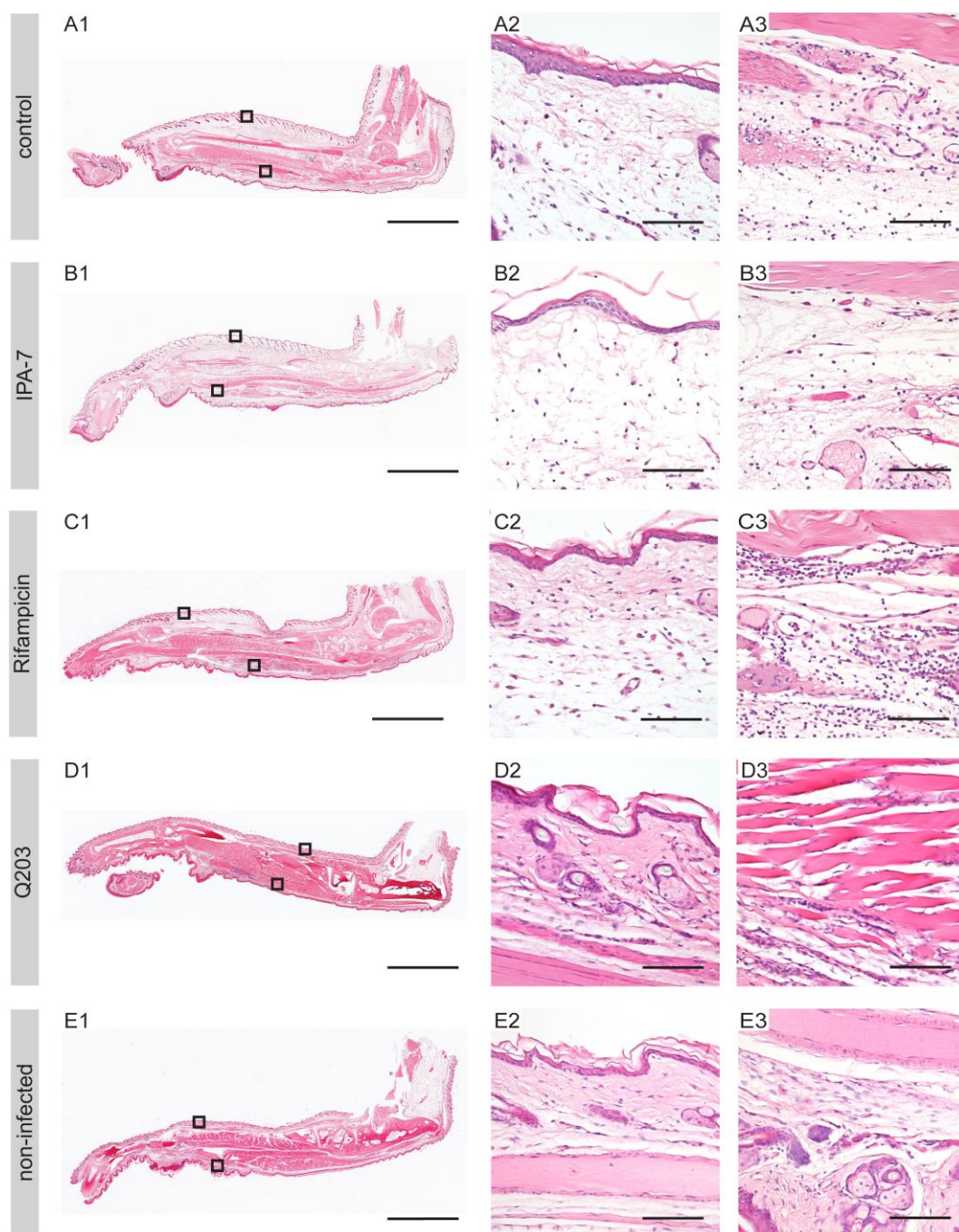


Figure 5: Absence of tissue necrosis and oedema formation in Q203 treated mice.

HE stained histological sections of foot pads from representative control (A), IPA-7 (B), rifampicin (C), or Q203 (D) treated mice as well as of a non-infected control foot pad (E). Scans of whole foot pads (A1, B1, C1, D1 and E1) as well as pictures taken at the epidermis (A2, B2, C2, D2 and E2) and at the site of infection (A3, B3, C3, D3 and E3) are shown. Scale bars represent 5 mm (A1, B1, C1, D1 and E1), and 80 μm (A2, A3, B2, B3, C2, C3, D2, D3, E2 and E3).

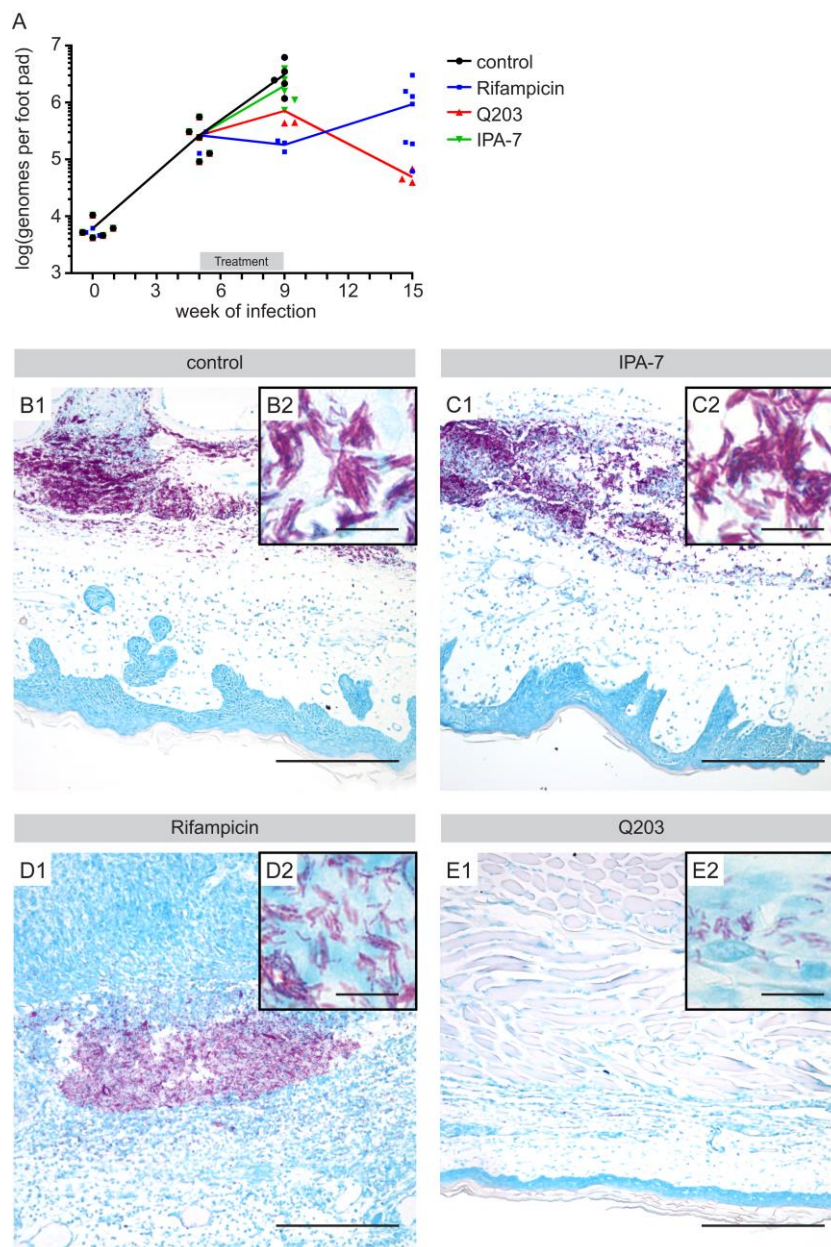
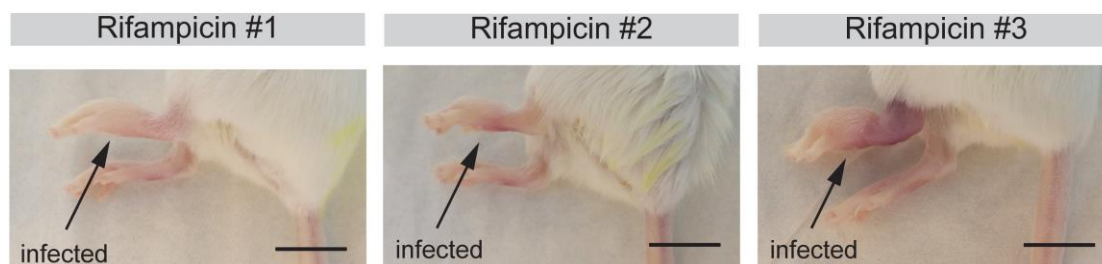


Figure 6: Treatment with Q203 results in a strong reduction of the bacterial load and induces killing of AFB.

(A) Bacterial load during the course of infection as determined by IS2404-specific qPCR. Individual animals are depicted, values are shown as log₁₀ (genomes per foot pad) and mean values are linked by connecting lines. (B-E) Tissue sections of foot pads from representative control (B1 and B2), IPA-7 (C1 and C2), rifampicin (D1 and D2) and Q203 treated (E1 and E2) mice stained with ZN for visualization of AFB. Scale bars represent 200 μm (B1, C1, D1 and E1) and 10 μm (B2, C2, D2 and E2).



Supplementary Figure 1: Wide range of responses in mice treated with rifampicin.

Mice treated with rifampicin showed a wide response range to the treatment, as illustrated by pictures taken at the end of the treatment (week 9). Scale bars represent 1 cm.

Methods

Bacterial strains, general growth conditions and reagents

M. ulcerans strains S1012, S1013, S1047 and S1298 (isolated in 2010, 2011 and 2013 from Cameroonian BU patients; also see [29]) were routinely propagated at 30 °C in BacT/Alert culture bottles supplemented with enrichment medium (bioMérieux). For *in vitro* compound testing, bacteria were grown either in liquid 7H9 medium or on 7H10 agar, supplemented with 10 % (vol/vol) OADC. The *M. ulcerans* strain S1014 (Togo) was received from F. Portaels (ITM, Antwerp) and the Australian strain S1251 from J. Fyfe (VIDRL, Melbourne).

Q203, used for initial screenings, was kindly provided by K. Pethe (Pasteur Institute Korea). For subsequent *in vitro* and *in vivo* experiments, re-synthesized Q203 was provided by K. Pethe (University of Singapore). The IPA screening panel encompassing 85 IPA compounds was received from BASF SE, Ludwigshafen.

Drug susceptibility assays

Minimal inhibitory concentrations (MIC) were determined as described before [17] by performing resazurin-based metabolic activity assays in the 96-well plate format. Briefly, two-fold serial dilutions of compounds were set up in duplicates or triplicates in a volume of 100 µl. Then, 100 µl of a diluted *M. ulcerans* culture (OD=0.04) was added and incubated at 30 °C for 8 days in the presence of the compounds. Upon resazurin (0.125 mg/ml) addition, plates were transferred to 37 °C and incubated o/n. Compound activities were determined by fluorescence measurements ($\lambda=540/588$ nm). Unless otherwise stated, the determined MIC values refer to the actual measured minimal concentrations at which growth was still completely inhibited. The MIC values obtained were then classified into different activity categories.

Kinetic survival assays

Serial dilutions of compounds Q203 and IPA-7 (0.25, 1, 2, 4, 8 and 16 fold the corresponding MIC value) were set up in a volume of 100 µl. Then 100 µl of a diluted *M. ulcerans* S1013 (OD₆₀₀=0.04) was added and bacteria were incubated at 30°C for 0, 3, 7,

14, 21 and 28 days in the presence of the compound. At every time point, bacteria were washed and 100 µl of undiluted, 1:100 or 1:1000 diluted bacterial suspension was plated on 7H10 agar. CFUs were assessed after 16 weeks of incubation at 30 °C.

Infection of mice

All mice were maintained in specific pathogen-free facilities at the Ecole Polytechnique Fédérale de Lausanne (EPFL, Switzerland) and the studies were performed under BSL-3 conditions in eight weeks old female BALB/c mice (Harlan). For the infection of mice, the *M. ulcerans* strain S1013 was used [29]. For preparing the inoculum, the bacteria were cultivated for 6-8 weeks in Bac/T medium (Biomerieux, 251011), pelleted by centrifugation and resuspended in sterile PBS to a stock concentration of 125 mg/ml wet weight. The infection was performed by injecting 30 µl (about 6×10^3 bacilli) of an appropriate dilution of the stock solution in sterile PBS into the hind left foot pad of the mice. The course of infection was followed by weekly measurements of the foot pad thickness using a caliper.

Mice were euthanized at treatment start (week 5), at the end of the treatment (week 9) and 6 weeks after completion of the treatment (week 15). Pictures of the feet were taken using a compact camera (WG-20, RICOH). Foot pads were aseptically removed for the determination of the bacterial load by quantitative RT-PCR or for histopathological analysis.

Treatment of mice

Treatment was started 5 weeks after infection when the first macroscopic signs such as foot pad swelling and reddening of the skin were observed. Treatment was given orally on three days per week during a period of four weeks (18 mice per treatment group). Q203 and IPA-7 were dissolved in 20 % D- α -Tocopherol polyethylene glycol 1000 succinate (TPGS) (Sigma, 57688) / H₂O containing 1 % Dimethyl Sulfoxide (Sigma, D2650) and administered at a concentration of 0.5 mpk. Rifampicin (Sigma, R3501) was dissolved in H₂O and given at a concentration of 10 mpk. As a control, 20 % TPGS / H₂O containing 1 % DMSO was administered.

Determination of the bacterial load by quantitative RT-PCR

After euthanasia, mouse feet designated for quantification of *M. ulcerans* bacteria by qPCR were removed above the ankle, cleaned by 70 % EtOH, cut into 4 pieces and transferred to hard tissue grinding tubes (MK28-R, Precellys, KT03961-1-008.2). For the preparation of foot pad lysates, 750 µl sterile 7H9 medium was added and homogenization was performed using a Precellys 24-Dual tissue homogenizer (3 x 20 s at 5000 rpm with 30 s break). Afterwards, the lysate was transferred into a new tube and the remaining and still intact tissue was homogenized for a second time after addition of 750 µl of sterile 7H9 medium. The lysates were pooled and DNA was isolated from 100 µl of a 1/20 dilution of the pooled lysate as described by Lavender and Fyfe [21]. After DNA isolation, the bacterial load was determined by performing IS2404-specific quantitative RT-PCR analysis as previously described [21]. Ct values were converted into genome numbers per foot pad by making use of the standard curve established by Fyfe *et al.* [22].

Histopathology

Mouse feet used for histopathological analysis were removed above the ankle and fixed at room temperature during 48 hours in 10 % neutral-buffered Formalin solution (4 % formaldehyde, Sigma, HT501128-4L). The feet were decalcified in Formic Acid Bone Decalcifier (Immunocal™, StatLab, 1414A) for 6 days at room temperature and subsequently transferred to 70 % ETOH for storage. After dehydration and paraffin embedding, 5 µm thin sections were cut, de-paraffinised, rehydrated, and stained according to WHO standard protocols with Haematoxylin/Eosin (HE, Sigma, 51275-500ML, J.T. Baker, 3874) to stain for connective tissue or Ziehl-Neelsen/Methylene blue (ZN, Sigma, 21820-1L and 03978-250ML) to stain for mycobacteria. The stained sections were mounted with the Eukitt® mounting medium (Fluka, 03989) and pictures were taken using a Leica® DM2500B microscope or an Aperio scanner.

References

1. Mak PA, Rao SPS, Ping Tan M, Lin X, Chyba J, Tay J, et al. A high-throughput screen to identify inhibitors of ATP homeostasis in non-replicating *Mycobacterium tuberculosis*. *ACS Chem Biol*. 2012;7: 1190–1197. doi:10.1021/cb2004884
2. Abrahams KA, Cox JAG, Spivey VL, Loman NJ, Pallen MJ, Constantinidou C, et al. Identification of novel imidazo[1,2-a]pyridine inhibitors targeting *M. tuberculosis* QcrB. *PloS One*. 2012;7: e52951. doi:10.1371/journal.pone.0052951
3. Ballell L, Bates RH, Young RJ, Alvarez-Gomez D, Alvarez-Ruiz E, Barroso V, et al. Fueling open-source drug discovery: 177 small-molecule leads against tuberculosis. *ChemMedChem*. 2013;8: 313–321. doi:10.1002/cmdc.201200428
4. Pethe K, Bifani P, Jang J, Kang S, Park S, Ahn S, et al. Discovery of Q203, a potent clinical candidate for the treatment of tuberculosis. *Nat Med*. 2013;19: 1157–1160. doi:10.1038/nm.3262
5. Kang S, Kim RY, Seo MJ, Lee S, Kim YM, Seo M, et al. Lead optimization of a novel series of imidazo[1,2-a]pyridine amides leading to a clinical candidate (Q203) as a multi- and extensively-drug-resistant anti-tuberculosis agent. *J Med Chem*. 2014;57: 5293–5305. doi:10.1021/jm5003606
6. Moraski GC, Markley LD, Cramer J, Hipskind PA, Boshoff H, Bailey M, et al. Advancement of Imidazo[1,2-a]pyridines with Improved Pharmacokinetics and Nanomolar Activity Against *Mycobacterium tuberculosis*. *ACS Med Chem Lett*. 2013;4: 675–679. doi:10.1021/ml400088y
7. Moraski GC, Oliver AG, Markley LD, Cho S, Franzblau SG, Miller MJ. Scaffold-switching: an exploration of 5,6-fused bicyclic heteroaromatics systems to afford antituberculosis activity akin to the imidazo[1,2-a]pyridine-3-carboxylates. *Bioorg Med Chem Lett*. 2014;24: 3493–3498. doi:10.1016/j.bmcl.2014.05.062
8. Cheng Y, Moraski GC, Cramer J, Miller MJ, Schorey JS. Bactericidal activity of an imidazo[1, 2-a]pyridine using a mouse *M. tuberculosis* infection model. *PloS One*. 2014;9: e87483. doi:10.1371/journal.pone.0087483
9. Andries K, Verhasselt P, Guillemont J, Göhlmann HWH, Neefs J-M, Winkler H, et al. A diarylquinoline drug active on the ATP synthase of *Mycobacterium tuberculosis*. *Science*. 2005;307: 223–227. doi:10.1126/science.1106753
10. Koul A, Dendouga N, Vergauwen K, Molenberghs B, Vranckx L, Willebrords R, et al. Diarylquinolines target subunit c of mycobacterial ATP synthase. *Nat Chem Biol*. 2007;3: 323–324. doi:10.1038/nchembio884
11. Hards K, Robson JR, Berney M, Shaw L, Bald D, Koul A, et al. Bactericidal mode of action of bedaquiline. *J Antimicrob Chemother*. 2015;70: 2028–2037. doi:10.1093/jac/dkv054
12. Kim M-S, Jang J, Ab Rahman NB, Pethe K, Berry EA, Huang L-S. Isolation and Characterization of a Hybrid Respiratory Supercomplex Consisting of *Mycobacterium tuberculosis* Cytochrome bcc and *Mycobacterium smegmatis* Cytochrome aa3. *J Biol Chem*. 2015;290: 14350–14360. doi:10.1074/jbc.M114.624312
13. Kakkar AK, Dahiya N. Bedaquiline for the treatment of resistant tuberculosis: promises and pitfalls. *Tuberc Edinb Scotl*. 2014;94: 357–362. doi:10.1016/j.tube.2014.04.001
14. Klis S, Stienstra Y, Phillips RO, Abass KM, Tuah W, van der Werf TS. Long Term Streptomycin Toxicity in the Treatment of Buruli Ulcer: Follow-up of Participants in the BURULICO Drug Trial. *PLoS Negl Trop Dis*. 2014;8. doi:10.1371/journal.pntd.0002739
15. WHO | Treatment of *Mycobacterium ulcerans* disease (Buruli Ulcer). Available: <http://www.who.int/buruli/treatment/en/>. Accessed 9 November 2015.
16. Marsollier L, Honoré N, Legras P, Manceau AL, Kouakou H, Carbonnelle B, et al. Isolation of three *Mycobacterium ulcerans* strains resistant to rifampin after experimental chemotherapy of mice. *Antimicrob Agents Chemother*. 2003;47: 1228–1232.
17. Scherr N, Röltgen K, Witschel M, Pluschke G. Screening of antifungal azole drugs and agrochemicals with an adapted alamarBlue-based assay demonstrates antibacterial activity of croconazole against

- Mycobacterium ulcerans*. *Antimicrob Agents Chemother.* 2012;56: 6410–6413. doi:10.1128/AAC.01383-12
18. Käser M, Rondini S, Naegeli M, Stinear T, Portaels F, Certa U, et al. Evolution of two distinct phylogenetic lineages of the emerging human pathogen *Mycobacterium ulcerans*. *BMC Evol Biol.* 2007;7: 177. doi:10.1186/1471-2148-7-177
 19. Guarner J, Bartlett J, Whitney EAS, Raghunathan PL, Stienstra Y, Asamoia K, et al. Histopathologic features of *Mycobacterium ulcerans* infection. *Emerg Infect Dis.* 2003;9: 651–656.
 20. Junghanss T, Johnson RC, Pluschke G. 42 - *Mycobacterium ulcerans* Disease. *Manson's Tropical Infectious Diseases (Twenty-Third Edition)*. London: W.B. Saunders; 2014. pp. 519–531.e2. Available: <http://www.sciencedirect.com/science/article/pii/B9780702051012000431>. Accessed 9 November 2015.
 21. Lavender CJ, Fyfe JAM. Direct detection of *Mycobacterium ulcerans* in clinical specimens and environmental samples. *Methods Mol Biol Clifton NJ.* 2013;943: 201–216. doi:10.1007/978-1-60327-353-4_13
 22. Fyfe JAM, Lavender CJ, Johnson PDR, Globan M, Sievers A, Aзуolas J, et al. Development and application of two multiplex real-time PCR assays for the detection of *Mycobacterium ulcerans* in clinical and environmental samples. *Appl Environ Microbiol.* 2007;73: 4733–4740. doi:10.1128/AEM.02971-06
 23. Bolz M, Kerber S, Zimmer G, Pluschke G. Use of Recombinant Virus Replicon Particles for Vaccination against *Mycobacterium ulcerans* Disease. *PLoS Negl Trop Dis.* 2015;9: e0004011. doi:10.1371/journal.pntd.0004011
 24. Doig KD, Holt KE, Fyfe JAM, Lavender CJ, Eddyani M, Portaels F, et al. On the origin of *Mycobacterium ulcerans*, the causative agent of Buruli ulcer. *BMC Genomics.* 2012;13: 258. doi:10.1186/1471-2164-13-258
 25. Röltgen K, Stinear TP, Pluschke G. The genome, evolution and diversity of *Mycobacterium ulcerans*. *Infect Genet Evol J Mol Epidemiol Evol Genet Infect Dis.* 2012;12: 522–529. doi:10.1016/j.meegid.2012.01.018
 26. Zhang T, Bishai WR, Grosset JH, Nuermberger EL. Rapid assessment of antibacterial activity against *Mycobacterium ulcerans* by using recombinant luminescent strains. *Antimicrob Agents Chemother.* 2010;54: 2806–2813. doi:10.1128/AAC.00400-10
 27. Thangaraj HS, Adjei O, Allen BW, Portaels F, Evans MR, Banerjee DK, et al. In vitro activity of ciprofloxacin, sparfloxacin, ofloxacin, amikacin and rifampicin against Ghanaian isolates of *Mycobacterium ulcerans*. *J Antimicrob Chemother.* 2000;45: 231–233.
 28. Portaels F, Traore H, De Ridder K, Meyers WM. In vitro susceptibility of *Mycobacterium ulcerans* to clarithromycin. *Antimicrob Agents Chemother.* 1998;42: 2070–2073.
 29. Bratschi MW, Bolz M, Minyem JC, Grize L, Wantong FG, Kerber S, et al. Geographic distribution, age pattern and sites of lesions in a cohort of Buruli ulcer patients from the Mapé Basin of Cameroon. *PLoS Negl Trop Dis.* 2013;7: e2252. doi:10.1371/journal.pntd.0002252

General Discussion

The WHO currently lists 17 diseases as neglected tropical diseases (NTDs), whereof BU belongs to one of four caused by bacteria. Altogether, these NTDs are responsible for substantial illness of more than one billion people worldwide and affect the world's poorest population by impairing their physical and cognitive development and by limiting the productivity at the workplace, thereby making it difficult to earn a living [1,2].

With the WHO's acknowledgement of BU as a NTD in 1998, a new era of BU research was initiated and since then, the number of scientific reports on this devastating disease has strongly increased [3,4]. However, despite continuous research efforts, major aspects of the disease have remained mysterious such as the unidentified reservoir, the transmission of *M. ulcerans* or the mode of action of mycolactone. In addition to these open research questions, numerous aspects of BU care, such as early case detection or a more effective and well-tolerated treatment beyond the currently used R/S antibiotic combination therapy clearly need further improvement.

Within the framework of this thesis, we have tackled some of the most relevant open research questions for the understanding of BU by studying the molecular pathways underlying the cytotoxic activity of mycolactone (Results Chapter 1) and by investigating the nature of protective immune responses against *M. ulcerans* infections (Results Chapter 2). Furthermore, important progress has been made towards a future treatment option by repurposing a highly active TB compound whose impressive anti-BU activity could be demonstrated both *in vitro* and *in vivo* (Results Chapter 3).

What has been learned about the molecular mechanisms underlying the cytotoxic activity of mycolactone and their impact on the pathogenesis of Buruli ulcer (Results Chapter 1)?

Already 15 years ago it was demonstrated for the first time that mycolactone can induce apoptosis in cultured L929 fibroblasts and J774 macrophages as well as in the skin of guinea pigs [5]. However, five years later, results of another study published by the same group suggested that mycolactone-exposed cells might rather undergo a mix of

apoptosis and necrosis [6]. Since then, no substantial progress in the understanding of the molecular mechanisms underlying mycolactone-induced cell death has been made and despite the major importance of this issue for the pathogenesis of BU, the cellular receptor responsible for triggering these pathways has still not been identified [7].

By using a set of selective inhibitors for apoptosis, programmed necrosis (necroptosis) and autophagy, we could show that mycolactone-exposed L929 fibroblasts exclusively die by apoptosis without an involvement of necroptosis or autophagy. These results could be reconfirmed in a follow-up quantitative real-time PCR (qPCR) screening approach for the most prominent genes involved in the regulation of apoptosis, necroptosis and autophagy, in which the pro-apoptotic Bcl-2 interacting mediator of cell death (Bim) was identified as a potential candidate gene responsible for mycolactone-induced apoptosis. Subsequent analyses showed that Bim was highly up-regulated by mycolactone at mRNA as well as at protein levels in several cell types including L929 fibroblasts, Jurkat T cells and J774 macrophages. It is important to mention that the up-regulation of Bim protein levels was never observed before 24 hours of mycolactone treatment and that this up-regulation always directly preceded the induction of apoptosis in all cell types analyzed. To test whether Bim represents indeed the key regulator of mycolactone-promoted apoptosis, we silenced this gene by RNA interference and found that this results in an almost complete protection of mycolactone-induced apoptosis. Encouraged from the outcome of our promising *in vitro* studies we decided to perform an *in vivo* validation of our results by making use of an experimental BU mouse model. To that end, Bim-deficient mice were infected with *M. ulcerans* and the course of infection was compared to wild-type control animals. In contrast to the wild-type mice, Bim-deficient mice displayed a complete lack of tissue necrosis and oedema formation after five weeks of infection. Furthermore, Bim knockout mice were able to contain *M. ulcerans* infection and showed a significantly lower bacterial burden. A close vicinity of the remaining AFB to intact nuclei was indicative of the uptake of the bacteria by viable and functional phagocytes.

Coagulative necrosis is a frequently used term in the BU field and describes the presence of extensive cell death and the pathogenesis of the disease due to tissue ischemia [8–11]. However, the *de facto* complete absence of tissue necrosis in *M. ulcerans*-infected Bim knockout mice and the detection of strong expression levels of Bim in clinical specimens of human BU patients suggest that the pathogenesis of BU is largely driven by the

induction of Bim-dependent apoptosis, raising the question whether coagulative necrosis is indeed involved in the pathogenesis of the disease. However, it should be emphasized that there might be discrepancies between the pathogenesis of BU in humans and mice, since a recently published study showed that mycolactone causes a depletion of endothelial cell thrombomodulin which is associated with the deposition of fibrin in BU lesions, a mechanism that might contribute to the formation of coagulative necrosis [10]. Yet, this study entirely relied on histopathological analyses without the demonstration of any mechanistic data and consequently it is not clear, whether these processes are indeed relevant for the initiation of the pathogenesis of the disease.

After having identified Bim as the central mediator of mycolactone-induced apoptosis, we were wondering which molecular mechanisms might underlie its massive up-regulation in mycolactone-exposed cells. Since the cellular effects of mycolactone reminded us of the mode of action of mTOR inhibitors, and since functional parallels between mycolactone and the natural mTOR inhibitor rapamycin have previously been postulated [7], we hypothesized that mycolactone might also act as an inhibitor of the mTOR pathway. In subsequent experiments we were not only able to demonstrate that mycolactone indeed has potent mTOR inhibitory activity, but we also found that the kinetics of mTOR inhibition caused by mycolactone and rapamycin were almost identical, suggesting that the two molecules might even share a similar mode of action. However, one major difference between the two compounds became evident. While the non-cytotoxic rapamycin was, as expected, primarily acting as an inhibitor of mTORC1, we found that mycolactone additionally possesses a very powerful mTORC2 inhibitory activity, leading to complete dephosphorylation and inactivation of the mTORC2-targeted Akt kinase.

The ultimate aim of the following experiments was to identify the molecular mechanisms linking the early mTOR inhibition with the subsequent up-regulation of Bim, finally resulting in Bim-promoted apoptosis. In search of potential factors we primarily focused on transcriptional regulators that are known to be activated in mTOR-inhibited cells and which are able to directly induce the gene expression of Bim. One class of proteins that fulfilled both criteria was the so-called FoxO family of transcriptional regulators, a sub-family of the Forkhead family of transcription factors.

In mammalian cells, the FoxO family is comprised of four members: FoxO1, FoxO3, FoxO4 and FoxO6 [12]. While FoxO4 is mainly expressed in muscle, kidney and colorectal tissue, FoxO6 is primarily expressed in the brain and liver. In contrast, FoxO1 and FoxO3 are expressed in nearly all tissues and therefore represented two promising candidate molecules for mediating the up-regulation of Bim [12]. By analyzing the expression levels of FoxO1 and FoxO3 in L929 fibroblasts, we found that predominantly FoxO3 was highly expressed in these cells. Therefore, we decided to silence this factor through RNA interference and evaluated the impact on cell viability. We found that knockdown of FoxO3 resulted in a decreased up-regulation of Bim and a significant protection from Bim-dependent apoptosis. The results of this experiment confirmed that FoxO3 constitutes the main factor linking mycolactone-induced mTOR inhibition and Bim up-regulation in mycolactone-treated cells. However, while knockdown of Bim resulted in an almost complete rescue of the phenotype, silencing of FoxO3 only partially protected the cells from mycolactone cytotoxicity, suggesting that also other FoxO family members might be involved in this process.

After having demonstrated that the mTORC2-Akt-FoxO3-Bim axis represents the central pathway underlying mycolactone cytotoxicity, we aimed at characterizing the mechanism of mycolactone-mediated mTOR inhibition in more detail. Given that mycolactone and rapamycin share similar cellular effects such as the induction of an early cell-cycle arrest or the downregulation of various cytokines [7] as well as the observation of an almost identical kinetics of the mTOR inhibition induced by these two molecules it is tempting to speculate whether they might even share the same cellular receptor.

In fact, by using an ELISA-based approach and biotinylated synthetic mycolactone derivatives with an unmodified, lower or upper side chain, respectively [13], we were able to show that mycolactone also binds to the intracellular 12kDa FK506-binding protein (FKBP12). To test whether mycolactone binding to FKBP12 is required for the cytotoxic activity of the molecule, we performed a competition experiment using FK506 (Tacrolimus), an immunosuppressive drug binding to the conserved active site of FKBP12 [14–16]. Indeed, administration of a 10-fold molar excess of FK506 already resulted in a significant protection from mycolactone-induced apoptosis in L929 fibroblasts, and a 1000-fold excess completely protected the cells. Based on the results

of these experiments we could draw two major conclusions. Firstly, mycolactone and rapamycin share a highly similar mode of action by binding to the same site of FKBP12. Secondly the existence of a secreted, so far unidentified factor required for the induction of mycolactone-induced apoptosis as previously speculated [17] can most likely be excluded. Hence, the recently published mechanism of mycolactone-mediated blockade of protein translocation to the ER, resulting in a nearly complete loss of all secreted and glycosylated proteins, is obviously relevant for mycolactone-induced immunosuppression by affecting the secretion of various cytokines [17]. However, this blockade is clearly not involved in the pathways constituting the molecular basis of mycolactone cytotoxicity. In addition, among all factors that are part of the mycolactone-induced apoptosis pathway, Bim is the only protein that has to be *de-novo* synthesized. Since Bim is a non-glycosylated cytosolic protein, it is most likely not affected by the mycolactone-mediated inhibition of protein translocation [17].

Could the new mechanistic insights into mycolactone cytotoxicity be used for the development of a novel therapeutic approach?

The identification of the mTORC2-Akt-FoxO3-Bim axis as the central mechanism underlying mycolactone-induced apoptosis raises questions about the potential for therapeutic interventions affecting this pathway. Although we can conclude from the outcome of our *in vitro* and *in vivo* experiments that targeting Bim would be a promising strategy to treat BU, such a therapy would most likely be accompanied by strong side effects, since Bim is essential for apoptosis in various mature organ cell types, including osteoblasts, endothelial cells, epithelial cells and neurons [18]. Furthermore, Bim-dependent apoptosis is absolutely critical for the maintenance and proper functioning of the immune system. For instance, it has been demonstrated that Bim deficiency results in an abnormal accumulation of myeloid and lymphoid cells as well as in an impaired development and function of B- and T-lymphocytes [19].

The most promising approach to specifically interfere with the action of mycolactone might be an inhibition of the binding of the toxin to FKBP12. First of all, the competition experiments using FK506 (Tacrolimus) provided strong evidence that blocking of the conserved binding site of FKBP12 results in a nearly complete abolishment of the

cytotoxic activity of mycolactone. Furthermore, interfering with mycolactone binding to FKBP12 could additionally result in a reduction of the immunosuppressive activity of the toxin. Additional experiments are required to evaluate whether blocking the mycolactone/FKBP12 complex formation can also prevent the pathogenesis of BU *in vivo*. However, due to potential calcineurin-mediated side effects and the strong immunosuppressive characteristics of FK506 [20], a non-immunosuppressive analog such as FK1706 should be used in such an experimental setup [21].

What is the significance of the mTORC2-Akt-FoxO3-Bim pathway for the immunosuppression mediated by mycolactone?

In general, the immunosuppressive effects of mycolactone should be subdivided into two independent branches; a local and a systemic one. At a local level, the cytotoxic activity of mycolactone is responsible for the efficient killing of infiltrating immune cells and it has been demonstrated that *M. ulcerans* can proliferate for short time periods and at low multiplicity of infections (MOI) inside murine macrophages, until mycolactone causes apoptosis of the host cells, resulting in the release of the bacteria into the intercellular space [22]. For these processes, Bim-dependent apoptosis seems to be central as Bim-deficient mice showed only small numbers of acid-fast bacilli after 5 weeks of infection. Furthermore, the bacteria were predominantly found in close vicinity of intact nuclei, indicative of the uptake by viable phagocytic cells, probably resulting in the destruction of the bacteria and the containment of the infection. In contrast, in wild-type mice, the bacilli were found – as also typically observed in human BU lesions - in large extracellular clusters, suggesting that the host cells were killed during the early intracellular stage of the infection.

On the other hand mycolactone additionally induces systemic immunosuppression and the functional parallels between mycolactone and the immunosuppressant rapamycin raised questions about the impact of the pathway underlying mycolactone-induced apoptosis on this systemic immunosuppression. In 1999, rapamycin was approved by the US Food and Drug Administration (FDA) for use in the prevention of kidney allograft rejection and nowadays, rapamycin and its derivative everolimus are still used for immunosuppressive treatment in solid organ transplantation [23].

The mechanisms of rapamycin-mediated immunosuppression are multi-layered and highly complex. While the FK506 (Tacrolimus) / FKBP12 complex inhibits calcineurin phosphatase and the subsequent activation of the nuclear factor of activated T-cells (NFAT), thereby blocking the transcription of cytokines such as IL-2 and progression of the T-cell cycle from G₀ to G₁ [24], rapamycin / FKBP12 inhibits IL-2 signaling and other cytokine receptor-dependent signaling pathways via mTOR, a central downstream mediator of IL signaling, thus preventing the activation of T- and B-cells [25,26].

Most likely, mycolactone also interferes with cytokine receptor-dependent signaling and the activation of T- and B-cells, since it showed even more potent mTOR inhibitory activity than rapamycin. This hypothesis is supported by observations from our lab showing that infection with mycolactone producing *M. ulcerans* bacteria leads to a complete suppression of humoral immune responses against the pathogen, an effect that is not observed during an infection with *M. marinum*, a close relative of *M. ulcerans* which is lacking the pMUM plasmid required for the production of mycolactone [27,28].

In addition to the interference with cytokine receptor signaling, mycolactone might act, like FK506, as a calcineurin inhibitor. In fact, NFAT-dependent inhibition of cytokine transcription might be involved in mycolactone-mediated immunosuppression, since it is well-known that the toxin is a potent suppressor of the expression of many cytokines, such as IL-2 in human T-cells *in vitro* and in BU patients [7,29–31].

Finally, in the past few years, research groups have provided us with a wealth of information demonstrating an important role for mTOR signaling in the regulation of innate immune responses by orchestrating a complex network of cellular and metabolic activities in myeloid cells. Activation of innate immune cells via Toll-like receptor (TLR) ligands, growth factors or cytokines triggers mTOR signaling, which is critical for shaping innate immune effector functions by controlling various cellular processes including cell migration, antigen presentation, T-cell stimulation or synthesis of inflammatory mediators such as cytokines, chemokines, prostaglandins and leukotrienes [32]. Despite major progress in the understanding of mycolactone-mediated immunosuppression during the last few years [29], it is not clear to what extent these processes are also affected by mycolactone. Further studies should therefore aim at answering these open research questions, as they are crucial for a better understanding of the immunosuppression mediated by the toxin and for the pathophysiology of BU disease in general.

What is the impact of this work for the understanding of immunity and for the treatment of Buruli ulcer (Results Chapter 2 and 3)?

Although knowledge about the mechanisms of mycolactone-mediated immunosuppression has considerably increased during the last decade, drawing conclusions on the type of immune effector functions relevant for defense against *M. ulcerans* has remained rather difficult [7]. The results of our experimental infection experiments with wild-type and IFN γ -deficient mice have indicated that the outcome of an infection with *M. ulcerans* may depend strongly on the induction of early cellular immune defense mechanisms. The absence of significant amounts of bacterial debris in IFN γ -deficient mice during the early intracellular stage of the infection was indicative of a reduced capacity of macrophages to kill intracellular *M. ulcerans* bacteria. As a consequence, a faster increase in the bacterial burden and an accelerated pathogenesis were observed.

Beside a central role for innate immune effector mechanisms, there is mounting evidence for the generation of adaptive immune responses during *M. ulcerans* infection. For instance, it has been shown that sera of people living in BU endemic regions frequently contain *M. ulcerans*-specific antibodies, demonstrating that many individuals develop immune responses associated with exposure to *M. ulcerans* without developing clinical disease [33,34]. In line with this are the observation of a partial protection by Bacille Calmette-Guérin (BCG) vaccination in humans and mice [35–38] and reports on spontaneous healing of BU [39,40].

Clearance of *M. ulcerans* infections by the immune system might in particular be possible before large clusters of mycolactone-producing extracellular bacilli have formed. In advanced BU lesions, the high mycolactone concentrations seem to interfere efficiently with the activation of the immune system by the mechanisms described before.

Immunosuppression seems to be reverted during treatment of BU [41]. Histopathological studies indicated that the production of mycolactone might decline early after start of R/S treatment, leading to a rapid onset of local cellular immune responses as characterized by a chronic leukocyte infiltration, the formation of defined granulomas and an efficient phagocytosis of extracellular bacteria [42,43]. In fact, we observed a massive cellular infiltration and a predominantly intracellular localization of AFB after 4 weeks of rifampicin treatment and to a lesser extent after Q203 treatment.

The reactivation of the immune system during R/S treatment might probably also be responsible for the strong reduction in relapse rates after the introduction of the R/S combination therapy in 2004 [44–46], in comparison to purely surgical treatment. However, although the recurrence rates could be reduced to around 2 % with the R/S treatment [45], it has also a number of disadvantages. First of all, the need for daily injection of streptomycin hinders decentralization of treatment in rural areas, where there is only limited access to health centers. The introduction of a solely oral treatment regimen is therefore one of the main goals of the WHO for the future treatment of BU [47]. In addition streptomycin may have severe side effects, such as nephrotoxicity and ototoxicity [47] and in a clinical trial, R/S treatment has led to hearing loss in more than 25 % of the BU patients receiving this treatment [48].

In view of all these disadvantages, potent new drugs for treatment of BU are urgently needed. Since the IPA class of compounds showed potent activity against TB and had desirable safety- and pharmacokinetic profiles [49], we initiated a study in which we tested a selected panel of IPA compounds including the compound Q203 which was optimized for use as a TB drug, *in vitro* and *in vivo* on *M. ulcerans*. We found that Q203 is more active against *M. ulcerans* than for *M. tuberculosis* [49] and may thus have great potential for treatment of BU. While the strategy of repurposing compounds has many advantages, one disadvantage could be that use of a TB drug for BU treatment in a TB endemic region may be problematic, in particular when the duration of treatment required for BU therapy is shorter than for TB. This is the case for R/S treatment, which has raised concerns with respect to the potential enhancement of drug resistance development in *M. tuberculosis* in patients with co-infections, but also in cases where cutaneous TB is misdiagnosed as BU [50].

However, this potential disadvantage is outbalanced by all the positive aspects of Q203. Beside the striking activity against *M. ulcerans*, a phase 1 clinical trial for the treatment of pulmonary tuberculosis is currently in preparation for Q203 [51]. Approval of this compound for the treatment of TB would strongly facilitate subsequent clinical testing and introduction of it for BU therapy. In contrast, it would hardly be possible to find sufficient financial resources for an independent full drug development process for this neglected disease.

Conclusions

In this PhD thesis, the molecular mechanisms underlying mycolactone cytotoxicity, a key factor in the pathogenesis of BU, were unraveled. In addition, by making use of the BU mouse foot pad model, the role of interferon- γ in immune defense against *M. ulcerans* was studied and the therapeutic potential of a novel tuberculosis drug candidate against BU was evaluated. The key findings of this thesis were:

1. Mycolactone binds to the 12-kDa FK506-binding protein and acts as a potent mTOR inhibitor. Mycolactone-mediated inhibition of mTORC2 results in inactivation of Akt and dephosphorylation and activation of the Akt-targeted transcription factor FoxO3. Subsequent up-regulation of the FoxO3 target gene *Bim* leads to Bim-promoted apoptosis.
2. Interferon- γ plays an important role during early host immune defense against *M. ulcerans* infection. Mice lacking this cytokine show a faster increase in bacterial burden and an accelerated pathogenesis.
3. The tuberculosis drug candidate Q203 is highly active against *M. ulcerans* and may be suitable for replacing rifampicin as first line therapeutic option.

References

1. WHO | World Health Organization. Available: http://www.who.int/neglected_diseases/diseases/en/. Accessed 9 November 2015.
2. CDC - Global Health - Neglected Tropical Diseases. Available: <http://www.cdc.gov/globalhealth/ntd/>. Accessed 9 November 2015.
3. WHO | The Yamoussoukro Declaration on Buruli ulcer. Available: http://www.who.int/buruli/yamoussoukro_declaration/en/. Accessed 9 November 2015.
4. Converse PJ, Nuermberger EL, Almeida DV, Grosset JH. Treating Mycobacterium ulcerans disease (Buruli ulcer): from surgery to antibiotics, is the pill mightier than the knife? *Future Microbiol.* 2011;6: 1185–1198. doi:10.2217/fmb.11.101
5. George KM, Pascopella L, Welty DM, Small PL. A Mycobacterium ulcerans toxin, mycolactone, causes apoptosis in guinea pig ulcers and tissue culture cells. *Infect Immun.* 2000;68: 877–883.
6. Adusumilli S, Mve-Obiang A, Sparer T, Meyers W, Hayman J, Small PLC. Mycobacterium ulcerans toxic macrolide, mycolactone modulates the host immune response and cellular location of M. ulcerans in vitro and in vivo. *Cell Microbiol.* 2005;7: 1295–1304. doi:10.1111/j.1462-5822.2005.00557.x
7. Demangel C, Stinear TP, Cole ST. Buruli ulcer: reductive evolution enhances pathogenicity of Mycobacterium ulcerans. *Nat Rev Microbiol.* 2009;7: 50–60. doi:10.1038/nrmicro2077
8. Merone A, Saggiomo G, Severino G, Capone D, De Vincentiis G. [Buruli ulcer. A case report]. *Minerva Pediatr.* 2001;53: 587–590.
9. Guarner J, Bartlett J, Whitney EAS, Raghunathan PL, Stienstra Y, Asamoia K, et al. Histopathologic features of Mycobacterium ulcerans infection. *Emerg Infect Dis.* 2003;9: 651–656.
10. Ogbechi J, Ruf M-T, Hall BS, Bodman-Smith K, Vogel M, Wu H-L, et al. Mycolactone-Dependent Depletion of Endothelial Cell Thrombomodulin Is Strongly Associated with Fibrin Deposition in Buruli Ulcer Lesions. *PLoS Pathog.* 2015;11: e1005011. doi:10.1371/journal.ppat.1005011
11. WHO | Laboratory diagnosis of buruli ulcer. Available: http://www.who.int/buruli/laboratory_diagnosis/en/. Accessed 9 November 2015.
12. Wang Y, Zhou Y, Graves DT. FOXO transcription factors: their clinical significance and regulation. *BioMed Res Int.* 2014;2014: 925350. doi:10.1155/2014/925350
13. Scherr N, Gersbach P, Dangy J-P, Bomio C, Li J, Altmann K-H, et al. Structure-Activity Relationship Studies on the Macrolide Exotoxin Mycolactone of Mycobacterium ulcerans. *PLoS Negl Trop Dis.* 2013;7: e2143. doi:10.1371/journal.pntd.0002143
14. Harding MW, Galat A, Uehling DE, Schreiber SL. A receptor for the immunosuppressant FK506 is a cis-trans peptidyl-prolyl isomerase. *Nature.* 1989;341: 758–760. doi:10.1038/341758a0
15. Siekierka JJ, Hung SH, Poe M, Lin CS, Sigal NH. A cytosolic binding protein for the immunosuppressant FK506 has peptidyl-prolyl isomerase activity but is distinct from cyclophilin. *Nature.* 1989;341: 755–757. doi:10.1038/341755a0
16. Galat A. Peptidylprolyl cis/trans isomerases (immunophilins): biological diversity--targets--functions. *Curr Top Med Chem.* 2003;3: 1315–1347.
17. Hall BS, Hill K, McKenna M, Ogbechi J, High S, Willis AE, et al. The Pathogenic Mechanism of the Mycobacterium ulcerans Virulence Factor, Mycolactone, Depends on Blockade of Protein Translocation into the ER. *PLoS Pathog.* 2014;10: e1004061. doi:10.1371/journal.ppat.1004061
18. Akiyama T, Dass CR, Choong PFM. Bim-targeted cancer therapy: a link between drug action and underlying molecular changes. *Mol Cancer Ther.* 2009;8: 3173–3180. doi:10.1158/1535-7163.MCT-09-0685
19. Akiyama T, Tanaka S. Bim: guardian of tissue homeostasis and critical regulator of the immune system, tumorigenesis and bone biology. *Arch Immunol Ther Exp (Warsz).* 2011;59: 277–287. doi:10.1007/s00005-011-0126-1
20. Liu J, Farmer JD, Lane WS, Friedman J, Weissman I, Schreiber SL. Calcineurin is a common target of cyclophilin-cyclosporin A and FKBP-FK506 complexes. *Cell.* 1991;66: 807–815.

21. Price RD, Yamaji T, Yamamoto H, Higashi Y, Hanaoka K, Yamazaki S, et al. FK1706, a novel non-immunosuppressive immunophilin: neurotrophic activity and mechanism of action. *Eur J Pharmacol.* 2005;509: 11–19. doi:10.1016/j.ejphar.2004.12.023
22. Torrado E, Fraga AG, Castro AG, Stragier P, Meyers WM, Portaels F, et al. Evidence for an intramacrophage growth phase of *Mycobacterium ulcerans*. *Infect Immun.* 2007;75: 977–987. doi:10.1128/IAI.00889-06
23. Touzot M, Soulillou JP, Dantal J. Mechanistic target of rapamycin inhibitors in solid organ transplantation: from benchside to clinical use. *Curr Opin Organ Transplant.* 2012;17: 626–633. doi:10.1097/MOT.0b013e32835a4be2
24. Manez R, Jain A, Marino IR, Thomson AW. Comparative evaluation of tacrolimus (Fk506) and cyclosporin a as immunosuppressive agents. *Transplant Rev.* 1995;9: 63–76. doi:10.1016/0955-470X(95)80026-5
25. Halloran PF. Immunosuppressive drugs for kidney transplantation. *N Engl J Med.* 2004;351: 2715–2729. doi:10.1056/NEJMra033540
26. Feske S, Giltman J, Dolmetsch R, Staudt LM, Rao A. Gene regulation mediated by calcium signals in T lymphocytes. *Nat Immunol.* 2001;2: 316–324. doi:10.1038/86318
27. Stinear TP, Jenkin GA, Johnson PD, Davies JK. Comparative genetic analysis of *Mycobacterium ulcerans* and *Mycobacterium marinum* reveals evidence of recent divergence. *J Bacteriol.* 2000;182: 6322–6330.
28. Stinear TP, Mve-Obiang A, Small PLC, Frigui W, Pryor MJ, Brosch R, et al. Giant plasmid-encoded polyketide synthases produce the macrolide toxin of *Mycobacterium ulcerans*. *Proc Natl Acad Sci U S A.* 2004;101: 1345–1349. doi:10.1073/pnas.0305877101
29. Hall B, Simmonds R. Pleiotropic molecular effects of the *Mycobacterium ulcerans* virulence factor mycolactone underlying the cell death and immunosuppression seen in Buruli ulcer. *Biochem Soc Trans.* 2014;42: 177–183. doi:10.1042/BST20130133
30. Hong H, Stinear T, Porter J, Demangel C, Leadlay PF. A novel mycolactone toxin obtained by biosynthetic engineering. *Chembiochem Eur J Chem Biol.* 2007;8: 2043–2047. doi:10.1002/cbic.200700411
31. Phillips R, Sarfo FS, Guenin-Macé L, Decalf J, Wansbrough-Jones M, Albert ML, et al. Immunosuppressive Signature of Cutaneous *Mycobacterium ulcerans* Infection in the Peripheral Blood of Patients with Buruli Ulcer Disease. *J Infect Dis.* 2009;200: 1675–1684. doi:10.1086/646615
32. Weichhart T, Hengstschläger M, Linke M. Regulation of innate immune cell function by mTOR. *Nat Rev Immunol.* 2015;15: 599–614. doi:10.1038/nri3901
33. Diaz D, Döbeli H, Yeboah-Manu D, Mensah-Quainoo E, Friedlein A, Soder N, et al. Use of the immunodominant 18-kiloDalton small heat shock protein as a serological marker for exposure to *Mycobacterium ulcerans*. *Clin Vaccine Immunol CVI.* 2006;13: 1314–1321. doi:10.1128/CVI.00254-06
34. Yeboah-Manu D, Röltgen K, Opore W, Asan-Ampah K, Quenin-Fosu K, Asante-Poku A, et al. Seroprevalence as a tool to screen populations for exposure to *Mycobacterium ulcerans*. *PLoS Negl Trop Dis.* 2012;6: e1460. doi:10.1371/journal.pntd.0001460
35. Dobos KM, Spotts EA, Marston BJ, Horsburgh CR, King CH. Serologic response to culture filtrate antigens of *Mycobacterium ulcerans* during Buruli ulcer disease. *Emerg Infect Dis.* 2000;6: 158–164. doi:10.3201/eid0602.000208
36. Okenu DMN, Ofielu LO, Easley KA, Guarner J, Spotts Whitney EA, Raghunathan PL, et al. Immunoglobulin M antibody responses to *Mycobacterium ulcerans* allow discrimination between cases of active Buruli ulcer disease and matched family controls in areas where the disease is endemic. *Clin Diagn Lab Immunol.* 2004;11: 387–391.
37. Smith PG, Revill WD, Lukwago E, Rykushin YP. The protective effect of BCG against *Mycobacterium ulcerans* disease: a controlled trial in an endemic area of Uganda. *Trans R Soc Trop Med Hyg.* 1976;70: 449–457.

38. Fraga AG, Martins TG, Torrado E, Huygen K, Portaels F, Silva MT, et al. Cellular immunity confers transient protection in experimental Buruli ulcer following BCG or mycolactone-negative *Mycobacterium ulcerans* vaccination. *PloS One*. 2012;7: e33406. doi:10.1371/journal.pone.0033406
39. Revill WD, Morrow RH, Pike MC, Ateng J. A controlled trial of the treatment of *Mycobacterium ulcerans* infection with clofazimine. *Lancet*. 1973;2: 873–877.
40. Gordon CL, Buntine JA, Hayman JA, Lavender CJ, Fyfe JA, Hosking P, et al. Spontaneous clearance of *Mycobacterium ulcerans* in a case of Buruli ulcer. *PLoS Negl Trop Dis*. 2011;5: e1290. doi:10.1371/journal.pntd.0001290
41. Yeboah-Manu D, Peduzzi E, Mensah-Quainoo E, Asante-Poku A, Ofori-Adjei D, Pluschke G, et al. Systemic suppression of interferon-gamma responses in Buruli ulcer patients resolves after surgical excision of the lesions caused by the extracellular pathogen *Mycobacterium ulcerans*. *J Leukoc Biol*. 2006;79: 1150–1156. doi:10.1189/jlb.1005581
42. Schütte D, UmBoock A, Pluschke G. Phagocytosis of *Mycobacterium ulcerans* in the course of rifampicin and streptomycin chemotherapy in Buruli ulcer lesions. *Br J Dermatol*. 2009;160: 273–283. doi:10.1111/j.1365-2133.2008.08879.x
43. Ruf M-T, Sopoh GE, Brun LV, Dossou AD, Barogui YT, Johnson RC, et al. Histopathological Changes and Clinical Responses of Buruli Ulcer Plaque Lesions during Chemotherapy: A Role for Surgical Removal of Necrotic Tissue? *PLoS Negl Trop Dis*. 2011;5: e1334. doi:10.1371/journal.pntd.0001334
44. WHO | Provisional guidance on the role of specific antibiotics in the management of *Mycobacterium ulcerans* disease (Buruli ulcer). Available: <http://www.who.int/buruli/information/antibiotics/en/index1.html>. Accessed 9 November 2015.
45. Chauty A, Ardant M-F, Adeye A, Euverte H, Guédénon A, Johnson C, et al. Promising Clinical Efficacy of Streptomycin-Rifampin Combination for Treatment of Buruli Ulcer (*Mycobacterium ulcerans* Disease). *Antimicrob Agents Chemother*. 2007;51: 4029–4035. doi:10.1128/AAC.00175-07
46. Sarfo FS, Phillips R, Asiedu K, Ampadu E, Bobi N, Adentwe E, et al. Clinical efficacy of combination of rifampin and streptomycin for treatment of *Mycobacterium ulcerans* disease. *Antimicrob Agents Chemother*. 2010;54: 3678–3685. doi:10.1128/AAC.00299-10
47. WHO | Treatment of *Mycobacterium ulcerans* disease (Buruli Ulcer). Available: <http://www.who.int/buruli/treatment/en/>. Accessed 9 November 2015.
48. Klis S, Stienstra Y, Phillips RO, Abass KM, Tuah W, van der Werf TS. Long Term Streptomycin Toxicity in the Treatment of Buruli Ulcer: Follow-up of Participants in the BURULICO Drug Trial. *PLoS Negl Trop Dis*. 2014;8. doi:10.1371/journal.pntd.0002739
49. Pethe K, Bifani P, Jang J, Kang S, Park S, Ahn S, et al. Discovery of Q203, a potent clinical candidate for the treatment of tuberculosis. *Nat Med*. 2013;19: 1157–1160. doi:10.1038/nm.3262
50. Bratschi MW, Njih Tabah E, Bolz M, Stucki D, Borrell S, Gagneux S, et al. A Case of Cutaneous Tuberculosis in a Buruli Ulcer-Endemic Area. *PLoS Negl Trop Dis*. 2012;6. doi:10.1371/journal.pntd.0001751
51. A Dose-Escalation Study to Evaluate Safety, Tolerability and Pharmacokinetics of Single Doses of Q203 in Normal, Healthy, Male and Female Volunteers. Available: <https://clinicaltrials.gov/ct2/show/NCT02530710>. Accessed 9 November 2015.

Appendix Chapter 1

Mycolactone binds to FKBP12 and promotes Bim-dependent apoptosis in Buruli ulcer through inhibition of mTOR

Raphael Bieri^{1,2}, Nicole Scherr^{1,2}, Marie-Thérèse Ruf^{1,2}, Jean-Pierre Dangy^{1,2}, Flurina Pletscher³, Philipp Gersbach⁴, Matthias Gehringer⁴, Thomas Junghanss⁵, Karl-Heinz Altmann⁴ and Gerd Pluschke^{1,2*}

¹Swiss Tropical and Public Health Institute, Socinstrasse 57, 4002 Basel, Switzerland

²University of Basel, Petersplatz 1, 4003 Basel, Switzerland

³Department of Biomedicine at University of Basel and University Hospital Basel, Hebelstrasse 20, 4031 Basel, Switzerland,

⁴Department of Chemistry and Applied Biosciences, Institute of Pharmaceutical Sciences, Swiss Federal Institute of Technology (ETH) Zurich, Vladimir-Prelog-Weg 1-5 / 10, 8093 Zurich, Switzerland

⁵Section of Clinical Tropical Medicine, Heidelberg University Hospital, Im Neuenheimer Feld 324, 69120 Heidelberg, Germany

* Corresponding author

This article is under revision (November 2015) in:
Nature Chemical Biology

Supplementary Table 1

Gene Symbol	0.5 h	3 h	12 h	24 h
9430015G10Rik	1.28	-1.02	1.11	-2.58
Abl1	1.25	1.06	-1.55	-1.16
Akt1	1.13	-1.13	-1.99	-2.49
Apaf1	1.17	-1.22	-1.04	-1.64
App	1.13	-1.07	-2.10	-1.27
Atg12	-1.21	-1.17	-1.27	-1.16
Atg16l1	1.14	1.12	-1.81	-2.21
Atg3	1.02	-1.03	-2.00	-2.01
Atg5	1.07	-1.10	-1.84	-2.56
Atg7	1.12	-1.07	-1.16	-1.27
Atp6v1g2	1.00	1.06	1.43	1.88
Bax	-1.03	-1.19	-1.24	-2.75
Bcl2	-1.21	-1.30	-4.92	-7.72
Bcl2a1a	-1.07	-1.10	-1.58	-1.86
Bcl2l1	1.08	-1.39	-3.70	-2.91
Bcl2l11	-1.22	-1.76	4.02	10.02
Becn1	-1.05	-1.05	-1.20	-1.42
Birc2	1.12	-1.41	1.12	1.38
Birc3	-2.67	-4.15	-4.08	-16.94
Bmf	-1.03	-1.55	2.57	10.70
Casp1	1.03	-1.19	-1.16	1.23
Casp2	1.24	1.02	-1.45	-1.48
Casp3	1.10	-1.12	-1.87	-1.87
Casp6	1.19	-1.29	1.65	2.01
Casp7	1.01	1.00	-2.06	-2.19
Casp9	1.19	-1.24	1.25	1.96
Ccdc103	-1.41	-3.12	1.42	2.55
Cd40	1.02	1.26	-2.08	-4.99
Cd40lg	1.11	1.18	-1.19	-1.00
Cflar	-1.02	-1.49	-2.73	-1.97
Commd4	1.04	-1.13	-1.07	1.05
Ctsb	1.13	-1.23	-1.23	1.45
Ctss	-4.04	-1.85	-3.40	1.28

Appendix

Cyld	1.05	-1.23	-1.43	-1.61
Defb1	-1.23	-1.85	-4.71	-5.82
Dennd4a	-1.04	-1.01	-2.42	-2.72
Dffa	1.26	-1.02	-1.12	1.18
Dpysl4	-1.25	-1.30	1.02	-4.54
Eif5b	-1.01	-1.22	-2.33	-3.04
Esr1	-1.10	-1.35	1.00	1.64
Fas	1.23	1.60	5.10	3.09
Fasl	-2.34	-2.22	-2.91	-2.61
Foxi1	-1.26	1.06	-2.50	-2.96
Gaa	1.11	-1.12	-1.45	-1.14
Gadd45a	1.19	2.01	1.88	3.21
Galnt5	1.11	1.18	-1.19	-1.00
Grb2	1.13	-1.03	-1.47	-1.36
Hspbap1	-1.22	-1.38	-1.17	-1.40
Htt	1.06	-1.16	-2.03	-2.80
Ifng	3.43	-1.21	1.65	1.59
Igf1	1.08	-1.54	-2.53	2.31
Igf1r	1.01	-1.13	-1.50	-1.33
Ins2	-1.06	1.39	-1.25	-1.45
Irgm1	1.13	1.04	-1.48	1.22
Jph3	-1.85	-1.20	-1.76	-5.00
Kcnip1	1.96	1.30	-1.04	-1.21
Mag	-1.32	1.09	-1.85	-2.56
Map1lc3a	-1.03	-1.39	1.38	3.89
Mapk8	-1.06	1.01	-2.24	-3.06
Mcl1	-1.09	-1.37	-3.37	-4.23
Nfkb1	1.11	1.01	-2.07	-1.96
Nol3	1.16	-1.01	1.28	2.76
Olfr1404	1.12	1.15	-1.30	-2.61
Parp1	1.14	-1.07	-1.73	-2.87
Parp2	1.07	-1.19	-1.65	-4.06
Pik3c3	1.10	-1.17	1.26	1.06
Pvr	-1.54	-1.42	-4.48	-8.53
Rab25	2.53	-1.17	-2.69	-2.14
Rps6kb1	1.10	1.02	-1.90	-2.69

S100a7a	1.79	1.44	-2.44	1.12
Snca	1.11	1.57	-1.20	-1.01
Spata2	-1.43	-1.11	-2.49	-3.11
Sqstm1	1.17	1.23	1.57	1.97
Sycp2	1.11	1.18	-1.19	-1.00
Tmem57	-1.18	-1.13	1.01	-1.16
Tnf	1.04	-1.47	-10.56	-9.24
Tnfrsf10b	-1.03	1.21	-1.27	-2.42
Tnfrsf11b	1.11	1.18	-1.19	-1.00
Tnfrsf1a	1.05	-1.06	-1.27	-1.24
Traf2	-1.03	1.05	-1.77	-2.97
Trp53	1.17	-1.01	-1.59	-2.69
Txnl4b	1.24	-1.10	-1.28	-1.58
Ulk1	1.17	-1.07	1.99	2.21
Xiap	-1.01	-1.27	-1.77	-1.65

Supplementary Table 1: Results of a quantitative RT-PCR screen in L929 fibroblasts.

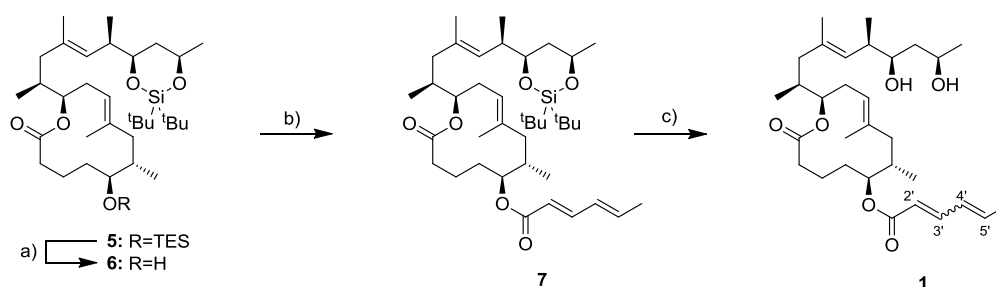
Expression levels of 84 key genes involved in the regulation of apoptosis, necrosis and autophagy were determined in L929 fibroblasts treated for 0.5, 3, 12 and 24 h with 80 nM mycolactone. Values are displayed as fold change compared to DMSO control cells. One of two independent experiments, yielding similar results, is shown.

Synthesis of mycolactone derivatives

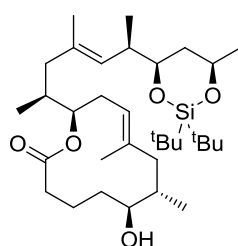
General

All non-aqueous reactions were carried out under argon atmosphere. All solvents used for reactions were purchased as anhydrous grade from Fluka. Solvents for extractions, flash column chromatography (FC) and thin layer chromatography (TLC) were commercial grade and distilled before use. Reactions were monitored by TLC using Merck TLC aluminum sheets (silica gel 60 F254). Visualization was achieved either by fluorescence quenching under UV light ($\lambda=254$ nm) or by staining with cerium sulfate / phosphomolybdic acid stain. FC was performed using Fluka silica gel 60 for preparative column chromatography (40-63 μm). Concentration under reduced pressure was performed by rotary evaporation at the appropriate temperature and pressure. NMR spectra were recorded on a Bruker AV-400 400 MHz and a Bruker DRX-500 500 MHz spectrometer at room temperature. Chemical shifts are reported as δ values (ppm). The solvent peaks were used as internal standards: Chloroform (δ 7.26), methanol (δ 3.31), or acetone (δ 2.05) for ^1H spectra, and chloroform (δ 77.0), methanol (δ 49.0), or acetone (δ 29.84) for ^{13}C spectra. Data are reported as follows: s = singlet, d = doublet, t = triplet, q = quartet, m = multiplet, br = broad signal. For inseparable isomers, ^1H -NMR and ^{13}C -NMR signals were assigned by HSQC and HMBC experiments. Infrared spectra (IR) were recorded on a Jasco FT/IR-6200 spectrometer. The absorption bands are given in wave numbers (cm^{-1}). Optical rotations were measured on a Jasco P-1020 polarimeter. Mass spectra were recorded on a Waters Micromass AutoSpec Ultima (EI-Sector) or a Varian IonSpec Ultima (MALDI/ESI-FT-ICR) (both MS service of Laboratory of Organic Chemistry (LOC) at the ETH Zurich). Except when noted otherwise, high pressure liquid chromatography (HPLC) analyses were carried out using a Waters Symmetry column (C18, 3.5 μm , 4.6 x 100 mm). Preparative HPLC was carried out using Waters Symmetry columns (C18, 5 μm , 7.8 x 100 mm; C18, 5 μm , 19 x 100 mm). The absorbance of HPLC samples was recorded for wavelengths between 200 nm and 400 nm. HPLC purity was determined by combining total absorbance from 200 nm to 400 nm ("Max Plot").

Truncated mycolactone analog 1

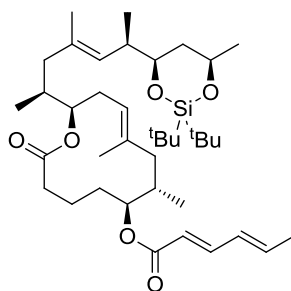


Scheme S1: a) THF/H₂O/AcOH 2:1:1, rt, 2.5 h, 90 %. b) sorbic acid, Cl₃C₆H₂COCl, DIPEA, DMAP, THF, 2 h, rt, quant; c) HF-pyridine, THF/pyridine 6:1, rt, 2 h, 49 %.



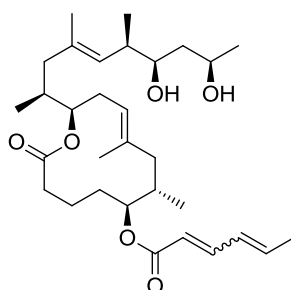
(6*S*,7*S*,12*R*,*E*)-12-((2*S*,6*R*,*E*)-6-((4*R*,6*R*)-2,2-di-tert-butyl-6-methyl-1,3,2-dioxasilinan-4-yl)-4-methylhept-4-en-2-yl)-6-hydroxy-7,9-dimethyloxacyclododec-9-en-2-one (6).

To a solution of TES-protected alcohol **5**¹ (19.7 mg, 29 μmol) in THF (1.0 mL) were added H₂O (0.5 mL) and HOAc (0.5 mL) at ambient temperature and the reaction mixture was stirred for 2½ h. Sat. aq. NaHCO₃-solution was then added until no more gas evolved. EtOAc was added, the layers were separated, and the aq. layer was extracted with EtOAc (2 x 10 mL). The combined org. extracts were washed with brine, dried over MgSO₄ and concentrated under reduced pressure. Purification of the residue by flash column chromatography (*n*-hexane/EtOAc 9:1) yielded 14.8 mg (90 %) of alcohol **6** as colorless oil. *R*_f (*n*-hexane/EtOAc 2:1) = 0.53; [α]_D²⁵ = -36.2° (*c* = 0.47, CHCl₃); ¹H-NMR (400 MHz, CDCl₃): δ 5.05 – 4.93 (m, 3H), 4.18 – 4.08 (m, 1H), 3.69 (ddd, *J* = 11.3, 7.5, 1.8 Hz, 1 H), 3.54 – 3.47 (m, 1 H), 2.46 (dt, *J* = 14.2, 11.5 Hz, 1H), 3.48 – 2.20 (m, 3H), 2.14 – 2.05 (m, 2H), 2.02 – 1.83 (m, 4H), 1.79 – 1.57 (m, 5H), 1.62 (s, 3H), 1.60 (d, *J* = 1.2 Hz, 3H), 1.38 – 1.27 (m, 3H), 1.18 (d, *J* = 6.1 Hz, 3H), 1.04 – 0.92 (m, 6H), 1.00 (s, 9H), 0.98 (s, 9H), 0.85 (d, *J* = 6.6 Hz, 3H); ¹³C-NMR (100 MHz, CDCl₃): δ 175.2, 137.0, 132.6, 129.9, 123.1, 77.8, 77.2, 71.0, 70.5, 45.4, 43.3, 41.7, 40.4, 35.0, 34.9, 34.8, 34.1, 30.0, 27.6 (3C), 27.2 (3C), 24.9, 22.7, 20.3, 19.6, 16.7, 16.5, 16.1, 14.7; IR (neat): $\tilde{\nu}$ 3672, 2967, 2931, 2905, 2361, 2339, 1713, 1470, 1454, 1379, 1251, 1161,



(2E,4E)-((6S,7S,12R,E)-12-((2S,6R,E)-6-((4R,6R)-2,2-di-tert-butyl-6-methyl-1,3,2-dioxasilinan-4-yl)-4-methylhept-4-en-2-yl)-7,9-dimethyl-2-oxooxacyclododec-9-en-6-yl)hexa-2,4-dienoate (7).

To a solution of sorbic acid (3.1 mg, 28 μmol) in THF (1.0 mL) was added DIPEA (0.02 mL, 0.11 mmol), DMAP (17 mg, 0.14 mmol), and $\text{Cl}_3\text{C}_6\text{H}_2\text{COCl}$ (9 μL , 55 μmol). Immediately, the colorless solution turned turbid. Alcohol **6** (7.8 mg, 14 μmol) in THF (1.0 mL) was added. The white suspension was stirred at ambient temperature for 2 h. The reaction was quenched by adding sat. aq. NaHCO_3 -solution (5 mL), EtOAc (15 mL) and little water. The layers were separated and the aq. layer was extracted with EtOAc (2 x 15 mL). The combined org. layers were washed with brine, dried over MgSO_4 and concentrated under reduced pressure. Purification by flash column chromatography (*n*-hexane/EtOAc 20:1) yielded 9.6 mg (quant.) of ester **7** as an inseparable mixture of isomers (*trans/cis* 84:16) as slightly yellow oil. R_f (*n*-hexane/EtOAc 9:1) = 0.48; $[\alpha]_{\text{D}_{25}} = -18.64^\circ$ ($c = 2.40$, CHCl_3); $^1\text{H-NMR}$ (400 MHz, CDCl_3): δ 7.33 – 7.18 (m, 1H), 6.29 – 6.01 (m, 2H), 5.76 (d, $J = 15.7$ Hz, 1H), 5.06 (d, $J = 10.6$ Hz, 1H), 4.95 (d, $J = 9.5$ Hz, 1H), 4.92 – 4.82 (m, 1H), 4.80 – 4.68 (m, 1H), 4.19 – 4.06 (m, 1H), 3.69 (dd, $J = 9.5, 7.7$ Hz, 1H), 2.52 – 2.25 (m, 3H), 2.16 – 1.87 (m, 7H), 1.85 (d, $J = 5.8$ Hz, 3H), 1.82 – 1.50 (m, 6H), 1.68 (s, 3H), 1.60 (d, $J = 1.2$ Hz, 3H), 1.39 – 1.23 (m, 1H), 1.17 (t, $J = 5.8$ Hz, 3H), 1.00 (s, 9H), 0.98 (d, $J = 6.7$ Hz, 3H), 0.98 (s, 9H), 0.94 – 0.88 (m, 3H), 0.85 (d, $J = 6.7$ Hz, 3H); $^{13}\text{C-NMR}$ (100 MHz, CDCl_3): δ 173.2, 166.6, 144.8, 139.1, 136.7, 132.7, 129.9, 129.8, 122.6, 119.3, 78.8, 77.9, 76.0, 70.5, 45.6, 43.4, 41.7, 40.4, 35.5, 34.8, 31.9, 30.2, 29.7, 27.6 (3C), 27.2 (3C), 24.9, 22.7, 20.4, 20.0, 19.6, 18.6, 16.7, 16.1, 15.7, 14.5; IR (film, CHCl_3): $\tilde{\nu}$ 2962, 2931, 2857, 1729, 1712, 1646, 1473, 1456, 1376, 1328, 1243, 1164, 1136, 1109, 998, 982, 940, 885, 826, 650; HR-ESI-MS calc. 659.4701 for $\text{C}_{39}\text{H}_{67}\text{O}_6\text{Si}^+$, $[\text{M}+\text{H}]^+$, found 659.4713.



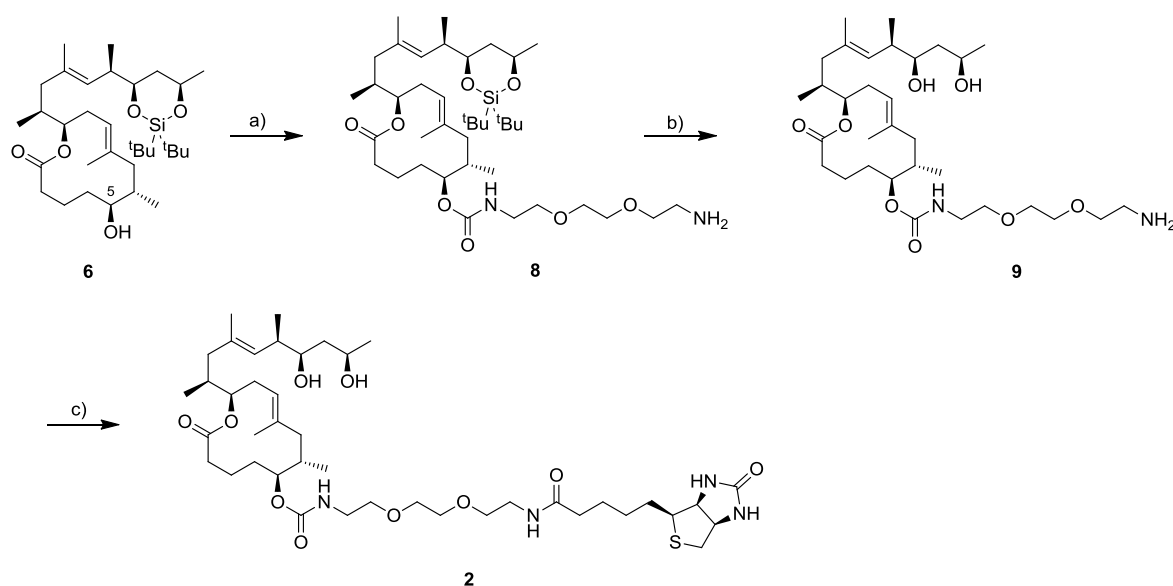
(2E,4E)-((6S,7S,12R,E)-12-((2S,6R,7R,9R,E)-7,9-dihydroxy-4,6-dimethyldec-4-en-2-yl)-7,9-dimethyl-2-oxooxacyclododec-9-en-6-yl)hexa-2,4-dienoate (1).

To a solution of protected diol **7** (9.6 mg, 14.6 μmol) in THF (2.0 mL) and pyridine (0.34 mL) in a 10 mL Falcon tube was added HF-pyridine (ca. 70 % HF, 38 μL). The yellow solution was stirred at ambient temperature for 2 h. The reaction was quenched by adding sat. aq. NaHCO_3 -solution (10 mL) until the gas evolution ceased. Subsequently brine (2 mL) and EtOAc (15 mL) were added and layers were separated. The aq. layer was extracted with EtOAc (3 x 15 mL). The combined org. layers were dried over MgSO_4 and concentrated under reduced pressure. Purification by flash column chromatography (*n*-hexane/ EtOAc 4:1 to 3:2, 0.1 % MeOH) yielded 3.7 mg (49 %) of diol **1** as an inseparable mixture of isomers (2'*E*,4'*E* isomer/minor isomer 91:11). R_f (*n*-hexane/EtOAc 1:1) = 0.47; $[\alpha]_D^{25} = -40.3^\circ$ ($c = 1.10$, CHCl_3); $^1\text{H-NMR}$ (400 MHz, acetone- d_6 , 2'*E*,4'*E* isomer): δ 7.24 (dd, $J = 15.3$ Hz, 10.0, 1H), 6.33 – 6.17 (m, 2H), 5.82 (d, $J = 15.3$ Hz, 1H), 5.12 (d, $J = 10.7$ Hz, 1H), 5.04 (d, $J = 9.8$ Hz, 1H), 4.93 – 4.86 (m, 1H), 4.71 – 4.65 (m, 1H), 4.22 – 4.16 (m, 2H, 2x OH), 4.00 – 3.92 (m, 1H), 3.54 – 3.47 (m, 1H), 2.55 – 2.44 (m, 1H), 2.44 – 2.33 (m, 2H), 2.16 – 1.91 (m, 7H), 1.90 – 1.79 (m, 1H), 1.84 (d, $J = 5.8$ Hz, 3H), 1.74 – 1.62 (m, 3H), 1.71 (s, 3H), 1.64 (d, $J = 1.3$ Hz, 3H), 1.62 – 1.52 (m, 2H), 1.44 – 1.34 (m, 1H), 1.14 (d, $J = 6.2$ Hz, 3H), 0.98 (d, $J = 6.6$ Hz, 3H), 0.90 – 0.87 (m, 6H); $^{13}\text{C-NMR}$ (125 MHz, acetone- d_6 , 2'*E*,4'*E* isomer): δ 173.3, 166.7, 145.5, 139.9, 137.3, 133.4, 131.2, 130.7, 123.9, 120.3, 79.3, 76.9, 76.3, 68.9, 46.4, 44.4, 43.8, 40.5, 35.9, 35.4, 32.8, 31.4, 29.8 (obscured by solvent signal), 24.6, 20.8, 20.4, 18.6, 17.1, 16.2, 15.9, 15.0; IR (film, acetone): $\tilde{\nu}$ 2952, 2929, 2889, 2857, 1727, 1613, 1514, 1472, 1464, 1249, 1102, 1037, 1006, 836, 777; HR-ESI-MS calc. 519.3680 for $\text{C}_{31}\text{H}_{51}\text{O}_6^+$, $[\text{M}+\text{H}]^+$, found 519.3671.

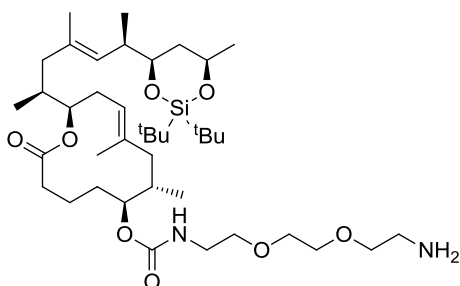
Determination of HPLC purity: Purity of **1** was determined by HPLC (Water Symmetry C18 column, 3.5 μm , 4.6 x 100 mm, injection: 10 μL , eluent: $\text{CH}_3\text{CN}/\text{H}_2\text{O}$ 75:25 to 85:15, flow 1.0 mL/min).

HPLC purification: 3.7 mg of **1** (HPLC purity >88 %) were purified by HPLC (Water Symmetry C18 column, 19 x 100 mm, 5 μm , injection 1.0 + 0.1 mL MeOH, $\text{CH}_3\text{CN}/\text{H}_2\text{O}$ 75:25 isocratic) yielded two product containing fractions. The fractions were combined, concentrated under reduced pressure and lyophilized overnight to yield 1.84 mg of **1** (*trans/cis* 84:13, HPLC purity >99 %).

C5 Biotin-tagged mycolactone analog 3



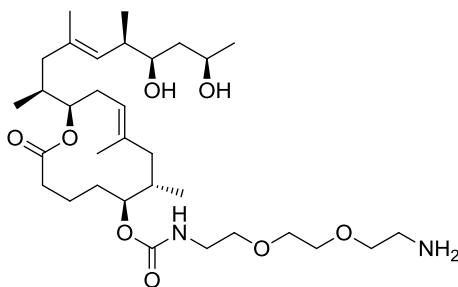
Scheme S2: a) (1) CDI, THF, rt, 2 d; (2) H₂O, rt, 45 min; (3) 1,2-bis(2-aminoethoxy)ethane, rt, 1 d, 81 %; b) HF·pyridine, THF/pyridine (4:1), rt, 2 h, 96 %; c) (+)-biotin, PyBop, DIPEA, DMF, rt, 30 min, 54 %.



(6*S*,7*S*,12*R*,*E*)-12-((2*S*,6*R*,*E*)-6-((4*R*,6*R*)-2,2-di-*tert*-butyl-6-methyl-1,3,2-dioxasilinan-4-yl)-4-methylhept-4-en-2-yl)-7,9-dimethyl-2-oxooxacyclododec-9-en-6-yl-(2-(2-(2-aminoethoxy)ethoxy)ethyl)carbamate (8).

To alcohol **6** (36 mg, 64 μmol) in THF (4.0 mL) was added CDI (83 mg, 510 μmol) at ambient temperature. The suspension was stirred at 40 °C for 1 d and subsequently at ambient temperature for 1 d. After 19 h, CH₂Cl₂ (2 mL) and additional CDI (4 x 21 mg, 510 μmol) were added. When conversion was complete, water (28 μL, 1.53 mmol) was added and the solution stirred for another 45 min. 1,2-bis(2-aminoethoxy)ethane (162 μL, 1.59 mmol) was added subsequently. The resulting milky suspension was stirred at ambient temperature for 1 d. Water (20 mL) and CH₂Cl₂ (20 mL) were added, the layers were separated and the aq. layer was extracted with CH₂Cl₂ (2 x 20 mL). The combined org. layers were washed with water (10 mL), dried over MgSO₄ and concentrated under reduced pressure. Purification by flash column chromatography (CH₂Cl₂ to CH₂Cl₂/MeOH, 50:1 to 9:1) yielded 16 mg (34 %) of the product as a

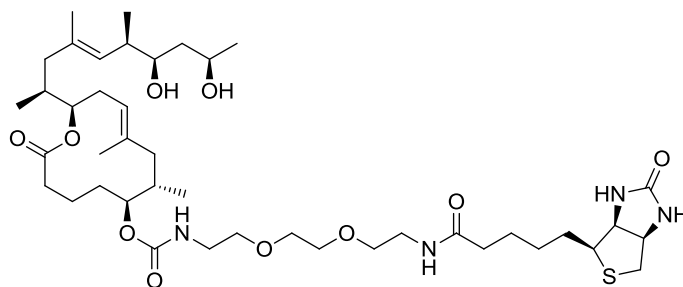
colorless oil and 38 mg of a mixture of activated imidazolyl carbamate and the product. The mixture was dissolved in THF (2.0 mL) and 1,2-bis(2-aminoethoxy)ethane (97 μ L, 0.96 mmol) and a catalytic amount of DMAP were added. The colorless solution was stirred at ambient temperature for 1 d. Water (20 mL) and CH_2Cl_2 (20 mL) were added, the layers were separated and the aq. layer was extracted with CH_2Cl_2 (2 x 10 mL). The combined org. layers were washed with water (10 mL), dried over MgSO_4 and concentrated under reduced pressure. Purification by flash column chromatography ($\text{CH}_2\text{Cl}_2/\text{MeOH}$ 50:1 to 9:1) yielded another 22 mg (47 %) of the product as a colorless oil to give a total of 38 mg (81 %) of amine **8**. R_f ($\text{CH}_2\text{Cl}_2/\text{MeOH}$ 4:1) = 0.16; $[\alpha]_D^{25} = -26.7^\circ$ ($c = 0.53$, CHCl_3); $^1\text{H-NMR}$ (400 MHz, CDCl_3): δ 5.27 – 5.15 (m, 1H), 5.02 (d, $J = 10.2$ Hz, 1H), 4.94 (d, $J = 9.4$ Hz, 1H), 4.86 (ddd, $J = 11.7, 5.7, 2.9$ Hz, 1H), 4.58 – 4.45 (m, 1H), 4.20 – 4.06 (m, 1H), 3.75 – 3.47 (m, 9H), 3.41 – 3.29 (m, 2H), 2.88 (t, $J = 5.2$ Hz, 2H), 2.50 – 2.22 (m, 3H), 2.18 – 1.45 (m, 19H), 1.32 (dt, $J = 13.9, 11.2$ Hz, 1H), 1.17 (d, $J = 6.1$ Hz, 3H), 1.02 – 0.87 (m, 24H), 0.83 (d, $J = 6.7$ Hz, 3H); $^{13}\text{C-NMR}$ (100 MHz, CDCl_3): δ 173.2, 156.4, 136.7, 132.7, 129.8, 122.4, 79.4, 77.8, 75.9, 73.3, 70.5, 70.3, 70.2, 70.1, 45.6, 43.4, 41.7 (2C), 40.7, 40.4, 35.5, 34.7, 32.0, 30.6, 29.6, 27.5 (3C), 27.2 (3C), 24.9, 22.7, 20.3, 19.8, 19.5, 16.7, 16.0, 15.7, 14.4; IR (film, MeOH): $\tilde{\nu}$ 2961, 2931, 2858, 2357, 1722, 1524, 1473, 1457, 1374, 1251, 1162, 1133, 1109, 1064, 1015, 982, 912, 886, 826, 650; HR-ESI-MS calc. 739.5287 for $\text{C}_{40}\text{H}_{75}\text{N}_2\text{O}_8\text{Si}^+$, $[\text{M}+\text{H}]^+$, found 739.5280.



(6*S*,7*S*,12*R*,*E*)-12-((2*S*,6*R*,7*R*,9*R*,*E*)-7,9-dihydroxy-4,6-dimethyldec-4-en-2-yl)-7,9-dimethyl-2-oxooxacyclododec-9-en-6-yl (2-(2-(2-aminoethoxy)ethoxy)ethyl)carbamate (9**).**

To the protected diol **8** (16 mg, 22 μ mol) in THF (1.0 mL) and pyridine (0.26 mL) was added HF·pyridine (70 % in pyridine, 28 μ L, 1.08 mmol) at ambient temperature. The colorless solution was stirred at ambient temperature for 120 min. The reaction was quenched by adding sat. aq. NaHCO_3 -solution (ca. 10 mL) until the evolution of gas ceased. CH_2Cl_2 (10 mL) was added and the layers were separated. The aq. layer was extracted with CH_2Cl_2 (3 x 5 mL). The combined org. layers were washed with brine, dried over MgSO_4 and concentrated under reduced pressure. Purification by flash column chromatography (CH_2Cl_2 to $\text{CH}_2\text{Cl}_2/\text{MeOH}$, 19:1 to 9:1 then 4:1) yielded 12.4 mg (96 %) of the diol **9** as colorless oil. R_f ($\text{CH}_2\text{Cl}_2/\text{MeOH}$ 4:1) = 0.06; $[\alpha]_D^{25} = -14.5^\circ$ ($c = 0.42$, MeOH); $^1\text{H-NMR}$ (400 MHz, methanol- d_4): δ 5.09 (d, $J = 10.2$ Hz, 1H), 5.00 (d, $J = 9.8$ Hz, 1H), 4.93 – 4.83 (m, 1H, partly obscured by H_2O signal), 4.50 – 4.39 (m, 1H), 4.01 – 3.90 (m, 1H), 3.74 – 3.62 (m, 6H), 3.58 – 3.51 (m, 2H), 3.42 (ddd, $J = 10.1, 7.7, 2.5$ Hz, 1H), 3.36 – 3.25 (m, 2H, obscured by solvent signal), 3.16 – 3.09 (m, 2H), 2.60 – 2.33 (m, 3H), 2.21 – 1.79 (m, 8H), 1.72 – 1.57 (m,

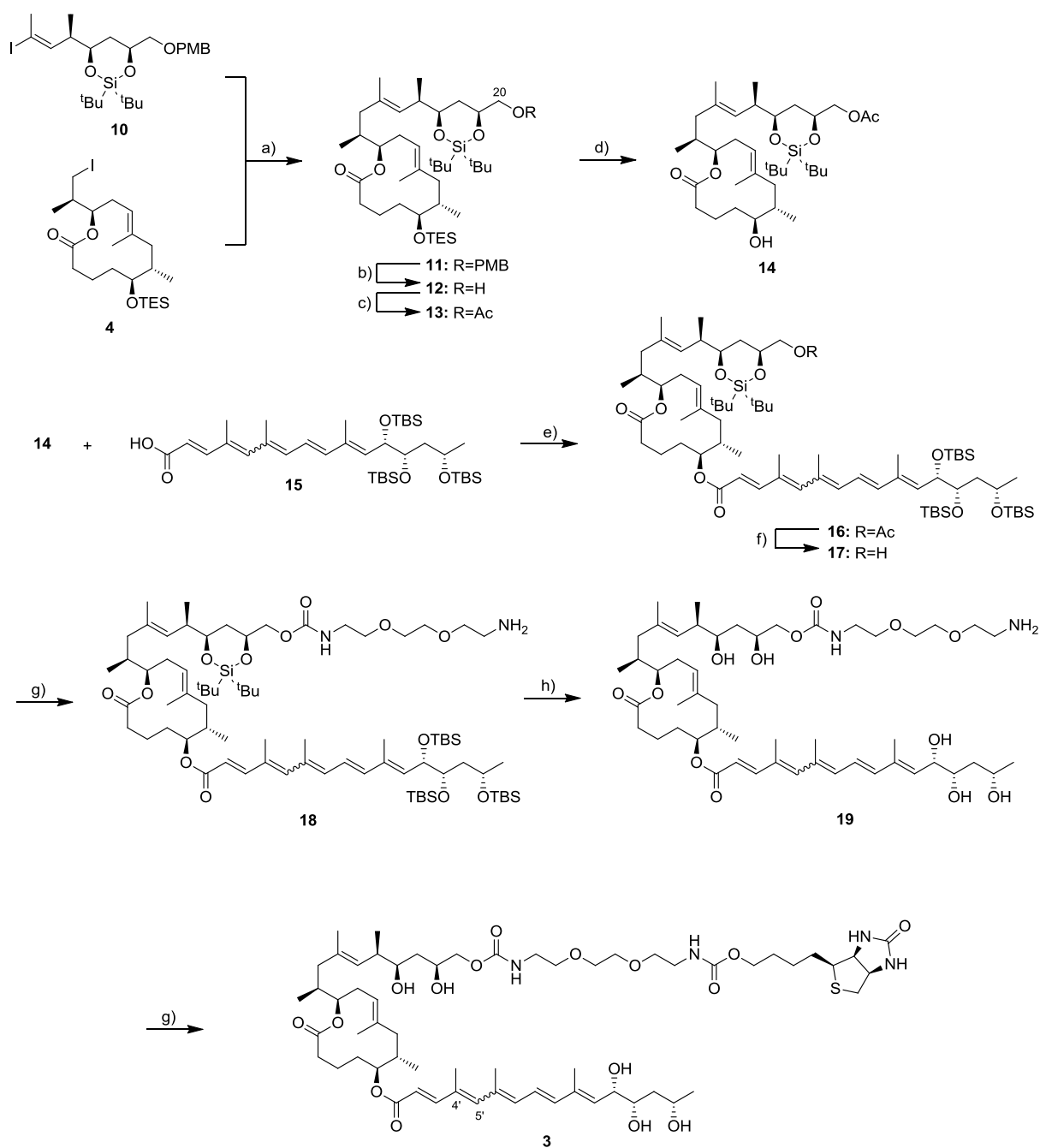
11H), 1.49 (ddd, $J = 14.0, 10.3, 7.4$ Hz, 1H), 1.16 (d, $J = 6.2$ Hz, 3H), 1.01 – 0.87 (m, 9H); ^{13}C -NMR (100 MHz, methanol- d_4): δ 175.3, 159.1, 138.0, 134.2, 131.2, 123.9, 80.6, 77.6, 76.4, 71.4, 71.3, 71.2, 68.3, 67.9, 46.9, 44.6, 44.3, 41.5, 40.8, 40.7, 36.4, 35.9, 33.5, 32.3, 29.9, 23.5, 21.0, 20.3, 17.2, 16.2, 15.9, 15.0; IR (film, MeOH): $\tilde{\nu}$ 3350, 2962, 2927, 1699, 1521, 1453, 1377, 1325, 1255, 1120, 1016, 941; HR-ESI-MS calc. 599.4266 for $\text{C}_{32}\text{H}_{59}\text{N}_2\text{O}_8^+$, $[\text{M}+\text{H}]^+$, found 599.4263.



(6*S*,7*S*,12*R*,*E*)-12-((2*S*,6*R*,7*R*,9*R*,*E*)-7,9-dihydroxy-4,6-dimethyldec-4-en-2-yl)-7,9-dimethyl-2-oxooxacyclododec-9-en-6-yl-(2-(2-(2-(5-((3*aS*,4*S*,6*aR*)-2-oxohexahydro-1*H*-thieno[3,4-*d*]imidazol-4-yl)pentanamido)ethoxy)ethoxy)ethyl)carbamate (2).

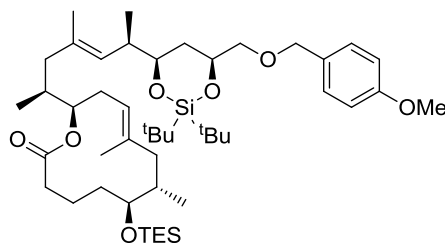
To (+)-biotin (18 mg, 74 μmol) in DMF (2.0 mL) were added DIPEA (43 μL , 247 μmol) and PyBop (51 mg, 99 μmol) at ambient temperature. The colorless solution was stirred at ambient temperature for 30 min. At this point all biotin had been consumed (TLC). The activated biotin (38 μmol) in DMF (1.0 mL; 50 % of the above solution) was transferred dropwise to a flask charged with amine **9** (15 mg, 25 μmol). The colorless solution was stirred at ambient temperature for 30 min. Sat. aq. NH_4Cl -solution (5 mL), water (15 mL) and EtOAc (10 mL) were added, the layers were separated and the aq. layer was extracted with EtOAc (3 x 10 mL). The combined org. layers were washed with sat. aq. NaHCO_3 -solution (2 x 3 mL) and brine, dried over MgSO_4 and concentrated under reduced pressure. Purification by flash column chromatography (CH_2Cl_2 to $\text{CH}_2\text{Cl}_2/\text{MeOH}$, 96:4 to 93:7 then 90:10) yielded 11.1 mg (54 %) of amide **2** as colorless oil. R_f ($\text{CH}_2\text{Cl}_2/\text{MeOH}$ 9:1) = 0.36; $[\alpha]_D^{25} = +9.6^\circ$ ($c = 0.56$, MeOH); ^1H -NMR (400 MHz, methanol- d_4): δ 5.09 (d, $J = 10.4$ Hz, 1H), 5.00 (d, $J = 9.7$ Hz, 1H), 4.89 (ddd, $J = 11.7, 5.0, 2.7$ Hz, 1H), 4.54 – 4.41 (m, 2H), 4.31 (dd, $J = 7.9, 4.5$ Hz, 1H), 4.00 – 3.87 (m, 1H), 3.66 – 3.58 (m, 4H), 3.58 – 3.50 (m, 4H), 3.42 (ddd, $J = 10.2, 7.6, 2.5$ Hz, 1H), 3.39 – 3.33 (m, 2H), 3.34 – 3.25 (m, 2H, partly obscured by solvent signal), 3.24 – 3.18 (m, 1H), 2.93 (dd, $J = 12.7, 5.0$ Hz, 1H), 2.71 (d, $J = 12.7$ Hz, 1H), 2.57 – 2.33 (m, 3H), 2.23 (t, $J = 7.4$ Hz, 2H), 2.16 – 1.42 (m, 26H), 1.16 (d, $J = 6.2$ Hz, 3H), 0.98 (d, $J = 6.7$ Hz, 3H), 0.93 (d, $J = 6.5$ Hz, 3H), 0.89 (d, $J = 6.7$ Hz, 3H); ^{13}C -NMR (100 MHz, methanol- d_4): δ 176.1, 175.2, 166.1, 159.0, 138.0, 134.3, 131.2, 123.9, 80.7, 77.6, 76.4, 71.3 (2C), 71.0, 70.6, 68.3, 63.4, 61.6, 57.0, 46.9, 44.6, 44.3, 41.6, 41.1, 40.8, 40.3, 36.7, 36.4, 35.9, 33.5, 32.3, 30.0, 29.8, 29.5, 26.8, 23.5, 21.0, 20.5, 17.2, 16.2, 15.9, 15.0; IR (film, EtOAc): $\tilde{\nu}$ 3319, 2930, 2871, 2360, 2338, 1695, 1540, 1454, 1374, 1332, 1312, 1253, 1160, 1129, 1093, 1016, 845, 558; HR-ESI-MS calc. 825.5042 for $\text{C}_{42}\text{H}_{73}\text{N}_4\text{O}_{10}\text{S}^+$, $[\text{M}+\text{H}]^+$, found 825.5045.

C20 Biotin-tagged mycolactone analog 2



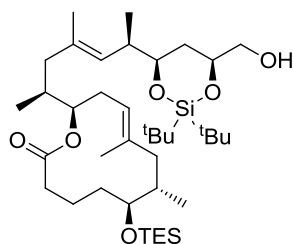
Scheme S3: a) (1) **4**¹, *t*-BuLi (2.4 eq), MeO-9-BBN, Et₂O/THF 1:1, -78 °C to rt, 45 min; (2) **10**¹ (0.85 eq), Pd(dppf)Cl₂ (0.1 eq), AsPh₃, aq. Cs₂CO₃, DMF, rt, 19 h, 66 %; b) DDQ, CH₂Cl₂/water 5:1, rt, 2 h, 75 %; c) Ac₂O, DIPEA, DMAP, CH₂Cl₂, rt, 30 min, quant.; d) THF/H₂O/HOAc 3:1:1, rt, 6 h, 89 %. e) Cl₃C₆H₂COCl, DIPEA, DMAP, rt, 16 h, 88 % (*E*-Δ^{4,5'}/*Z*-Δ^{4,5'} 4.3:1); f) K₂CO₃, MeOH, rt, 180 min, 90 % (*E*-Δ^{4,5'}/*Z*-Δ^{4,5'} 4:1). g) (1) CDI (12 eq), THF, rt, 5 h; (2) H₂O, rt, 30 min; (3) 1,2-bis(2-aminoethoxy)ethane (25 eq), rt, 90 min,

87 % (*E*- $\Delta^{4,5'}$ /*Z*- $\Delta^{4,5'}$ 3:1); h) (1) TBAF, THF, rt, 4 h; (2) NH₄F, rt, 17 h, quant. (*E*- $\Delta^{4,5'}$ /*Z*- $\Delta^{4,5'}$ 3:1); g) (+)-biotin, DIPEA, PyBop, DMF, rt, 30 min, 63 % (*E*- $\Delta^{4,5'}$ /*Z*- $\Delta^{4,5'}$ /other isomers 63:29:8)



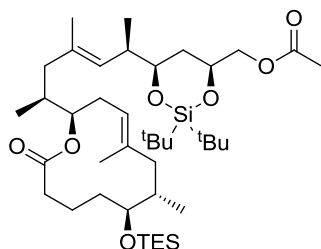
(6*S*,7*S*,12*R*,*E*)-12-(((2*S*,6*R*,*E*)-6-((4*R*,6*S*)-2,2-di-*tert*-butyl-6-(((4-methoxybenzyl)oxy)-methyl)-1,3,2-dioxasilinan-4-yl)-4-methylhept-4-en-2-yl)-7,9-dimethyl-6-((triethylsilyl)oxy)oxacyclododec-9-en-2-one (11).

To a solution of alkyl iodide **4** [1] (80 mg, 0.16 mmol) and MeO-9-BBN (1.0 M in hexane, 0.41 mL, 0.41 mmol) in diethyl ether (1.0 mL) in a 20 ml *Schlenk* flask was added *t*-BuLi (1.6 M in pentane, 0.24 mL, 0.38 mmol) and THF (1.0 mL) slowly *via* syringe at -78°C . The resulting yellow mixture was stirred at -78°C for 10 min and was then allowed to warm to ambient temperature. It was stirred at ambient temperature for 45 min while it turned almost colorless. The solution was transferred into a solution of vinyl iodide **10**¹ (75 mg, 0.13 mmol), Pd(dppf)Cl₂ (11.5 mg, 16 μmol), AsPh₃ (14.5 mg, 47 μmol), and aq. Cs₂CO₃-solution (3.0 M in H₂O, 178 μL , 0.54 mmol) in DMF (1.0 mL) *via* syringe. The yellow suspension was stirred in darkness at ambient temperature for 19 h over which period it turned orange. H₂O (20 mL) and Et₂O (20 mL) were added, the layers were separated and the aq. layer was extracted with diethyl ether (2 x 20 mL). The combined org. layers were washed with brine (3 mL) and dried over MgSO₄. The solvents were evaporated under reduced pressure. Purification by flash column chromatography (*n*-hexane/EtOAc 50:1 to 20:1) yielded 72 mg (66 %) of coupling product **11** as colorless oil. R_f (*n*-hexane/EtOAc 9:1) = 0.46; $[\alpha]_D^{25} = -17.89^{\circ}$ ($c = 0.66$, CHCl₃); ¹H-NMR (400 MHz, CDCl₃): δ 7.26 (d, $J = 8.6$ Hz, 2H), 6.87 (d, $J = 8.6$ Hz, 2H), 5.00 – 4.95 (m, 2H), 4.84 (ddd, $J = 11.7, 6.0, 3.0$ Hz, 1H), 4.52 (s, 3H), 4.22 – 4.15 (m, 1H), 3.80 (s, 3H), 3.75 (ddd, $J = 11.5, 7.2, 1.6$ Hz, 1H), 3.49 (dd, $J = 10.0, 5.4$ Hz, 1H), 3.41 – 3.36 (m, 1H), 3.33 (d, $J = 10.0, 5.9$ Hz, 1H), 2.53 – 2.31 (m, 3H), 2.12 (dd, $J = 13.2, 4.2$ Hz, 1H), 2.06 – 1.65 (m, 10H), 1.66 (s, 3H), 1.59 (d, $J = 1.0$ Hz, 3H), 1.45 – 1.25 (m, 3H), 1.02 – 0.96 (m, 6H), 1.01 (m, 9H), 0.97 (s, 9 H), 0.95 (t, $J = 7.8$ Hz, 9H), 0.83 (d, $J = 6.8$ Hz, 3H), 0.60 (q, $J = 7.8$ Hz, 6H); ¹³C-NMR (100 MHz, CDCl₃): δ 173.5, 159.1, 137.3, 132.8, 130.8, 129.6, 129.2, 129.1 (2C), 121.5, 113.8 (2C), 113.7, 77.8, 77.7, 75.7, 75.2, 73.5, 73.0, 55.3, 45.4, 43.1, 40.4, 36.9, 35.9, 35.0, 33.5, 30.1, 27.5 (3C), 27.2 (3C), 22.8, 21.8, 19.7, 18.7, 16.5, 16.2, 15.6, 7.0 (3C), 5.1 (3C); IR (film, CHCl₃): $\tilde{\nu}$ 2956, 2933, 2875, 2857, 2359, 1727, 1513, 1472, 1464, 1458, 1385, 1374, 1363, 1304, 1247, 1164, 1125, 1103, 1024, 985, 928, 825, 805, 783, 779, 762, 742, 724, 651; HR-ESI-MS calc. 832.5937 for C₄₇H₈₆NO₇Si₂⁺, [M+NH₄]⁺, found 832.5946.



(6S,7S,12R,E)-12-((2S,6R,E)-6-((4R,6S)-2,2-di-tert-butyl-6-(hydroxymethyl)-1,3,2-dioxasilinan-4-yl)-4-methylhept-4-en-2-yl)-7,9-dimethyl-6-((triethylsilyl)oxy)oxacyclododec-9-en-2-one (12).

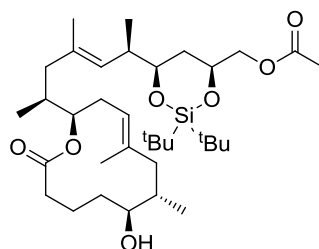
To a solution of PMB-protected alcohol **11** (72 mg, 88 μmol) in $\text{CH}_2\text{Cl}_2/\text{water}$ (5:1, 6 mL) was added DDQ (27 mg, 119 μmol) at ambient temperature. The brown two-layer system was stirred at ambient temperature for 2 h. The reaction was quenched by adding sat. aq. NaHCO_3 -solution (10 mL) and little water. EtOAc (20 mL) was added and the layers were separated. The aq. layer was extracted with EtOAc (2 x 10 mL), the combined org. layers were washed with water (3 mL), brine, dried over MgSO_4 and concentrated under reduced pressure. Purification by flash column chromatography (*n*-hexane/EtOAc 100:7) yielded 46 mg (75 %) of primary alcohol **12** as colorless oil. R_f (*n*-hexane/EtOAc 9:1) = 0.38; $[\alpha]_D^{25} = -28.5^\circ$ ($c = 0.84$, CHCl_3); $^1\text{H-NMR}$ (400 MHz, CDCl_3): δ 4.98 – 4.90 (m, 2H), 4.83 (ddd, $J = 11.8, 5.7, 3.0$ Hz, 1H), 4.14 – 4.07 (m, 1H), 3.75 (ddd, $J = 11.5, 7.8, 1.9$ Hz, 1H), 3.58 – 3.51 (m, 1H), 3.47 – 3.36 (m, 2H), 2.53 – 2.26 (m, 3H + OH), 2.09 (dd, $J = 13.0, 5.4$ Hz, 1H), 2.04 – 1.57 (m, 10H), 1.66 (s, 3H), 1.60 (d, $J = 1.0$, 3H), 1.48 – 1.33 (m, 3H), 1.02 (s, 9H), 1.02 – 0.97 (m, 6H), 0.99 (s, 9H), 0.95 (t, $J = 7.8$ Hz, 9H), 0.85 (d, $J = 6.6$ Hz, 3H), 0.60 (q, $J = 7.8$ Hz, 6H); $^{13}\text{C-NMR}$ (100 MHz, CDCl_3): δ 173.6, 137.5, 133.2, 129.4, 121.4, 77.8, 77.7, 75.4, 74.7, 67.6, 45.4, 43.4, 40.6, 35.9, 35.8, 34.8, 33.5, 33.4, 29.5, 27.5 (3C), 27.1 (3C), 22.8, 21.8, 19.7, 18.7, 16.8, 16.1, 15.6, 14.5, 7.0 (3C), 5.1 (3C); IR (film, CHCl_3): $\tilde{\nu}$ 2956, 2933, 2876, 2858, 1728, 1473, 1458, 1385, 1249, 1165, 1128, 1103, 1087, 1067, 1024, 985, 949, 927, 826, 764, 738, 650; HR-ESI-MS calc. 717.4916 for $\text{C}_{39}\text{H}_{74}\text{NaO}_6\text{Si}_2^+$, $[\text{M}+\text{Na}]^+$, found 717.4918.



((4S,6R)-2,2-di-tert-butyl-6-((2R,6S,E)-6-((2R,7S,8S,E)-5,7-dimethyl-12-oxo-8-((triethylsilyl)oxy)oxacyclododec-4-en-2-yl)-4-methylhept-3-en-2-yl)-1,3,2-dioxasilinan-4-yl)methyl acetate (13).

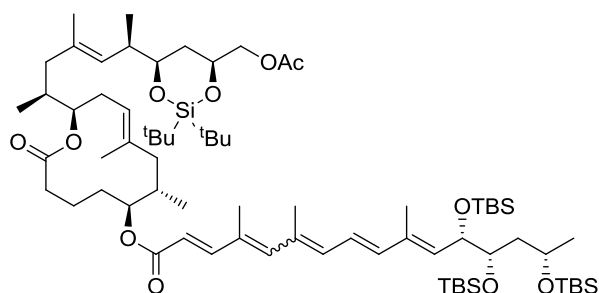
To a solution of primary alcohol **12** (46 mg, 66 μmol) in CH_2Cl_2 (2.0 mL) were added DIPEA (0.11 mL, 662 μmol), acetic anhydride (19 μL , 199 μmol) and a catalytic amount of DMAP (ca. 2 mg) at ambient temperature. The reaction was stirred at ambient temperature for 30 min before additional CH_2Cl_2 (10 mL) was added and the org. layer was washed with sat. aq. NaHCO_3 -solution (5 mL). The aq. layer was extracted with CH_2Cl_2 (2 x 5 mL). The combined org. layers were dried over MgSO_4 and concentrated

under reduced pressure. Purification by flash column chromatography (*n*-hexane/EtOAc 25:1) afforded 49 mg (quant.) of acetylated alcohol **13** as colorless oil. R_f (*n*-hexane/ EtOAc 9:1) = 0.56; $[\alpha]_D^{25} = -19.1^\circ$ ($c = 0.83$, CHCl_3); $^1\text{H-NMR}$ (400 MHz, CDCl_3): δ 4.97 (d, $J = 9.7$ Hz, 2H), 4.87 – 4.80 (m, 1H), 4.24 – 4.16 (m, 1H), 4.07 – 3.99 (m, 2H), 3.74 (ddd, $J = 11.1, 7.4, 1.8$ Hz, 1H), 3.38 (d, $J = 9.3$ Hz, 1H), 2.53 – 2.31 (m, 3H), 2.12 (dd, $J = 13.1, 4.4$ Hz, 1H), 2.06 (s, 3H), 2.05 – 1.58 (m, 10H), 1.66 (s, 3H), 1.60 (d, $J = 1.0$ Hz, 3H), 1.50 – 1.38 (m, 3H), 1.00 (d, $J = 6.2$ Hz, 3H), 1.00 (s, 9H), 0.99 (d, $J = 3.6$ Hz, 3H), 0.98 (s, 9H), 0.95 (t, $J = 7.8$ Hz, 9H), 0.84 (d, $J = 6.8$ Hz, 3H), 0.60 (q, $J = 7.8$ Hz, 6H); $^{13}\text{C-NMR}$ (100 MHz, CDCl_3): δ 173.5, 170.9, 137.4, 133.1, 129.4, 121.4, 77.8, 77.5, 75.6, 72.0, 68.6, 45.4, 43.2, 40.4, 36.2, 35.9, 35.0, 33.5, 33.5, 30.0, 27.5 (3C), 27.0 (3C), 22.7, 21.8, 20.9, 19.7, 18.7, 16.6, 16.2, 15.7, 14.5, 7.0 (3C), 5.1 (3C); IR (film, CHCl_3): $\tilde{\nu}$ 2956, 2932, 2876, 2858, 1742, 1728, 1473, 1459, 1385, 1365, 1245, 1163, 1131, 1109, 1084, 1069, 1040, 1024, 985, 905, 825, 763, 742, 723, 651; HR-ESI-MS calc. 759.5022 for $\text{C}_{41}\text{H}_{76}\text{NaO}_7\text{Si}_2^+$, $[\text{M}+\text{Na}]^+$, found 759.5003.



((4*S*,6*R*)-2,2-di-*tert*-butyl-6-((2*R*,6*S*,*E*)-6-((2*R*,7*S*,8*S*,*E*)-8-hydroxy-5,7-dimethyl-12-oxooxacyclo-dodec-4-en-2-yl)-4-methylhept-3-en-2-yl)-1,3,2-dioxasilinan-4-yl)methyl acetate (14**).**

To a solution of TES-protected alcohol **13** (49 mg, 66 μmol) in THF (2.0 mL) were added H_2O (0.66 mL) and HOAc (0.66 mL) at ambient temperature. The reaction was stirred at ambient temperature for 6 h. Subsequently, sat. aq. NaHCO_3 -solution (20 mL) was added until the evolution of gas stopped. EtOAc (20 mL) was added and the layers were separated. The aq. layer was extracted with EtOAc (2 x 10 mL). The combined org. layers were washed with sat. aq. NaHCO_3 -solution, brine, dried over MgSO_4 and concentrated under reduced pressure. Purification by flash column chromatography (*n*-hexane/ EtOAc 20:1 to 3:1, 0.5 % MeOH) yielded 37 mg (89 %) of secondary alcohol **14** as colorless oil. R_f (*n*-hexane/EtOAc 2:1) = 0.37; $[\alpha]_D^{25} = -32.1^\circ$ ($c = 0.56$, CHCl_3); $^1\text{H-NMR}$ (400 MHz, CDCl_3): δ 5.06 – 4.93 (m, 3H), 4.24 – 4.16 (m, 1H), 4.04 (d, $J = 4.9$ Hz, 2H), 3.71 (ddd, $J = 11.3, 7.5, 1.7$ Hz, 1H), 3.55 – 3.48 (m, 1H), 2.46 (dt, $J = 14.2, 11.5$ Hz, 1H), 2.40 – 2.20 (m, 3H), 2.15 – 2.04 (m, 2H), 2.07 (s, 3H), 2.02 – 1.82 (m, 4H), 1.77 – 1.51 (m, 5H), 1.61 (s, 3H), 1.60 (d, $J = 1.2$ Hz, 3H), 1.46 (dt, $J = 13.8, 11.3$ Hz, 1H), 1.37 – 1.27 (m, 1H), 1.01 (d, $J = 6.5$ Hz, 3H), 1.01 (s, 9H) 0.98 (s, 9H), 0.95 (d, $J = 6.8$ Hz, 3H), 0.85 (d, $J = 6.7$ Hz, 3H); $^{13}\text{C-NMR}$ (100 MHz, CDCl_3): δ 175.2, 171.0, 137.1, 133.0, 129.5, 123.0, 77.5, 76.7, 72.0, 70.8, 68.6, 45.4, 43.2, 40.5, 36.1, 35.1, 31.5, 34.9, 34.2, 30.1, 27.5 (3C), 27.0 (3C), 22.7, 20.9, 20.4, 19.7, 16.6, 16.4, 16.2, 15.9, 14.8; IR (film, CHCl_3): $\tilde{\nu}$ 2960, 2932, 2858, 1743, 1733, 1727, 1715, 1474, 1464, 1456, 1386, 1364, 1243, 1156, 1134, 1107, 1041, 1012, 985, 962, 940, 905, 826, 793, 651; HR-ESI-MS calc. 623.4338 for $\text{C}_{35}\text{H}_{63}\text{O}_7\text{Si}^+$, $[\text{M}+\text{H}]^+$, found 623.4339.

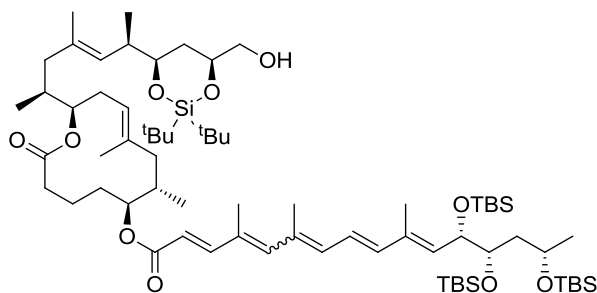


(2E,8E,10E,12S,13S,15S)-(6S,7S,12R,E)-12-((2S,6R,E)-6-((4R,6S)-6-(acetoxymethyl)-2,2-di-*tert*-butyl-1,3,2-dioxasilinan-4-yl)-4-methylhept-4-en-2-yl)-7,9-dimethyl-2-oxooxacyclododec-9-en-6-yl 12,13,15-tris((*tert*-butyldimethylsilyl)oxy)-4,6,10-trimethylhexadeca-2,4,6,8,10-pentaenoate (16).

To a solution of acid **15**¹ (98 mg, 0.14 mmol) in THF (2.0 mL) was added DIPEA (0.10 mL, 0.58 mmol), Cl₃C₆H₂COCl (45 μL, 0.29 mmol) and DMAP (53 mg, 0.43 mmol) at ambient temperature. After a few seconds the bright yellow solution became turbid. After 10 min alcohol **14** (42 mg, 67 μmol) in THF (2.0 mL) was added. The yellow suspension was stirred at ambient temperature for 16½ h protected from light. The reaction was quenched by adding sat. aq. NaHCO₃-solution (10 mL) and EtOAc (15 mL), the layers were separated and the aq. layer was extracted with EtOAc (2 x 10 mL). The combined org. layers were washed with brine, dried over MgSO₄ and concentrated under reduced pressure. Purification by flash column chromatography (1. *n*-hexane/EtOAc 12:1 to 4:1 to 4:1, 0.25 % HCOOH; 2. *n*-hexane/EtOAc 25:1 to 9:1) yielded 76 mg (88 %) of ester **16** as an inseparable mixture of isomers (*E*-Δ^{4',5'}/*Z*-Δ^{4',5'} 4.3:1)

as a yellow oil and 38 mg (39 %) of starting acid **14**. R_f(*n*-hexane/EtOAc 9:1) = 0.35; **Z**-Δ^{4',5'} **isomer**: ¹H-NMR (400 MHz, acetone-*d*₆): δ 7.93 (d, *J* = 15.3 Hz, 1H), 6.74 – 6.61 (m, 1H), 6.47 (d, *J* = 19.6 Hz, 1H), 6.34 (s, 1H), 6.19 (d, *J* = 10.6 Hz, 1H), 5.93 (d, *J* = 15.3 Hz, 1H), 5.71 – 5.64 (m, 1H), 5.15 – 5.05 (m, 2H), 4.90 (ddd, *J* = 11.8, 5.1, 2.8 Hz, 1H), 4.77 – 4.68 (m, 1H), 4.58 (dd, *J* = 9.2, 3.4 Hz, 1H), 4.36 – 4.27 (m, 1H), 4.09 – 3.94 (m, 3H), 3.86 (ddd, *J* = 11.1, 7.6, 1.7 Hz, 1H), 3.82 – 3.75 (m, 1H), 2.59 – 2.29 (m, 3H), 2.29 – 1.77 (m, 10H), 2.05 (s, 3H), 2.02 (s, 3H), 1.98 (d, *J* = 1.0 Hz, 3H), 1.94 (d, *J* = 1.0 Hz, 3H), 1.77 – 1.47 (m, 6H), 1.71 (s, 3H), 1.67 (d, *J* = 1.04 Hz, 3H), 1.18 (d, *J* = 5.9 Hz, 3H), 1.06 (d, *J* = 6.6 Hz, 3H), 1.04 (s, 9H), 1.02 (s, 9H), 0.94 – 0.87 (m, 33H), 0.37 – 0.18 (m, 18H). ¹³C-NMR (100 MHz, acetone-*d*₆): δ 173.3, 170.8, 166.9, 143.0, 141.8, 140.0, 137.4, 135.7, 135.0, 135.0, 134.7, 134.3, 132.0, 130.2, 125.3, 123.8, 119.7, 79.2, 78.6, 76.2, 74.4, 73.2, 72.2, 69.0, 66.8, 46.3, 44.3, 44.1, 41.4, 36.9, 36.0, 35.5, 32.9, 31.4, 29.6, 27.9 (3C), 27.6 (3C), 26.4 (3C), 26.3 (3C), 26.3 (3C), 24.3, 23.3, 21.1, 20.8, 20.8, 20.5, 20.3, 18.7, 18.6, 18.6, 17.7, 17.0, 16.4, 15.9, 15.1, 13.9, –3.8, –3.9, –3.9, –4.1, –4.3, –4.4; **E**-Δ^{4',5'} **isomer**: ¹H-NMR (400 MHz, acetone-*d*₆): δ 7.37 (d, *J* = 15.5 Hz, 1H), 6.74 – 6.61 (m, 1H), 6.48 (d, *J* = 14.5 Hz, 1H), 6.48 (s, 1H), 6.39 (d, *J* = 11.7 Hz, 1H), 5.89 (d, *J* = 15.5 Hz, 1H), 5.71 – 5.64 (m, 1H), 5.15 – 5.05 (m, 2H), 4.90 (ddd, *J* = 11.8, 5.1, 2.8 Hz, 1H), 4.77 – 4.68 (m, 1H), 4.58 (dd, *J* = 9.2, 3.4 Hz, 1H), 4.36 – 4.27 (m, 1H), 4.09 – 3.94 (m, 3H), 3.86 (ddd, *J* = 11.1, 7.6, 1.7 Hz, 1H), 3.82 – 3.75 (m, 1H), 2.59 – 2.29 (m, 3H), 2.29 – 1.77 (m, 10H), 2.09 (s, 3H), 2.06 (s, 3H), 2.02 (s, 3H), 1.94 (d, *J* = 1.0 Hz, 3H), 1.77 – 1.47 (m, 6H), 1.71 (s, 3H), 1.67 (d, *J* = 1.04 Hz, 3H), 1.18 (d, *J* = 5.9 Hz, 3H), 1.06 (d, *J* = 6.6 Hz, 3H), 1.04 (s, 9H), 1.02 (s, 9H), 0.94 – 0.87 (m, 33H), 0.37 – –0.18 (m, 18H); ¹³C-NMR (100 MHz,

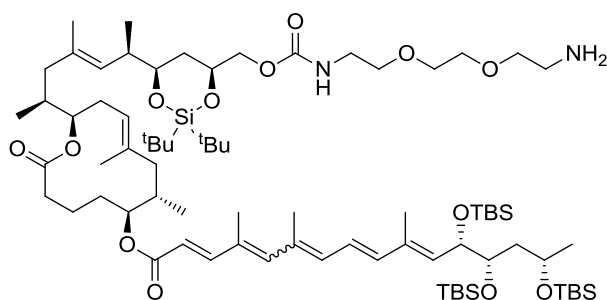
acetone- d_6): δ 173.3, 170.8, 166.9, 151.2, 144.3, 140.3, 137.4, 136.2, 135.7, 135.4, 135.0, 134.3, 133.2, 130.2, 125.3, 123.8, 117.5, 79.2, 78.6, 76.2, 74.4, 73.2, 72.2, 69.0, 66.8, 46.3, 44.3, 44.1, 41.4, 36.9, 36.0, 35.5, 32.9, 31.4, 29.6, 27.9 (3C), 27.6 (3C), 26.4 (3C), 26.3 (3C), 26.3 (3C), 24.3, 23.3, 20.8, 20.8, 20.5, 20.3, 18.7, 18.6, 18.6, 17.2, 17.0, 16.4, 15.9, 15.1, 14.4, 13.9, -3.8, -3.9, -3.9, -4.1, -4.3, -4.4; IR (film, acetone): $\tilde{\nu}$ 2955, 2931, 2895, 2857, 1740, 1728, 1707, 1650, 1604, 1509, 1472, 1463, 1442, 1386, 1362, 1304, 1284, 1252, 1215, 1167, 1157, 1133, 1093, 1061, 1036, 985, 962, 938, 927, 835, 810, 807, 771, 759; HR-ESI-MS calc. 1283.8763 for $C_{72}H_{131}O_{11}Si_4^+$, $[M+H]^+$, found 1283.8764.



(2E,8E,10E,12S,13S,15S)-(6S,7S,12R,E)-12-((2S,6R,E)-6-((4R,6S)-2,2-di-*tert*-butyl-6-(hydroxymethyl)-1,3,2-dioxasilinan-4-yl)-4-methylhept-4-en-2-yl)-7,9-dimethyl-2-oxooxacyclododec-9-en-6-yl-12,13,15-tris((*tert*-butyldimethylsilyl)oxy)-4,6,10-trimethyl hexadeca-2,4,6,8,10-pentaenoate (17).

To a solution of acetylated alcohol **16** (76 mg, 59 μ mol) in MeOH (4 mL) was added K_2CO_3 (41 mg, 296 μ mol) at ambient temperature. The solution was stirred at ambient temperature for 180 min. Aq. buffer solution (pH = 7.2, 10 mL) and EtOAc (15 mL) were added. The layers were separated and the aq. layer was extracted with EtOAc (1 x 5 mL). The combined org. layers were washed with brine, dried over $MgSO_4$ and concentrated under reduced pressure. Purification by flash column chromatography (*n*-hexane/EtOAc 20:1 to 7:3) furnished 66 mg (90 %) of primary alcohol **17** as yellow oil as an inseparable mixture of isomers (*E*- $\Delta^{4,5'}$ /*Z*- $\Delta^{4,5'}$ 4:1). R_f (*n*-hexane/EtOAc 4:1) = 0.58; **Z- $\Delta^{4,5'}$ isomer**: 1H -NMR (400 MHz, acetone- d_6): δ 7.93 (d, J = 15.5 Hz, 1H), 6.72 – 6.62 (m, 1H), 6.53 – 6.29 (m, 2H), 6.19 (d, J = 10.7 Hz, 1H), 5.93 (d, J = 15.5 Hz, 1H), 5.70 – 5.64 (m, 1H), 5.13 (d, J = 10.4 Hz, 1H), 5.07 (d, J = 9.9 Hz, 1H), 4.94 – 4.84 (m, 1H), 4.75 – 4.69 (m, 1H), 4.58 (dd, J = 9.2, 3.4 Hz, 1H), 4.14 – 4.06 (m, 1H), 4.01 (dd, J = 12.3, 6.3 Hz, 1H), 3.90 – 3.73 (m, 2H), 3.59 – 3.48 (m, 2H, OH), 3.47 – 3.40 (m, 1H), 2.61 – 2.36 (m, 3H), 2.22 – 1.77 (m, 19H), 1.77 – 1.52 (m, 5H), 1.71 (s, 3H), 1.66 (d, J = 1.2 Hz, 3H), 1.44 (ddd, J = 14.1, 11.4, 11.4 Hz, 1H), 1.17 (d, J = 6.0 Hz, 3H), 1.05 (d, J = 5.3 Hz, 3H), 1.04 (s, 9H), 1.00 (s, 9H), 0.96 – 0.79 (m, 33H), 0.24 – -0.11 (m, 18H); ^{13}C -NMR (100 MHz, acetone- d_6): δ 173.3, 166.8, 143.0, 141.8, 140.0, 137.3, 135.7, 135.1, 134.7, 134.3, 133.9, 132.0, 130.4, 125.2, 123.8, 119.7, 79.2, 78.8, 76.2, 76.2, 74.3, 72.1, 68.0, 66.7, 46.3, 44.3, 44.0, 41.4, 37.3, 36.0, 35.4, 32.6, 31.3, 29.8, 28.0 (3C), 27.6 (3C), 26.4 (3C), 26.3 (3C), 26.3 (3C), 24.3, 23.4, 21.2, 20.8, 20.6, 20.3, 18.7, 18.6 (2C), 17.7, 17.2, 16.3, 15.9, 15.0, 13.9, -3.7, -3.8, -3.9, -4.1, -4.2, -4.3; **E- $\Delta^{4,5'}$ isomer**: 1H -NMR (400 MHz, acetone- d_6): δ 7.37 (d, J = 15.0 Hz, 1H), 6.72 – 6.62 (m, 1H), 6.53 – 6.29 (m, 3H), 5.89 (d, J = 15.7 Hz, 1H), 5.70 – 5.64 (m, 1H), 5.13 (d, J = 10.4 Hz, 1H), 5.07 (d, J = 9.9 Hz, 1H), 4.94 – 4.84 (m, 1H), 4.75 –

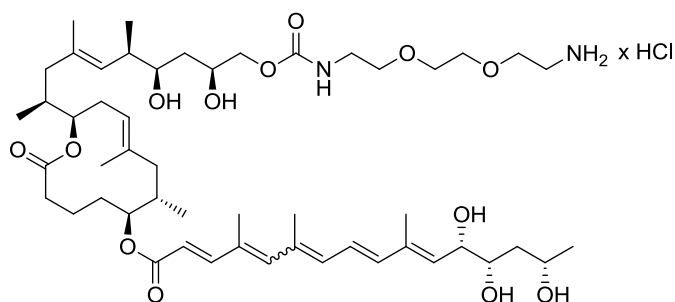
4.69 (m, 1H), 4.58 (dd, $J = 9.2, 3.4$ Hz, 1H), 4.14 – 4.06 (m, 1H), 4.01 (dd, $J = 12.3, 6.3$ Hz, 1H), 3.90 – 3.73 (m, 2H), 3.59 – 3.48 (m, 2H, OH), 3.47 – 3.40 (m, 1H), 2.61 – 2.36 (m, 3H), 2.22 – 1.77 (m, 16H), 2.09 (s, 3H), 1.77 – 1.52 (m, 5H), 1.71 (s, 3H), 1.66 (d, $J = 1.2$ Hz, 3H), 1.44 (ddd, $J = 14.1, 11.4, 11.4$ Hz, 1H), 1.17 (d, $J = 6.0$ Hz, 3H), 1.05 (d, $J = 5.3$ Hz, 3H), 1.04 (s, 9H), 1.00 (s, 9H), 0.96 – 0.79 (m, 33H), 0.24 – -0.11 (m, 18H); $^{13}\text{C-NMR}$ (100 MHz, acetone- d_6): δ 173.3, 166.8, 151.2, 144.3, 140.3, 137.3, 136.2, 135.7, 135.3, 134.9, 133.9, 133.2, 130.4, 125.2, 123.8, 117.4, 79.2, 78.8, 76.2, 76.2, 74.3, 72.1, 68.0, 66.7, 46.3, 44.3, 44.0, 41.4, 37.3, 36.0, 35.4, 32.6, 31.3, 29.8, 28.0 (3C), 27.6 (3C), 26.4 (3C), 26.3 (3C), 26.3 (3C), 24.3, 23.4, 20.8, 20.6, 20.3, 18.7, 18.6 (2C), 17.2, 17.2, 16.3, 15.9, 15.0, 14.4, 13.9, -3.8, -3.9, -3.9, -4.1, -4.3, -4.3; IR (film, acetone): $\tilde{\nu}$ 2956, 2929, 2857, 1709, 1614, 1472, 1386, 1252, 1156, 1131, 1093, 1065, 983, 960, 898, 835, 774, 652; HR-ESI-MS calc. 1258.8923 for $\text{C}_{70}\text{H}_{132}\text{NO}_{10}\text{Si}_4^+$, $[\text{M}+\text{NH}_4]^+$, found 1258.8931.



(2*E*,8*E*,10*E*,12*S*,13*S*,15*S*)-(6*S*,7*S*,12*R*,*E*)-12-((2*S*,6*R*,*E*)-6-((4*R*,6*S*)-6-(12-amino-3-oxo-2,7,10-trioxa-4-azadodecyl)-2,2-di-*tert*-butyl-1,3,2-dioxasilan-4-yl)-4-methylhept-4-en-2-yl)-7,9-dimethyl-2-oxooxacyclododec-9-en-6-yl-12,13,15-tris((*tert*-butyldimethylsilyl)oxy)-4,6,10-trimethylhexadeca-2,4,6,8,10-pentaenoate (18**).**

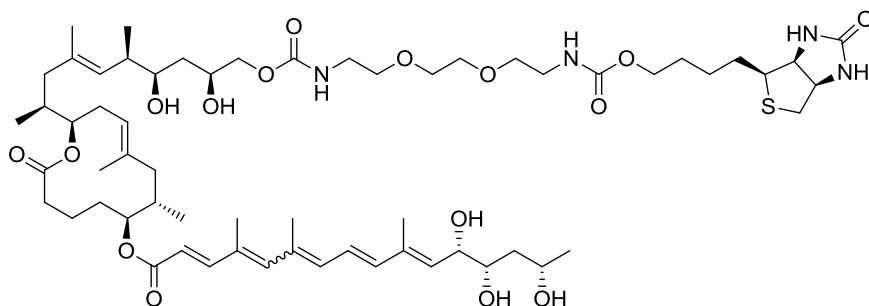
To a solution of primary alcohol **17** (15 mg, 12.1 μmol) in THF (1.5 mL) was added CDI (7.8 mg, 48 μmol) at ambient temperature. The solution was stirred at ambient temperature for 4 $\frac{3}{4}$ h. Additional CDI (2 x 7.8 mg, 2 x 48 μmol) was added after 1 h and 2 h. Water (4.4 μL , 242 μmol) was added and the solution stirred at ambient temperature for 30 min. 1,2-bis(2-aminoethoxy)ethane (30 μL , 302 μmol) was added and the resulting turbid solution was stirred at ambient temperature for 90 min while it turned clear again. Water (10 mL) and CH_2Cl_2 (15 mL) were added, the layers were separated and the org. layer was extracted with CH_2Cl_2 (3 x 5 mL). The combined org. layers were washed with water (5 mL) and brine (3 mL), dried over MgSO_4 and concentrated under reduced pressure. Purification by flash column chromatography (CH_2Cl_2 to $\text{CH}_2\text{Cl}_2/\text{MeOH}$, 50:1 to 9:1) gave 15.2 mg (87 %) of amino carbamate **18** as an inseparable mixture of isomers (*E*- $\Delta^{4,5'}$ /*Z*- $\Delta^{4,5'}$ 3:1) obtained as intensely colored yellow oil. R_f ($\text{CH}_2\text{Cl}_2/\text{MeOH}/\text{Et}_3\text{N}$ 90:10:1) = 0.17; **Z**- $\Delta^{4,5'}$ isomer: $^1\text{H-NMR}$ (400 MHz, methanol- d_4): δ 7.93 (d, $J = 15.6$ Hz, 1H), 6.71 – 6.50 (m, 1H), 6.48 – 6.29 (m, 2H), 6.13 (d, $J = 11.3$ Hz, 1H), 5.92 (d, $J = 15.6$ Hz, 1H), 5.73 – 5.52 (m, 1H), 5.09 (d, $J = 10.1$ Hz, 1H), 5.03 (d, $J = 9.7$ Hz, 1H), 4.97 – 4.81 (m, 1H), 4.80 – 4.68 (m, 1H), 4.53 (dd, $J = 9.1, 3.4$ Hz, 1H), 4.36 – 4.17 (m, 1H), 4.08 (dd, $J = 11.1, 3.9$ Hz, 1H), 4.03 – 3.91 (m, 2H), 3.89 – 3.70 (m, 2H), 3.69 – 3.41 (m, 8H), 3.33 – 3.27 (m, 3H), 2.85 (t, $J = 5.2$ Hz, 2H), 2.62 – 2.29 (m, 3H), 2.17 – 1.42 (m, 15H), 2.01 (s, 3H), 1.97 (s, 3H), 1.89 (s, 3H), 1.71 (s, 3H), 1.65 (s, 3H), 1.17 (d, $J = 6.0$ Hz, 3H), 1.10 –

0.96 (m, 3H), 1.03 (s, 9H), 1.01 (s, 9H), 0.96 – 0.81 (m, 33H), 0.16 – –0.05 (m, 18H); $^{13}\text{C-NMR}$ (100 MHz, methanol- d_4): δ 175.2, 168.6, 158.9, 144.3, 142.7, 140.2, 138.1, 136.1, 135.7, 135.3, 134.9, 134.6, 132.5, 130.7, 125.5, 124.0, 119.3, 80.1, 79.1, 77.3, 74.8, 74.1, 72.6, 72.4, 71.6, 71.3, 71.1, 70.1, 67.4, 46.7, 44.9, 44.3, 41.8 (2C), 41.7, 37.4, 36.4, 35.8, 33.5, 31.8, 29.7, 28.1 (3C), 27.7 (3C), 26.5 (3C), 26.5 (3C), 26.4 (3C), 24.3, 23.7, 21.2, 21.0, 20.6, 20.4, 19.0, 19.0, 18.9, 17.7, 17.1, 16.3, 16.0, 15.1, 14.0, –3.8, –3.8, –3.9, –4.1, –4.2, –4.3; ***E*- $\Delta^{4',5'}$ isomer**: $^1\text{H-NMR}$ (400 MHz, methanol- d_4): δ 7.38 (d, J = 15.5 Hz, 1H), 6.71 – 6.50 (m, 1H), 6.48 – 6.29 (m, 3H), 5.88 (d, J = 15.5 Hz, 1H), 5.73 – 5.52 (m, 1H), 5.09 (d, J = 10.1 Hz, 1H), 5.03 (d, J = 9.7 Hz, 1H), 4.97 – 4.81 (m, 1H), 4.80 – 4.68 (m, 1H), 4.53 (dd, J = 9.1, 3.4 Hz, 1H), 4.36 – 4.17 (m, 1H), 4.08 (dd, J = 11.1, 3.9 Hz, 1H), 4.03 – 3.91 (m, 2H), 3.89 – 3.70 (m, 2H), 3.69 – 3.41 (m, 8H), 3.33 – 3.27 (m, 3H), 2.85 (t, J = 5.2 Hz, 2H), 2.62 – 2.29 (m, 3H), 2.17 – 1.42 (m, 15H), 2.09 (s, 3H), 2.05 (s, 3H), 1.89 (s, 3H), 1.71 (s, 3H), 1.65 (s, 3H), 1.17 (d, J = 6.0 Hz, 3H), 1.10 – 0.96 (m, 3H), 1.03 (s, 9H), 1.01 (s, 9H), 0.96 – 0.81 (m, 33H), 0.16 – –0.05 (m, 18H); $^{13}\text{C-NMR}$ (100 MHz, methanol- d_4): δ 175.2, 168.6, 158.9, 152.4, 145.3, 140.6, 138.1, 136.7, 136.1, 136.1, 135.3, 134.6, 133.5, 130.7, 125.5, 124.0, 117.1, 80.1, 79.1, 77.3, 74.8, 74.1, 72.6, 72.4, 71.6, 71.3, 71.1, 70.1, 67.4, 46.7, 44.9, 44.3, 41.8 (2C), 41.7, 37.4, 36.4, 35.8, 33.5, 31.8, 29.7, 28.1 (3C), 27.7 (3C), 26.5 (3C), 26.5 (3C), 26.4 (3C), 24.3, 23.7, 21.2, 20.6, 20.4, 19.0, 19.0, 18.9, 17.2, 17.1, 16.3, 16.0, 15.1, 14.4, 14.0, –3.8, –3.8, –3.9, –4.1, –4.2, –4.3; IR (film, MeOH): $\tilde{\nu}$ 2956, 2928, 2856, 2360, 2344, 2328, 1725, 1616, 1559, 1539, 1472, 1463, 1386, 1362, 1297, 1250, 1156, 1131, 1094, 1004, 982, 961, 938, 897, 835, 773, 651; HR-ESI-MS calc. 1415.9662 for $\text{C}_{77}\text{H}_{143}\text{N}_2\text{O}_{13}\text{Si}_4^+$, $[\text{M}+\text{H}]^+$, found 1415.9636.



(2*E*,8*E*,10*E*,12*S*,13*S*,15*S*)-(6*S*,7*S*,12*R*,*E*)-12-((13*S*,15*R*,16*R*,20*S*,*E*)-1-amino-13,15-dihydroxy-16,18-dimethyl-10-oxo-3,6,11-trioxa-9-azahenicos-17-en-20-yl)-7,9-dimethyloxoxacyclododec-9-en-6-yl-12,13,15-trihydroxy-4,6,10-trimethylhexadeca-2,4,6,8,10-pentaenoate (19). To a solution of silyl-protected pentol **18** (19.1 mg, 13.5 μmol) in THF (1.5 mL) was added TBAF (1 M in THF, 162 μL , 162 μmol) at ambient temperature. The solution was stirred at ambient temperature for 2 h. Subsequently, NH_4F (25 mg, 674 μmol) was added and the solution was stirred at ambient temperature for 17 h. Sat. aq. NH_4Cl -solution (3 mL), water (5 mL) and CH_2Cl_2 (10 mL) were added, the layers were separated and the aq. layer was extracted with $\text{CH}_2\text{Cl}_2/\text{MeOH}$ 100:1 (5 x 5 mL). The combined org. layers were washed with sat. aq. NH_4Cl -solution (3 mL) and brine, dried over MgSO_4 and concentrated under reduced pressure. Purification by FC ($\text{CH}_2\text{Cl}_2/\text{MeOH}$ 20:1 to 10:1 to 4:1) gave 15.3 mg (quant) of pentol **19** as an inseparable mixture of isomers (*E*- $\Delta^{4',5'}$ /*Z*- $\Delta^{4',5'}$ 3:1) obtained as strongly colored yellow oil. R_f ($\text{CH}_2\text{Cl}_2/\text{MeOH}$ 4:1) = 0.20; ***Z*- $\Delta^{4',5'}$ isomer**: $^1\text{H-NMR}$ (400 MHz, methanol- d_4): δ 7.91 (d, J = 15.6 Hz, 1H), 6.70 – 6.50 (m, 1H), 6.50

– 6.27 (m, 2H), 6.11 (d, $J = 10.9$ Hz, 1H), 5.94 (d, $J = 15.6$ Hz, 1H), 5.60 – 5.54 (m, 1H), 5.12 (d, $J = 11.1$ Hz, 1H), 5.01 (d, $J = 9.5$ Hz, 1H), 4.95 – 4.89 (m, 1H, obscured by H₂O signal), 4.78 – 4.69 (m, 1H), 4.43 – 4.29 (m, 1H), 4.11 – 3.93 (m, 4H), 3.77 – 3.41 (m, 10H), 3.40 – 3.24 (m, 2H, obscured by solvent signal), 3.15 (dd, $J = 12.0, 6.9$ Hz, 2H), 2.61 – 2.31 (m, 3H), 2.16 – 1.43 (m, 16H), 2.00 (s, 3H), 1.97 (s, 3H), 1.93 (s, 3H), 1.71 (s, 3H), 1.65 (s, 3H), 1.23 – 1.11 (m, 3H), 0.99 (d, $J = 6.6$ Hz, 3H), 0.94 – 0.87 (m, 6H); ¹³C-NMR (100 MHz, methanol-*d*₄): δ 175.3, 168.6, 159.0, 144.4, 142.6, 140.0, 138.6, 138.0, 135.6, 135.0, 134.4, 133.6, 132.6, 131.1, 125.8, 124.0, 119.3, 80.1, 77.5, 75.6, 75.1, 72.7, 71.3, 71.3, 71.0, 70.3, 69.6, 67.8, 67.5, 46.7, 44.7, 42.0, 41.6, 40.7 (2C), 39.0, 36.4, 35.9, 33.4, 31.8, 29.9, 23.5, 21.2, 20.9, 20.4, 17.6, 17.2, 16.2, 15.9, 15.0, 13.4; ***E*- $\Delta^{4,5}$ -isomer**: ¹H-NMR (400 MHz, methanol-*d*₄): δ 7.38 (d, $J = 15.3$ Hz, 1H), 6.70 – 6.50 (m, 1H), 6.50 – 6.27 (m, 3H), 5.89 (d, $J = 15.3$ Hz, 1H), 5.60 – 5.54 (m, 1H), 5.12 (d, $J = 11.1$ Hz, 1H), 5.01 (d, $J = 9.5$ Hz, 1H), 4.95 – 4.89 (m, 1H, obscured by H₂O signal), 4.78 – 4.69 (m, 1H), 4.43 – 4.29 (m, 1H), 4.11 – 3.93 (m, 4H), 3.77 – 3.41 (m, 10H), 3.40 – 3.24 (m, 2H, obscured by solvent signal), 3.15 (dd, $J = 12.0, 6.9$ Hz, 2H), 2.61 – 2.31 (m, 3H), 2.16 – 1.43 (m, 16H), 2.08 (s, 3H), 2.05 (s, 3H), 1.93 (s, 3H), 1.71 (s, 3H), 1.65 (s, 3H), 1.23 – 1.11 (m, 3H), 0.99 (d, $J = 6.6$ Hz, 3H), 0.94 – 0.87 (m, 6H); ¹³C-NMR (100 MHz, methanol-*d*₄): δ 175.3, 168.7, 159.0, 152.3, 145.1, 140.4, 138.6, 138.0, 136.5, 135.9, 134.4, 133.6, 133.5, 131.1, 125.8, 124.0, 117.1, 80.1, 77.5, 75.6, 75.1, 72.7, 71.3, 71.3, 71.0, 70.3, 69.6, 67.8, 67.5, 46.7, 44.7, 42.0, 41.6, 40.7 (2C), 39.0, 36.4, 35.9, 33.4, 31.8, 29.9, 23.5, 21.2, 20.4, 17.2, 17.1, 16.2, 15.9, 15.0, 14.3, 13.4; IR (film, MeOH): $\tilde{\nu}$ 3339, 2970, 1697, 1647, 1559, 1456, 1302, 1270, 1251, 1159, 1131, 1089, 982, 652; HR-ESI-MS calc. 955.5866 for C₅₁H₈₄N₂NaO₁₃⁺, [M+Na]⁺, found 955.5874.



(2*E*,8*E*,10*E*,12*S*,13*S*,15*S*)-(6*S*,7*S*,12*R*,*E*)-12-((19*S*,21*R*,22*R*,26*S*,*E*)-19,21-dihydroxy-22,24-dimethyl-5,16-dioxo-1-((3*aS*,4*S*,6*aR*)-2-oxohexahydro-1*H*-thieno[3,4-*d*]imidazol-4-yl)-9,12,17-trioxa-6,15-diazaheptacos-23-en-26-yl)-7,9-dimethyl-2-oxooxacyclododec-9-en-6-yl 12,13,15-trihydroxy-4,6,10-trimethylhexadeca-2,4,6,8,10-pentaenoate (3).

To a solution of (+)-biotin (11.3 mg, 46 μ mol) in DMF (2.0 mL) were added DIPEA (26.7 μ L, 154 μ mol) and (benzotriazol-1-yloxy)tripyrrolidinophosphonium hexafluorophosphate (PyBop; 32 mg, 62 μ mol) at ambient temperature. The colorless solution was stirred at ambient temperature for 20 min. The activated biotin (11.6 μ mol) in DMF (0.5 mL; 25 % of the above solution) was transferred dropwise to a flask charged with amine **19** (7.2 mg, 7.7 μ mol). The yellow solution was stirred at ambient temperature for 30 min. Sat. aq. NH₄Cl-solution (3 mL), water (10 mL) and EtOAc (10 mL) were added. The layers were

separated and the aq. layer was extracted with and EtOAc (3 x 5 mL). The combined org. extracts were washed with sat. aq. NH₄Cl-solution (3 mL), sat. aq. NaHCO₃-solution (3 x 2 mL) and brine, dried over MgSO₄ and concentrated under reduced pressure. Purification by flash column chromatography (CH₂Cl₂ to CH₂Cl₂/MeOH, 50:1 to 10:1 then 5:1) yielded 5.6 mg (63 %, HPLC purity: >79 %) of amide **3** as an inseparable mixture of isomers (*E*-Δ^{4',5'}/*Z*-Δ^{4',5'}/minor isomers 63:29:8) as a yellow oil. *R_f* (CH₂Cl₂/MeOH 85:15) = 0.38; **Z**-Δ^{4',5'} **isomer**: ¹H-NMR (400 MHz, methanol-*d*₄): δ 7.92 (d, *J* = 15.6 Hz, 1H), 6.71 – 6.58 (m, 1H), 6.49 – 6.28 (m, 2H), 6.12 (d, *J* = 10.6 Hz, 1H), 5.94 (d, *J* = 15.6 Hz, 1H), 5.61 – 5.54 (m, 1H), 5.13 (d, *J* = 10.4 Hz, 1H), 5.01 (d, *J* = 9.4 Hz, 1H), 4.96 – 4.80 (m, 1H), 4.79 – 4.67 (m, 1H), 4.49 (dd, *J* = 7.8, 4.9 Hz, 1H), 4.35 – 4.25 (m, 2H), 4.16 – 3.91 (m, 4H), 3.68 – 3.42 (m, 10H), 3.41 – 3.28 (m, 4H), 3.26 – 3.14 (m, 1H), 2.93 (dd, *J* = 12.8, 5.0 Hz, 1H), 2.71 (d, *J* = 12.7 Hz, 1H), 2.60 – 2.32 (m, 3H), 2.22 (t, *J* = 7.4 Hz, 2H), 2.18 – 1.89 (m, 7H), 2.01 (s, 3H), 1.97 (s, 3H), 1.92 (s, 3H), 1.89 – 1.36 (m, 15H), 1.71 (s, 3H), 1.65 (s, 3H), 1.17 (d, *J* = 6.1 Hz, 3H), 0.99 (d, *J* = 6.6 Hz, 3H), 0.96 – 0.82 (m, 6H); ¹³C-NMR (100 MHz, methanol-*d*₄): δ 176.2, 175.3, 168.7, 166.1, 159.0, 144.4, 142.6, 140.1, 138.3, 138.4, 135.5, 135.2, 134.4, 133.8, 132.6, 131.2, 125.7, 124.1, 119.3, 80.1, 77.6, 75.6, 74.9, 72.6, 71.3, 71.3, 71.0, 70.7, 70.3, 69.7, 67.4, 63.4, 61.6, 57.0, 46.7, 44.7, 42.3, 41.7, 41.1, 40.8, 40.3, 39.0, 36.8, 36.4, 35.9, 33.4, 31.8, 30.0, 29.8, 29.5, 26.9, 23.4, 21.2, 20.9, 20.4, 17.6, 17.2, 16.3, 16.0, 15.1, 13.4; **E**-Δ^{4',5'} **isomer**: ¹H-NMR (400 MHz, methanol-*d*₄): δ 7.38 (d, *J* = 15.4 Hz, 1H), 6.71 – 6.58 (m, 1H), 6.49 – 6.28 (m, 3H), 5.89 (d, *J* = 15.4 Hz, 1H), 5.61 – 5.54 (m, 1H), 5.13 (d, *J* = 10.4 Hz, 1H), 5.01 (d, *J* = 9.4 Hz, 1H), 4.96 – 4.80 (m, 1H), 4.79 – 4.67 (m, 1H), 4.49 (dd, *J* = 7.8, 4.9 Hz, 1H), 4.35 – 4.25 (m, 2H), 4.16 – 3.91 (m, 4H), 3.68 – 3.42 (m, 10H), 3.41 – 3.28 (m, 4H), 3.26 – 3.14 (m, 1H), 2.93 (dd, *J* = 12.8, 5.0 Hz, 1H), 2.71 (d, *J* = 12.7 Hz, 1H), 2.60 – 2.32 (m, 3H), 2.22 (t, *J* = 7.4 Hz, 2H), 2.18 – 1.89 (m, 7H), 2.08 (s, 3H), 2.05 (s, 3H), 1.92 (s, 3H), 1.89 – 1.36 (m, 15H), 1.71 (s, 3H), 1.65 (s, 3H), 1.17 (d, *J* = 6.1 Hz, 3H), 0.99 (d, *J* = 6.6 Hz, 3H), 0.96 – 0.82 (m, 6H); ¹³C-NMR (100 MHz, methanol-*d*₄): δ 176.2, 175.3, 168.7, 166.1, 159.0, 152.3, 145.2, 140.5, 138.4, 138.4, 136.6, 135.8, 134.4, 133.8, 133.6, 131.2, 125.7, 124.1, 117.1, 80.1, 77.6, 75.6, 74.9, 72.6, 71.3, 71.3, 71.0, 70.7, 70.3, 69.7, 67.4, 63.4, 61.6, 57.0, 46.7, 44.7, 42.3, 41.7, 41.1, 40.8, 40.3, 39.0, 36.8, 36.4, 35.9, 33.4, 31.8, 30.0, 29.8, 29.5, 26.9, 23.4, 21.2, 20.4, 17.2, 17.1, 16.3, 16.0, 15.1, 14.4, 13.4; IR (film, MeOH): $\tilde{\nu}$ 3323, 2928, 2361, 2338, 1700, 1555, 1454, 1256, 1159, 984, 846; HR-ESI-MS calc. 1181.6642 for C₆₁H₉₈N₄NaO₁₅S⁺ [M+Na]⁺, found 1181.6644.

Determination of HPLC purity: Purity of **3** was determined by HPLC (Water Symmetry C18 column, 3.5 μm, 4.6 x 100 mm, sample concentration: 1.0 mg/mL in MeOH, injection: 10 μL, eluent: H₂O/CH₃CN 90:10 to 40:60, flow: 1 mL/min).

References

1. Gersbach P, Jantsch A, Feyen F, Scherr N, Dangy J-P, Pluschke G, et al. A ring-closing metathesis (RCM)-based approach to mycolactones A/B. Chem Weinh Bergstr Ger. 2011;17: 13017–13031. doi:10.1002/chem.201101799

Appendix Chapter 3

The anti-TB drug candidate Q203 is highly active against Mycobacterium ulcerans, the causative agent of Buruli ulcer

Nicole Scherr^{1,2#}, Raphael Bieri^{1,2#}, Paul Schneide³, Kevin Pethe⁴, Matthias Witschel³, and
Gerd Pluschke^{1,2*}

¹Swiss Tropical and Public Health Institute, Socinstrasse 57, 4002 Basel, Switzerland

²University of Basel, Petersplatz 1, 4003 Basel, Switzerland

³BASF SE, Carl-Bosch-Strasse 38, 67056 Ludwigshafen, Germany

⁴Lee Kong Chian School of Medicine and School of Biological Sciences, Nanyang Technological University,
30 Biopolis Street, #B2-15a, Singapore 138671, Singapore

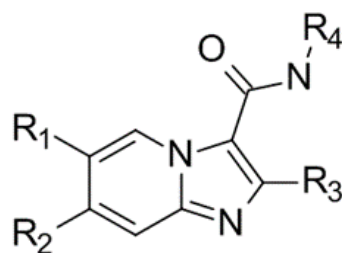
Contributed equally

* Corresponding author

This article is ready for submission (November 2015) to:
The Journal of Infectious Diseases
(Confidential until publication)

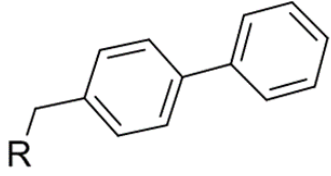
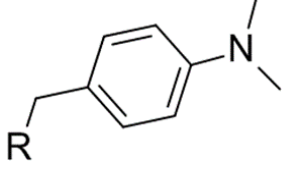
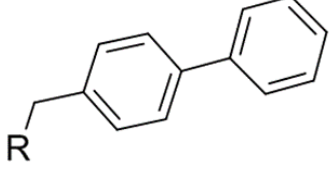
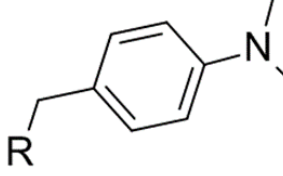
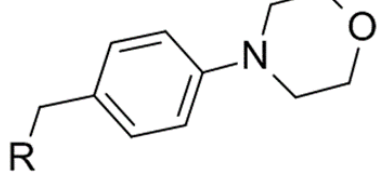
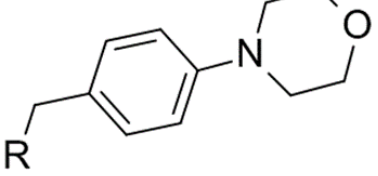
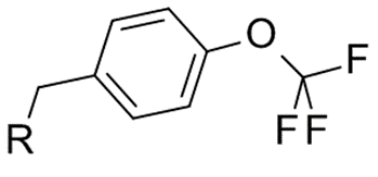
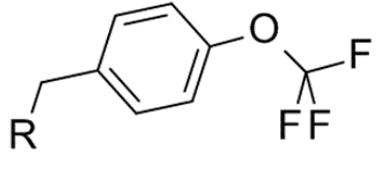
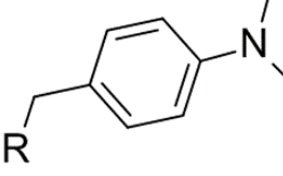
Supplementary Table 1

$\mu\text{g/ml}$	N (cpds)
< 0.001	1
0.001 - 0.01	8
0.01 - 0.1	11
0.1 - 1	20
1.0 - 10.0	14
> 10	31
total	85

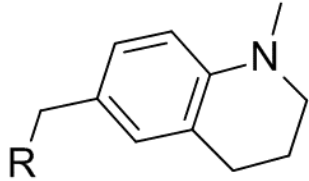
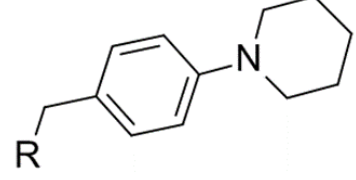
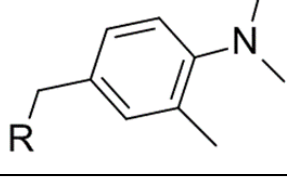
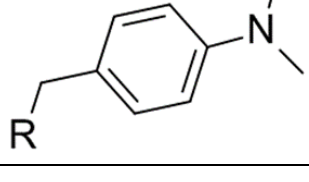
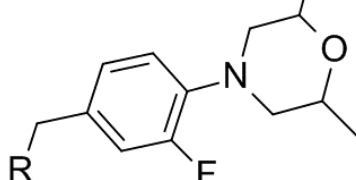
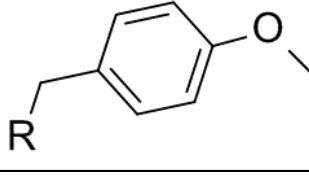
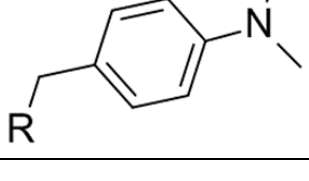
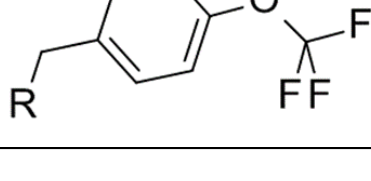


Number	R1	R2	R3	R4	MIC range
Q203 (1)	Cl	H	Et		
2	Me	H	Me		
3	H	Me	Me		
4	Me	H	Me		
5	Cl	H	Et		
6	Br	H	Me		

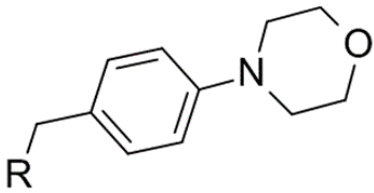
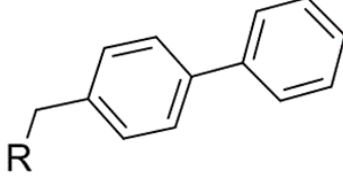
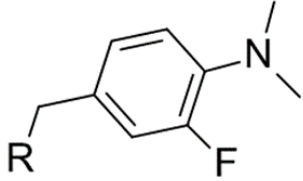
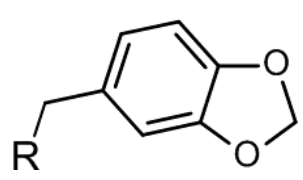
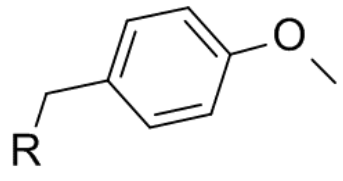
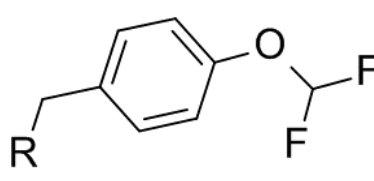
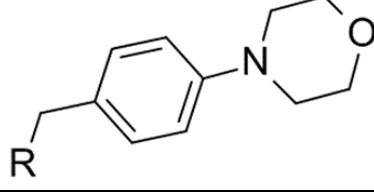
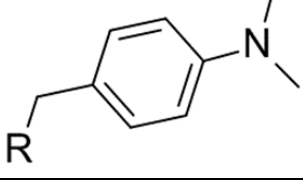
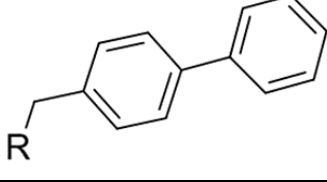
Appendix

7	Cl	H	Et		
8	Cl	H	Et		
9	Cl	H	Me		
10	Me	H	Me		
11	Br	H	Me		
12	Cl	H	Me		
13	Cl	H	Et		
14	Me	H	Me		
15	Br	H	Me		

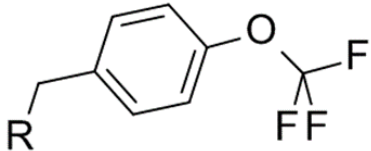
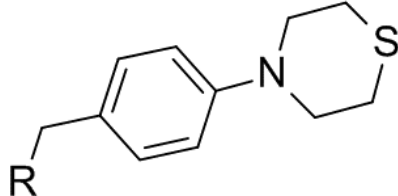
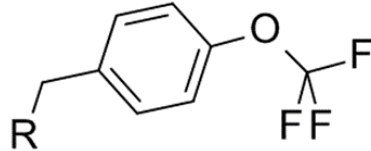
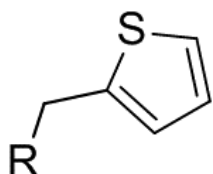
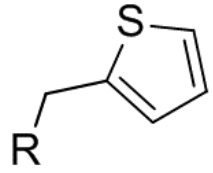
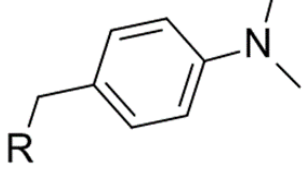
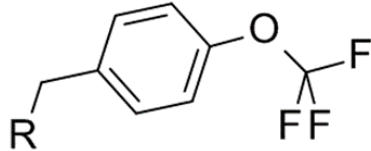
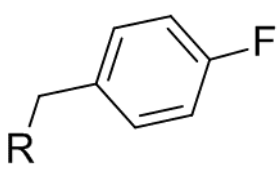
Appendix

16	H	H	Cl		
17	H	H	Cl		
18	H	H	Cl		
19	Cl	H	Me		
20	H	H	Cl		
21	H	H	Cl		
22	H	H	Me		
23	Cl	H	Me		

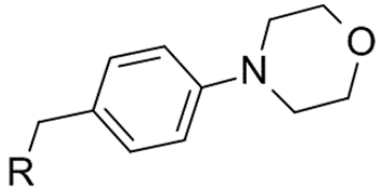
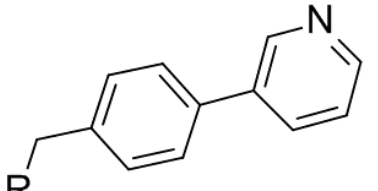
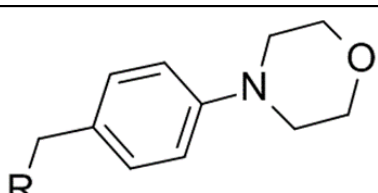
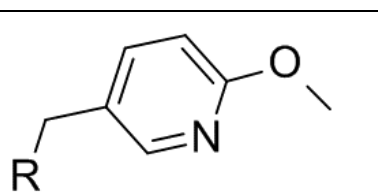
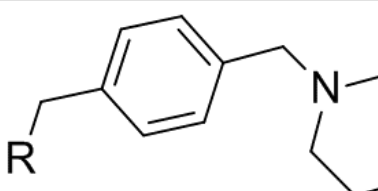
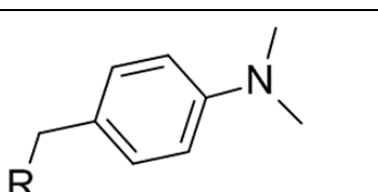
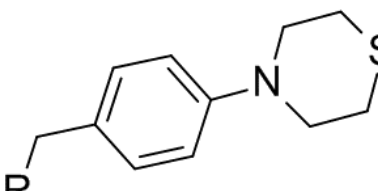
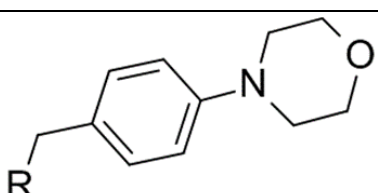
Appendix

24	H	Me	Me		
25	H	H	Me		
26	H	H	Cl		
27	H	H	Me		
28	H	H	Cl		
29	H	H	Cl		
30	Cl	H	Et		
31	H	H	Cl		
32	H	Me	Me		

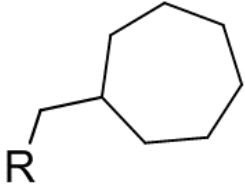
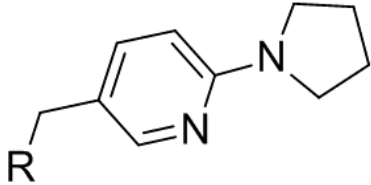
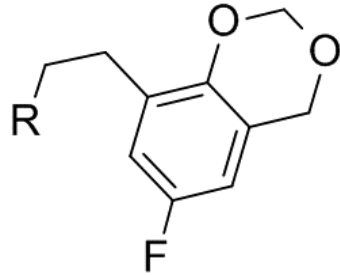
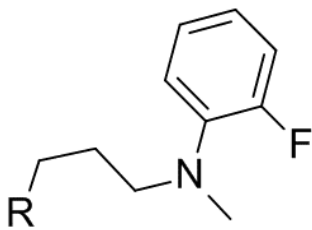
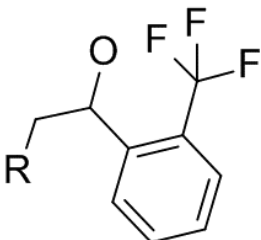
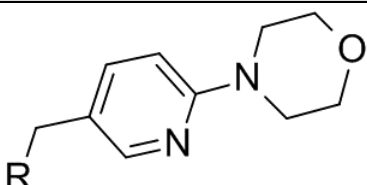
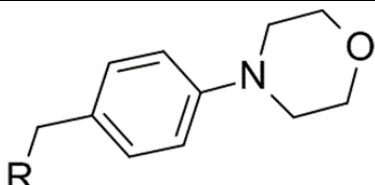
Appendix

33	H	H	Me		
34	H	H	Cl		
35	Br	H	Me		
36	H	H	Me		
37	H	H	Cl		
38	H	Me	Me		
39	H	Me	Me		
40	H	H	Cl		

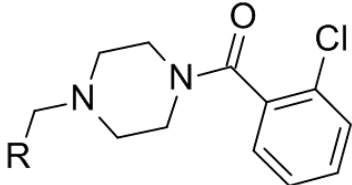
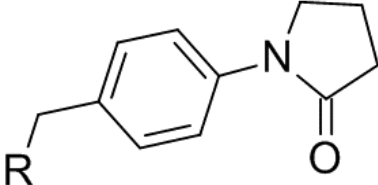
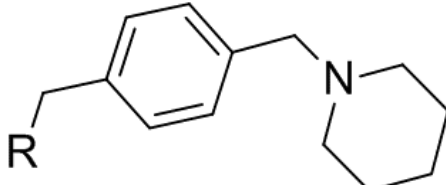
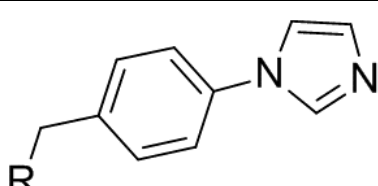
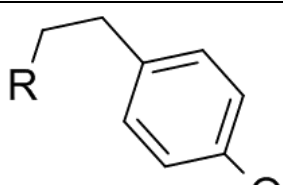
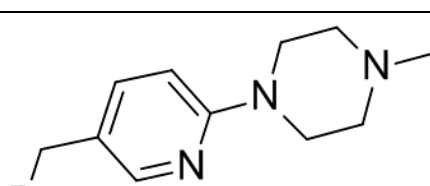
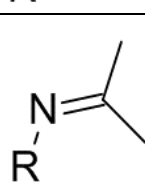
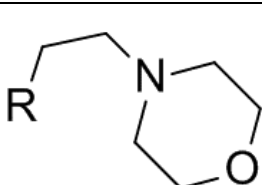
Appendix

41	H	H	Me		
42	H	H	Cl		
43	H	H	Cl		
44	H	H	Cl		
45	H	H	Cl		
46	Me	H	H		
47	Me	H	H		
48	Me	H	Me		

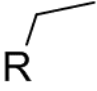

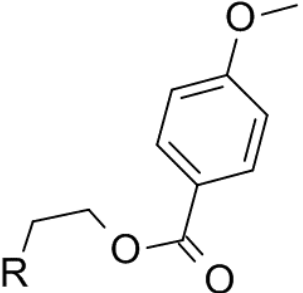
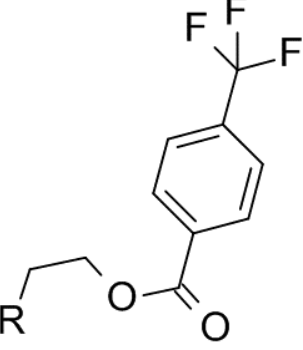
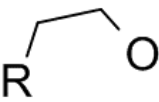
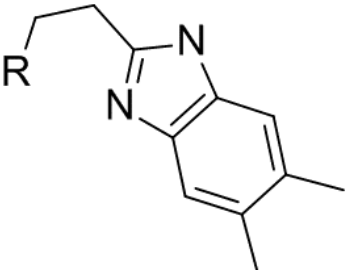
Appendix

49	H	H	Me		
50	H	H	Cl		
51	H	H	Cl		
52	H	H	Cl		
53	H	H	Cl		
54	H	H	Cl		
55	Me	H	H		

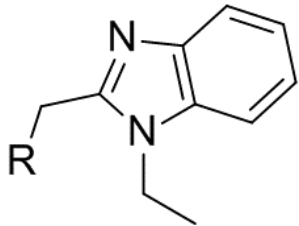
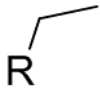
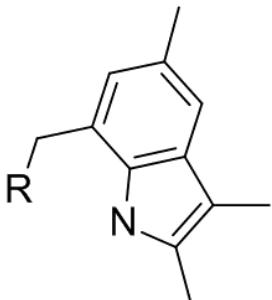
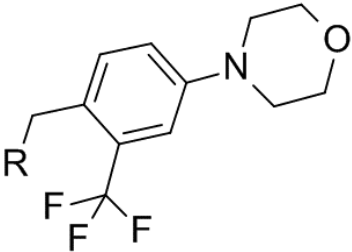
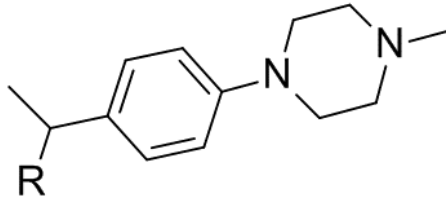
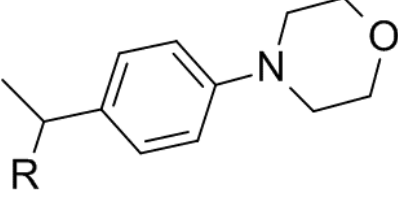
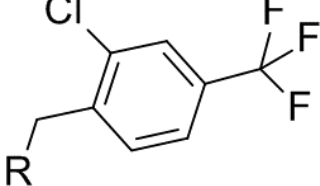
Appendix

56	H	H	Me		
57	H	H	Cl		
58	H	H	Cl		
59	H	H	Cl		
60	H	H	Cl		
61	H	H	Cl		
62	H	Me	Me		
63	H	H	Me		

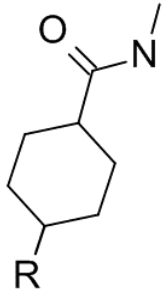
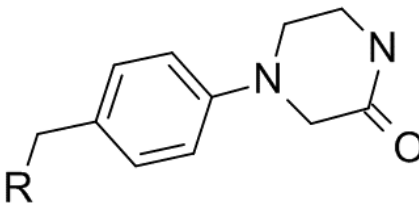
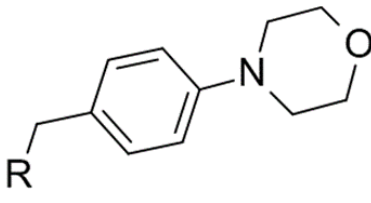
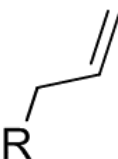
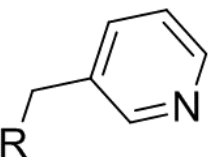
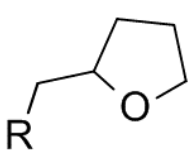
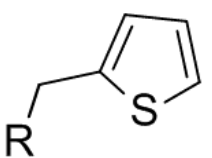

Appendix

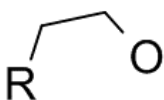
64	H	H	Me		
65	H	H	p-Me-Ph		
66	H	H	Cl		
67	H	H	Cl		
68	H	H	Cl		
69	Cl	H	Me		

Appendix

70	Me	H	m-Me-Ph		
71	H	H	Cl		
72	H	H	Cl		
73	H	H	Cl		
74	H	H	Cl		
75	H	Me	Me		
76	H	H	Cl		

Appendix

77	H	H	Cl		
78	H	Me	H		
79	H	H	Me		
80	H	H	Me		
81	H	H	Me		
82	H	Me	Me		
83	H	H	Me		
84					

85					
----	--	--	--	---	--

Supplementary Table 1: List of tested IPA compounds ranked according to their activity against *M. ulcerans*.

Curriculum Vitae

Raphael Bieri

Personal Information

Date of birth	20.02.1986
Nationality	Swiss
Current affiliation	Swiss Tropical and Public Health Institute
Address	Socinstrasse 57, CH – 4002 Basel
Phone	+41 61 284 82 77
E-mail	raphael.bieri@unibas.ch

Languages

German	mother tongue
English	fluent
French	basic knowledge

Academic Education

Since 05/2012	PhD candidate Molecular Immunology group, Swiss Tropical and Public Health Institute, University of Basel, Switzerland
03/2011 – 11/2011	Employed as a PhD student in the group of PD Dr. Jean-Pierre Bourquin, Children's Hospital, University of Zurich Member of the Cancer Biology Ph.D Program, University and ETH Zurich
09/2009 – 10/2010	Master of Science in Molecular Biology ("Functional evaluation of the role of Paralemmin-1 in lymphatic endothelial cells") Laboratory of Prof. Gerhard Christofori, Department of Biomedicine, Biozentrum, University of Basel
09/2006 – 08/2009	Bachelor of Science in Molecular Biology Biozentrum, University of Basel

Further Activities

Since 12/2013 **Visiting researcher**
Laboratory of Prof. Stewart Cole, Global Health Institute,
EPFL, Lausanne, Switzerland
Activity: Running and further development of the Buruli ulcer
mouse model

Conferences

23/03 – 25/03/2015 **Presentation** (“The *Mycobacterium ulcerans* toxin
mycolactone is an mTOR inhibitor promoting FoxO3- and
Bim-dependent apoptosis in Buruli ulcer”)
WHO Meeting on Buruli ulcer, Geneva, Switzerland

13/01 - 18/01/2015 **Poster** (“Pathogenesis of Buruli ulcer induced by the
Mycobacterium ulcerans macrolide toxin mycolactone is
caused by mTOR inhibition and Bim-dependent apoptosis”)
Keystone Symposia, PI 3-Kinase Signaling Pathways in
Disease, Vancouver, Canada

Teaching Activities

2013 - 2015 **Presentation** (Lecture Series on Advanced Immunology of
Infection)
University of Basel, Switzerland

01/2014 – 04/2014 **Supervision of a BSC Student**
 (“Molecular Basis of Mycolactone Cytotoxicity”)

Experimental Methods

Molecular biology

- Cloning
- DNA and RNA extraction from cell lines and animal tissue
- Conventional and real-time PCR

Cell biology

- Cell culture
- siRNA transfection
- Immunoprecipitation
- Generation of cell lines stably expressing lentiviral vectors

- FACS

Biochemistry

- Western Blot
- ELISA

Histology and Microscopy

- HE and ZN staining
- Immunohistochemical stainings on human and mouse tissues
- Light, fluorescence and confocal microscopy

Microbiology

- Cultivation of bacteria
- Colony forming unit assays (CFU)
- Trained to work under BSL-3 conditions

Mouse work

- Running the Buruli ulcer mouse model under BSL3 conditions
- Infection of mice with *M. ulcerans*
- Treatment and bleeding of mice
- Isolation and preparation of organs

Publications

- 11/2015 **Bieri, R., Scherr, N., Ruf, M.-T., Dangy, J.-P., Pletscher, F., Gersbach, P., Gehringer, M., Junghanss, T., Altmann, K.-H., and Pluschke, G.**
Mycolactone binds to FKBP12 and promotes Bim-dependent apoptosis in Buruli ulcer through inhibition of mTOR
Nature Chemical Biology, under revision
- 11/2015 **Bieri, R., Bolz, M., Ruf, M.-T., and Pluschke, G.**
Interferon- γ is a Crucial Activator of Early Host Immune Defense against Mycobacterium ulcerans Infection in Mice
PLOS Neglected Tropical Diseases, under revision
- 11/2015 **Bieri, R.*, Scherr, N.*, Schneide, P., Pethe, K., Witschel, M., and Pluschke, G. (*contributed equally)**
The anti-TB drug candidate Q203 is highly active against Mycobacterium ulcerans, the causative agent of Buruli ulcer
Ready for submission to The Journal of Infectious Diseases
Confidential until publication

10/2013

Albrecht, I., Bieri, R., Leu, A., Granacher, P., Hagmann, J., Kilimann, M.W., and Christofori, G.

Paralemmin-1 is expressed in lymphatic endothelial cells and modulates cell migration, cell maturation and tumor lymphangiogenesis

Angiogenesis. 2013 Oct;16(4):795-807